



THE
Water
Research
FOUNDATION



PROJECT NO.

4326



Advanced Condition Assessment and Failure Prediction Technologies for Optimal Management of Critical Water Supply Pipes

Advanced Condition Assessment and Failure Prediction Technologies for Optimal Management of Critical Water Supply Pipes

Prepared by:

Jayantha Kodikara
Monash University

2018



The Water Research Foundation (WRF) is a nonprofit (501c3) organization that provides a unified source for One Water research and a strong presence in relationships with partner organizations, government and regulatory agencies, and Congress. WRF conducts research in all areas of drinking water, wastewater, stormwater, and water reuse. The Water Research Foundation's research portfolio is valued at over \$700 million.

WRF plays an important role in the translation and dissemination of applied research, technology demonstration, and education, through creation of research-based educational tools and technology exchange opportunities. WRF serves as a leader and model for collaboration across the water industry and its materials are used to inform policymakers and the public on the science, economic value, and environmental benefits of using and recovering resources found in water, as well as the feasibility of implementing new technologies.

For more information, contact:

The Water Research Foundation

Alexandria, VA Office

1199 North Fairfax Street, Suite 900
Alexandria, VA 22314-1445
Tel: 571.384.2100
www.werf.org
werf@werf.org

Denver, CO Office

6666 West Quincy Avenue
Denver, Colorado 80235-3098
Tel: 303.347.6100
www.waterrf.org
Info@WaterRF.org

©Copyright 2018 by The Water Research Foundation. All rights reserved. Permission to copy must be obtained from The Water Research Foundation.

WRF ISBN: 978-1-60573-334-0

WRF Project Number: 4326

This report was prepared by the organization(s) named below as an account of work sponsored by The Water Research Foundation. Neither The Water Research Foundation, members of The Water Research Foundation, the organization(s) named below, nor any person acting on their behalf: (a) makes any warranty, express or implied, with respect to the use of any information, apparatus, method, or process disclosed in this report or that such use may not infringe on privately owned rights; or (b) assumes any liabilities with respect to the use of, or for damages resulting from the use of, any information, apparatus, method, or process disclosed in this report.

Prepared by Monash University.

This document was reviewed by a panel of independent experts selected by The Water Research Foundation. Mention of trade names or commercial products or services does not constitute endorsement or recommendations for use. Similarly, omission of products or trade names indicates nothing concerning The Water Research Foundation's positions regarding product effectiveness or applicability.

CONTENTS

LIST OF TABLES	ix
LIST OF FIGURES	xi
EXECUTIVE SUMMARY	xv
CHAPTER 1: INTRODUCTION	1
1.1 Background	1
1.2 Project Partners	2
1.3 Project Scope.....	2
1.3.1 Round 1	2
1.3.2 Deliverables	3
1.3.3 Round 2.....	4
1.3.4 Deliverables	4
PART 1: ACTIVITIES 1 AND 4E - HOW, WHEN, AND WHERE WILL PIPES FAIL WITHIN THE ENTIRE NETWORK AND HOW CAN PROBABILITY OF FAILURE BE ESTIMATED?	7
CHAPTER 2: ACTIVITY 1 AND 4E SUMMARY.....	9
2.1 Historical Information on Large-Diameter Pipe Failure.....	9
2.2 Pipe Traffic Loading Tests in Sydney Water Test Bed	9
2.3 Pressure-Transient Monitoring and Modelling.....	10
2.4 Cast-Iron Pipe Cohort Properties	10
2.5 Large-Diameter Pipe Burst Tests.....	11
2.6 Fatigue Mechanisms in Cast Iron Water Mains.....	11
2.7 Finite Element Modelling of Pressurised Corroded Cast Iron Pipes	12
2.8 Physical Modelling for Prediction of Failure Probability	13
2.9 Distributed Optical Fibre Sensors.....	13
2.10 Future Research Directions.....	14
CHAPTER 3: ACTIVITY 1 AND 4E REPORT	15
3.1 Summary	15
3.2 Introduction.....	16
3.3 Historical Information on Large-Diameter Pipe Failure.....	17
3.3.1 Introduction.....	17
3.3.2 Methodology	18
3.3.3 Findings.....	18
3.4 Pipe Traffic Loading Tests.....	19
3.4.1 Introduction.....	19
3.4.2 Instrumentation of Sydney Water Test Bed.....	19
3.4.3 Important Results and Discussion.....	20
3.4.4 Discussion	22
3.4.5 Conclusions.....	22

3.5 Pressure Transient Monitoring and Modelling	23
3.5.1 Introduction.....	23
3.5.2 Pressure Transient Monitoring Program.....	24
3.5.3 Pressure Transient Modelling Program	27
3.5.4 Conclusions.....	30
3.6 Cast Iron Pipe Cohort Properties	30
3.6.1 Introduction.....	30
3.6.2 Material and Methods	31
3.6.3 Results and Discussion	33
3.6.4 Conclusions.....	35
3.7 Large-Diameter Pipe Burst Tests.....	36
3.7.1 Introduction.....	36
3.7.2 Material and Methods	36
3.7.3 Results and Discussion	37
3.7.4 Conclusions.....	41
3.8 Fatigue Mechanisms in Cast Iron Water Mains.....	42
3.8.1 Introduction.....	42
3.8.2 Research Aims	42
3.8.3 Initiation of a Through-Wall Crack by Cyclic Pressures.....	43
3.8.4 Propagation of a Through Crack by Cyclic Pressures	45
3.8.5 Fatigue: Key Findings.....	47
3.9 Finite Element Modelling of Pressurised Corroded Cast Iron Pipes	48
3.9.1 Introduction.....	48
3.9.2 FE Modelling to Develop a Closed-Form Stress-Estimate Equation	48
3.9.3 FE Modelling of Burst Pipe Testing	53
3.9.4 Conclusions.....	57
3.10 Physical Modelling for Prediction of Probability of Failure	58
3.10.1 Overview.....	58
3.10.2 Deterioration of Pipe Structural Capacity Due to Corrosion.....	59
3.10.3 Prediction of Pipe Lifetime Probability of Failure	59
3.10.4 Prediction of Failure Rate of Pipe Cohorts	61
3.10.5 Summary	62
3.11 Distributed Optical Fibre Sensors.....	63
3.11.1 Introduction.....	63
3.11.2 Accuracy of Distributed Optical Fibre Sensors	64
3.11.3 Pressure Transient Monitoring.....	65
3.11.4 Fatigue Damage Monitoring.....	68
3.11.5 Summary of Optical Fibre Studies.....	69
3.12 Conclusions.....	70
PART 2: ACTIVITIES 2 AND 4A – RESEARCH ACTIVITIES INTO DIRECT CONDITION ASSESSMENT TECHNOLOGIES AND “ALONG-THE-PIPE” FRAMEWORK FOR CONDITION ASSESSMENT OF CICL CRITICAL WATER MAINS.....	73
CHAPTER 4: ACTIVITY 2 AND 4E SUMMARY.....	75

4.1 Scope.....	76
4.2 Test Bed and Verification	77
CHAPTER 5: RESEARCH ACTIVITIES INTO CONDITION ASSESSMENT	
TECHNOLOGIES FOR CICL CRITICAL WATER MAINS.....	
5.1 Magnetic Flux Leakage (MFL) Technology.....	81
5.1.1 Technical Description	81
5.1.2 Observations during Trials.....	82
5.1.3 Recommendations.....	82
5.1.4 Vendors of MFL Technology in the Market.....	83
5.1.5 Summary of UTS Research Outcomes	83
5.2 Remote Field Eddy Current Technology	84
5.2.1 Technical Description	84
5.2.2 Observations during Trials.....	85
5.2.3 Recommendations.....	86
5.2.4 Vendors of RFEC Technology in the Market.....	86
5.2.5 Summary of UTS Research Outcomes	86
5.3 Pulse Eddy Current Technology	87
5.3.1 Technical Description	87
5.3.2 Observations during Trials.....	88
5.3.3 Recommendations.....	89
5.3.4 Vendors of PEC Technology in the Market.....	90
5.3.5 Summary of UTS Research Outcomes	90
5.4 Pressure Wave Propagation Technologies.....	90
5.4.1 Technical Description	90
5.4.2 Technology Vendors of Pressure Wave Propagation Technology in the Market.....	91
5.5 Magnetoelastic Sensing Technologies.....	97
5.5.1 Technical Description	97
5.5.2 Vendors of Magnetoelastic Sensing Technology in the Market.....	97
5.6 Summary Table of Technology Capabilities	99
5.7 Condition Assessment Technologies – Concluding Remarks	102
CHAPTER 6: RESEARCH ACTIVITIES INTO AN “ALONG-THE-PIPE”	
FRAMEWORK FOR CONDITION ASSESSMENT OF CICL CRITICAL	
WATER MAINS	
6.1 Introduction.....	105
6.2 “Along-the-Pipe” Framework for Condition Assessment	105
6.2.1 Screening and Local Inspection Data Gathering	106
6.2.2 “Along-the-Pipe” Learning and Generalisation.....	107
6.2.3 “Along-the-Pipe” Flow Chart	109
6.2.4 Extreme Value Analysis	110
6.3 Experimental Validation: A Case Study from the Sydney Water Test Bed	111
6.3.1 Results.....	112
6.4 Conclusions and Relevance for Utilities.....	114

PART 3: ACTIVITY 3 – HOW DO WE CALCULATE PIPE DETERIORATION RATES ACCURATELY WITH RESPECT TO THE PIPE ENVIRONMENT?.....	117
CHAPTER 7: ACTIVITY 3 BACKGROUND, AIMS, AND PROPOSED METHOD.....	119
7.1 Field Data Collection.....	119
7.2 Conceptual Corrosion Model.....	120
7.3 Analysis of the Field Data in the Context of the Conceptual Corrosion Model.....	121
7.4 Preliminary Version of the Corrosion Model.....	122
7.5 Corrosion after Pipe Perforation.....	122
7.6 Recommendations for Future Work.....	123
PART 4: ACTIVITY 4B - IMPROVING CONFIDENCE IN CRITICAL PIPE FAILURE PREDICTION.....	125
CHAPTER 8: ACTIVITY 4B SUMMARY.....	127
8.1 Introduction.....	127
8.2 Results.....	128
8.2.1 Review of Theoretical and Practical Application of LPR.....	128
8.2.2 Quantification of the Current Level of Confidence in LPR Corrosion Predictions.....	129
8.2.3 Development of an Improved Model for LPR Prediction of Corrosion Rates.....	130
PART 5: ACTIVITY 4C - PREDICTING THE LIKELIHOOD OF PIPE CORROSION AND ITS SEVERITY ALONG THE PIPE TO FORECAST FAILURE.....	133
CHAPTER 9: ACTIVITY 4C SUMMARY.....	135
9.1 Introduction.....	135
9.2 Results.....	135
9.2.1 Interpolation of Soil Properties along the Pipe.....	135
9.2.2 Feasibility Assessment for an Advanced Monitoring Tool.....	138
9.2.3 Method of Soil Property Estimation.....	138
9.3 Conclusions and Recommendations for Future Work.....	141
CHAPTER 10: ACKNOWLEDGEMENTS.....	143
CHAPTER 11: APPENDICES.....	145
11.1 Appendix 1A: Explanatory Notes for Monash Tool.....	145
11.1.1 Introduction to Monash Tool.....	145
11.1.2 Evaluation Methods.....	145
11.1.3 Disclaimer.....	151
11.2 Appendix 1A: Definitions of Statistical Functions and Failure Data.....	151
11.2.1 PDF.....	151
11.2.2 CDF.....	151
11.2.3 Hazard Rate.....	152

11.3 Activity 2 Appendix 1: Procedure for Obtaining Ground Truth of Remaining Wall Thickness of Critical Pipes	154
11.3.1 Preface.....	154
11.3.2 Introduction.....	154
11.3.3 EXAscan 3D Scanner - Operating Principle.....	154
11.3.4 Recommendations for Best Practice	156
11.3.5 Safety Precautions.....	156
11.3.6 Obtaining Point Clouds.....	157
11.3.7 Computing Ground Truth	177
11.4 Activity 2 Appendix 2: Influence of Material Properties on Critical Pipe Non-Destructive Evaluation Techniques	178
11.4.1 Preamble	178
11.4.2 Measuring Electrical and Magnetic Properties of Pipe Materials	178
11.4.3 Typical Variation of Critical Pipe Electrical and Magnetic Properties	183
11.4.4 Effect of Critical Pipe Electrical and Magnetic Properties on the Accuracy of a Defect Depth Predicted by MFL	185
11.4.5 Effect of Critical Pipe Electrical and Magnetic Properties on the Accuracy of Average Wall Thickness Predicted by PEC (BEM).....	186
11.4.6 Effect of Critical Pipe Electrical and Magnetic Properties on the Accuracy of Wall Loss and Local Thickness Estimates Predicted by RFT	186
11.5 Activity 4b and 4c Appendices.....	187
11.5.1 Activity 4b: LPR Data for Verona St Test Bed Site (Sydney)	187
11.5.2 Activity 4b: LPR Field Data for Perth Subiaco and Fremantle Sites.....	195
11.5.3 Activity 4b: Report on the Current Knowledge of the Theoretical Basis of Linear Polarisation Resistance	198
11.5.4 Activity 4b: Report on the Relationship between the Theoretical Basis and Practical Application of Linear Polarisation Resistance Technology	235
11.5.5 Activity 4c: Soils Data for Verona St Test Bed Site.....	265
11.5.6 Activity 4c: Soils Data for Perth Subiaco and Fremantle Sites.....	283
11.5.7 Activity 4c: Long-Term Soil Moisture Data for Verona St Test Bed (Sydney).....	293
REFERENCES	299

TABLES

Table 3.1. General range of material properties for cast iron pipe cohorts tested	34
Table 3.2. Pipe corrosion patch information for each test	37
Table 3.3. Failure data for each pipe test	40
Table 3.4. Effect of fatigue damage in cast iron pipelines.....	44
Table 3.5. Results of fracture toughness and FCGR tests.....	45
Table 3.6. Physical properties of large-diameter cast iron buried pipes.....	50
Table 3.7. Approximate values of measured and predicted leak and burst water pressures.....	57
Table 4.1 List of test bed activities	78
Table 5.1. Summary table of technology capabilities.....	100
Table 6.1. Lowest thickness and largest patch geometries found in the pipeline (as given by G2)	113
Table 6.2. “Along-the-pipe” framework results on predicting extreme conditions in the pipeline.....	114

FIGURES

Figure 3.1. Layout of Sydney Water test bed	20
Figure 3.2. Relationship between hoop strain on pipe crown and tyre load.....	21
Figure 3.3. Relationship between ground pressure on pipe crown and tyre load	21
Figure 3.4. Pressure transients generated at Section A due to pumps during high demand	25
Figure 3.5. Pressure transients generated at Section A due to pumps during low demand (rise of steady-state pressure).....	25
Figure 3.6. Severe pressure transient generated due to combined action of two booster pumps and an automated inlet valve.....	26
Figure 3.7. Sample pressure map developed using results of the pressure transient analysis of Section B (results for Scenarios 4 and 5); new data layer in the GIS database.....	29
Figure 3.8. Timeline of ferrous pipe material in eastern Australia.....	31
Figure 3.9. Typical cast iron pipe cohort groups used in eastern Australia.....	33
Figure 3.10. Relationship between cast iron pipe class, diameter, and wall thickness.....	35
Figure 3.11. Large-diameter cast iron pipe burst test facility (Test 1 pipe in place)	37
Figure 3.12. Large-diameter cast iron pipes leaking water with corrosion patch size.....	39
Figure 3.13. Test 3 burst failure (piece blown out) and longitudinal split.....	41
Figure 3.14. Conceptual diagrams: (a) crack propagation from the corroded patched areas; (b) fatigue cumulative damage of cast iron pipes	43
Figure 3.15. FCGR of a full-scale fatigue test	46
Figure 3.16. Leakage rates by measuring and simulation in TBF1	47
Figure 3.17. Finite element model of a buried pipe in subgrade	49
Figure 3.18. Numerical modelling of clustering configuration of two pits	49
Figure 3.19. Screenshot of Monash Tool (MT)	52
Figure 3.20. Variations in maximum tensile stresses due to the increase of L	53
Figure 3.21. Tested CI pipes including machined corrosion patches	55

Figure 3.22. Numerical results of tensile stress and hoop strains of burst tests on pipe 2 shown in (a) and (b), pipe 3 in (c) and (d), and pipe 4 in (e) and (f).	56
Figure 3.23. Simplified pipe burial conditions for water mains	58
Figure 3.24. Configurations of corrosion in CI pipes	59
Figure 3.25. Concepts of prediction of lifetime probability of failure.....	60
Figure 3.26. Lifetime probability of failure of CI pipes	61
Figure 3.27. Failure rate of CI pipes derived from physical modelling.....	62
Figure 3.28. Comparison of distributed optical fibre sensors of different spatial resolutions with theoretical solution as well as strain gauge measurements.....	64
Figure 3.29. (a) Time series (4s) of strain measurement at 2000 $\mu\epsilon$ loading regime, and (b) Fast Fourier Transform (FFT) of time series	65
Figure 3.30. Distributed strain measured during transient events (due to valve closure and turning on the pump).....	66
Figure 3.31. Dynamic strain response (time series) measured at section B-B in Figure 3.30.....	67
Figure 3.32. (a) Comparison between the dynamic strain measurement with pressure profile measured by pressure transducer during a pressure transient event (due to operating pump), and (b) dynamic strain measurement at location B-B when subjected to multiple sets of pressure transient events	67
Figure 3.33. Dynamic strain measurement along the monitored pipe with the presence of localised damage.....	68
Figure 3.34. Strain measurement at a point along the distributed optical fibre sensor vs. number of cycles	69
Figure 3.35. Fatigue crack growth monitoring using distributed optical fibre sensors	69
Figure 4.1. Project test bed provided by Sydney Water. Longitudinal section (above) and view on a map (bottom) with spot CA inspections shown in blue	77
Figure 5.1. Leakage of magnetic flux due to a reduction in wall thickness in area 'B' is shown to illustrate the principle of operation of MFL. 'A' represents an area without any material losses due to corrosion	81
Figure 5.2. AIA Smart-CAT MFL tool used during the trials at Sydney Water test bed.....	82
Figure 5.3. Schematic of a RFEC tool showing the path of the electro-magnetic field within a section of a pipe	84

Figure 5.4. PICA Corp SeeSnake tool deployed during the trials at Sydney Water test bed	85
Figure 5.5. Typical sensor design and signal conditioning circuitry (left). Cross view of the PEC sensor coils sitting on top of a pipe. The top two larger circles represent the cross section of the exciter coil, while the bottom, smaller circles represent the detector coils. A cross section of the pipe wall is seen under the sensor, with the induced Eddy currents shown in yellow on the pipe wall (right)	88
Figure 5.6. RSG HSK PEC tool with a single antenna used during the trials at Sydney Water test bed	89
Figure 5.7. Typical acoustic pressure wave signal at the exciter (top) and receiver	91
Figure 5.8. Pure Technologies Sahara II acoustic PWA tool as trialled on Sydney Water test bed (top left), a schematic of the actual tool sensor configuration arrangement (bottom left), and an illustration of the deployment mechanism (right).....	92
Figure 5.9. PCA-Echologics ePulse typical deployment scenario with two acoustic receivers	94
Figure 5.10. Detection Services p-CATTM typical deployment scenario with two acoustic receivers	95
Figure 5.11. Illustrative example of the Magnetoelastic principle on a pipeline.....	97
Figure 5.12. An illustration (left) of the Smartball® device hosting the EM PWA sensor and during the test bed trial (right)	98
Figure 6.1. Along-the-pipe framework for CA.....	106
Figure 6.2. Step 1: learn data correlation models from local inspection results. Step 2: sample from the “along-the-pipe” model on area without any additional input	108
Figure 6.3. Two representative random realisations of a pipe spool generated by the framework	109
Figure 6.4. Flow chart for the “along-the-pipe” generic framework	110
Figure 6.5. Ground truth data obtained from exhumed, grit-blasted, and laser-profiled sections.....	112
Figure 8.1. Schematic of pipe failure information flow.....	128
Figure 8.2. Variation of LPR Rp values for 3 clusters of soils sampled along the Verona St test bed	130
Figure 9.1. The variation in soil nitrate levels observed above the buried pipe, at the mid depth of the pipe, and underneath the pipe	136
Figure 9.2. Variation in soil nitrate levels along the length of the Verona St test bed.....	137

Figure 9.3. Long-term variation in soil moisture at site 6 - Verona St test bed, Sydney.....137

Figure 9.4. Soil moisture recorded at pipe depth along the Verona St test bed at 7 sites.....138

EXECUTIVE SUMMARY

KEY FINDINGS

- A new Excel-based pipe stress prediction tool (“Monash Tool”) was developed for large-diameter cast iron (CI) water pipes.
- A leak-before-break (LBB) concept was proposed for pipe failure prevention.
- Managing internal pressure may extend CI pipe life.
- Corrosion does not progress as a linear function from its origin. Therefore, a corrosion “rate” is highly misleading.
- Moisture/wetness is a critical issue.

BACKGROUND

Cast iron pipes remain a substantial component of buried pipe cohorts of water utilities, and many are over one hundred years old. Although these pipes were significantly overdesigned with high factors of safety at the time of installation, pipes have variably deteriorated over time, primarily due to corrosion in the soil environment, and pipe failures have become common. Consequently, utility managers are interested in determining the optimal replacement schedule for these critical mains.

In 2011, a consortium of Australian water utilities led by Sydney Water (SW) joined forces with WRF and UK Water Industry Research (UKWIR) to initiate a five-year research program, the Advanced Condition Assessment and Pipe Failure Prediction Project (ACAPFP). The goal of the project was to advance critical pipe condition assessment (CA) and failure prediction.

APPROACH

The research team divided the project into four activities or research questions:

- 1) How, when, and where will pipes fail within the network?
- 2) How do we assess the condition of the pipe cost effectively?
- 3) How do we calculate pipe deterioration rates accurately with respect to the pipe environment?
- 4) How do we assess the time-dependent probability of failure along the pipeline?

This research focused on CI pipes, specifically on pipe materials and data from Australian utilities. The cast iron pipes in Australia are mostly cement-lined (some in-situ and some from factory); therefore, no significant effort was directed to examine the progression of internal corrosion. Nonetheless, internal corrosion could be incorporated in the failure analysis developed by approximating the internal corrosion to be uniform. Furthermore, the effects of temperature changes (e.g., freezing weather conditions) were not considered in since, under Australian conditions, such changes are less common.

Monash University led Activity 1, supervised by Professor Jayantha Kodikara, who was also the Principal Investigator of the overall project. Activity 2 was led by UTS (University Technology Sydney), led by Associate Professor Jaime Valls Miro and Professor Gamini Dissanayaka. Professor Rob Melchers at The University of Newcastle, with the support of Dr.

Robert Peterson, led Activity 3. UTS, University of Newcastle, and Monash University all participated in Activity 4.

FINDINGS

Activity 1: How, When, and Where Will Pipes Fail within the Network?

The research team defined the failure of a large-diameter pipe as a major burst leading to uncontrollable losses of water, requiring immediate attention. Failures were placed into two categories: failures in the pipe barrel and failures in the joint, with the emphasis on pipe barrel failures. The barrel failures were considered to occur mostly through longitudinal fracture, since typical circumferential failures or “broken backs” for large-diameter pipes are not common due to the pipe’s relatively high bending stiffness. The research primarily considered the deterministic aspects of stresses due to external and internal loads, original cast iron material properties, failure mechanisms, and failure state prediction.

Most large-diameter pipes lay under roadways, and the researchers examined the influence of traffic loads on pipe failure. It was found that traffic loading did not exert significant stress on the pipe even under simulated truck braking, cornering, and going over a speed bump. In contrast, 660 kPa (95.7 psi) of water pressure exerted seven times more strain on the pipe, highlighting the importance of internal water pressure in contrast to traffic loads. The instrumentation also provided validation of 3D finite element models for simulation of other traffic loading scenarios.

The research revealed that pressure transients might be responsible for many pipe failures. A monitoring program was initiated to study pressure and water pressure transient development in two utility networks. The team found that significant transient water pressures can develop due to operational changes, and these pressures can become magnified within the network. Due to low demand, nighttime water pressure can increase substantially, making pipe failures more likely.

The stress analysis of corroded cast iron pipes was advanced by considering corrosion in three main categories; namely, uniform corrosion, pit or patch corrosion, and corrosion clusters. Using 3D finite element modelling, a new stress analysis tool (the Monash Tool) was developed to analyze these corrosion configurations and to determine the remaining life of pipes.

Guided by numerical modelling and various forensic analyses of corrosion patches in failed and unfailed exhumed pipes, it was found that a substantially large corrosion patch with extensive corrosion (as much as 80% of wall thickness) is normally required to cause longitudinal failures in the pipe barrel. The first failure is most likely to occur as a fracture in the corroded patch, which may lead to water leakage. In many instances, this fracture may not be large enough to cause pipe burst in the first occurrence. Therefore, the concept of leak-before-burst (LBB) was developed for cast iron water pipes, where a generated fracture could grow with transient loadings and corrosion until fast fracture occurs. It was found that the first failure leading to leakage was controlled by a pipe material’s tensile strength, whereas the subsequent burst was controlled by a pipe material’s fracture toughness, highlighting the two main material properties that are given emphasis in cohorting of cast iron pipes based on their type and place of manufacture.

To further examine the LBB concept, a pipe burst facility was developed at Monash University. A series of pipes with natural and simulated corrosion patches were tested to examine the new concepts. The tests validated the theoretical findings and the LBB concept was confirmed.

Activity 2: How Do We Assess the Condition of the Pipe Cost Effectively?

Activity 2 sought to advance the understanding of the most widely used technologies employed for the condition assessment of critical cast iron pipes, to appreciate their strengths and weaknesses, and to investigate their benefits. The team sought to improve the interpretation of the signals acquired by condition assessment (CA) tools, utilizing modern machine learning algorithms to better capture pipeline wall geometries. The findings are generic to the underlying techniques studied: Magnetic Flux Leakage (MFL), Broadband Electromagnetics (BEM)—also known as pulsed eddy currents, Remote Field Eddy Currents, and in-pipe acoustic waveforms.

The UTS team also performed trials of emerging technologies, including additional external and in-pipe acoustic wave propagation methodologies, in-pipe ultrasonics, and the Magnetostriction technique.

The research team found that some techniques better represent point measurement of wall thickness, while others represent measures of average volume of material under the sensor antennae. A third class of techniques aims to capture average or extreme parameters from the pipeline (e.g., remaining wall thickness) over long distances. Some techniques have been shown to lack the necessary sensitivity to be able to detect pipe wall losses/defects in large metallic pipes. This applies most notably to acoustic-based techniques.

These results have allowed CA technology vendors to incorporate findings into their future strategies, and to participate more closely in shaping their interpretations and reporting for the benefit of the utility industry—as specified through utilities’ review of their CA contract specifications. A feedback loop to providers of CA tools appears critical to push utilities toward more targeted critical asset management and renewals.

Activity 3: How Do We Calculate Pipe Deterioration Rates Accurately with Respect to the Pipe Environment?

Previous efforts to predict the failure likelihood of cast iron pipe buried in soil have been limited by data and difficulties in interpretation. The research team worked from the premise that corrosion of cast iron in soils should follow the same basic ideas as those for corrosion of cast iron and other ferrous metals in other natural environments, such as fresh water, seawater, and tidal and atmospheric zones.

To facilitate the interpretation of data from actual operational pipes, more than 30 pipe exhumations were undertaken. In each case, the exhumed pipe was grit blasted to remove the graphitized layer, followed by laser scanning to characterize the corroded surface (Figure ES.1).

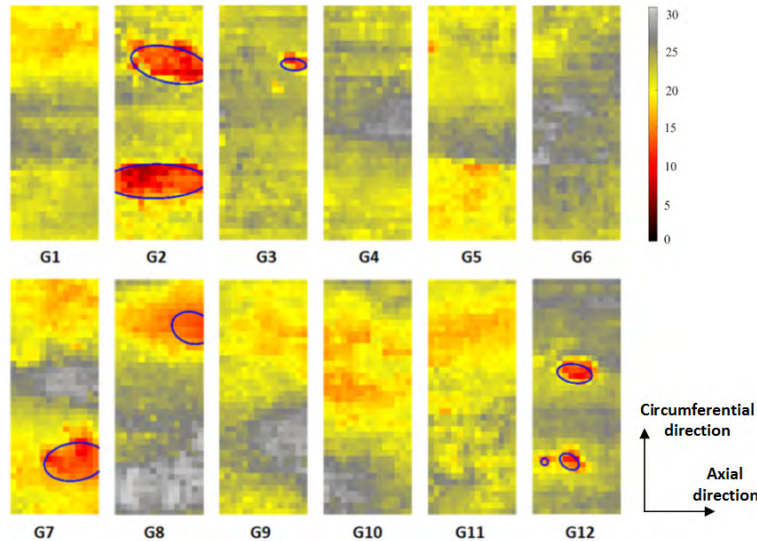


Figure ES.1. Data obtained from exhumed, grit-blasted, and laser-profiled sections

At each location, soil samples were taken of the undisturbed backfill adjacent to the pipe and analyzed for a range of properties.

Finally, closer examination of the patterns of corrosion and failure surfaces was conducted. It appears that perforation from the outside allows freshwater from inside the pipe to be forced out under pressure, which causes a different type of more general corrosion under the graphitized layer that then causes sufficient large area mass loss for pipe fracture to become possible. This explains the time between the first occurrence of a leak and the eventual bursting of a pipe under pressure.

The key findings of Activity 3 can be summarized as follows:

- Long-term cast iron corrosion in soils follows a non-linear bi-modal pattern with time and not the power law. This means that the corrosion rate is not a constant, but reaches an approximately constant rate after 10 to 15 years. Since most cast iron water pipes are over 50 years old, they can be considered to have reached this “steady” state.
- Water content and oxygen availability are critical parameters in the development of corrosion with time, but oxygen is less important for longer-term corrosion and pitting.
- Soils with higher moisture content tend to show elevated levels of corrosion.
- There appears to be no significant effect of chlorides and sulphates for corrosion losses even though these usually are considered important influences, with chlorides contributing to enhanced pit depth development.
- Soils with some nitrate content show higher levels of corrosion, attributed to microbiological influenced corrosion (MIC).
- A mechanism is now available to explain the time between the first occurrence of a leak and eventual pipe failure through bursting under internal pressure.

Activity 4: How Do We Assess the Time-Dependent Probability of Failure along the Pipeline?

This activity focused on prioritizing sections of a pipeline for replacement. The probability of failure calculation is an extension of the deterministic estimation of remaining life developed in Activities 1, 2, and 3, taking into account the uncertainties in input of loading, material properties,

and corrosion progression along the pipeline.

As part of this activity, the research team applied the Linear Polarisation Resistance (LPR) technique to water pipes buried in soils to reduce the uncertainties associated with its use. An extensive LPR survey of several sites showed that variations in soil properties over very short sampling distances may be significant contributors to uncertainty in LPR-based predictions. In practice, this issue is overcome by statistical analyses and by averaging many LPR samples. Whether this approach can be improved to produce more refined predictions remains an open question.

The research team also sought to establish a methodology for interpolating soil properties relevant to water pipe corrosion between sites where measurements could be obtained to predict current and likely future corrosion along the pipe, i.e., between measured points.

The researchers found that the following soil properties impact corrosion rates of buried cast iron mains: soil moisture; concentrations of nutrients, including nitrate, chlorine, sulphate, phosphate, and carbonate; and soil physical properties that impact soil water holding capacity and moisture transport.

A review of currently available technologies showed that of the above listed variables, only soil nitrates can be measured in situ; however, even for this property, commercially available equipment is insufficiently sensitive. Further work is required to assess the immediate and long-term viability of in-situ monitoring.

The team also developed a methodology for evaluating the lifetime probability of failure of cast iron (CI) pipes and predicting the pipe remaining life. The probability of failure is greatly affected by wall thickness, water pressure, and corrosion rate. Extra effort to determine the original wall thickness (or the class of the pipe) has definite advantages in failure prediction. The physical modelling results showed that the lifetime probability of failure follows a Weibull distribution, which was reasonably consistent with the observed failure data. Once the failure rate (or “decay”) curves are calibrated, other scenarios such as pressure management and cathodic protection could also be simulated to extend to the remaining lives of CI pipes. The Monash Tool can also be used to evaluate pipe failure probability.

APPLICATIONS/RECOMMENDATIONS

- The MFL technology provider currently does not provide the shapes of corrosion patches or thickness maps. This research has shown that the signals measured by MFL tools can be processed to capture this information. Furthermore, as MFL measurements are continuous, it may be possible to recover thickness maps with a higher resolution than currently feasible with other technologies. It is recommended that utilities using the tools developed by the ACAPFP project request the shapes of corrosion patches and thickness maps from the technology vendors.
- It is important to note that algorithms used by technology providers for interpreting information from their tools are continuously evolving. It is, therefore, recommended that utilities develop a regime for validating reports provided by all technology providers. UTS has developed a methodology for this purpose, which is explained in detail in the ground-truth generation document in Appendix Section 11.3.
- Variations in soil properties over short distances are likely to be significant contributors to uncertainty in corrosion rates predicted using the LPR technique. Consequently, corrosion rates specified at a specific location from the analysis of a single soil sample

should be treated with caution. In practice, this issue is overcome by statistical analysis and averaging of many LPR samples taken over the region of interest. This research clearly indicated the factors that are likely to improve the LPR to corrosion rate predictive model. To progress this work, it will be necessary to assemble a significant data base of soil, pipe, and corrosion data to allow for model development and validation.

- The highly uncorrelated nature of the soil properties observed at the Verona Street test bed and at the Perth sites suggests that a classical interpolation procedure is not appropriate for estimating soil properties and corrosion behavior along the pipe. Instead, a procedure has been proposed which enables the average soil property to be estimated for a given level of confidence within certain bounds.

The findings of this study are based on soil surveys conducted at a limited number of sites and will need to be verified at future locations because similar studies, albeit for shallower soils, indicate that the high level of variability observed in this work may not be universal. It is also important that the approach to estimating soil property averages outlined here be verified at a number of future sites.

MULTIMEDIA

A website for the ACAPFP Project at www.criticalpipes.com was published in December 2012.

Developed as part of Activity 1, the Monash Tool is posted on the #4326 project page of the WRF website under Web Tools.

RESEARCH PARTNERS

ACAPFP is a collaborative project funded by Sydney Water Corporation, Water Research Foundation, Melbourne Water, Water Corporation (WA), UK Water Industry Research Ltd (UKWIR), South Australia Water Corporation, South East Water, Hunter Water Corporation, City West Water, Queensland Utilities, and Yarra Valley Water. The research team is comprised of Monash University, University Technology Sydney (UTS), and the University of Newcastle of Australia.

RELATED WRF RESEARCH

- Condition Assessment of Large-Diameter Iron Pipe, project #4391
- Fracture Failure of Large Diameter Cast Iron Water Mains, project #4035
- Non-Destructive Condition Assessment for Small Diameter Cast and Ductile Iron Pipe, project #4230
- Potable Water Pipeline Defect Condition Rating, project #4498
- Selecting Techniques for the Rehabilitation of Small Diameter Cast Iron Pipes, project #4234

1 INTRODUCTION

1.1 BACKGROUND

The Advanced Condition Assessment and Pipe Failure Prediction (ACAPFP) Project was developed and funded by the Australian, US and UK water industries to undertake fundamental research aimed at solving an intractable problem – the failure of ageing, large diameter (i.e., >300 mm) main (“critical”) water pipes.

Maintenance of ageing water pipe infrastructure is a major challenge for the world’s water industry and can be very costly. Estimates of the total replacement cost of pipe networks in Australia exceed AU\$100 billion (Nicholas and Moore 2009). Over the five years from 2009, the costs of urgently needed asset replacement were estimated at around AU\$5 billion. Estimates of maintenance costs over the same period were some AU\$2.5 billion (WSAA 2009, Nicholas and Moore 2009).

Cast iron pipes remain a substantial component of buried pipe cohorts of water utilities, and many are over one hundred years old. Although these pipes were significantly overdesigned at the time of installation, pipes have variably deteriorated over time, due to corrosion, and pipe failures have become common. The non-homogeneous nature of this material presents challenges when compared to materials used in other industries. Also, the cement lining of cast iron water pipes presents challenges for condition assessment (CA) technologies in assessing the extent of corrosion, which are critical for failure. While utility managers are interested in determining the optimal replacement schedule for these critical mains, current methodologies are primarily based on technologies and prediction tools applied in the oil and gas industries, where mostly steel pipelines are used. In general, critical water pipe networks operate at considerably lower pressures and are predominantly made from cast iron.

In July 2011 seven Australian water utilities joined two UK and US water industry research organisations and three Australian universities to conclude a Collaborative Research Agreement (CRA) and form the ACAPFP Project.

The CRA provided for cash and in-kind funding of AU\$13 million over five years for Round 1 to cover Activities 1, 2 and 3. As well as its cash and in-kind contributions to the Project, Sydney Water made available for testing purposes a 1.2km long 600 mm diameter cement-lined cast iron water pipeline in Strathfield. Research on Round 1 began in the second half of 2011. In 2013 Sydney Water took the initiative to fund Round 2, covering Activities 4 and 5, by providing a cash contribution of approximately AU\$1.7 million. The three universities supplied additional support funding for project management to bring the total additional funding to approximately AU\$1.9 million. In February 2014 the partners concluded a variation to the Collaborative Research Agreement for this Round 2 funding and research on additional activities began soon thereafter.

The inclusion of two more Australian utilities in 2015 and 2016 secured additional contributions to fund research.

A website for the ACAPFP Project at www.criticalpipes.com was published in December 2012.

The ACAPFP Project lasted from 2011 to 2017.

1.2 PROJECT PARTNERS

The original partners in the ACAPFP Project were Sydney Water Corporation, UK Water Industry Research Ltd., Water Research Foundation of the USA, Water Corporation (WA), City West Water, Melbourne Water, South Australia Water Corporation, South East Water Ltd, and Hunter Water Corporation. Water Environment Research Foundation of the USA was an affiliate partner. Monash University led the research supported by University of Technology Sydney and the University of Newcastle. Other collaborators included Dr Balvant Rajani of Canada, private consultant and former researcher of the National Research Council of Canada. Queensland Urban Utilities joined the Project in 2015 and Yarra Valley Water in 2016.

1.3 PROJECT SCOPE

According to the Project Outline in Schedule D of the CRA, the following Activities and Deliverables were to make up Round 1 of the Advanced Condition Assessment and Pipe Failure Prediction Project. The pipes to be considered as part of the Activities include cast iron and steel pipes. It should be also noted that emphasis was placed on pipe materials and data from Australian utilities. The cast iron pipes in Australia are mostly cement lined (some in situ and some from factory) and hence no significant effort was directed to examine the progression of internal corrosion. None the less, internal corrosion could be incorporated in the failure analysis developed, by approximating the internal corrosion to be uniform. Furthermore, the effects of temperature changes (e.g., freezing weather conditions etc) were not considered in this study since under Australian conditions, they were found to be less important.

1.3.1 Round 1

1.3.1.1 Activity 1 – How, When, and Where Will Pipes Fail within the Entire Network?

The aim of this activity is to establish improved methodologies to predict remaining physical life of critical pipes taking into account the effect of external/internal factors, different material types and critical locations and factors within the network. This activity will draw from Activity 2 and 3 to establish failure state and to determine the physical remaining life of pipes.

This activity has mainly two sub-activities:

- 1a - Measurement and calculation of internal/external loads and pipe response,
- 1b - Failure mechanisms and failure states

This activity was led by Professor Jayantha Kodikara of Monash University.

1.3.1.2 Activity 2 – How Do We Assess the Condition of the Pipe Cost Effectively?

Assessment of pipe condition is central to pipe failure prediction and management. Water utilities lack confidence in current commercial techniques available for condition assessment. This project will advance the knowledge in the areas of development of direct and indirect methods for condition assessment using advanced sensor package development and associated data fusion techniques successfully used in the field of automation.

This activity had two sub-activities:

- 2a - Indirect condition assessment methods
- 2b - Direct condition assessment methods

This activity was jointly led by Professor Gamini Dissanayake and Associate Professor Jaime Valls Miro of University of Technology Sydney.

1.3.1.3 Activity 3 – How Do We Calculate Pipe Deterioration Rates Accurately with Respect to the Pipe Environment?

One of the foremost requirements of pipe failure prediction is the accurate estimation of pipe deterioration rates. Most ferrous pipes deteriorate due to various forms of corrosion and asbestos cement pipes degrade due to cement leaching. The methods currently available for estimation of pipeline deterioration are purely empirical, of insufficient accuracy, and limited in application. The present project will develop calibrated theoretical models to predict significant deterioration in the structural strength of buried pipelines on the basis of established scientific principles.

Professor Robert Melchers, The University of Newcastle, NSW, led this Activity.

1.3.2 Deliverables

1.3.2.1 Activity 1

- (a) Compilation of available data and critique on external factors and stresses on pipes.
- (b) Compilation of available data and synthesis of failure mechanisms of cast iron and steel pipes.
- (c) Measured data on pipe stresses including pressure transients and traffic loading on selected pipe networks.
- (d) Identification of key stress drivers for pipe networks.
- (e) Validated and improved methods for computation of stresses on buried pipes due to external and internal factors taking into account their intensity and time spectra.
- (f) Establishment of failure mechanisms for buried pipes on the basis of forensic studies during the project and in the past. Identification of key failure mechanisms.
- (g) Validated methods to predict the pipe failure and physical remaining life of pipes, and identification of where, when and how pipes are most likely to fail.
- (h) Preliminary proof of concept for monitoring of new pipes using optical fibre technology subject to fund availability.

1.3.2.2 Activity 2

- (i) Establishment of a comprehensive test bed for assessing and developing condition assessment technologies.
- (j) Development of experimentally validated MFL and BEM interpretative numerical models for simulating sensor behaviour under different operating modes, and enhance current/future partner's sensors accordingly.
- (k) Provision of mathematical models and software modules for generating pipe maps based on MFL and BEM technology.

1.3.2.3 Activity 3

- (l) Identification of main critical parameters that affect corrosion in the longer term.
- (m) Calibrated Mathematical model for long-term prediction of steel and cast iron pipeline corrosion as a function of the main environmental and other parameters.

According to the Project Outline – Extension in Annexure 3 of the Deed of Variation of February 2014 to the Collaborative Research Agreement, the following Activities and Deliverables were to make up Round 2 of the Advanced Condition Assessment and Pipe Failure Prediction Project.

1.3.3 Round 2

1.3.3.1 Activity 4 – Improving Confidence in Critical Pipe Failure Prediction

The aim of this activity is to improve current capacities to predict likelihood of pipe failure for a given length of pipe. It has five sub-activities to be carried out by the three universities as shown here.

- Sub-activity 4a - Enhancing the reliability of condition assessment of buried large diameter water mains. (UTS)
- Sub-activity 4b - Reducing the uncertainty in the use of non-destructive, indirect measurement with LPR. (University of Newcastle and UTS)
- Sub-activity 4c - Predicting the likelihood of pipe corrosion and its severity along the pipe to forecast failure. (University of Newcastle)
- Sub-activity 4d - Enhancing the reliability of emerging technologies that have not yet been incorporated into the current research project (UTS)
- Sub-activity 4e - The probability of failure (Monash University)

1.3.4 Deliverables

1.3.4.1 Sub-Activity 4a

Enhanced reliability of condition assessment of buried large diameter water mains

1.3.4.2 Sub-Activity 4b

Reduced uncertainty in the use of non-destructive, indirect measurement with LPR

1.3.4.3 Sub-Activity 4c

Enhanced ability to predict the likelihood of pipe corrosion and its severity along the pipe to forecast failure

1.3.4.4 Sub-Activity 4d

Enhanced reliability of emerging technologies that have not yet been incorporated into the current research project.

This Final Technical Report contains the results of the research conducted from 2011 to 2017 at Monash University, UTS and the University of Newcastle. It reports the findings from Activities 1, 2, 3, 4a, 4b, 4c, 4d and 4e of the Project.

PART 1
ACTIVITIES 1 AND 4E - HOW, WHEN, AND WHERE WILL PIPES FAIL
WITHIN THE ENTIRE NETWORK AND HOW CAN PROBABILITY OF
FAILURE BE ESTIMATED?

Project Team (Monash University):

Professor Jayantha Kodikara (Lead)
Professor Xiao-Ling Zhao
Professor Wing Kong Chiu
Dr. Asadul Haque
Dr. Chunshun Zhang
Dr. Jian Ji
Dr. Derek Chan
Dr. Suranji Rathnayaka (ex PhD student)
Dr. Benjamin Shannon
Dr. Leslie Wong (ex PhD student)
Rui Jiang (current PhD student)
Dr. Rajeev Pathnamanathan (formerly Monash University)
Dr. Dilan Robert (formerly Monash University)

2 ACTIVITY 1 AND 4E SUMMARY

This report covers the main summaries of Activity 1 and 4e in the Advanced Condition Assessment and Pipe Failure Prediction (ACAPFP) Project, which are listed in the sections below. The ACAPFP project focussed mainly on barrel failures of buried large diameter (>300 mm) cast iron (CI) water pipes.

2.1 HISTORICAL INFORMATION ON LARGE-DIAMETER PIPE FAILURE

This historical information was gathered at the beginning of the project and would reflect primarily Australian water utility conditions.

The findings on pipe failure analysis are as follows:

- Longitudinal splitting is one of the most frequent failure modes observed in water utilities for critical water pipes. Failure due to spiral fracture or circumferential fracture is observed less often than other failure modes. Through-wall pit wall corrosion was observed in many pipes after grit blasting, but through-wall pits may not lead to major bursts or fractures. In many cases, these pits were plugged by graphitised material.
- A larger number of failures was observed in uncoated pipes. This was evident for all utilities.
- Based on the data, corrosion is the main cause of failure in the pipe barrel. However, significant contributions from other factors such as pressure transients were also evident.
- There were significant numbers of failures at the road verge (i.e., edge of the road).

More details can be found in the following publications: Rajeev et al. 2013b and Rajeev et al. 2014. These preliminary findings provided initial background and were then examined and analysed in the light of the research undertaken in the project as described in the following sections.

2.2 PIPE TRAFFIC LOADING TESTS IN SYDNEY WATER TEST BED

Based on the field test results:

- Changes in pipe strains from trucks passing at different speeds and braking tests are similar, with differences less than 20 microstrain (CI failure strain is around 4000 microstrain)
- Changes in pipe hoop strains due to internal water pressure (50 m head) showed that under normal operational pressure, pipe strain is within the elastic region with the maximum strain of 126 microstrain. On this basis, internal water pressure exerts over six times the strain than that due to traffic loads under the conditions studied.
- Truck test results showed small differences in hoop strains measured by different tests (i.e., passing, braking, standing)
- Pressure differences between braking and other tests are less significant at the depth of 860 mm tested (less than 5 kPa)

- As recommended in some design guides, the use of a uniform vertical pressure of about 25 kPa across the pipe crown level due to traffic load is conservative, since vertical pressure drops away from the pipe crown laterally.
- The instrumentation undertaken at the nature strip indicated that, although the pipe barrel can experience stresses due to seasonal moisture changes in clayey soil, most of the loads are transferred to joints in larger diameter pipes due to higher moments of inertia. Therefore, for larger diameter pipes buried in shrinking/swelling soils, joints can be damaged although the pipe barrel may not bend. The same reasoning is applicable to general ground movement due to other reasons for large diameter pipes.

More details can be found in the following publications: Robert et al. 2016b, Wong et al. 2017b, Ji et al. 2015b, Vitanage et al. 2013, Rajeev et al. 2013b, Vitanage et al. 2014.

2.3 PRESSURE-TRANSIENT MONITORING AND MODELLING

The following conclusions were drawn from the pressure transient monitoring and modelling studies:

- Severe pressure transients from multiple start- ups, shut-downs or automated controls are a major concern for pipe bursting.
- Direct evidence was obtained that repetition of pressure cycles can lead to bursting, even if bursting may not occur at the first instance of pressure cycling.
- Generated pressure transients dissipate rapidly with distance from the site of the transient origin.
- Reasonable agreement between measured transient pressure values and those of models was found.
- Main sites found to be vulnerable for high pressure transients are: downstream of main and booster pump stations, upstream and downstream of automated control valves, and reticulation networks that are in close proximity to pump stations and control valves.

More details can be found in the following publications: Rathnayaka et al. 2016a; Rathnayaka et al. 2016b; Chan, forthcoming; Chan 2016; Chan 2014.

2.4 CAST-IRON PIPE COHORT PROPERTIES

The pipe cohort physical parameters that contribute most to the failure mechanism have been reviewed. By doing so, the large uncertainty of physical properties was narrowed, which will help in the investigation of past failure events and making future failure predictions. Furthermore, for a certain utility, the gaps in knowledge in terms of relevant material properties can be identified, and where to direct efforts in data collection can be identified. Some key findings were as follows:

- In cohorting CI water mains, the pipe diameter, wall thickness, cement lining condition, pipe coating, and material tensile strength (depending on manufacturing process and location) are keys to distinguishing the cohort. Another key material property, fracture toughness, may not show wide variations within cohorts.

- The tensile strength required to pass pipes in the factory before placement in the field was found to be greater than some of the measured samples of exhumed pipes.
- Manufacturing flaws in the tested samples significantly reduced the material strength.
- Yennora spun cast had the greatest strengths (tensile, compressive and bending) and fracture toughness.

More details can be found in the following publication: Jiang et al. 2016

2.5 LARGE-DIAMETER PIPE BURST TESTS

Based on the lessons learned from CI pipe burst testing, the following suggestions are made:

- For large-diameter CI pipes, a large corrosion patch with significantly deep corrosion (over 80%) is required to cause failure at operational pressures. The first failure was observed as a fracture at the base of the patch that eventually led to water leakage. Major longitudinal fractures occurred at higher pressures when cracks grew to a critical length. However, there could be exceptions, if the patch size is excessively large where a critical crack length causing a burst could develop in the first instance.
- Many of the large-diameter pipe test samples tested had natural corrosion and relatively small pits of variable sizes and depth, some almost through-wall. None of these led to failure, even at pressures of 3000 kPa (or 300 m head).
- These observations with numerical and field evidence gave rise to the “Leak-Before-Break” (LBB) concept as a common mechanism for failure of CI pipes.
- The most important parameters for the prediction of pipe failure are tensile strength (for initiation of fracture) and fracture toughness (for burst).
- On this basis, it is suggested that condition assessment for large-diameter pipes should focus on identifying large and deep corrosion patches rather than smaller pits. However, smaller pits at the base of a large patch could increase the chance of failure. Therefore, the resolution of the condition assessment technique needs to be considered.
- Leaks may be monitored to detect pipes that are close to failure, thereby possibly preventing future failures.

More details can be found in the following publications: Rathnayaka et al. 2016c, Zhang et al. 2017a, Shannon et al. 2016a, Chan 2014.

2.6 FATIGUE MECHANISMS IN CAST IRON WATER MAINS

Crucial findings to date from this ongoing study are as follows:

- Internal cyclic pressures are the predominant stress for fatigue damage in aged CI pipelines.
- In order for fatigue to be prominent for crack initiation in CI pipe barrels, stresses in excess of about 50% of the tensile strength may be needed.
- A through-wall crack is able to propagate under cyclic pressures.

- Fatigue damage is severe when the maximum pipe stress is over 90% of the material tensile strength. This category of fatigue falls into “low-cycle fatigue,” where the number of cycles needed may be less than 10,000 and in many cases hundreds or less. This can be converted to days, if the rate of cycling is available within a network section.
- Leak rates in pressurised CI pipes can be estimated, if the crack length and operating pressure are known. In other words, if leak rates can be measured, it is possible to detect the crack length and, therefore, the remaining life before a burst. However, more targeted research is needed in this area.
- The LBB window period in practice is between the occurrence of detectable leakage and the final burst event, and this period depends mainly on operating pressures, corrosion patch configurations and leak detection methods. In this context, there is merit in advancing leak detection methods to improve condition assessment.
- CI pipelines that experience transient pressures or frequent adjacent burst/refill events may be more likely to be influenced by fatigue damage.
- In order to reduce fatigue damage, operational transients should be reduced or dissipated, and large pressure changes need to be controlled. Theoretical models can be developed to assist these decisions.

More details can be found in the following publications: Zhang et al. 2017b, Shannon et al. 2016c.

2.7 FINITE ELEMENT MODELLING OF PRESSURISED CORRODED CAST IRON PIPES

- Three-dimensional finite element analysis of a large number of CI pipe models was used to develop stress prediction models that are expressed in closed-form equations. These equations are embedded in the Monash Tool developed for pipe failure prediction.
- The Monash Tool provides guidance on the conduct of longitudinal failure analysis of pipe barrels with uniform corrosion or remaining wall corrosion defects that are idealised into ellipsoids. A methodology to analyse a cluster of pits or patches has also been developed. Attention needs to be given to the resolution of condition assessment techniques in determining patch size and depth.
- The Monash Tool provides a deterministic approach to assess: 1) nominal (hoop) tensile stress, 2) stress concentration factor (SCF) and maximum tensile stress for fracture initiation, 3) critical crack length for pipe burst, and 4) remaining life to initiation of local failure leading to a leak.
- Another set of numerical analyses focussed on the study of the non-linearity of corroded CI pipes, and a relatively simple hyperbolic constitutive model, as opposed to the complex elastoplastic models in the research literature, has been developed and implemented in finite element analysis. However, the Monash Tool is designed using linear elastic analysis but indirectly considering non-linear effects.
- With appropriate scanning data on a naturally corroded CI pipe, the proposed numerical method with the hyperbolic model can be readily used for structural and mechanical analysis of pipes under various loading conditions.

More details can be found in the following publications: Ji et al. 2015a, Wong et al. 2016b, Wong et al. 2017a, Rathnayaka et al. 2016e, Shannon et al. 2016a.

2.8 PHYSICAL MODELLING FOR PREDICTION OF FAILURE PROBABILITY

The quantification of the lifetime probability of corroded CI pipes was introduced in this section. It was found that:

- The probability of failure is greatly affected by the wall thickness, water pressure and corrosion rate. Therefore, these parameters need most attention for pipe barrel failure. Therefore, extra effort to determine the original wall thickness (or the class of the pipe) has definite advantages in failure prediction.
- The physical modelling results showed that the lifetime probability of failure follows a Weibull distribution, which was reasonably consistent with the observed failure data.
- Once the failure rate (or “decay”) curves are calibrated, other scenarios such as pressure management and cathodic protection could also be simulated to extend to the remaining lives of CI pipes.
- Monash Tool can also be used to evaluate pipe failure probability.

More details can be found in the following publications: Ji et al. 2015a, Ji et al. 2016, Wong et al. 2014.

2.9 DISTRIBUTED OPTICAL FIBRE SENSORS

- The concept of smart pipes for new pipes where fibre optic sensors are deployed to provide information on pipe condition continually was introduced with some proof-of-concept testing.
- Validation: The strain measured by distributed optical fibre sensors corresponded to the fatigue loading profile accurately, whilst also providing real-time structural health monitoring capabilities. The durability and dynamic strain response along the length of the test specimen was evident from testing.
- Transient monitoring. The distributed strain responses due to pressure transients were monitored accurately using distributed optical fibre sensors. However, more robust sensing arrangements are necessary for buried pipe line deployments. A concerted research project is needed in this area.
- Detection of anomalies. The presence of localised damage along the pipe and the features of localised damage are accentuated during pressure transient events recorded by the fibres. This provides evidence that a suitable fibre optic sensor can detect local damage in buried CI pipelines.

More details can be found in the following publications: Rajeev et al. 2013a, Lim et al. 2016, Wong et al. 2016a, Rathnayaka et al. 2016d, Zhang et al. 2017b, Rathnayaka et al. 2013, Shannon et al. 2016c.

2.10 FUTURE RESEARCH DIRECTIONS

The main findings of the Advanced Condition Assessment and Pipe Failure Prediction Project Activities 1 and 4e run by Monash University are provided in this document. Some areas are identified as needing further research as follows:

1. Further research is needed on the “Leak-Before-Break” concept using the newly developed Transient Pressure Testing Facility at Monash, and on the development of the LBB Time Window calculation for burst time prediction. It should be noted that to date, all the testing was performed on test bed pipe, which is a vertically pit-cast CI pipe with a nominal wall thickness of about 25 mm. Therefore, additional testing to include different materials, transient pressure configurations and associated material testing of fracture growth will be beneficial. In addition, the capture of water leak acoustic signatures while a pipe segment is buried in soil would be beneficial to relate the leak signatures to the likely crack lengths. Once developed, the LBB methodology will have potential to be applied for prevention of pipeline failures.
2. Building on current research findings, advanced fibre optic sensing can be further developed as a comprehensive condition assessment method for buried water pipes that measures transient pressure signatures and acoustic signals along the pipeline at intervals of around 1 m. Future research could develop theoretical procedures to analyse the results and determine the pipe condition, remaining life and time window for a burst (LBB Time Window), if a leak is already present. A new fibre-optic based sensor is being researched for deploying in existing buried pipelines for condition assessment and leak detection.
3. The current ACAPFP project has developed failure mechanisms and failure prediction methodologies for CI pipe barrels for large-diameter pipes. However, the case studies indicate that pipe joints can fail without much corrosion and failures are attributed to ground movement predominantly, while other factors such as water pressure and traffic load have some influence. In colder climates, the temperature differential can also add to the joint stress. Based on the current work, research can be undertaken to develop a failure prediction methodology for large-diameter pipe joints. The current Monash Tool can then be extended to also consider joint failure mode.
4. The current ACAPFP project undertook research mainly into CI pipes. Other metallic pipes were considered to some extent and it was found that in the respective material’s pipe barrel, failure was mainly through extensive corrosion and leakage. Research can be undertaken to develop failure prediction methodologies for other pipe materials, such as steel, ductile iron, plastics and HDPE.
5. On the basis of the research undertaken, it is possible to examine and develop effective pipe rehabilitation technologies in situations where extension of pipe life is preferred in contrast to replacement.

3 ACTIVITY 1 AND 4E REPORT

3.1 SUMMARY

The advanced condition assessment and failure prediction project (the critical pipe project) final key findings and Activities 1 and 4 are presented in this report, which covers the following aspects of large diameter cast iron (CI) water main pipes: historical information, pipe traffic loading tests, pressure transient modelling, cohort properties, pipe burst tests, fatigue mechanisms, finite element modelling, physical modelling for prediction of failure probability, and distributed optical fibre sensors. A summary of the main findings of each section is given below.

Historical information on large diameter failure on past data: Most pipe failures were observed in cast iron or steel pipes for all the water utilities studied with pieces blown out and pin hole or perforation failure observed as major failure modes in CI and steel pipes. Longitudinal splitting is a common failure mode and spiral or circumferential fractures are less common than other failure modes. A larger number of failures was observed in uncoated pipes. Corrosion is considered to be the main cause of failure for pipe barrel, with significant contributions from pressure transients, traffic load and material flaws. The average life-time of pipe material varies significantly, depending on the location and corrosion rate variables. This preliminary information formed the background for research in Activity 1, the outcomes of which are summarised below.

Pipe traffic loading tests: In pipe traffic loading tests, traffic loading had a small influence on changes in pipe hoop strain on the large diameter pipe. Higher pipe strain (well below typical failure strain) was recorded from internal pressure rather than traffic loading. In terms of pipe strain, the importance of internal water pressure was 6–7 times greater than traffic loading.

Pressure-transient monitoring and modelling: Severe pressure transients from multiple start-ups, shut-downs or automated controls are a major concern for pipe bursting. Routine pressure transients do not provide an immediate risk of pipe failure, but could cause damage that could accumulate leading to failure. Pressure transients dissipate rapidly with distance from the site of pressure transient generation. Reasonable accuracy between monitoring sites and numerical models was found. The main sites found to be vulnerable for high pressure transients are downstream of main and booster pump stations, upstream and downstream of automated control valves, and reticulation networks that are in close proximity to pump stations and control valves.

Cast iron cohort properties: In CI water mains, the pipe diameter, wall thickness, cement lining condition, pipe coating, and material tensile strength are keys factors that distinguish the cohort. The factory tensile strength required to pass pipes before field placement was found to be greater than some of the measured samples of exhumed pipes. Manufacturing flaws in the tested samples significantly reduced the material strength, when present in significant proportions.

Large diameter pipe burst tests: Large-diameter pipe burst test facility sample testing found that a large corrosion patch with significantly deep corrosion, the presence of a leak, and sufficiently high internal water pressures were required before longitudinal splitting occurs. The leak-before-break (LBB) method and condition assessment for large diameter pipes should focus upon locating large corrosion patches running along the pipe with low remaining wall thickness (>80% corrosion depth) are introduced. Leaks should be monitored for examination of remaining pipe life.

Fatigue mechanisms in cast iron water mains: The internal cyclic pressures are the predominant cause of stress for fatigue damage in aged CI pipelines. A through-wall crack can propagate in a corrosion patch of a CI pipe barrel by cyclic pressures. The fatigue damage is severe

when the maximum pipe stress is over 90% of material tensile strength, and may be ignored if the maximum stress is less than 50% of material tensile strength in CI pipe barrels. CI pipelines that experience transient pressures or frequent burst/refill events are more likely to be influenced by fatigue damage. The LBB window period in practice is between the occurrence of detectable leakage and the final burst event, and this period is mainly dependent on operating pressures and transient frequency, corrosion patch configurations and leak detection methods. In order to reduce the fatigue damage, operational transients should be reduced, and dramatic pressure changes need to be controlled.

Finite element modelling of pressurised corroded cast iron pipes: A stress prediction model, expressed in a closed-form equation and implemented in Monash Tool (MT), is proposed on the basis of numerical analyses of a large number of CI pipes. MT provides guidance to conduct longitudinal failure analysis of pipe barrels with uniform corrosion or single remaining wall corrosion defects that are idealised into ellipsoids. The MT provides a deterministic approach to assess 1) nominal (hoop) tensile stress, 2) stress concentration factor (SCF) and maximum tensile stress for fracture initiation, 3) critical crack length for pipe burst, and 4) remaining life to initiation of local failure leading to a leak. In addition, the probability calculation of the pipe failure prediction and remaining life is incorporated along with the production of hazard curves.

A simple hyperbolic constitutive model was implemented in finite element analysis to study the non-linearity of corroded CI pipes. The hyperbolic model allows much simpler and quicker numerical analysis with reasonably good accuracy, compared with the existing elastoplastic models. With appropriate scanning data of a naturally corroded CI pipe, the proposed numerical method with the hyperbolic model can be readily used for structural and mechanical analysis of a pipe under various loading conditions.

Physical modelling for prediction of failure probability: The probability of failure is greatly affected by the wall thickness, water pressure and corrosion rate. The physical modelling results showed that the lifetime probability of failure follows a Weibull distribution, and they agreed reasonably well with the observed failure data. Once the failure rate curves are calibrated, scenarios such as pressure management and cathodic protection can also be simulated to extend the remaining lives of CI pipes.

Distributed optical fibre sensors: Strains measured by distributed optical fibre sensors corresponding to the fatigue loading profile and pressure transients are accurate, whilst also providing real-time structural health monitoring capabilities. The durability and dynamic strain response along the length of the test specimen was evident from testing. The presence of localised damage along the pipe is accentuated during pressure transient events recorded by the fibres. The orientation and distance of the distributed optical fibres is crucial for strain measurement, as a distance up to 40 mm from the fatigue crack point tip can be detected by the fibre.

3.2 INTRODUCTION

This report covers the main findings of Activity 1 in the Critical Pipes Project.

The aim was to establish improved methodologies to predict the remaining physical life of critical pipes, taking into account the effect of external and internal factors, different material types, and critical locations and factors within the network. This activity draws information from Activities 2 and 3 to establish the failure state and to determine the remaining life of pipes.

The intended outcomes of Activity 1 were to:

- 1) Improve methods for estimation of pipe remaining life considering the information available, including condition assessment data;

- 2) Develop practical concepts for monitoring of new pipelines using optical fibres and other sensors.

The final work included in this report includes the following:

- Pipe historical failure analysis
- Test bed pipe truck tests
- Pressure transient network modelling
- Large-diameter pipe burst tests
- Cast iron pipe cohort properties
- Pipe fatigue testing
- Finite element modelling of pressurised cast iron pipes
- Probability modelling
- Fibre optic pipe measurement

3.3 HISTORICAL INFORMATION ON LARGE-DIAMETER PIPE FAILURE

3.3.1 Introduction

The water industry operates a supply and distribution network consisting of ageing, predominantly cast iron (CI) and steel mains. Failures of large diameter pipes can be highly disruptive to both the water industry and to the public. They can have major consequences in terms of economic loss to water utilities, public safety, and damage to property, and can adversely affect the overall performance of the assets. The structural failure of large-diameter water mains is due to a combination of factors, but is mainly due to deterioration by corrosion when the pipe is subjected to internal and external loadings. Therefore, the quantification of the relative contributions of each factor (i.e., physical issues and corrosion) is often a complex process and not yet completely resolved. The factors contributing to pipe failure can be summarised as follows: (a) pipe structural properties, material type, pipe-soil interaction, and quality of installation, (b) internal loads due to operational and transient pressures and external loads due to soil overburden, traffic loads, frost loads and third-party interference, and (c) material deterioration due largely to external and internal chemical factors, including the bio-chemical, microbiological and electro-chemical environment leading to corrosion.

Existing physical and statistical models for the prediction of failures in individual water mains address only one or a few factors. Neglecting to account for important factors can lead to inaccurate conclusions, resulting in sub-optimal failure prediction and renewal strategies. The statistical analysis of past pipe failure data in large-diameter mains is an effective way to study the pipe failure mechanism and causes of failure and deterioration. Statistical analysis uses historical data on past failures to identify the possible factors leading to pipe failure. However, failure data on large diameter pipes are limited.

The objectives of this project section were as follows:

- Collect and critically assess pipe failure data provided by industry partners and identify factors that control failure in large-diameter (i.e., pipe diameter ≥ 300 mm) pipes);
- Collect failure inspection reports and photographs to obtain the corrosion pit geometries and their influence on failure mechanisms;

- Estimate the average corrosion rates of failed pipes at various ages using the failure database and failure inspection reports collected by industry partners;
- Estimate the contribution of corrosion rate and other factors to the failure of large pipes;
- Categorise corrosion patterns for structural analysis;
- Identify knowledge gaps that need to be filled to further focus the experimental program; and
- Collect and review condition assessment reports to identify their limitations and ways of using these data in pipe failure prediction.

The section focused on collecting the pipe failure data, failure inspection reports and condition assessment reports from 8 water utilities to identify important factors controlling failure.

3.3.2 Methodology

An extensive review of the literature both in the public domain and partner organisations relevant to large-diameter pipes summarised (a) failures to establish the possible external/internal factors causing failure and the failure modes, (b) condition assessment, (c) corrosion modelling, and (d) condition monitoring techniques. A detailed review of past pipe failure data from partner organisations was used to establish a consistent dataset. Statistical analysis of past pipe failure data was used to determine the critical factors leading to failure of pipes. Failure inspection reports obtained from partner organisations were used to establish the corrosion pit depth and shape geometry. A relationship was developed between the average corrosion rate, the lifetime of pipes and the failure mode.

3.3.3 Findings

The findings of the recorded pipe failure data analysis are as follows:

- Most failures were reported in cast iron (CI) or steel pipes for all the water utilities. The number of failures is lower in ductile iron pipes for all the water utilities.
- Pieces blown out and pin-hole or perforation failures are major failure modes in CI and steel pipes for all the water utilities.
- Longitudinal splitting is one of the common failures observed in most of the water utilities. Failures due to spiral or circumferential fractures are less frequent than other failure modes.
- A larger number of failures was observed in uncoated pipes. This was evident for all utilities.
- Based on the data, corrosion is the main cause of failure. However, significant contributions from other factors, such as pressure transients and traffic loads, are also evident.
- Most failures occur in the road or verge (i.e., edge of the road).
- The average life-time of pipe material varies significantly depending on the location. This may be due to the changes in corrosion rate that depend on the soil chemistry and soil moisture variations, etc.

More details can be found in the following publications: Vitanage et al. 2013 and Rajeev et al. 2013b. These preliminary findings provided initial background and were then examined and analysed in the light of the research undertaken in the project as described in the following sections.

3.4 PIPE TRAFFIC LOADING TESTS

3.4.1 Introduction

The performance of buried pipes is affected by both physical and environmental factors, such as water pressure, traffic, climate, soil, and pipe deterioration (Chan, 2014, Rajani and Kleiner, 2010). These internal and external factors determine the failure mode and how close the pipe is to failure. Determination of the pipe failure mechanisms and the influence of different factors on buried pipes can be undertaken by monitoring the working environment, the corresponding response of the buried pipe, and measurement of the soil properties in the vicinity.

Since the majority of large-diameter pipes are buried under major roads, the influence of traffic loads on the pipe behaviour has been a concern. Some failure data and anecdotal evidence from water utility personnel have highlighted the varying influences of traffic loads on pipe failure. In addition, anecdotal evidence gathered as part of this study suggests that it is possible for pipes to be adversely affected due to dynamic loading of trucks when they brake at traffic lights, turn at bends, or go over speed humps. Therefore, a field study was undertaken by instrumenting a large diameter CI water pipe buried across a road in Strathfield, Sydney, which is known as the Sydney Water test bed. This work was intended to study the effect of external and internal factors on the buried pipeline.

3.4.2 Instrumentation of Sydney Water Test Bed

The Sydney Water test bed pipe is a decommissioned 600 mm diameter CI pipe buried in natural clay. The average pipe wall thickness is 25 to 30 mm with a relatively uniform thickness all around without significant corrosion. Soil resistivity at the pipe depth is fairly to highly corrosive. Figure 3.1 shows the layout of the site on the road cross-section and the instrumentation locations. The instrumentation was undertaken on two sections along the pipeline: (1) the main section buried under the road and (2) a small section buried under the nature strip. Pipe strain, ground pressure, joint displacement, and soil moisture were measured on site.

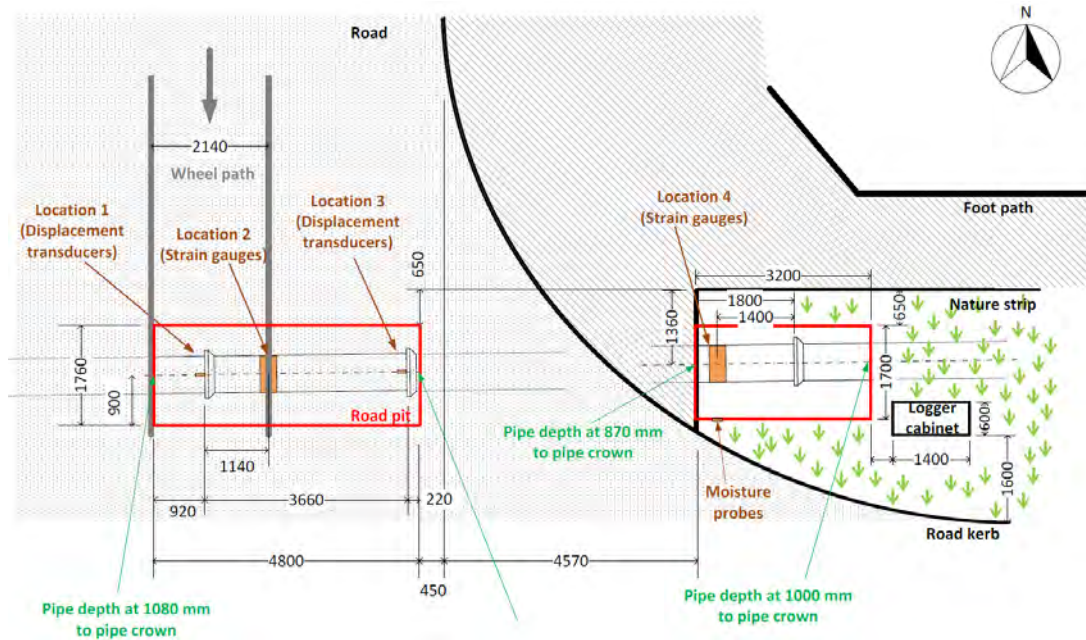


Figure 3.1. Layout of Sydney Water test bed

3.4.3 Important Results and Discussion

3.4.3.1 Traffic Trigger Events

Field data were measured from traffic events since instrumentation in March to May 2013 with the fast data logging triggered by heavy vehicles. It was found that approximately 82% of the triggered events were due to the local bus services, which generated approximately 30 events a day. Therefore, the daily operation of buses can create cyclic traffic loading on buried pipes in suburban areas.

The maximum pressure due to traffic events was measured at 100 mm above the pipe crown. The maximum measured pressure was 18.9 kPa due to a passing bus. These results suggest that the common assumption in pipe design of uniform stress of 25 kPa directly above the pipe to represent the traffic load may be conservative for the remaining life analysis of buried aged pipes. The road surface, road base and soil provide substantial support to traffic loadings so that the pressure effect due to traffic loading on the pipe is not significant.

3.4.3.2 Traffic Tests

A series of tests was performed using two test trucks in order to examine the behaviour of buried pipes due to traffic loading. The traffic tests simulated scenarios include stopped, passing, braking, cornering, and passing over a pot-hole. A 22.5 tonne three-axle truck and a 38.5 tonne semi-trailer were used for the test on the road base, bitumen road surface and concrete road surface.

Since the traffic test results showed similar magnitudes of strains measured from the different types of tests, the influence of the type of traffic tests on the pipe is not significant. Figure 3.2 shows a plot of the pipe strain measured on the pipe crown against the tyre load resulting from various types of axle groups and road surface. The likely linear pipe strain and tyre load relationship are plotted, and the results may be used to back-calculate the tyre loads of passing vehicles from traffic events measured on site.

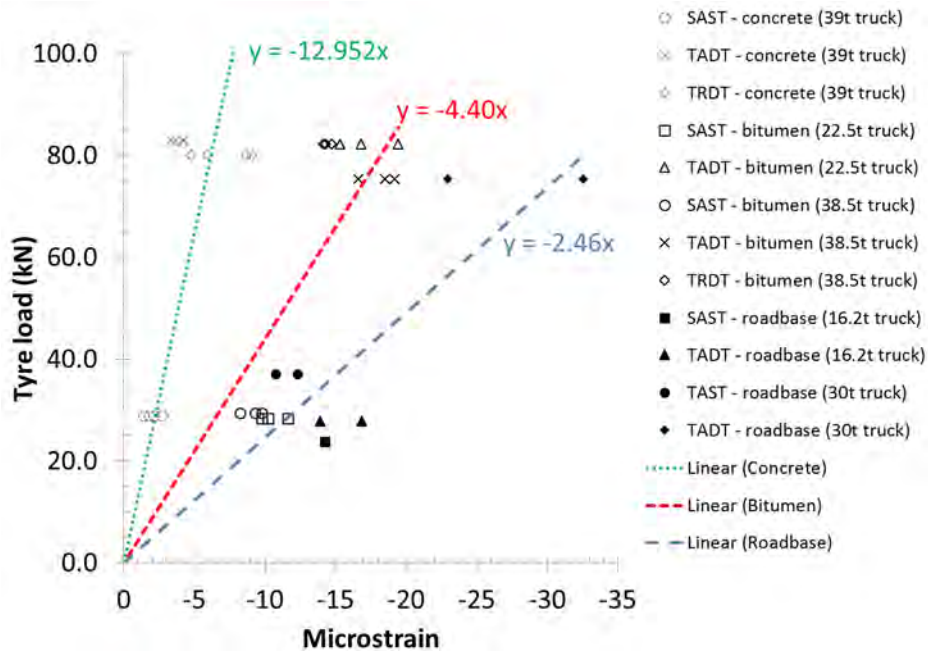


Figure 3.2. Relationship between hoop strain on pipe crown and tyre load

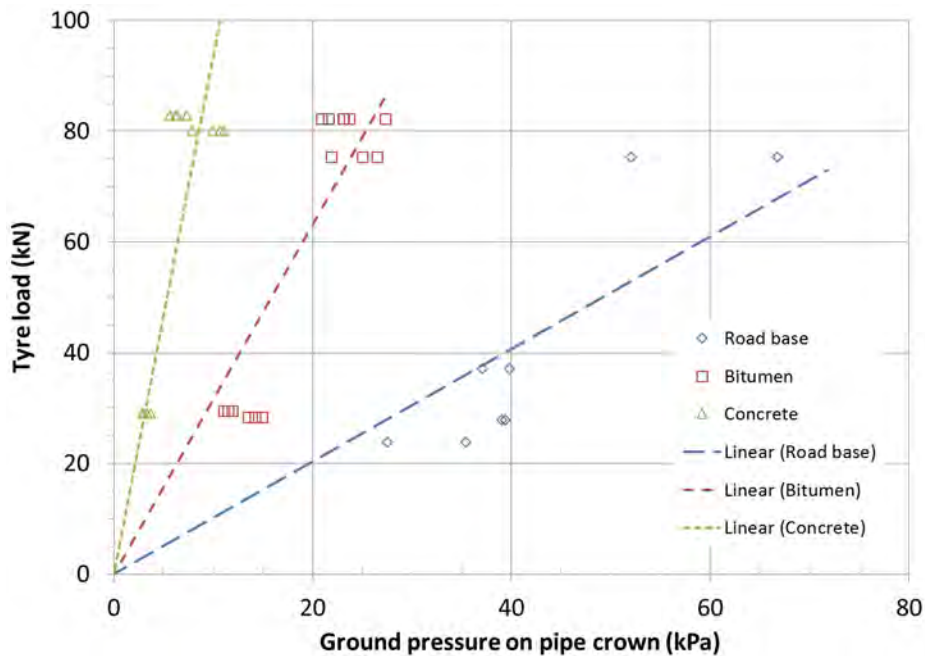


Figure 3.3. Relationship between ground pressure on pipe crown and tyre load

Ground pressures were measured at different depths from the road surface to the pipe crown. A significant decrease in pressure of up to 50 kPa was observed over the depth of 600 mm. Lower pressure in the range of 14 to 21 kPa was measured at the pipe crown. There was a small variation of pressure values that resulted from the different types of tests. Figure 3.3 shows the plot of ground pressures measured at various depths above the pipe against the tyre load resulting from various types of axle groups and road surfaces. The likely linear ground pressure and tyre

load relationships at each depth are plotted. Figure 3.3 can be used to determine the ground pressures due to traffic events when the weight of the passing vehicle is known, for similar ground and pipe conditions.

3.4.3.3 Internal Pressure Tests

Internal pressure tests were undertaken on the test bed in conjunction with the traffic tests. The test pipe was pressurised from 0 to 688 kPa and depressurised from 540 to 137 kPa. The loading and unloading path can be observed in the approximately linear relationship between internal pressure and measured pipe hoop strain, which shows that the change in strain is within the elastic region. The maximum pipe hoop strain was 126 microstrain at 688 kPa measured on the pipe crown. The strain value was about seven times greater than that resulting from traffic tests, but still well below the failure strain states of CI, which can range from 3000 to 6000 microstrain based on laboratory testing, under operational water pressures (i.e., 400 to 700 kPa). Note that the impact of operational water pressure loading on pipe deformation may be well below the failure strains of CI material if the pipe is not heavily corroded (generally or locally).

3.4.4 Discussion

Instrumentation of the Sydney test bed has provided results and evidence on the effect of dynamic traffic loading and internal water pressure on buried pipes. The behaviour of critical pipes and the buried environment can be understood from the measured pipe hoop strain and ground pressure.

Hoop strain measured around the outer surface of the pipe showed compression on the pipe crown and tension on the pipe springline, which suggest that the pipe behaves similar to a ring being loaded from the top due to soil and traffic loads. The maximum tensile strain measured is significantly small in relation to the average failure strain of tensile test coupons. A significant contribution of traffic loading arises from bus traffic for pipes buried in this suburban area, as 82% of measured traffic triggered events are due to the bus service.

Strains measured from different types of traffic tests have small differences and the magnitude of strain is small compared to the strains resulting from internal pressure. The small magnitude of strain suggests that the influence of traffic loading on pipe strain is insignificant.

The ground pressure measured from traffic loading tests and triggered events ranged from 5.2 to 18.9 kPa, suggesting that traffic loadings do not have a significant effect on the pipe for a relatively uncorroded pipe of this size. The common assumption in pipe design of uniform stress of 25 kPa directly above the pipe to represent the traffic loading may be too conservative for the remaining life analysis of buried aged pipes. This is mainly because the vertical pressure on the pipe decreases rapidly laterally away from the pipe crown.

The mode of loading arising from passing heavy traffic such as braking, cornering etc. had only a minor effect on the pipe strain and ground pressure close to the pipe crown.

3.4.5 Conclusions

Based on the field test results the following conclusions can be drawn:

- Changes in pipe strains from trucks passing at different speeds and braking tests are similar, with differences less than 20 microstrain (CI failure strain is around 4000

- microstrain)
- Changes in pipe hoop strains due to internal water pressure (688 kPa) showed that under normal operational pressure, pipe strain is within the elastic region with the maximum strain of 126 microstrain. On this basis, internal water pressure exerts over six times the strain than that due to traffic loads under the conditions studied.
 - Truck test results showed small differences in hoop strains measured by different tests (i.e., passing, braking, standing)
 - Pressure differences between braking and other tests are less significant at the depth of 860 mm tested (less than 5 kPa)
 - The use of a uniform vertical pressure of about 25 kPa across the pipe crown level due to traffic load is conservative, since vertical pressure drops away from the pipe crown laterally.
 - The instrumentation undertaken at the nature strip indicated that, although the pipe barrel can experience stresses due to seasonal moisture changes in clayey soil, most of the loads are transferred to joints in larger diameter pipes due to higher moments of inertia. Therefore, for larger diameter pipes buried in shrinking/swelling soils, joints can be damaged although the pipe barrel may not bend. The same reasoning is applicable to general ground movement due to other reasons.

More details can be found in the following publications: Robert et al. 2016b, Wong et al. 2017b, Ji et al. 2015b, Vitanage et al. 2013, Rajeev et al. 2013b, Vitanage et al. 2014.

3.5 PRESSURE TRANSIENT MONITORING AND MODELLING

3.5.1 Introduction

Internal water pressure is identified as a major factor that contributes to many large-diameter pipe failures. Internal water pressure can be sub-categorised as normal operational pressure and transient pressure. Estimation of steady-state pressure across an entire pipe network is relatively easy, since many water utilities have installed steady-state hydraulic models and pressure gauges covering the entire network. However, an estimation of the magnitude of pressure transients is particularly difficult, as the magnitude and the propagation of a transient pressure wave depend on additional factors, including the rate of change of flow, the hydraulic characteristics of system components, pipe material, pipe geometry (wall thickness and diameter), and pipe wall friction, which are often relatively difficult to obtain accurately. Therefore, information on the magnitude of pressure transients is often neglected or conservatively assumed during pipe failure prediction, due to the lack of knowledge about pressure transients. However, pressure transients can be a major contributor to pipe failures (Rezaei et al., 2015).

Therefore, significant research has been undertaken in the ACAPFP project to understand the propagation of pressure transients in water supply networks, to identify potential locations of pipe networks that are susceptible to severe pressure transients, and to quantify the magnitude of pressure transients for pipe failure prediction. In this project, a pressure transient monitoring and modelling program was conducted in four selected pressure zones (identified as Sections A, B, C and D) in the Hunter Water and South East Water networks. In subsequent sections, the methodology for pressure monitoring and transient modelling is explained and the major findings of the study are provided.

3.5.2 Pressure Transient Monitoring Program

3.5.2.1 Methodology

Pressure monitoring locations were selected on the basis of the operational experience of the water utility engineers and the results of preliminary pressure transient hydraulic modelling. Five units of Radcom pressure transient monitoring equipment (model RDL671LF) were installed in each pressure zone to monitor pressure transients generated due to pumps, valves and pressure regulating valve operations. The equipment is capable of recording 25 readings per second and is robust, waterproof, submersible and equipped with a long-life battery, which enables the data logger to log continuously for long periods of time in remote locations. The data logger is equipped with one input for an external pressure transducer and one output to download the data into a personal computer with the aid of Radwin software. In this particular field work, the data logger was often connected to fire hydrants using a hydrant cap and flexi-hose with a snap connection. In a few sites only, the data logger was installed upstream of the pressure regulating valve and directly on the trunk main using the small outlet taps. The frequency of the data logger was set to 20 readings per second with a tolerance setting of ± 5 k. The tolerance setting was used to enable the data logger to save a longer recording duration without clearing the memory of the data loggers. Pressure was monitored for a period of approximately one month in each selected section.

3.5.2.2 Discussion and Major Findings

Two sets of pump start-up events created during high and low system demand periods in network Section A indicated a significant rise of steady-state pressure during low system demand (i.e., early morning, 2:00 am to 4:00 am) as shown in Figure 3.4 and Figure 3.5, possibly due to less energy dissipation during low demand periods and closure of auto-inlet valves at closer reservoirs to the main pump station (i.e., development of high friction head when pumps are operated to pump water to far-end water reservoirs).

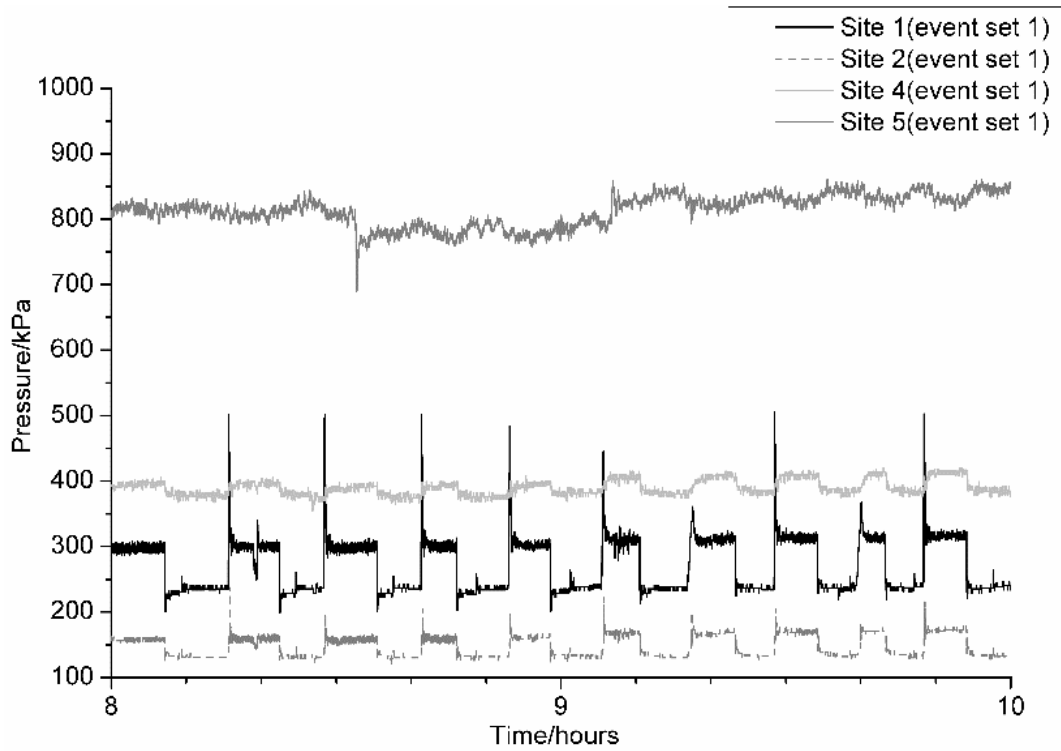


Figure 3.4. Pressure transients generated at Section A due to pumps during high demand

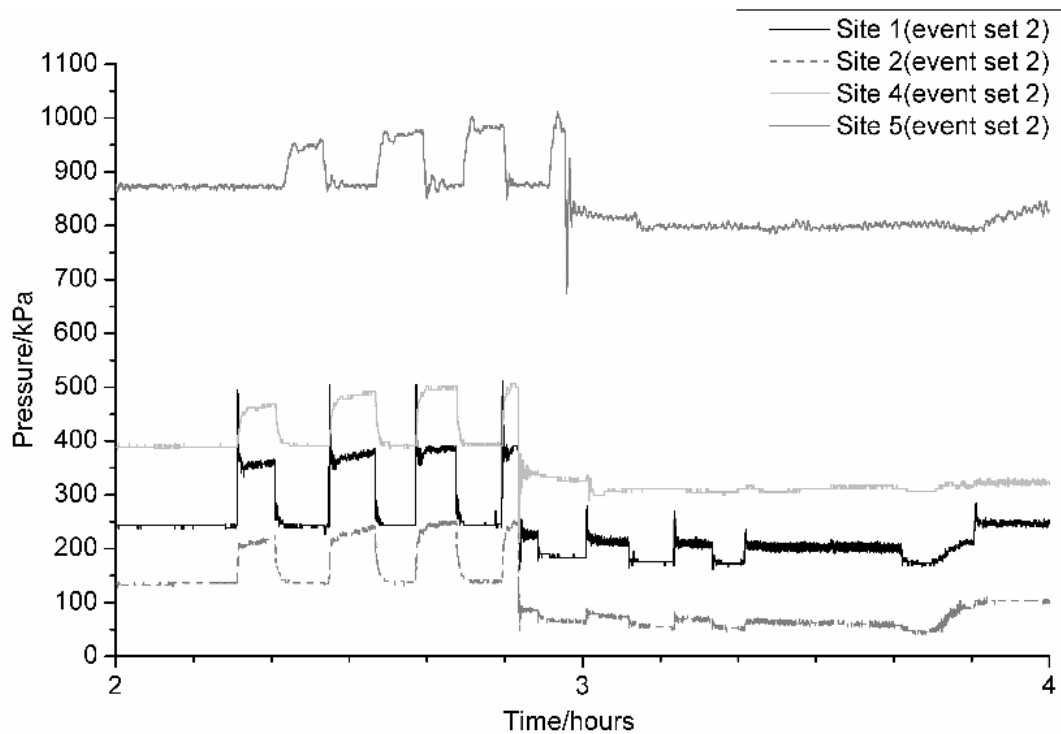


Figure 3.5. Pressure transients generated at Section A due to pumps during low demand (rise of steady-state pressure)

The settings of pipe network automated controls can lead to the development of severe pressure transients in water supply networks. The pressure transients shown in Figure 3.6 were created by the operation of an automated inlet valve and two booster pumps, which were automatically controlled by the water level of the downstream reservoir. The automated inlet valve was set to open when the reservoir water level dropped to 70 % of the maximum reservoir water level, and the valve was set to close when the reservoir water level reached 90 % of the maximum reservoir water level. When the reservoir water level drops to 55 % of the reservoir maximum water level, pump no. 1 in the booster pump station starts, and when the level drops to 35 % of the maximum water level, pump no. 2 starts to pump water to the reservoir. Pump no. 1 stops when the reservoir level reaches 85 % and pump no. 2 stops when the reservoir level reaches 80 % of maximum water level. The data obtained from SCADA showed that, although during this particular day the reservoir water level never dropped below 65 % of the maximum water level, each pump at the booster pump station started twice. The first three pressure spikes occurred due to the booster pump operational events. The very high pressure spike observed in the third event resulted from two pump start-ups and one shut-down event, which occurred at the booster pump station within a period of 32 s. The fourth pressure spike was a direct result of the closure of the automated inlet valve.

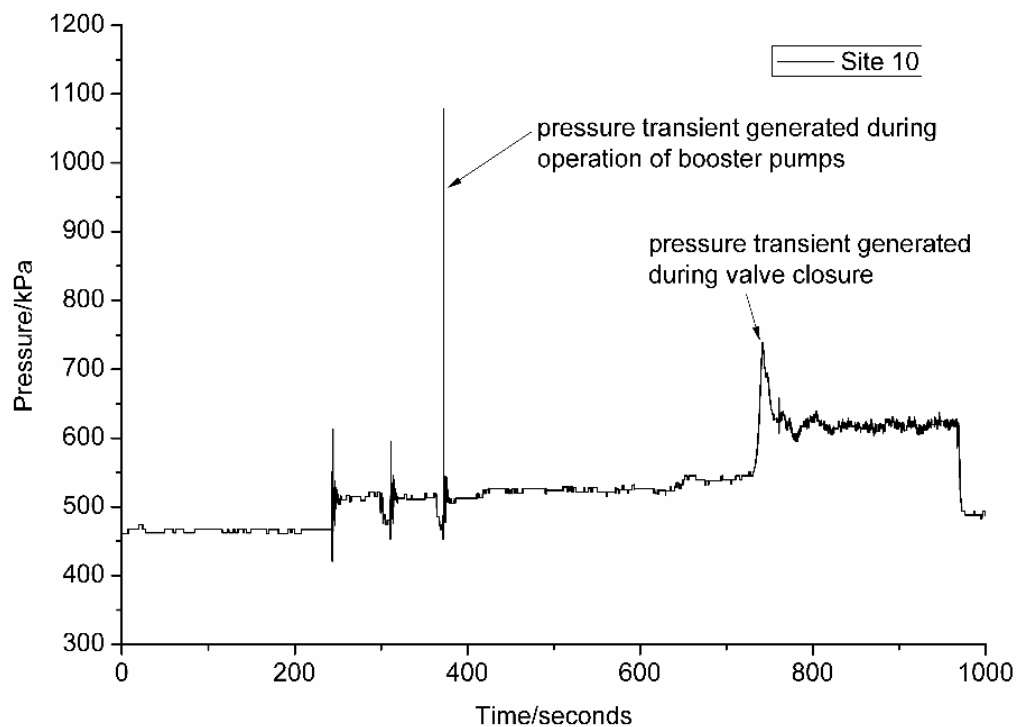


Figure 3.6. Severe pressure transient generated due to combined action of two booster pumps and an automated inlet valve

It was identified that routine pressure transients in water supply networks do not provide an immediate risk of pipe failure, unless the pipe deterioration is accelerated by an external cause. However, unintentional pressure transients similar to the two cases mentioned above provide the highest risk for failure of deteriorated pipes. Such a pipe failure was evident in this pressure monitoring program.

The generated transient pressure waves dissipated rapidly as they propagated along the trunk mains. In most cases, approximately 40–50 % reduction of pressure was observed within a distance of 2 to 3 km from the event origin when pressure transients occurred in comparatively high demand periods. However, pressure transient dissipation may depend on the pipe network configuration, and other energy dissipation mechanisms available in the individual network, which can dissipate extra energy during a pressure transient event.

3.5.3 Pressure Transient Modelling Program

3.5.3.1 Introduction

Field evidence suggests that transient water pressures can lead to pipe failures (e.g., a pipe failure occurred while generating pressure transients in the pressure monitoring study) seemingly due to damage accumulation in degraded or leaking pipes. The field pressure measurements mentioned above can only provide pressure information at the measuring site and there are no accurate methods to estimate the pressures at other pipes using the field data due to the complex nature of transient propagation through water-pipe networks. Therefore, the best method of obtaining the network-wide pressure transient data for pipe asset management is the use of validated pressure transient numerical models. Therefore, numerical models were developed and validated to obtain network-wide transient pressure distribution and an approach was shown to link the model results to the pipe asset management database.

3.5.3.2 Methodology

Using the network data provided by each water utility, first, extended period simulation (EPS) models were developed and validated using SCADA data to simulate a typical operational day for each network, so that steady-state operation could be established. Three pressure transient hydraulic models (for network sections A, B and C in the pressure monitoring program) were developed using the Surge2010-KYPIPE computer program. This program uses the wave characteristic method (WCM) to solve basic equations of unsteady flow and is customised for pressure transient analysis in water supply networks. Combining several smaller pipe segments (length < 1 m) into one longer section where possible, the size of the model (number of pipes) was reduced such that the model is efficient when analysed with the program (i.e., the presence of large numbers of short pipe segments could provide numerical convergence issues). During this simplification, demands associated with removed nodes were re-assigned to the closest retained node but the total demand remained unchanged. Except for house connections (diameter < 25 mm), the complete pipe network (including all reticulation pipes) was included when creating the pressure transient hydraulic models. As the wave propagation speed of each pipe is unique (calculated using Equation [3.1] and it has uncertainty associated with it, sensitivity analysis was conducted using four different types of wave speeds (i.e., (1) wave speed calculated using best available data for Equation [3.1], (2) single value of 915 m/s assigned for all pipes (3) single value of 1065 m/s assigned for all pipes and (4) introducing 0.1% air (α) into water and recalculating wave speed using Equation [3.2]:

$$c = \sqrt{\frac{E_f}{\rho(1 + K_R E_f D / E_c w)}} \quad [3.1]$$

$$c = \left\{ \left[\alpha \rho_a + (1 - \alpha) \rho_c \left[\frac{\alpha}{K_a} + \frac{(1 - \alpha)}{K_c} + \frac{D}{E_c t} \right] \right] \right\}^{-1/2} \quad [3.2]$$

where, E_c is the elastic modulus of the conduit in N/m^2 , E_f is the elastic modulus of the fluid in N/m^2 , ρ is the liquid density in kg/m^3 , K_R is the coefficient of restraint for the longitudinal pipe movement, D is the pipe diameter in m, and w is the pipe wall thickness in m, α is the local volumetric fraction of the air in water, ρ_a and ρ_c are the density of air and water in kg/m^3 , and K_c and K_a are the bulk moduli of the water and air in N/m^2 . The results of each simulated pressure transient scenario (i.e., the pressure rise from steady state for each scenario) were exported into the ArcGIS computer program to be integrated with other pipe information, in order to improve the pressure management and pipe failure prediction models. This process generated another data column in GIS that could be viewed, plotted, and mathematically manipulated in the GIS environment.

3.5.3.3 Discussion and Major Findings

All simulated scenarios showed reasonably accurate estimation of the magnitude of field-measured pressure transients for Sections A, B and C when the wave speed was assigned as 915 m/s for all pipes or when the wave speed was calculated using Equation [3.1] for individual pipes. This conclusion was drawn on the basis of the results of this research project, where the majority of trunk mains were made of CI, ductile iron and steel. Therefore, these results may be unique to the pipe networks studied, and caution should be exercised when using 915 m/s wave speed in other pipe networks in which plastic and other pipe materials are present in trunk mains.

Customer demands were not represented with complete accuracy, and the presence of leaks was unaccounted for during the simulation. Average daily customer demands and a diurnal curve provided by the water utility were used in the modelling, as records of metered water consumption for the dates on which the models were run could not be obtained. Discrepancies between actual water demand and the average data provided can result in different transient responses, because the nodal water demands can modify the shape and magnitude of moving pressure waves. Additional demand data, such as customer demand data measured using smart water meters at residential level, can be used to improve the predictability of pressure transients.

Until this study, no research has attempted to integrate validated pressure transient modelling results with pipe failure prediction models to improve pipe failure predictability. In this study, a method is proposed to incorporate pressure transient data into pipe asset management. It was developed by adding the maximum pressure rise above the steady state for all simulated pressure transient scenarios in Section B. With the addition of the maximum pressure rise above steady state in each of the two scenarios in Section B, for each pipe a new ArcGIS data column was generated, "Transient_pressure_rise," in the pipe asset data layer (Figure 3.7) that could be used for pipeline asset management. This is a conservative approach, because the likelihood of both scenarios occurring at the same time is very low. It is possible to identify pipes by either matching asset identification numbers in the hydraulic model and the asset database. It is also possible to develop pressure contour maps and running the GIS code to obtain the corresponding pressure for each pipe from the contour map. In preliminary decision making, water utilities can examine the pipes that experience high pressure to see if they have higher corrosion rates in those areas based on pipe condition assessments. A more rigorous approach would be to use these data

in physical-failure prediction models (including probabilistic modelling) or in statistical-failure prediction models using pressure as a covariant.

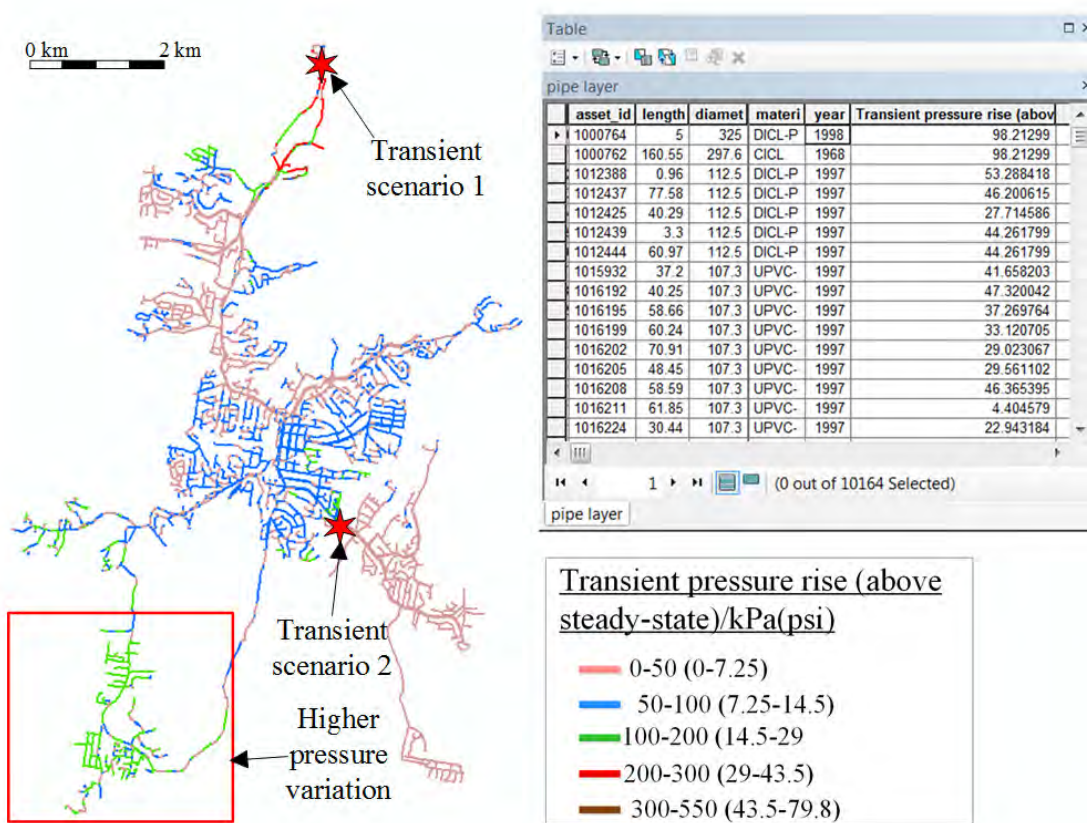


Figure 3.7. Sample pressure map developed using results of the pressure transient analysis of Section B (results for Scenarios 4 and 5); new data layer in the GIS database

During both pressure monitoring and transient modelling studies, the following locations were identified as vulnerable to high pressure transients. This list of locations may vary for each network, depending on network operations, the hydraulic equipment and the configuration of pipes in each network:

- Downstream of main and booster pump stations;
- Upstream and downstream of automated control valves;
- Reticulation networks that are in close proximity to pump stations and control valves (i.e., amplification of pressure transients when moving into reticulation from trunk main is possible);
- Reticulation sections connected by long pipelines without cross-connections, even some distance away from the transient sources (see the reticulation section marked in Figure 3.7); and
- Elevated locations with low operating pressure (these locations are susceptible to vapour cavity generation and collapse).

3.5.4 Conclusions

The following conclusions can be drawn from the pressure transient monitoring and modelling work:

- Severe pressure transients from multiple start-ups, shut-downs or automated controls are a major concern for pipe bursting.
- Routine pressure transients do not provide an immediate risk of pipe failure, but can contribute to damage accumulation.
- Generated pressure transients dissipate rapidly with distance from the generated pressure transient site.
- Reasonable accuracy between monitoring sites and models was found.
- New addition of maximum pressure rise above the steady state was developed for transient modelling and pipeline asset management.
- Main sites found to be vulnerable for high pressure transients are: downstream of main and booster pump stations, upstream and downstream of automated control valves, and reticulation networks that are in close proximity to pump stations and control valves.

More details can be found in the following publications: Rathnayaka et al. 2016a; Rathnayaka et al. 2016b; Chan, forthcoming; Chan 2016; Chan 2014.

3.6 CAST IRON PIPE COHORT PROPERTIES

3.6.1 Introduction

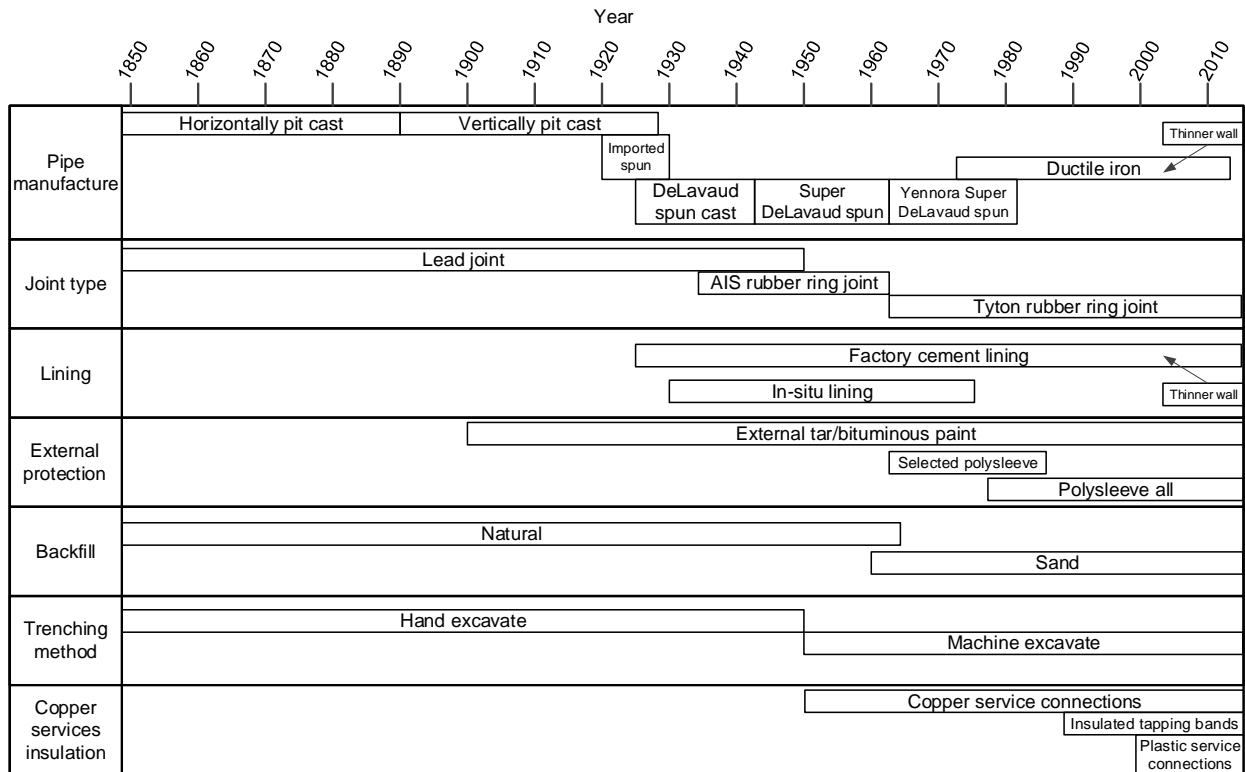
Buried ferrous water mains are subject to complex environmental conditions, which can cause deterioration over the water main's service lifetime. Significant variation of CI pipe physical properties exists as a result of the long span of manufacture and environmental changes (Rajani et al., 2000, Rajani et al., 2011). CI pipe properties are important to determine the remaining residual pipe strength (Fahimi et al., 2016), numerical modelling of tests (Ji et al., 2015a) and pipe failure prediction (Shannon et al., 2016b). Reports of significant testing of CI pipes in North America and the UK have been published (Conlin and Baker, 1991, Rajani et al., 2000, Seica and Packer, 2004, Makar and McDonald, 2007, Belmonte et al., 2008). However, the material properties of Australian CI pipes have been less documented.

Many of the examined water utilities' records have missing information about pipes, such as manufacturing type, wall thickness, failure data, repair data and correct location. This makes single value cohorts difficult to apply. As casting techniques improved, so did the strength of the CI pipe. However, this came at a cost with the coinciding reduction in wall thickness. The reduction in wall thickness meant a reduction in the time for corrosion to penetrate the CI and form a through-wall pit.

It is believed that the failure mode of ferrous water mains depends, to some extent, on both internal factors such as material tensile strength and fracture toughness and the pipe dimensions, as well as external factors such as corrosion, operating pressure, and surface load (Nicholas and Moore, 2009, Rajeev et al., 2013). To better understand the failure mechanism of Australian CI water mains manufactured from the mid-18th to late 19th centuries, the variations of these physical properties were narrowed by categorising the servicing water mains into a number of cohorts. In

this research study, the cohort properties were developed based on various tests and sources of data.

The CI pipe cohort was classified into main categories and further into sub-categories based on external and internal factors. The data classification uses Nicholas and Moore (2009), Scott (1990) and CI pipe design standards (British Standards, 1938, Australian Iron and Steel, 1941) to determine the main criteria. The main categories found in the literature include: pipe manufacturing process (pit and spun cast), joint type, pipe coating (tar or sleeve), internal lining, soil backfill, trenching method, copper services and pipe classes. Figure 3.8 shows a timeline of the pipes and construction methods used in some eastern Australian pipe utilities.



Source: Data from Scott 1990 and Nicholas and Moore 2009.

Figure 3.8. Timeline of ferrous pipe material in eastern Australia (overlapping of dates may be present in different water utilities)

3.6.2 Material and Methods

To calculate the remaining life of cast iron water mains, the key parameters used are: water pressure (maximum pressure the pipe experiences from daily pressure and pressure transients), pipe elastic modulus, pipe tensile strength, pipe fracture toughness, pipe wall thickness, pipe diameter, burial depth, soil modulus, soil density, soil lateral earth pressure coefficient, and soil/pipe corrosion rate. Water pressure is often monitored by water utilities and pressure data is included in most cohorts. However critical cast iron pipe properties are usually neglected when forming a pipe cohort. Most water utilities appear to have not documented the initial pipe wall thickness or the pipe class, when pipes were initially buried. Difficulties arise in classifying cast

iron pipes into the correct cohorts based upon pipes cast at a similar time, similar sizes and similar strengths.

3.6.2.1 Testing Methodology

Five large-diameter cast iron pipes of varying ages were selected from Victoria and NSW from decommissioned and burst water mains greater than 300 mm in diameter. The burial year of the pipes ranged from the 1920s to the 1970s. The five pipes tested were: Test Bed, Port Melbourne, Windale, Harris Street and Richmond, and their installation dates were 1922, 1937, 1956, 1961 and 1976 respectively. The CI pipes were tested for material structural properties including tension, compression, 4-point bending and fracture toughness. Metallurgy tests were conducted following ASTM A247 (ASTM International 2010).

In all mechanical property testing, specimens were cut using water-jet cutting and all internal and external corrosion was machined flat. Several tensile tests were performed on CI samples taken from numerous large diameter pipes in which the remaining CI was sufficient to run the tests. The tensile testing procedure followed ASTM E8M (ASTM International 2004). Strain gauges were placed in both the vertical and horizontal directions to measure tensile strains. A total of at least four tensile tests were conducted for each pipe.

Compression test sample preparation followed ASTM E9 (ASTM International 2009) with a diameter of 13 mm and a height three times the diameter (39 mm). If the wall thickness was less than 13 mm, the diameter of the sample was reduced to 10 mm (Richmond). At least three compression tests were conducted for each pipe. The bending tests were conducted in 4-point bending with a span of 240 mm. An LVDT measured the mid-span deflection at the base of the sample and a strain gauge measured bending strain. Two bending tests were conducted for each pipe.

The fracture toughness, which is widely used for describing crack mechanics, varies between CI cohorts. The fracture toughness was obtained from standard testing procedures using ASTM E399 (ASTM International 2008a). Single-edge notch bend (SENB) tests were used. A minimum of four tests were conducted on each of the five pipes.

3.6.2.2 Methodology of Cohorting Water Mains

Many mechanical characteristics, including tensile yield strength and fracture toughness, are closely related to the material type. This information should have been recorded by water utilities prior to pipe placement. However, material properties are usually not explicitly given in most water utility databases. After pipe casting at the factory, mechanical samples, primarily to test for tensile strength, were cast into separate moulds. The moulded samples were tested on whether the pipes met recommended strength standards such as AIS (1941) or BS 78 (1938). Pipe outer diameter was the major information water utilities gave when placing pipes. Information on initial pipe wall thickness and concrete lining thickness (in-situ or factory lined) is almost non-existent. Therefore, this crucial missing information makes the task of classification of pipes for cohorting very difficult.

Figure 3.9 shows the typical CI pipe cohort groups used in this section and the various differences exhibited between the cohort groups. The cohort groups are typical of the pipes used by eastern and south-eastern water utilities in Australia. The cohort groups were labelled according to the casting type: pit cast (PIT) or spun cast (SPUN), and casting method: horizontal (H), vertical (V), imported (I), DeLavaud (D) Super DeLavaud (S), and Yennora (Y). The numbers after the

casting method indicate variations, such as joint type, lining, external protection, backfill, trenching methods and copper installations, in cohort groups.

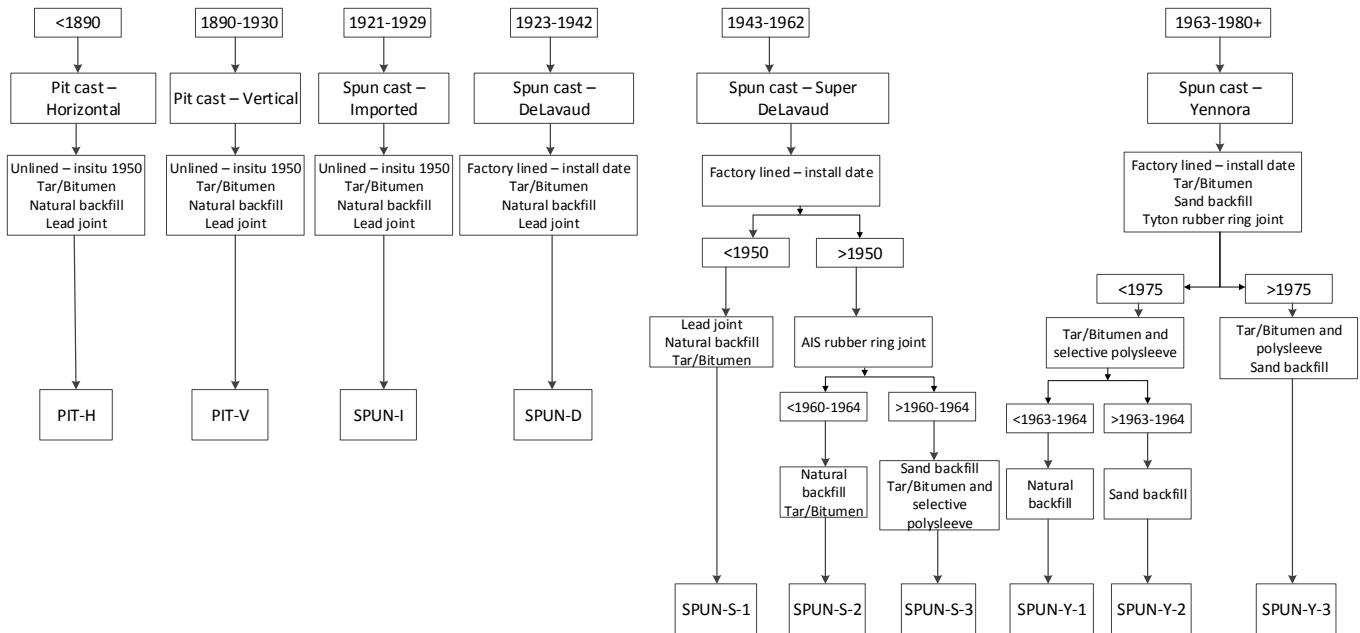


Figure 3.9. Typical cast iron pipe cohort groups used in eastern Australia

3.6.3 Results and Discussion

The tensile strength of intact pipes is an important parameter for pipe cohorting and for determining the remaining life of a pipe. For ferrous water mains, the British Standard (1938) specification for (vertically) cast iron pipes indicates that the minimum tensile breaking strength for tensile test bars should not less than 139.0 to 154.4 MPa, depending on the diameter of the test bar. According to Australia Iron & Steel Limited (1941), the design tensile strength of spun CI is to be taken as 169.9 MPa. However, the tensile tests reported in this paper indicated a range of average values for pit and spun cast between 83–235 MPa.

The average tensile strengths are shown in Table 3.1. A general trend in the data suggests that the older the pipe, the higher its tensile strength. This is true to a certain extent, but relies heavily on the manufacturing process and procedure. Initial spun cast pipes in Australia tend to have greater numbers of defects in casting than the super DeLavaud pipes. As a smaller number of defects may have been present in the factory-tested samples than in the in-situ CI pipes, the defects may have gone unnoticed when tensile strength tests were conducted on separate cast specimens. Due to the greater number of defects, the average strength of these pipes varies significantly and a lower resulting average tensile strength should be used.

The Young's (elastic) modulus of CI pipes increased with the more recent manufacturing year. Although the minimum rupture modulus for bending tests should be between 276–310 MPa for spun cast pipes (Rajani et al., 2000), the rupture modulus was found to be <276 MPa for all except Super DeLavaud and Yennora spun cast pipes. The compressive strengths ranged between 375–803 MPa for all pipes. A distinct difference between pit and spun cast pipes was seen. The Poisson's ratio of all the pipes ranged from 0.24–0.29. The fracture toughness from testing varied from 13.8 MPa m^{1/2} to 16.8 MPa m^{1/2} for the CI tested.

A range of material properties for the five pipes tested and various other research papers can be seen in Table 3.1, and the material properties can be linked with the cohort groups mentioned in Figure 3.9. This can help to give a range of material values that can be used in cohort modelling to estimate pipe remaining life.

Table 3.1
General range of material properties for cast iron pipe cohorts tested¹. Average values are in brackets

Pipe tested	PIT-H ²	PIT-V	SPUN-I ²	SPUN-D	SPUN-S	SPUN-Y
	²	Test bed	²	Port Melbourn e	Harris st/Windal e	Richmond
Graphite flake type	A	A	A & B	A & B	B	B & D
Graphite size	2	2	3	3	5	6
Graphite form	VII	VII	VII	VII	V	V
Tensile strength (MPa)	80– 120(100)	83–113 (103)	83–180 (130)	56 ³ –174 (127)	133–181 (156)	198–235 (214)
Tensile strain (µstrain)	1500– 4000 (3000)	1723– 4047 (3379)	2000– 3000 (2500)	657 ³ – 2765 (1692)	1843– 4097 (2827)	2764– 4038 (3460)
Young's Modulus (GPa)	70–99 (85)	72–99 (85)	110–120 (115)	110–122 (117)	104–113 (107)	109–146 (127)
Compressive strength (MPa)	375–450 (430)	375–455 (435)	520–600 (560)	540–589 (562)	523–715 (638)	546–803 (708)
Bending rupture strength (MPa)	220–260 (240)	242–243 (243)	180–240 (210)	197–234 (215)	299–348 (324)	348–403 (376)
Bending tensile strain (µstrain)	5000– 10000 (7500)	9517– 10075 (9796)	2500– 4000 (3000)	2589– 3574 (3081)	3245– 14970 (10303)	6508– 7185 (6847)
Fracture toughness (MPa m ^{1/2})	9.1–14.7 (12)	12.8–14.7 (13.8)	12.0–16.0 (14.0)	14.0–16.6 (15.3)	12.1–17 (14.5)	13.7–19.9 (16.8)

¹ Data obtained from large diameter (≥ 300 mm) pipe testing. Range of data may be higher or lower depending on pipe sample strength, size or flaws.

² No testing conducted on these pipe types. Data taken from past literature and similar pipe types (Gould, 2011).

³ Pipe sample had significant number of longitudinal flaws (casting defects).

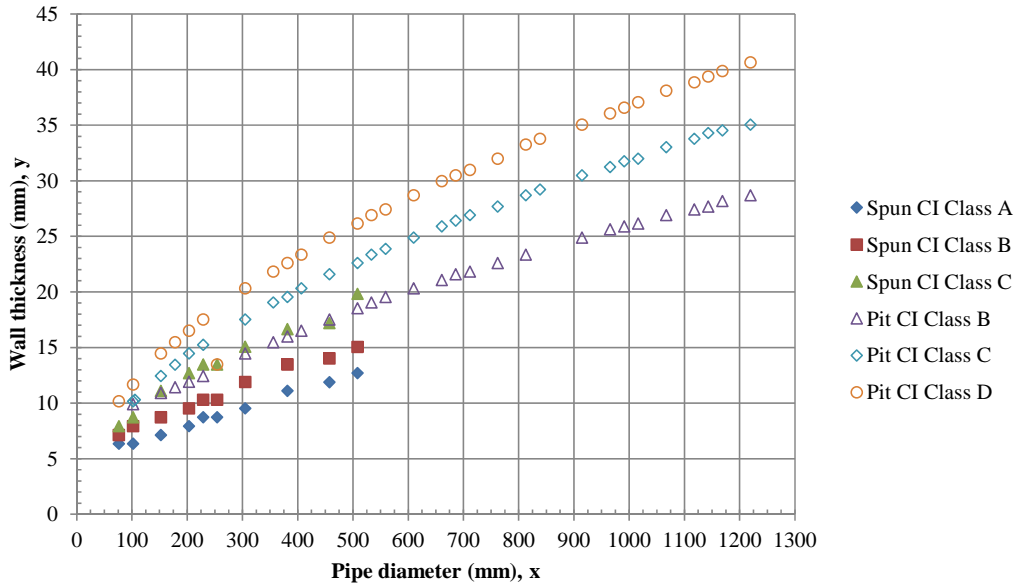


Figure 3.10. Relationship between cast iron pipe class, diameter, and wall thickness

Pipes were manufactured in different classes, mainly by varying the wall thickness for the same diameter and material. The class of pipe results in a large difference of mechanical resistance. Hence, wall thickness is another important element for cohorting the pipes. With respect to pit and spun CI pipes, Figure 3.10 shows the classes, specifying the design wall thickness. As manufacturing tolerance was applied to the products, there was a certain amount of variation in the pipe wall thickness for the same product class. The AIS (1941) allowed a maximum variation of wall thickness of $\pm 0.5\%$ of the pipe diameter. In the majority of water utilities, pipe wall thickness was not recorded when pipe placement took place. Therefore, wall thickness may have to be determined from the initial pressure for which the pipe sections were designed. Of the pipes tested, Test Bed was pit CI class D, Port Melbourne was spun CI class D, Windale was spun CI class C, Harris Street was spun CI class D, and Richmond was spun CI class B.

When CI pipes were originally cast into moulds, the pipes were pressure-checked for leakage and separate samples were tested for material tensile strength. This report found that there is a substantial difference between the measured strength of the pipes tested in Australia and the pipe manufactured pass strength. The strengths recorded tend to be on the low side of the manufactured pass strength, possibly due to manufacturing differences, defects or material degradation due to time. Nonetheless, the material properties used for cohorting should be sorted from actual tests conducted through laboratory testing of decommissioned, failed or exhumed ex-service CI pipes.

3.6.4 Conclusions

The pipe cohort physical parameters that contribute most to the failure mechanism have been reviewed. By doing so, the large variation of physical properties has been narrowed, which will help to investigate the past failure events and enable future failure prediction.

Some key findings are as follows:

- In cohorting CI water mains, the pipe diameter, wall thickness, cement lining condition, pipe coating, and material tensile strength are keys to distinguishing the cohort.
- The tensile strength required to pass pipes in the factory before placement in the field was found to be greater than some of the measured samples of exhumed pipes.
- Flaws in the tested samples significantly reduced the material strength.
- Yennora spun cast had the greatest strengths (tensile, compressive and bending) and fracture toughness.

More details can be found in the following publication: Jiang et al. 2016

3.7 LARGE-DIAMETER PIPE BURST TESTS

3.7.1 Introduction

A large-diameter cast iron pipe burst testing facility was set up in the basement at Monash University to test the burst capacity of grey CI pipes that have been subjected to different levels of corrosion. The main objective of the test was to investigate the burst capacity of old grey CI pipelines and to understand the relevant failure mechanisms. The testing facility consists of three main sections: the pipe containment (pipe section, two end plates and eight high tensile bolts, which are used to hold the water pressure inside: see Figure 3.11), the pressurising system and the data acquisition system. The base end plate and tensile bolts are fixed in position. The pipe section and top end plate are lowered onto the baseplate and carefully aligned with the tensile bolts. Gaskets made of composite material and petroleum jelly are used to create a good seal between the pipe and the end plates. Eight high tensile bolts are pre-tensioned to approximately equal pre-defined strains according to the estimated failure pressure in order to prevent water leakage and to seal the test pipe during pressurisation of the pipe section. As the pressure rises, the effect of the initial compression force applied to the pipe through the tensile bolts becomes minimal, due to the lifting of the top plate under pressure.

A 25-mm diameter pressure relief ball valve with a transparent tube is connected to the top end plate and the pressure relief valve is opened during filling of the pipe to allow the water to flush and to release the air trapped inside the pipe. After filling the pipe section with water using a 25-mm inlet hose attached to the bottom plate, the filling hose set-up is disconnected from the water supply using a ball valve attached to the bottom inlet hose, and the pressure relief ball valve at the top end plate is closed prior to beginning pressurisation. The pipe is then pressurised through a 10-mm diameter high-pressure hose through the top end plate. In the test reported here, the pipe section was pressurised using a pressure amplifier (HASKEL MS 21) which uses the laboratory air supply to amplify the water pressure inside the test pipe. An air pressure regulator installed on the upstream side of the pump was used to transfer air pressure into the water pump. Two digital and one analogue pressure transducers were used to monitor the water pressure inside the pipe during pressurisation. A data acquisition system recorded the pressure and strain gauge readings for up to 24 gauges at 1-second intervals. In addition, video cameras were placed next to the most critical corrosion patches on the CI pipe in order to capture the failure.

3.7.2 Material and Methods

Four 660 mm outer diameter vertically pit cast CI pipes, with initial wall thicknesses of ~25–27 mm, from a decommissioned pipeline in Sydney, NSW (Test bed pipeline) were tested at

the pipe burst test facility at Monash University. The operational pressure of the pipeline when in use varied from 500–750 kPa including pressure transients. To test the bursting capacity (internal pressure) of these CI pipes in the presence of corrosion, a variety of simulated and natural pipe thicknesses and corrosion patches were used. For information on the patch size for each of the tests see Table 3.2. The pipes were pressurised until either bursting occurred or the pipe leak rate was too high to continue testing. Pressure transducers were placed at the top and bottom of the pipe. Strain gauges were placed in the centre of each corrosion patch to measure hoop strain. Pressure and strain were monitored using pressure transducers and strain gauges at 1- second intervals. Figure 3.11 shows a decommissioned section of a large-diameter CI pipe in the burst test facility.

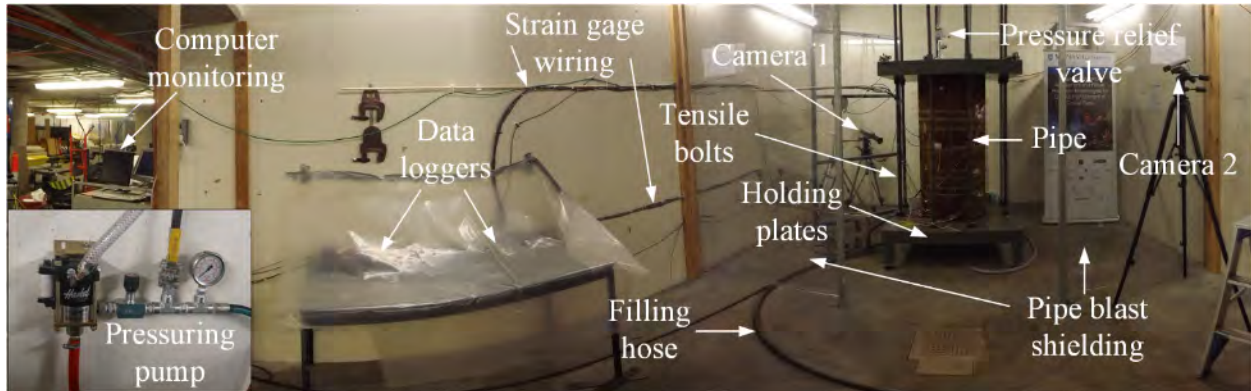


Figure 3.11. Large-diameter cast iron pipe burst test facility (Test 1 pipe in place)

**Table 3.2
Pipe corrosion patch information for each test**

Patch	Pipe 1	Pipe 2	Pipe 3	Pipe 4
Natural/artificial patch	Natural	Artificial	Artificial	Artificial
Shape of the corrosion patch	Varies	Circular	Elliptical	Elliptical
Internal corrosion	Yes	Yes	No	No
External corrosion	Yes	Yes	Yes	Yes
Axial length of the corrosion patch (mm)	125	190	330	400
Circumferential length of the corrosion patch (mm)	93	190	100	160
Average wall thickness (mm)	25	25	17	18
Remaining wall thickness (mm)	7.4	5.1	4.0	3.3
Round/flat patch base	Round	Round	Flat	Round

3.7.3 Results and Discussion

In all tests conducted, noticeable leaks were present before failure. These results show evidence of leak-before-break in large-diameter CI pipes (see Figure 3.12). For the CI pipes tested with smaller natural (Test pipe 1) and artificial (Test pipe 2) corrosion patches (approximately 125 mm and 190 mm in diameter and 7.4 mm and 5.1 mm thick in Test 1 and 2 respectively) no pipe burst was recorded. Test 1 and 2 pipe sections started to leak water from the locations of minimum pipe wall thickness around 3.2 MPa and 3.6 MPa internal pressures respectively. Increasing the internal water pressure beyond 3.6 MPa further increased the crack length in Test 2; however, as the corrosion patch diameter was small, the crack was arrested when the crack propagated to the

thicker part of the pipe wall (crack length 70 mm). Once the crack reached a greater remaining wall thickness, no further propagation of the crack occurred under the leaking pressure. It should be noted that the water pressures required, in both Test 1 and 2 (high remaining wall thickness and high nominal wall thickness), to initiate leaking were greater than 3.2 MPa. This is over five times greater than the typical water pressures of this pipeline in normal operation, which ranged from 500 to 700 kPa. Even considering catastrophic pressure transients (600 to 800 kPa), such high pressure is excessive for water pipelines. Therefore, if the rest of the water main was in similar condition to the pipes tested, it can be assumed that this pipe could have had a significant remaining service life if the pipe had continued to operate without being decommissioned.



Figure 3.12. Large-diameter cast iron pipes leaking water with corrosion patch size

In Test pipe 3, the pipe failed by piece blown out and longitudinal splitting within the range of typical operational water pressure (<1500 kPa). Once the pipe failed, the crack propagated at a fast rate, causing a chunk of the pipe to burst out from the patch (Figure 3.13). The crack further propagated through the thicker remaining wall section (~300 mm each side of the patch). In Test 4, the pressurisation process was stopped before failure at 1.5 MPa pressure. The pipe started to leak water at 0.8 MPa and the leak continued to grow with rising pressure. The final crack length in Test 4 was 75 mm. As the patch base was curved in Test 4, again the crack was arrested by the thicker section for the crack to propagate through before the bursting pressure. Lower remaining wall thickness is often seen in younger (spun cast) and smaller diameter CI pipes, which may be a

cause of the piece being blown out or longitudinal split failures. Table 3.3 shows the leak and failure data for the four pipes tested.

Table 3.3
Failure data for each pipe test

	Pipe 1	Pipe 2	Pipe 3	Pipe 4
Leak pressure (MPa)	3.4 ¹	3.2	0.8	0.8
Burst or final pressure (MPa)	3.6 ²	3.7 ²	1.4	1.5 ²
Leak strain (μstrain)	6100 ³	4000	2200	2100
Burst or final strain (μstrain)	NA ³	7200 ²	6400	5900 ²
Remaining life (years)	>30	>20	<1	<3

¹-Exact pressure not identified

²-Did not burst

³-Strain gauge failure before final pressure

The pipes tested were examined for remaining life using the Monash Tool: failure assessment of corroded grey CI pipe for longitudinal split failure (see Appendix Section 11.1). Based on a typical pitting corrosion rate for a moderately corrosive soil of 0.16 mm/year and a horizontal corrosion rate of 1 mm/year (Petersen and Melchers 2014 and the corrosion rates given in Activity 3), with an internal water pressure of 750 kPa (including pressure transients), the predicted life for each of the pipe sections tested varied from <1 year to >30 years and the values are shown in Table 3.3. The pipe sections used in Tests 3 and 4 indicate that if a patch this size was present in the field the remaining life would be very short. A similar corrosion patch with remaining wall thickness <20% would be the reason to replace this section soon. On the other hand, Tests 1 and 2 had smaller size corrosion patches and a remaining life of > 20 years. Although the thicknesses in both cases were slightly greater, the initial leaking pressure was significantly higher (about 4 times greater). Therefore, replacement of sections in this corrosion environment and in a similar state would be unnecessary in the short term. This assessment must be conducted thoroughly; as many variables can further influence the pipe's remaining service life.

In all cases a leak was present before bursting. The two smaller corrosion patches (Tests 1 and 2) did not cause failure at operational water pressures that would be present in the field. If the leak-before-break (LBB) theory for CI pipes is further refined, the theory could be used to help determine the remaining service life of a CI pipe. A leak detection tool in parallel with present condition assessment tools is recommended to determine the condition of the pipe. After a leak is found, the corrosion patch should be examined to determine whether the leak should be repaired or the pipe replaced. If the corrosion patch in a pipe is large, replacement should be conducted immediately to avoid pipe failure. However, if the leak is from a small pit, the pipe can be repaired and further monitored. If leak detection is not available, searching for large patches with <20% remaining wall thickness should be given priority.

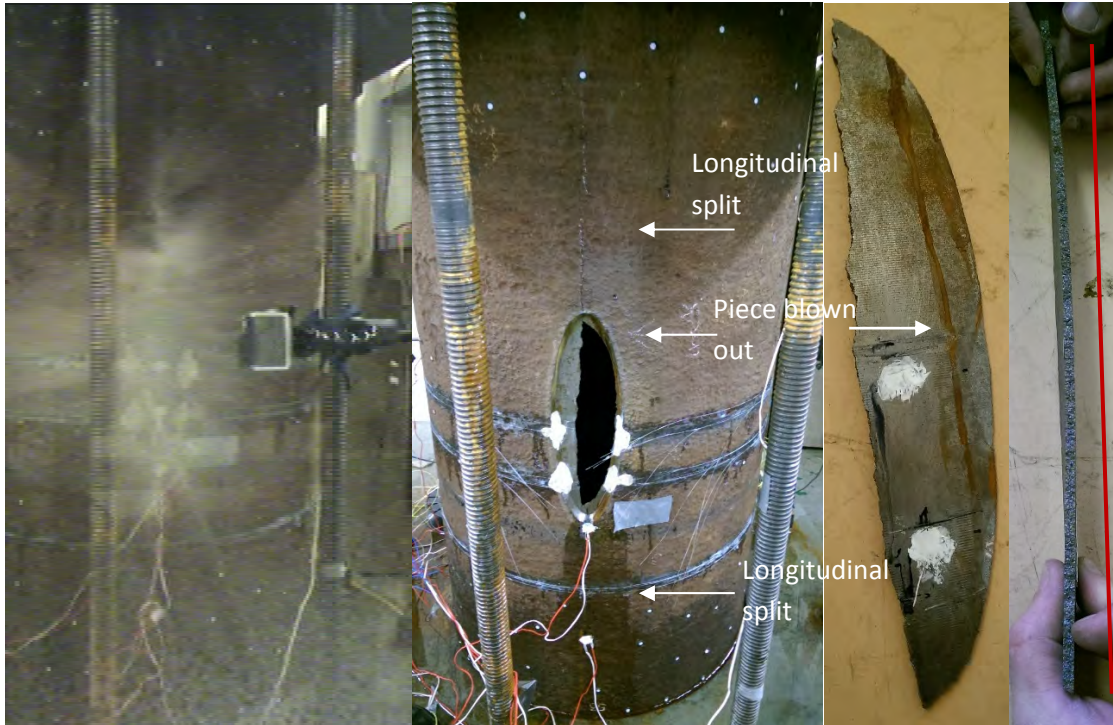


Figure 3.13. Test 3 burst failure (piece blown out) and longitudinal split

3.7.4 Conclusions

With the lessons learned from cast iron pipe burst testing, the following suggestions are made:

- For large-diameter CI pipes, a large corrosion patch with significantly deep corrosion (over 80%) is required to cause failure at operational pressures. The first failure was observed as a fracture at the base of the patch that eventually led to water leakage. Major longitudinal fractures occurred at higher pressures when cracks grew to a critical length.
- Many of the large-diameter pipe test samples tested had natural corrosion and relatively small pits of variable sizes and depth, some almost through-wall. None of these led to failure, even at pressures of 3000 kPa (or 300 m head).
- These observations with numerical and field evidence gave rise to the “Leak-Before-Break” (LBB) concept for CI pipes.
- The most important parameters for the prediction of pipe failure are tensile strength and fracture toughness.
- On this basis, it is suggested that condition assessment for large-diameter pipes should focus on identifying large and deep corrosion patches rather than smaller pits. However, smaller pits at the base of a large patch can increase the chance of failure. Therefore, the resolution of the condition assessment technique needs to be considered.
- Leaks may be monitored to detect pipes that are close to failure, thereby possibly preventing future failures.

More details can be found in the following publications: Rathnayaka et al. 2016c, Zhang et al. 2017a, Shannon et al. 2016a, Chan 2014.

3.8 FATIGUE MECHANISMS IN CAST IRON WATER MAINS

3.8.1 Introduction

Corrosion is generally considered as the predominant mechanism of pipe deterioration, which can reduce the thickness of the pipe wall and form stress concentrations in smooth pipes. Nevertheless, corrosion is a time-consuming process, and hence, soil corrosion is likely to be the major cause of crack initiation due to the generation of pits or patches, rather than the predominant mechanism of crack growth that eventually leads to catastrophic failure in many cases (Brevis et al., 2014, Rajani and Kleiner, 2013). However, some recent failure cases indicate that fatigue mechanisms may play a role in crack formation in CI pipes. Based on site observations, leakages of water trunk mains tend to happen prior to catastrophic fracture, and based on pipe failure analysis, different corrosive products along the fracture surface show different phases of fatigue crack growth.

Fatigue is a common failure mode for metal infrastructures, including bridges and buildings (Anderson, 2005, Schijve, 2001). Almost all the stresses in piping networks, including internal pressure, thermal stress and traffic loads, are time-various and can be considered as alternating stresses in fatigue analysis (Brevis et al., 2014, Rajani et al., 2012).

3.8.2 Research Aims

This section aims to explore the cumulative damage process and fatigue properties of aged CI pipes under the tension-to-tension stress range, by developing a new fatigue burst test and effective analytical models. A full-scale hydrostatic fatigue burst test has been established to simulate the changeable internal water conditions in practice and observe the crack propagation in aged water mains. Simultaneously, models of fatigue crack growth are verified by recorded data from full-scale tests, to enable the prediction of the window period of leak-before-break (LBB) to prevent pipe bursts.

In this study, the primary aim is to better understand the cumulative damage processes of large-diameter CI pipes before catastrophic fracture. Two research questions relate to this aim:

1. How does a through crack generate in corrosion pit via fatigue pressures?
2. How long will a macro-crack in CI pipes propagate to the critical length to cause the catastrophic fracture under fatigue stresses?

The core hypothesis of this section is longitudinal crack propagation in large diameter CI pipes is dominated by fatigue stresses. Apart from corrosion, fatigue or fatigue-related mechanisms play a vital role in the phase of crack propagation once a through-wall crack has initiated from pre-cracking or manufacturing defects. Moreover, corrosion patches or manufacturing defects may also lead to visible cracks in CI pipes, as these defect areas are subjected to relatively higher stresses (stress concentrators).

With regard to severely corroded pipes or pipes with existing sub-critical cracks, the phenomenon of low-cycle fatigue (LCF) may play a role in catastrophic fracture. First, relatively high hoop stress is produced in these thin-walled tubes, especially in areas with large patches due to the continuous loss of pipe wall. Second, the alternating internal pressure or unexpected transient pressures may initiate a crack, which tends to accumulate extremely high stress within the tip region (Figure 3.14). Thereafter, the crack may longitudinally propagate under relatively

low number of cycles until it reaches a certain length, resulting in the final fracture. Therefore, the remaining life of cracked pipes can be predicted by models of the fatigue crack growth rate.

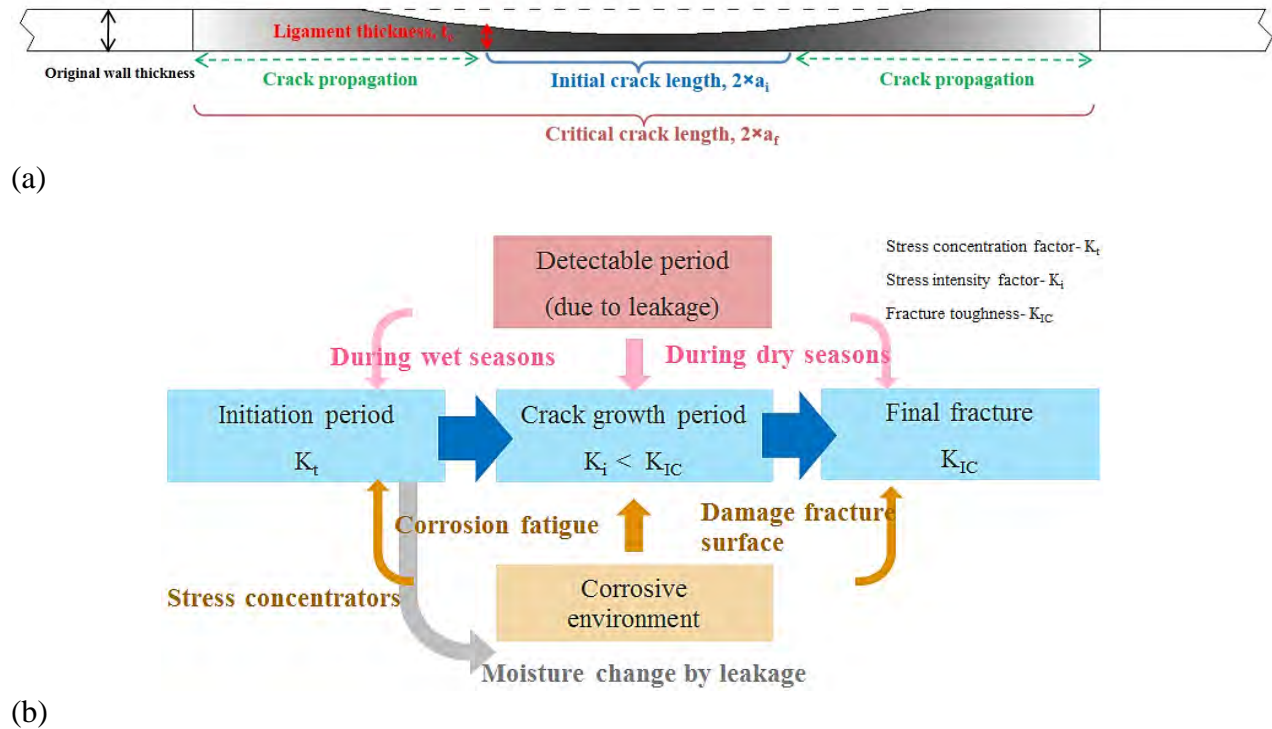


Figure 3.14. Conceptual diagrams: (a) crack propagation from the corroded patched areas; (b) fatigue cumulative damage of cast iron pipes

3.8.3 Initiation of a Through-Wall Crack by Cyclic Pressures

3.8.3.1 Introduction

Corrosion pits are normally generated in external pipe surfaces, which result in stress concentrations under the internal water pressure (Ji et al., 2015a). The maximum stress normally occurs in the centre of a circular or sub-circular corrosion patch. It was shown that a through-wall crack may be generated by the static increase of internal pressure. This phenomenon has been explained using the limit state design (LSD) method. A local crack is produced when the hoop stress is beyond the ultimate tensile strength of piping material in the centre of the corrosion patch centre. In water transportation networks, a single transient event (pressure surge) may result in a through-wall crack, which may cause either leakage or catastrophic fracture, depending on the particular corrosion patch configuration (Rathnayaka et al., 2016a).

The cyclic pressure may also contribute to the formation of through-wall cracks in corroded pipes, since pressure is continuously changing in transmission water pipelines. Fatigue damage is more likely to happen in networks with high ranges of cyclic pressures. Due to the fact that pressurised pipes are subjected to tension-to-tension cyclic stresses, a stress-controlled fatigue testing program was completed to reveal the stress-life of CI pipes.

3.8.3.2 Fatigue Tests

Stress-controlled fatigue tests were introduced to evaluate the risks of fatigue damage in deteriorated pipes, since cyclic pressures during transients and burst-refill events tend to be in fixed ranges of pressure change. Fatigue tests were conducted following ASTM E466 (2013a), and the specimens were carefully cut from the ex-service CI trunk mains detailed in Section 2.7. Fatigue tests were conducted on an Instron 4204 or 8800. Tests were carried out continuously until the specimens fractured, unless the specimens did not fail after 10 million cycles in a particular stress spectrum.

In fatigue tests, the stress ratio (R) is defined as the ratio between maximum stress (σ_{max}) and minimum stress (σ_{min}) in each cycle. Most of the specimens were tested under a stress ratio of 0.1, which indicates the fatigue strength in the tension range. In order to verify existing theories of mean stress effects, stress ratios of 0.3 and 0.5 were also applied to Test bed samples. The stress range ($\Delta\sigma$), alternating stress (σ_a) and mean stress (σ_m) are defined below.

$$R = \frac{\sigma_{min}}{\sigma_{max}} \quad [3.3]$$

$$\Delta\sigma = \sigma_{max} - \sigma_{min} \quad [3.4]$$

$$\sigma_a = \frac{1}{2} \Delta\sigma = \frac{1}{2} (\sigma_{max} - \sigma_{min}) \quad [3.5]$$

$$\sigma_m = \frac{1}{2} (\sigma_{max} + \sigma_{min}) \quad [3.6]$$

3.8.3.3 Results

With regard to aged CI pipes, the low cycle fatigue (LCG) phenomenon is more critical for failure prediction than the high-cycle fatigue life. The percentage of maximum fatigue stress to material tensile strength was used to analyse the test results. Table 3.4 shows the effects of fatigue damage in CI pipes depending on the amplitude of fatigue stress.

Table 3.4
Effect of fatigue damage in cast iron pipelines

Percentage of maximum stress to tensile strength	Cycles to failure	Effects of fatigue damage
>90%	1,000	Critical
65–90%	1,000–20,000	Considerable
50–65%	20,000–10,000,000	Minor
<50%	>10,000,000	Safe

3.8.4 Propagation of a Through Crack by Cyclic Pressures

3.8.4.1 Fracture Toughness and Fatigue Crack Growth Rates (FCGR)

Paris' law (Equation [3.7]) was adopted, in order to quantify the fatigue crack growth rates in CI pipes. There are three phases of fatigue crack growth: crack initiation (Phase I), stable crack growth (Phase II) and unstable crack growth/fracture (Phase III). The stable crack growth rates in Phase II can be described by Paris' constants:

$$\frac{da}{dN} = C \Delta K^m \quad [3.7]$$

$$\Delta K = K_{max} - K_{min} = Y \frac{P_{max} R_i}{t_n} \sqrt{\pi a} - Y \frac{P_{min} R_i}{t_n} \sqrt{\pi a} = \frac{\Delta P R_i}{t_n} Y \sqrt{\pi a} \quad [3.8]$$

where, C and m are Paris constants, a is half crack length, N is cycle number, K_{max} is maximum intensity factor, K_{min} is minimum intensity factor, P_{max} is maximum internal pressure, P_{min} is minimum internal pressure, t_n is the nominal wall thickness, and R_i is internal pipe radius.

The fracture toughness and fatigue crack growth rate (FCGR) tests were designed according to ASTM E1820 (2008b) and E647 (2013b) respectively. Single-edge-notched beam (SENB) specimens taken from the longitudinal direction were considered as the optimum method.

At least four specimens were tested from each pipe sample, and the Aramis digital image correlation system was used to record the surface deformation over the loading period. The tests were conducted using an Intron 4204 with a 50 kN load cell. The test results are summarised in Table 3.5.

Table 3.5
Results of fracture toughness and FCGR tests

Sample	Fracture Toughness, K_{max} (MPa m ^{3/2})		Average Paris' Constants	
	Average	S.D.	m	C (m/cycle)
Pit	13.8	1.1	10.1	6.4×10 ⁻¹⁴
Spun	15.4	2.5	9.2	9.6×10 ⁻¹³

3.8.4.2 Full-Scale Fatigue Tests

A large diameter pipe burst and the fatigue testing facility were used to monitor the behaviour of large-diameter corroded pipes under various internal pressures. In previous static bursting tests (see Section 2.7), when a longitudinal crack was generated in the patch centre, the internal pressure dropped due to leakage. The facility was upgraded to maintain pressure and to provide cyclic internal pressures whilst the pipe samples were leaking.

In a recent test, a 1.6 m long Test Bed pipe sample with an elliptical artificial patch was tested to failure. This pipe was previously pressurised in order to generate a sharp crack in the patch base. The maximum and minimum internal pressures were 1000 and 500 kPa respectively. After 2700 cycles, the surface crack length increased from 75 to 420 mm, despite the later pressure drop caused by high leakage rates. The test was halted after the crack had propagated past the leak-

rate capacity of the fatigue testing burst facility. The crack growth rates were plotted to obtain the Paris' constants (refer to Figure 3.15). The m and C are equal to 6.0 and 3.4×10^{-6} mm/cycle, respectively.

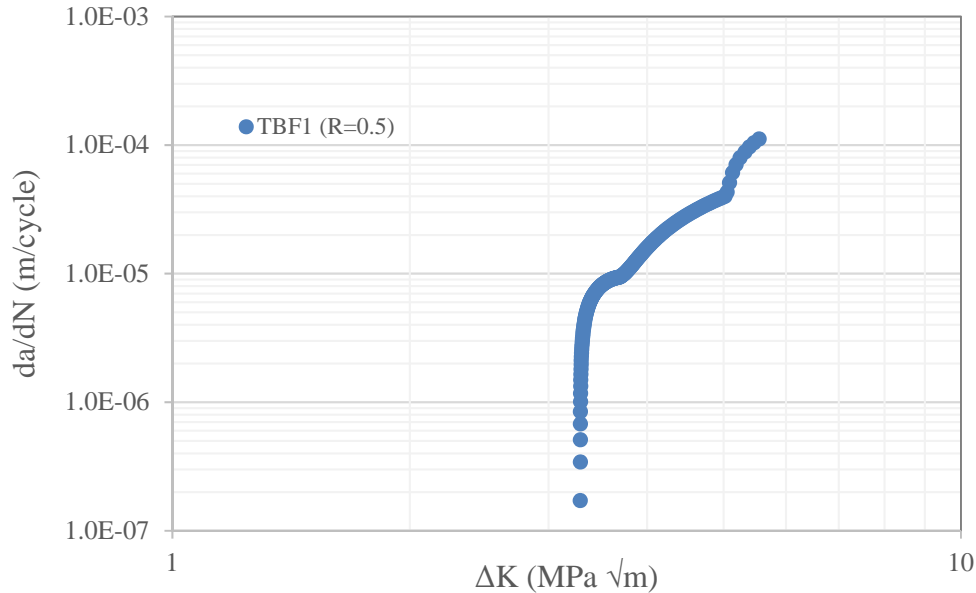


Figure 3.15. FCGR of a full-scale fatigue test

3.8.4.3 Window Period

The leak-before-break (LBB) window period can be defined as the period between the occurrence of detectable leakage and the final burst event. The window period is highly dependent on the leak detection methods. Fatigue crack growth models were applied to estimate the window period between a detectable leak and catastrophic break. The model of fatigue crack growth was established by the Paris' law and specific geometric factors from fracture mechanical theories. The initial crack length and final length can be determined by metallurgical analysis of corrosion products on the fracture surface (or corrosion patch configurations) and fracture toughness, respectively.

The leak rates during fatigue testing were measured and simulated for the mean operating pressure (refer to Figure 3.16). Equation [3.9] was used to estimate the leak rates throughout the service life of the target pipe (Cassa et al., 2010):

$$Q = C_d A \sqrt{2gh} \quad [3.9]$$

where, Q is the flow rate, C_d is the discharge coefficient; A is the orifice area, h is the operating water head (m) and g is the acceleration due to gravity. The C_d was assumed to be 0.6 (Mumovic and Santamouris, 2013).

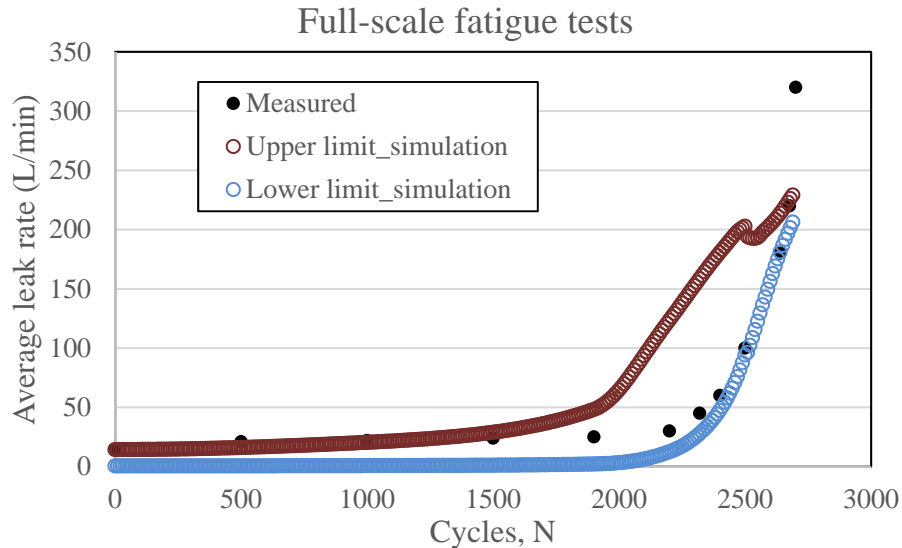


Figure 3.16. Leakage rates by measuring and simulation in TBF1

3.8.5 Fatigue: Key Findings

Some crucial findings of this ongoing study are as follows:

- The internal cyclic pressures are the predominant stress for fatigue damage in aged CI pipelines.
- A through-wall crack can be initiated in a corrosion patch of a CI pipe barrel by cyclic pressures.
- The fatigue damage is severe when the maximum pipe stress is over 90% of the material tensile strength. Fatigue analysis is required when the maximum stress is higher than 65% of the material tensile strength.
- Fatigue damage can be neglected if the maximum stress is less than 50% of the material tensile strength in CI pipe barrels.
- A through-wall crack is able to propagate under cyclic pressures.
- Leak rates in pressurised CI pipes can be estimated, and are directly controlled by corrosion patch configurations and operating pressures.
- The LBB window period in practice is between the occurrence of detectable leakage and the final burst event, and this period is mainly dependent on operating pressures, corrosion patch configurations and leak detection methods.
- CI pipelines that experience transient pressures or frequent burst/refill events may be more likely to be influenced by fatigue damage.
- In order to reduce fatigue damage, operational transients should be reduced or dissipated, and dramatic pressure changes need to be controlled.

More details can be found in the following publications: Zhang et al. 2017b, Shannon et al. 2016c.

3.9 FINITE ELEMENT MODELLING OF PRESSURISED CORRODED CAST IRON PIPES

3.9.1 Introduction

It has been established that if a CI pipe is corroded, the metal-loss area will suffer greater intensified stress than its previous area without corrosion. However, the amount of stress increase depends on the external and internal (water) pressures and corrosion patterns. Therefore, the appropriate corrosion condition should be taken into account in the stress estimate of corroded CI pipes.

This chapter is intended to summarise a large amount of numerical work on the evaluation of the influence of metal-loss corrosion on pressurised CI pipes. All the numerical analyses were conducted using the commercial software ABAQUS, based on the finite element (FE) method. The aim is to propose an appropriate closed-form equation to unite corrosion patterns (idealised *via* circular and elliptical shapes) and the induced concentrated tensile stress. Real pipes, of course, suffer from corrosion anomalies in irregular and complex configurations. Therefore, we have also developed a relatively simple and reliable constitutive model for CI material that can be used to compute stress-strain responses of CI pipes under real natural corrosion conditions.

3.9.2 FE Modelling to Develop a Closed-Form Stress-Estimate Equation

3.9.2.1 FE Modelling of Soil and CI Pipes with and without Corrosion

Figure 3.17 shows a typical FE model created to numerically analyse the corrosion-induced concentrated stress of a CI pipe. The complete modelling process is provided in Robert et al. (2016b) and Ji et al. (2015a), and only a brief introduction is given here.

1. The first stage is to model a uniform pipe without corrosion. The pipe is subject to gravity; overburden pressure from the soil, internal water pressure and traffic load, and the maximum tensile stress, $\sigma_{nominal}$, acting at the middle of the pristine pipe is obtained.
2. The second stage is to artificially create a corrosion patch or pit, which was idealised earlier by a circular and more recently by an elliptical shape, in the middle external surface of the pipe. A stress concentration factor (SCF), being the ratio of the maximum tensile stress of a corroded pipe to that of pristine pipe, is computed for each corroded pipe model. Where the term *corrosion* is used, it mostly refers to remaining-wall corrosion, although some through-wall corrosion cases were also investigated.
3. The third stage is to consider the interaction of corrosion pits, resulting in pipe failure at a lower pressure than would be expected in the case of single, separate pits. Since there are almost countless types of grouping or clustering configurations, such as two, three, four and more pits of different sizes, depths, orientation angles and so on, the present research mainly focused on two pits spaced longitudinally, as shown in Figure 3.18. This clustering pattern is found to have a more significant influence than circumferential spacing.

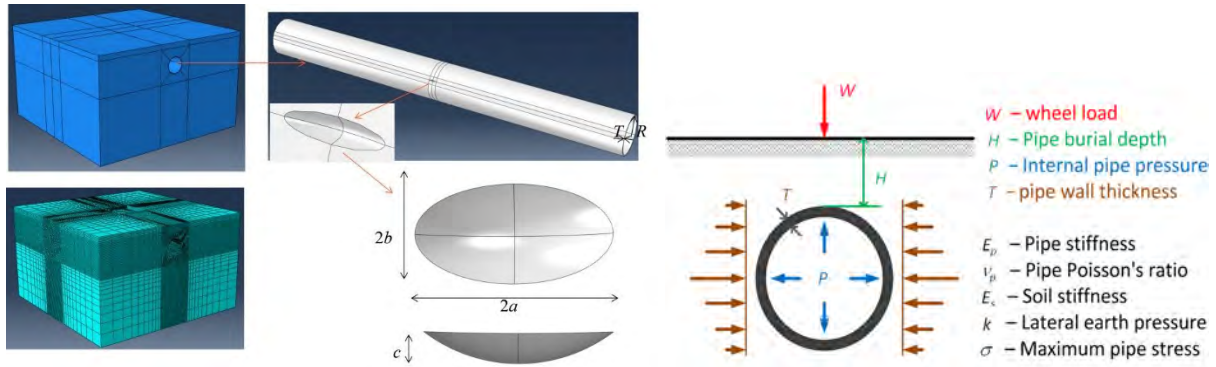


Figure 3.17. Finite element model of a buried pipe in subgrade

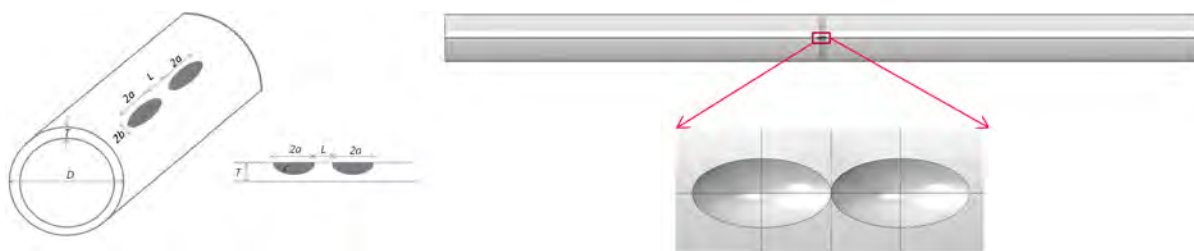


Figure 3.18. Numerical modelling of clustering configuration of two pits

Thousands of FE models have been created and analysed for the above intentions. The model parameters and dimensions of pipes and corrosion pits and patches are listed in Table 3.6. The purpose of these FE models was to derive an equation to predict maximum pipe stress due to internal and external loads on buried pipes.

Table 3.6
Physical properties of large-diameter cast iron buried pipes

Description of physical parameters		Symbol	Unit	Value for NLR
Location	Burial depth	H	m	0.3, 0.8, 1.3, 2.0
Backfill soil surrounding pipelines	Elastic modulus	E_s	MPa	2, 4, 10, 25, 50
	Unit weight	γ	kN/m ³	18.5
	Lateral earth pressure coefficient	k		0.1, 0.25, 0.4
	Poisson's ratio	ν_s		0.3
Pipe physical properties (cast iron)	Elastic modulus	E_p	GPa	100
	Poisson's ratio	ν_p		0.3
	Wall thickness	T	mm	4, 8, 10, 15, 27
	Pipe diameter	D	mm	200, 300, 660, 1000
Load	Surface load (traffic)	W	kN	0 to 75
	Operating water pressure	P	kPa	0, 300, 500, 800, 1000, 1300, 1500
Corrosion patch	Radius of major axis	a	mm	2.5 – 100
	Radius of minor axis	b	mm	1.375 – 100
	Corrosion depth	c	mm	5 – 28
Two-pit cluster	Longitudinally spaced distance/ wall thickness	L/T		0 – 4T

A dataset of $\sigma_{nominal}$ was obtained and evaluated, enabling the development of a closed-form equation [3.10] to estimate $\sigma_{nominal}$ for an embedded pristine pipe:

$$\sigma_{nominal} = \left(\frac{W + \gamma \cdot D^2 \cdot h}{D^2} \right) \left[\alpha_1 \left(\frac{E_p}{E_s} \right)^{\beta_1} \left(\frac{E_s}{\gamma \cdot h} \right)^{\beta_2} \left(\alpha_2 \frac{\left(\frac{P}{E_s} \right)^{\beta_3}}{\left(\frac{t}{D} \right)^{\beta_4} \left(\frac{W}{\gamma \cdot D^2 \cdot h} + 1 \right)^{\beta_5}} + \alpha_3 \frac{\left(\frac{t}{D} \right)^{\beta_6} \left(\frac{W}{\gamma \cdot D^2 \cdot h} + 1 \right)^{\beta_7}}{\alpha_4 \left(\frac{E_p}{E_s} \right) + \alpha_5 \left(\frac{P}{E_s} \right) + \alpha_6 \left(\frac{h}{D} \right) + \alpha_7 k} \right) \right] \quad [3.10]$$

where,

α_1	α_2	α_3	α_4	α_5	α_6	α_7
0.12	4.08	1.76E+06	7.65E+04	4.17E+06	3.23E+07	3.55E+07
β_1	β_2	β_3	β_4	β_5	β_6	β_7
0.086	0.94	0.89	0.88	0.94	-0.51	-0.71

On the other hand, the data set of the numerically-obtained SCF leads to another closed-form equation [3.11]:

$$SCF = 1 + \frac{\sqrt[3]{3(1-\nu^2)}}{2} \left\{ \frac{\alpha_1 \left(\frac{a}{\sqrt{RT}} \right)^{\beta_1} + \alpha_2 \left(\frac{b}{\sqrt{RT}} \right)^{\beta_2} + \alpha_3 \left(\frac{c}{\sqrt{RT}} \right)^{\beta_3}}{\alpha_4 \left(\frac{a}{\sqrt{RT}} \right)^{\beta_4} + \alpha_5 \left(\frac{b}{\sqrt{RT}} \right)^{\beta_5} + \alpha_6 \left(\frac{c}{\sqrt{RT}} \right)^{\beta_6}} \right\} \alpha_7 \left(\frac{c}{T-c} \right)^\beta, \quad 0 \leq b \leq \sqrt{R^2 - (R-T)^2} \quad [3.11]$$

where, the α and β parameters (regress model coefficients – note: coefficients were estimated based on the numerical analysis performed for the range of parameters in Table 3.6) are listed below and the condition of b in Equation [3.11] must be satisfied due to the curvature compatibility between an (idealised) semi-ellipsoid and the pipeline.

α_1	α_2	α_3	α_4	α_5	α_6	α_7
2.80E-05	3.00E-05	7.096	3.00E-06	3.00E-05	0.011	0.797
β_1	β_2	β_3	β_4	β_5	β_6	β_7
1.071	2.09	11.677	0.733	1.348	5.755	0.84

Equation [3.11] reveals that SCF is a function of the five geometric parameters that depict the sizes of the pipe and idealised corrosion pattern. This equation satisfies the minimum bound of SCF that shall be not less than unity:

$$SCF = \Omega(R, T, a, b, c) \geq 1.0 \quad [3.12]$$

In addition, the equation also indicates that SCF is unity if there is no corrosion on the pipe, such as for a pristine pipe:

$$\lim_{c \rightarrow 0} SCF = 1.0 \quad [3.13]$$

3.9.2.2 Monash Tool

With the implementation of Eqns. [3.10] and [3.11] and considering fundamental concepts of fracture mechanics, we have developed a Monash Tool (MT) as shown in Figure 3.19, for the condition assessment of pressurised CI pipelines. The MT is intended to serve for the estimation of:

1. nominal (hoop) tensile stress,
2. stress concentration factor (SCF) and maximum tensile stress for fracture initiation,
3. critical crack length for pipe burst, and
4. remaining life to initiation of local failure leading to a leak.

More information on how to use the MT is provided in Appendix Section 11.1: *Explanatory Notes for Monash Tool*. The MT is an easy-to-use deterministic tool, which is being improved to incorporate more functions, such as the probabilistic analysis of pipe failure.



Figure 3.19. Screenshot of Monash Tool (MT)

3.9.2.3 FE Modelling of Interaction of Corrosion Pits

To date, we have achieved some preliminary findings on the influence of pit clusters, although a large amount of modelling effort is still required. The findings are summarised as follows with a typical result of maximum tensile stress distribution shown in Figure 3.20:

1. When longitudinal distance, $L=0$ (i.e., the boundaries of the two corrosion pits are point-by-point connected), the maximum tensile stress is generally located within the local intersection region and extends to a minor depth below the pipe external surface, as shown in Figure 3.20(a).
2. When L is sufficiently small, the maximum tensile stress may be found on the top of the part between the two pits (Figure 3.20(b)). This may allay the stress intensity at the bottom, reducing the risk of punch-through failure. As L increases, the maximum tensile stress gradually shifts from the top to the bottom of the pits, decreasing in its amplitude, as shown in Figure 3.20(c). During this shifting procedure, the stress at the bottom of the pipe is likely to become higher than that of a single pit due to the pits' interaction, initiating pipe (local) failure at a lower water pressure. This mechanism is very complicated and needs further investigation.
3. The influence of L needs to be considered in developing the SCF for two-pit clusters. Many more models are being trialled to establish a mathematical equation to connect the SCF with L , on the basis of the following restraints:

$$SCF_{cluster} = \Omega(R, T, a, b, c, L) \geq 1.0 \quad [3.14]$$

$$\lim_{L \rightarrow L_c} SCF_{cluster} = SCF \quad [3.15]$$

where, L_c implies the critical longitudinally-spaced distance between two pits, beyond which the interacting influence can be considered to be negligible.

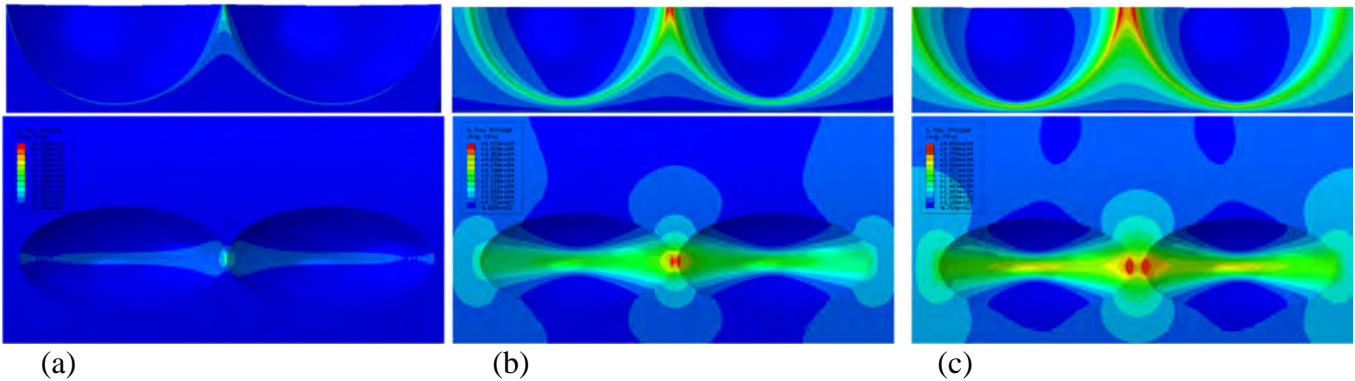


Figure 3.20. Variations in maximum tensile stresses due to the increase of L

3.9.3 FE Modelling of Burst Pipe Testing

Many tests of CI pipe materials have shown the non-linearity of CI materials subject to loads. Although in many cases CI pipe behaviours have been assumed to be linear, a nonlinear analysis may achieve more accurate results when studying the pipe responses. Therefore, some elastoplastic models based on classic and refined theories of plasticity have been proposed in the research literature to study the nonlinear behaviours of CI materials. Nevertheless, the existing elastoplastic models have not yet been widely used by general public, due to the difficulties in mathematical derivation and numerical implementation.

In the light of the above situation, instead of using complicated elastoplastic models, we have developed a much simpler and easy-to-use, nonlinear elastic constitutive model termed MHM-CI (Zhang et al., 2017b), which has been implemented in FEA for the numerical modelling of CI structures without loss of generality and accuracy. Details of the derivation of the model, together with the validation of laboratory tests (uniaxial tensile/compression, beam bending and ring tests) are provided by Zhang et al. (2017b). In this section, we summarise the key numerical results of three pressurised pipes tested in the newly developed burst test facility in the Monash Civil Engineering laboratory.

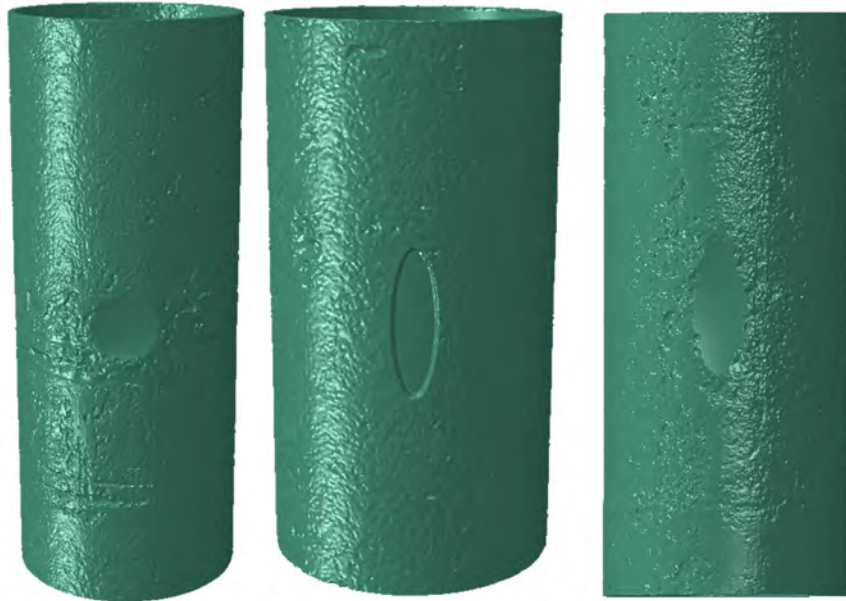
Figure 3.21 shows three of the CI pipes for burst testing (see Section 2.7 for further details) and the corresponding numerical counterparts that were developed by laser scanning and mapped into ABAQUS for numerical analysis. As the figure shows, large and deep corroded patches estimated based on preliminary modelling were artificially created for each pipe specimen so that the patch would leak and burst under operating pressure. Information on these artificially machined corroded patches and the pipes is summarised by Zhang et al. (2017b).

Using our numerical simulations, the scattered distributed stresses like the maximum tensile stresses, are shown in detail in Figure 3.21. The numerical results of the three pressurised pipes show that the stresses are quite scattered, with some local areas under significant tension, while their vicinities are under minor tension, depending on the severity of pitting corrosion in the pipes. The relatively deep corrosion areas, such as the machined corrosion patches, where the most significant tensile stresses are concentrated, are the most critical areas when estimating the likelihood of pipe leaks and bursts. These complicated stress distributions due to pitting corrosion are completely different from those in the pipe with a uniform or reduced wall thickness. The latter

approach using a reduced uniform wall thickness is a common treatment that has been widely adopted in practice and research in the analysis of corroded pipes. Based on our demonstrations in Figure 3.22, it is clear that the idealisation of the corroded pipes using a (reduced) uniform wall thickness may lead to a significantly inaccurate stress estimate of a corroded pipe, particularly when the pipe is severely corroded.



(a) Pipe burst test 2 (b) Pipe burst test 3 (c) Pipe burst test 4



(d) Scanned pipe 2 (e) Scanned pipe 3 (f) Scanned pipe 4

Figure 3.21. Tested CI pipes including machined corrosion patches

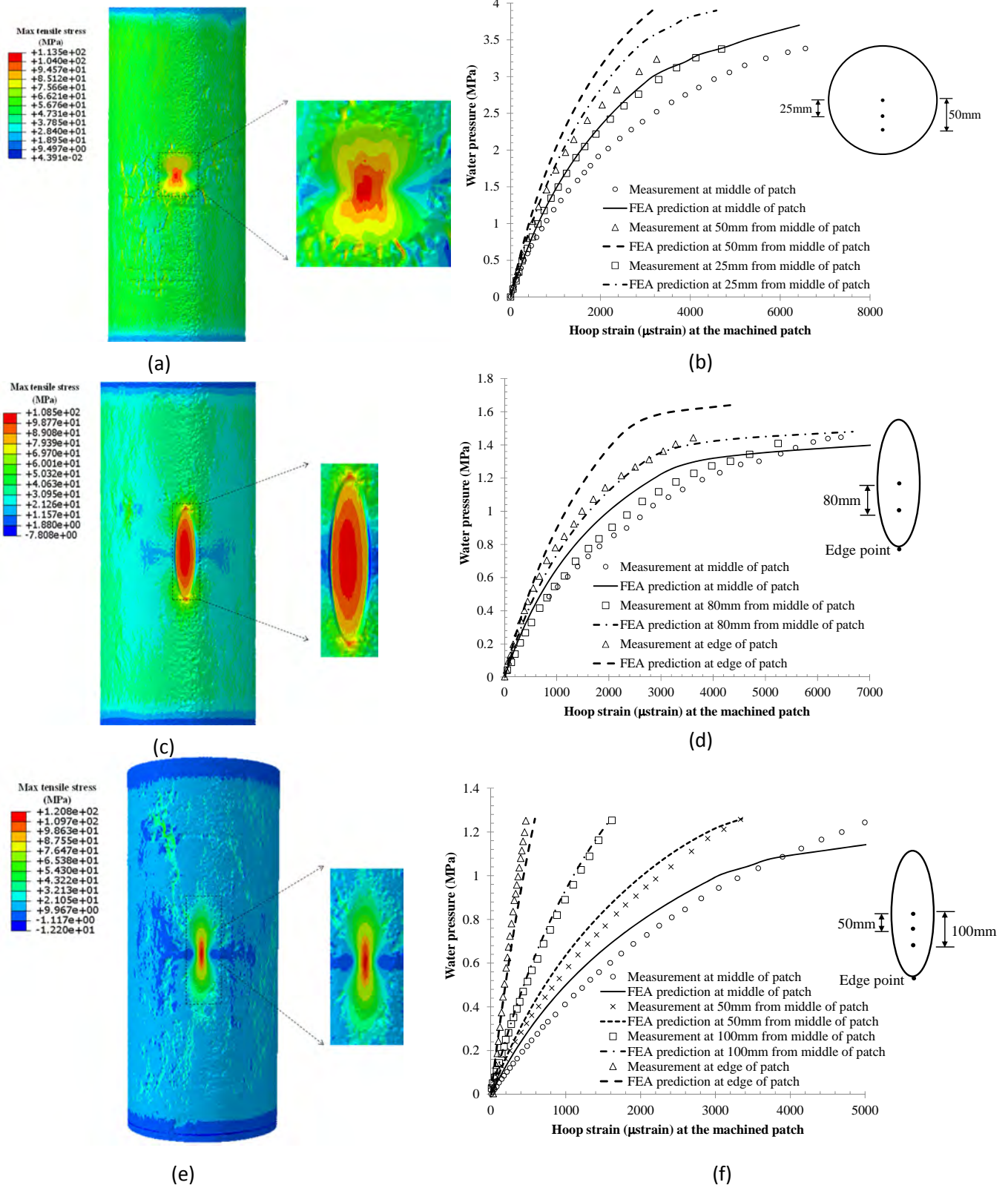


Figure 3.22. Numerical results of tensile stress and hoop strains of burst tests on pipe 2 shown in (a) and (b), pipe 3 in (c) and (d), and pipe 4 in (e) and (f)

The numerically-obtained water pressures corresponding to the start of cracking with possible leakage at the centre of the machined patches of pipes 2, 3 and 4, are approximately 3000 kPa, 1240 kPa and 970 kPa, respectively. In comparison, the measured water pressures at first leakage of the three pipes are approximately 3200 kPa, 1290 kPa and 800 kPa, indicating prediction errors of 6.25%, 3.86% and 21.25% respectively for pipe tests 1, 2 and 3. These errors may arise from a number of factors, including the applicability of the model parameters, the model itself and any other internal defects that CI may have in its microstructure. Unfortunately, however, such internal defects cannot be detected and scanned by the current laser scanning technique.

Once a crack is initiated, for the next phase of pressuring up to a burst, fracture mechanics theory is used to determine the critical crack length that would generate a fast fracture across the rest of the corroded as well as the un-corroded section of the pipe. This is appropriate since, as the experiments show, a sharp crack is likely to be generated during initial failure, leading to leakage. Together with the principles of fracture mechanics and the numerical results of the tensile stresses, the burst pressures for the three pipes can be estimated (Zhang et al., 2017b), as listed in Table 3.7.

Table 3.7
Approximate values of measured and predicted leak and burst water pressures

Pipe test	burst	Leak pressure (kPa)		Burst pressure (kPa)	
		Measured	Predicted	Measured	Predicted
Pipe 1		~3200	~3000	N/A ¹	~3550
Pipe 2		~1290	~1240	~1440	~1300
Pipe 3		~800	~970	N/A ²	~1310

Note 1: exact burst pressure is not available as the single small volume pump used in the test was not sufficiently powerful enough to produce high pressure when water leaked quickly. As a result, the maximum recorded water pressure is 3700 kPa, at which the pipe burst had not yet occurred.

Note 2: the pipe was intentionally left unbroken for subsequent fatigue tests.

3.9.4 Conclusions

- Numerical analyses of a large number of CI pipe models have led to the proposal of the stress prediction model that is expressed in a closed-form equation.
- The model has been implemented in Monash Tool to provide guidance to conduct longitudinal failure analysis of pipe barrels with uniform corrosion or single remaining wall corrosion defects that are idealised into ellipsoids.
- The Monash Tool provides a deterministic approach to assess 1) nominal (hoop) tensile stress, 2) stress concentration factor (SCF) and maximum tensile stress for fracture initiation, 3) critical crack length for pipe burst, and 4) remaining life to initiation of local failure leading to a leak. In addition, the probability calculation of the pipe failure prediction and remaining life is also being incorporated.
- Another set of numerical analyses focussed on the study of the nonlinearity of corroded CI pipes, where a relatively simple hyperbolic constitutive model, as opposed to the complex elastoplastic models in the literature, has been developed and implemented in FE analysis.

- The hyperbolic model has been shown to allow much simpler and quicker numerical analysis with reasonably good accuracy, than the existing elastoplastic models.
- With appropriate scanning data of a naturally corroded CI pipe, the proposed numerical method with the hyperbolic model can be readily used for structural and mechanical analysis of pipes under various loading conditions.

More details can be found in the following publications: Ji et al. 2015a, Wong et al. 2016b, Wong et al. 2017a, Rathnayaka et al. 2016e, Shannon et al. 2016a.

3.10 PHYSICAL MODELLING FOR PREDICTION OF PROBABILITY OF FAILURE

3.10.1 Overview

CI pipes used as water trunk mains are subjected to many internal and external factors (Figure 3.23), which involve some uncertainties. Because of continuing deterioration, the probability of failure of these ageing CI pipes increases over time. In order to make prudent renewal decisions, it is necessary to quantify the lifetime probability of failure of critical pipes. Typically, the risk of failure is defined as the product of the probability of failure and the consequence of failure, as given in Equation [3.16]:

$$\text{Risk of failure (\$)} = \text{probability of failure} \times \text{consequence (\$)} \quad [3.16]$$

Activity 1 has progressed in identifying and categorising failure mechanisms and developing field- and laboratory-validated theoretical solutions to evaluate the stress states on CI pipes, taking into account the most important external/internal factors. On the other hand, Activity 3 has progressed in developing field-validated practical solutions to estimate corrosion in CI pipes. Combining these outcomes and the inherent uncertainty of input variables, Activity 4e has developed a methodology for evaluating the lifetime probability of failure of CI pipes and predicting the pipe remaining life (Section 2.10). This section introduces this methodology without reference to any condition assessment. Hence, it is relevant to conduct first pass analysis of critical pipelines prior to undertaking condition assessment.

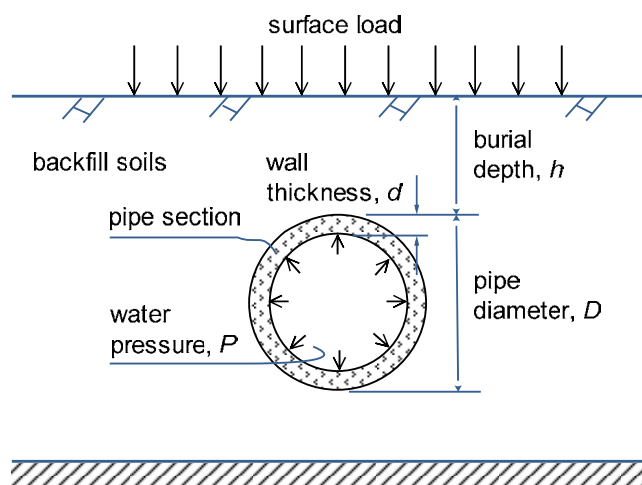


Figure 3.23. Simplified pipe burial conditions for water mains

3.10.2 Deterioration of Pipe Structural Capacity Due to Corrosion

The corrosion activity (internal and external) can manifest in various forms, but generally leads to a reduction in pipe thickness, thereby causing deterioration of the pipe structural capacity. On the basis of field evidence, the corrosion-induced thickness loss is idealised into two patterns: uniform corrosion and pitting corrosion. Uniform corrosion applies when there is an all-round reduction in pipe wall thickness, and pitting corrosion applies when there are localised corrosion patches or pits. Either may occur with or without the other. These idealised configurations are illustrated in Figure 3.24.

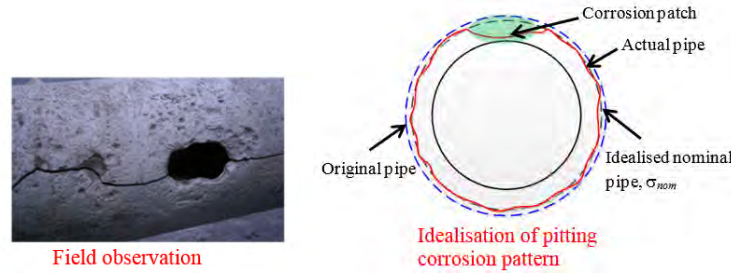


Figure 3.24. Configurations of corrosion in CI pipes

It is well recognised (from Activity 3) that the rate of corrosion is not constant but changes over time, featuring an initially high value and then reaching a steady state. In this study, a field-validated model developed from Activity 3 by Newcastle University is utilised. This model is described by:

$$\begin{cases} \tau(t) = c_s + r_s \times t, & \text{when } t \geq T^* \\ \tau(t) = (c_s / T^* + r_s) \times t, & \text{when } t < T^* \end{cases} \quad [3.17]$$

where $\tau(t)$ is corroded depth when pipe is aged t years, T^* is the transit point of time from where the corrosion rate approaches a steady state in equilibrium with the surrounding environment after an initially high value.

3.10.3 Prediction of Pipe Lifetime Probability of Failure

Based on FE analysis of stress concentrations of corrosion pits and laboratory/field validation, a predictive stress model for buried pipes has been derived from Activity 1. Details of these stress-based models regressed from FE analyses are referred to Section 3.9. Using the stress-based failure criterion, the *failure* or out-of-performance of CI pipes is defined as:

$$g(\mathbf{x}, t) = \sigma_y - \sigma_{nom}(\mathbf{x}, t) \cdot SCF(t) < 0 \quad [3.18]$$

where σ_y is the material failure stress, $\sigma_{nom}(\mathbf{x}, t)$ and $SCF(t)$ are nominal stress of the pipe due to uniform corrosion and stress concentration factor due to pitting/patch corrosion respectively, both being time-dependent variables, and \mathbf{x} denotes the vector of all relevant physical parameters.

When the physical parameter \mathbf{x} is appropriately assigned their statistical information, and pipe lifetime is discretised over the lifetime, the lifetime probability of failure is obtained following the procedure illustrated in Figure 3.25.

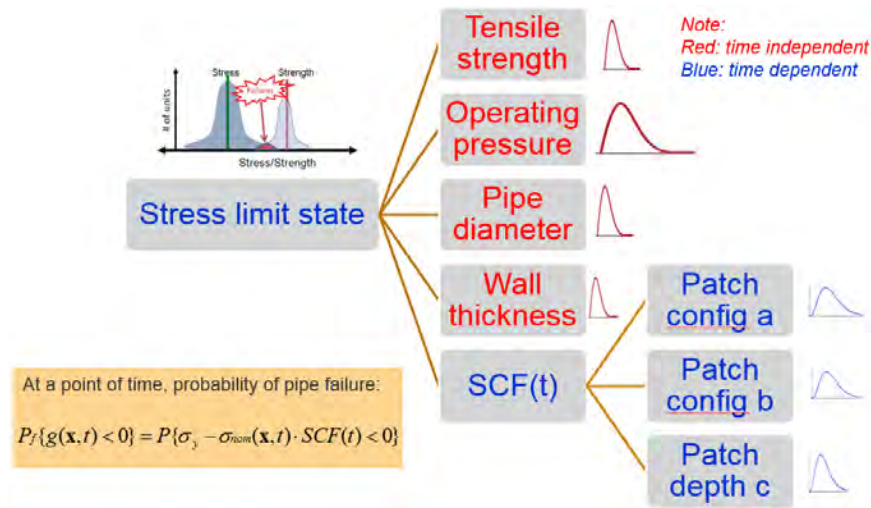


Figure 3.25. Concepts of prediction of lifetime probability of failure

Focusing specifically on Sydney Water utilities, typical results of cohort-based probability prediction are shown in Equation 3.19. These lifetime probabilities are regarded in time-to-failure reliability engineering as instantaneous failure probability $P_f(t)$. Over the lifetime, the cumulative distribution functions (CDF), $F(t)$ with respect to failure age/time t , can be estimated by

$$P_f(t) = f(t)/[1 - F(t)] \quad [3.19]$$

$$\text{or numerically, } F(t_{i+1}) = F(t_i) + P_f(t_i)[1 - F(t_i)] \quad [3.20]$$

where, $f(t)$ is the probability density function, which is the derivative of $F(t)$.

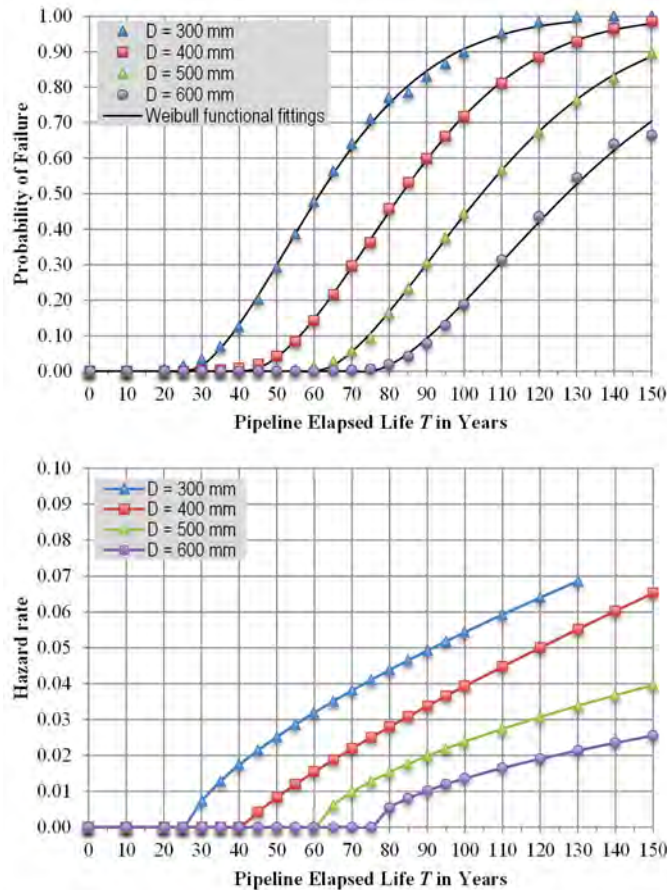
For the convenience of mathematical expression, the CDF can be analytically represented by fitting curves of the type of Weibull distribution:

$$F(t; \alpha, \beta) = 1 - e^{-((t-t_0)/\beta)^\alpha} \quad [3.21]$$

where, t_0 is the location parameter, α the shape parameter and β the scale parameter. Based on these expressions, the hazard rate function is readily inferred as

$$H(t; \alpha, \beta) = \frac{dF(t; \alpha, \beta)/dt}{1 - F(t; \alpha, \beta)} = \frac{\alpha}{\beta} \left(\frac{t-t_0}{\beta} \right)^{\alpha-1} e^{-((t-t_0)/\beta)^\alpha} \quad [3.22]$$

The best-fitted Weibull curves and hazard rate functions are also shown in Figure 3.26 with a coefficient of determinant r^2 of more than 0.99. Further definitions of these statistical functions can be found in Appendix Section 11.2.



Note: wall thickness linearly increases with pipe diameter
Figure 3.26. Lifetime probability of failure of CI pipes

3.10.4 Prediction of Failure Rate of Pipe Cohorts

The failure rate, in terms of number of failures per 100 km per year, is commonly recognised by water utilities as a basis for failure prediction for their assets. The hazard rate as obtained from probabilistic physical modelling, and statistical failure data analysis can be easily converted into this practically useful failure rate. Assuming statistical independence between pipe failures, the following relationship holds:

$$Q(t) = H(t) \times N_t \quad [3.23]$$

where, $Q(t)$ denotes failure rate, in units of number of failures per 100 km per year, $H(t)$ is hazard rate for a typical pipe (section), and N_t is the number of pipes (sections) for a 100-km cohort in a particular year t .

The Hunter Water failure data consists of a total of 832 CI pipe failures, with lengths varying from several metres up to 500 m. Some long pipes can experience multiple failures after repair. On average, each failure can happen on a typical length of 83 m. As a result, it is deemed that a 100-km cohort will roughly consist of $N_t = 1205$ such typically long pipes that are subject to risk of failure. This, in turn, is used to produce the predicted failure rate $Q(t)$, as shown in Figure 3.27(a) by the second vertical axis. Similarly, the predicted failure rate $Q(t)$ for Sydney Water is

shown in Figure 3.27(b). These curves are commonly referred to as “decay curves” in the water industry, but they are derived from statistical data only. The probabilistic physical modelling methodology developed in this report is capable of giving comparable prediction results by use of the physical mechanics and parameter variations. Hence, the prediction can be extended to any pipe cohorts.

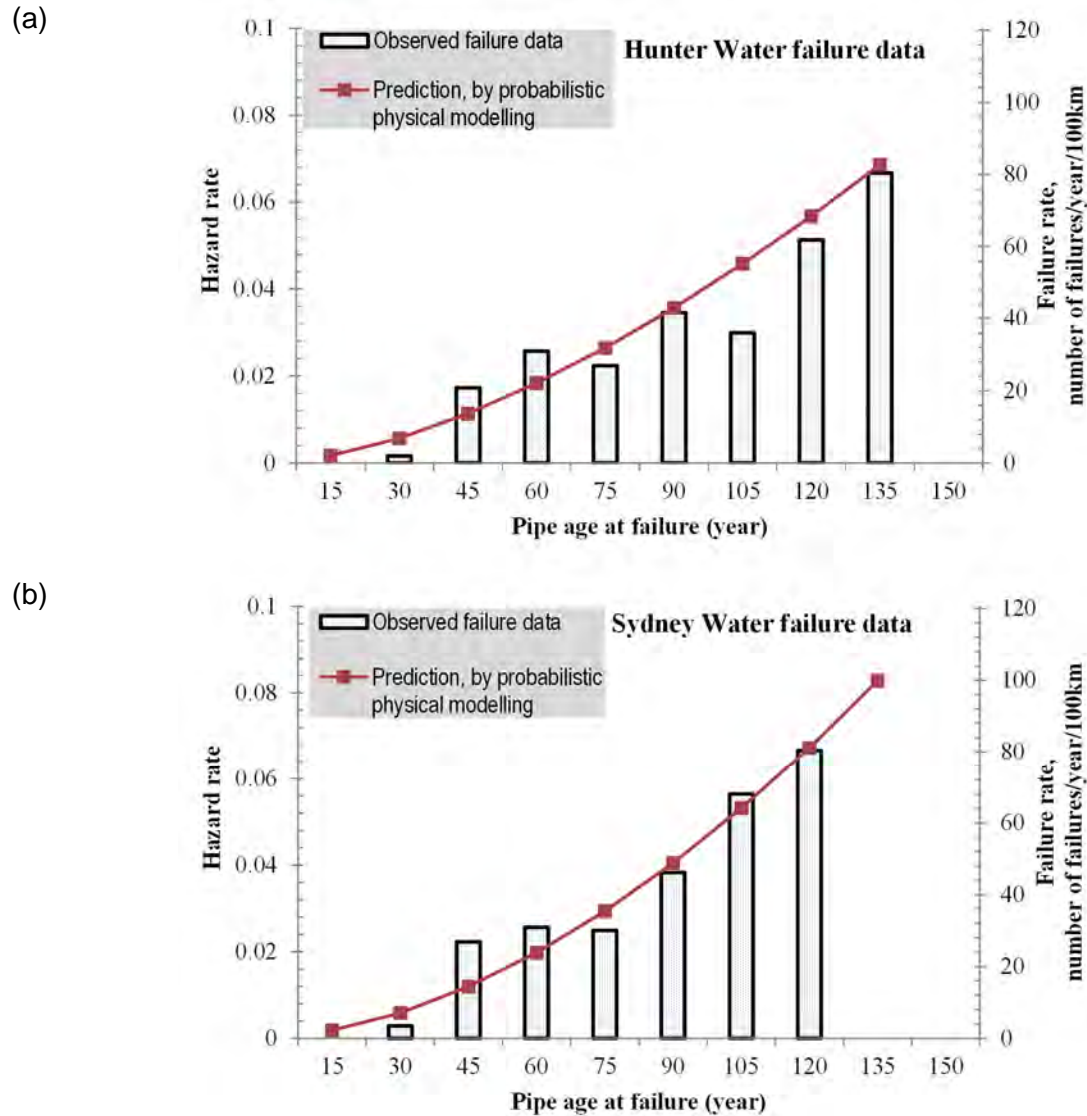


Figure 3.27. Failure rate of CI pipes derived from physical modelling

3.10.5 Summary

The quantification of the lifetime probability of corroded CI pipes is introduced in this section. It was found that:

- The probability of failure is greatly affected by the wall thickness, water pressure and corrosion rate. Therefore, these parameters need most attention for pipe barrel failure.

- Therefore, extra effort to determine the original wall thickness (or the class of the pipe) has definite advantages in failure prediction.
- The physical modelling results showed that the lifetime probability of failure follows a Weibull distribution, which was reasonably consistent with the observed failure data.
 - Once the failure rate (or “decay”) curves are calibrated, other scenarios such as pressure management and cathodic protection could also be simulated to extend to the remaining lives of CI pipes.
 - Monash Tool can also be used to evaluate pipe failure probability.

More details can be found in the following publications: Ji et al. 2015a, Ji et al. 2016, Wong et al. 2014.

3.11 DISTRIBUTED OPTICAL FIBRE SENSORS

3.11.1 Introduction

Pipeline structural health monitoring is a tool that assists the realisation of pro-active pipeline failure management. The implementation of the assessment tool can ideally provide information about where, when and how the water pipeline will fail. Its goal is to provide information on the pipeline’s integrity, which can then be used to manage the repair and maintenance of pipes. It has been estimated that Australia spends \$1.4 billion annually on reactive repairs and maintenance of its water mains (OAG, 2014). It is also predicted that the cost could be reduced by 50% if the repairs were done proactively instead of reactively (Vitanage and Zhang, 2014).

Most non-destructive evaluation (NDE) methods, such as magnetic flux, acoustic emission, radiography, ultrasonics and eddy current, have been developed to detect and monitor the structural health of pipelines. These methods are very useful for monitoring localised situations. However, many of these methods do not provide continuous and real-time monitoring. They may also suffer from distinct disadvantages, such as lack of portability, difficulty in installation over large and remote distances, and susceptibility to electromagnetic interference. In other words, none of the existing NDE methods are perfect. Therefore, new sensors and monitoring techniques are continuously being researched and developed in order to provide better solutions for pipeline structural health monitoring.

Over the past decades, distributed optical fibre sensors have demonstrated their potential for application to pipeline structural health monitoring. They are designed to measure strain or temperature, and can simultaneously make measurements at many points along the length of the fibre sensor. This is a very favourable feature, as much pipeline structural health information is reflected in terms of the strain and temperature distributed along the pipeline and its surroundings. The fibre sensors are made from silica, which makes them immune to many chemical attacks and therefore suitable for use in highly corrosive environments. Their chemical inertness also suggest that they do not react with the host structure and compromise its integrity.

Distributed optical fibre sensors are also very robust, allowing for use in very low temperature environments like tundras or high temperature environments like deserts. Their small packaging and light weight makes the footprint on the structure small and they add negligible extra weight. Their measurement length can also go up to a hundred kilometres, which is of the order of the length of pipelines. They can also complete kilometres worth of measurements in a matter of minutes, allowing thousands of measurements to be easily obtained. Common optical fibre cables

which are easily sourced can also be used as sensors. This lowers overall costs and allows them to be left in the field, as they do not cost much to replace if damaged. Therefore, distributed fibre optic sensors have the potential to be used for pipeline structural health monitoring. They could be installed on new pipelines so that the pipelines are intelligent enough to provide information on their structural health and any warnings of inhomogeneities or an abnormal environment that can lead to reduction of the lifespan of the pipelines. These pipelines can be called “smart” pipelines.

However, this technology is still relatively new for monitoring pipeline structural health and there are still many areas where research is required before field deployment. The contributions of the Critical Pipelines Project are (1) to show the accuracy of distributed sensing, (2) to show the ability to detect localised anomalies, (3) the ability to use the distributed optical fibre sensors for pressure transient monitoring, (4) to investigate the durability of distributed sensors by performing fatigue testing and (5) to investigate the response of the system when deployed on different pipe materials (flexible and rigid pipes). The research outcomes of using distributed optical fibre sensors for pipeline structural health monitoring have been documented and summarised.

3.11.2 Accuracy of Distributed Optical Fibre Sensors

The accuracy of distributed optical fibre sensors was studied on a cantilever. Strain gauges were instrumented on the cantilever to validate the distributed optical fibre sensors. A cantilever was chosen, because the strain profile of a cantilever loaded at the free end can be theoretically calculated and therefore used as another form of validation. The distributed sensor was continuously bonded to the cantilever with Loctite 406 adhesive. A bare single mode fibre was used as the sensor head of choice. The distributed strains measured in two different spatial resolutions (100 mm and 5 mm) were compared with theoretical solutions and strain gauge measurements as shown in Figure 3.28. It was found that the strain measurements made by distributed optical fibre sensors showed good agreement with those made by the strain gauges and theoretical calculation when the cantilever was loaded at the free end. This validated the distributed optical fibre sensor measurement technique.

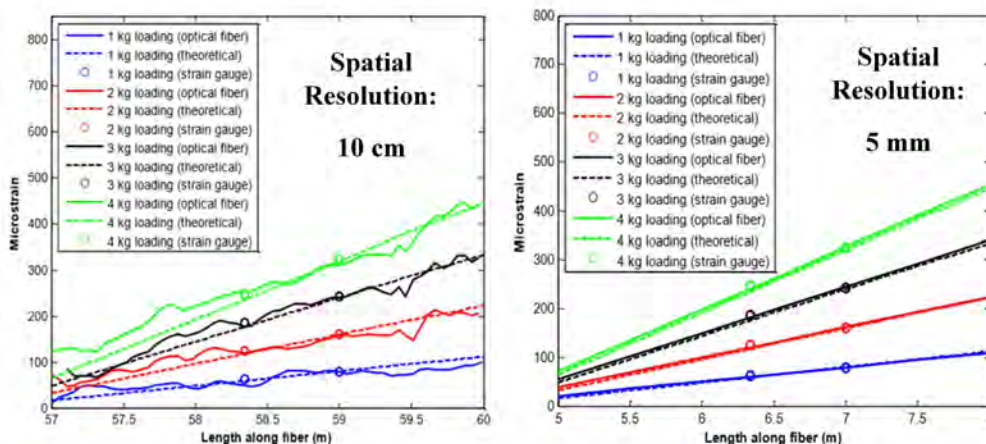


Figure 3.28. Comparison of distributed optical fibre sensors of different spatial resolutions with theoretical solution as well as strain gauge measurements

To show the ability to monitor the dynamic strain response of a structure, the distributed optical fibre sensors were bonded to a structure. The prepared specimen was set up on an INSTRON 100kN testing machine. The specimen was subjected to a tension-tension fatigue loading with peak strain of $2000 \mu\epsilon$ and R-ratio of 0.1. The fatigue test was conducted at a frequency of 5 Hz with a sinusoidal waveform and an extensometer was used to correlate strain to load. In the experiment, the distributed optical fibre sensors were sampled at 17 Hz. The strain measured at the centre point of the bonded fibre was displayed over a period of 4 seconds as shown in Figure 3.29(a). The measured strain shows a sinusoidal waveform with maximum and minimum strain recorded at approximately $2000 \mu\epsilon$ and $200 \mu\epsilon$, respectively. A Fast Fourier Transform (FFT) was performed on the time series and the result is shown in Figure 3.29(b). The cyclic frequency was calculated to be 5.11 Hz. The results clearly show that the strain measured by distributed optical fibre sensor corresponds to the fatigue loading profile whilst also providing real-time structural health monitoring capability. The potential for using this high-speed distributed optical fibre sensor to monitor the dynamic strain response along the length of the test specimen is evident.

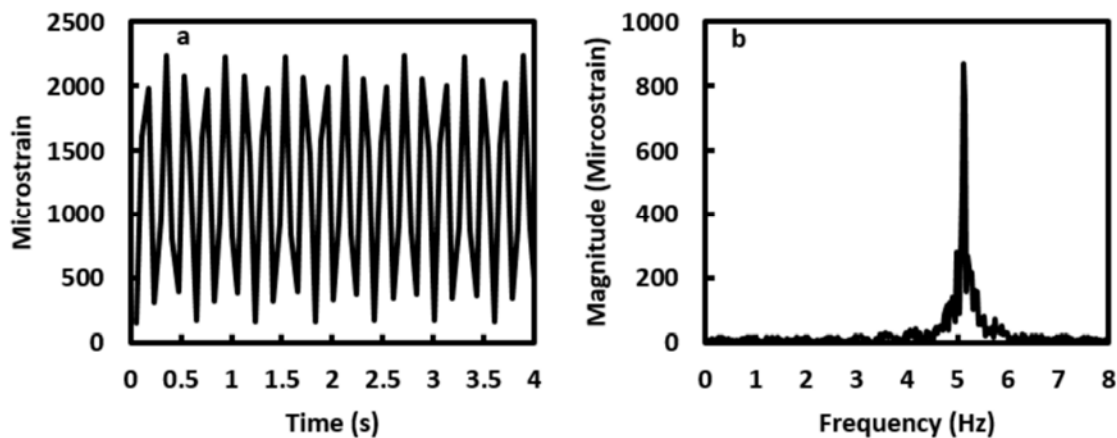


Figure 3.29. (a) Time series (4s) of strain measurement at $2000\mu\epsilon$ loading regime, and (b) Fast Fourier Transform (FFT) of time series

3.11.3 Pressure Transient Monitoring

According to the research literature, most studies show that distributed optical fibre sensors are very effective for static and quasi-static measurements and can be used for monitoring the condition of a pipeline. However, there is still a lack of research using distributed optical fibre sensors to monitor the dynamic response of pipelines. It is well known that pressure transients (water hammer) can occur in any pressurised pipeline system due to changes in the operating conditions. In addition, pressure transient responses can provide useful information to detect and monitor pipe condition.

The ability to use distributed optical fibre sensors to monitor pressure transients was demonstrated under laboratory conditions. Distributed optical fibre sensors were instrumented on a long small diameter pipeline subjected to pressure transients. The transient pressures were introduced into the experimental set-up by changing the operating conditions (valve closure and starting up the pump). The distributed optical fibre sensors were used to measure the dynamic response of the pipeline at a frequency of 100 Hz. The distributed strain response is shown in

Figure 3.30. A detailed picture at the strain measured (time series) by the distributed optical fibre sensor during these transient events at a given location (Section B-B in Figure 3.30) is shown in Figure 3.31. The results show that distributed optical sensing can provide continuous and real-time monitoring of pipes subjected to different transient events caused by the operation of valves and pumps.

To validate the dynamic response, the distributed optical fibre sensors were compared with the information collected by the pressure transducer, as shown in Figure 3.32(a). The results validate the distributed optical fibre sensor dynamic measurement technique. Multiple sets of the transient events were repeated to show that the experiment was repeatable (see Figure 3.32(b)). Distributed optical fibre sensors are not only able to monitor the pressure transient profile, but they are also able to monitor the distributed strain response along the pipeline due to pressure transients. Figure 3.33 shows that distributed optical fibre sensors can be used to detect the presence of localised damage along the pipe and the localised damage would be accentuated during pressure transient events.

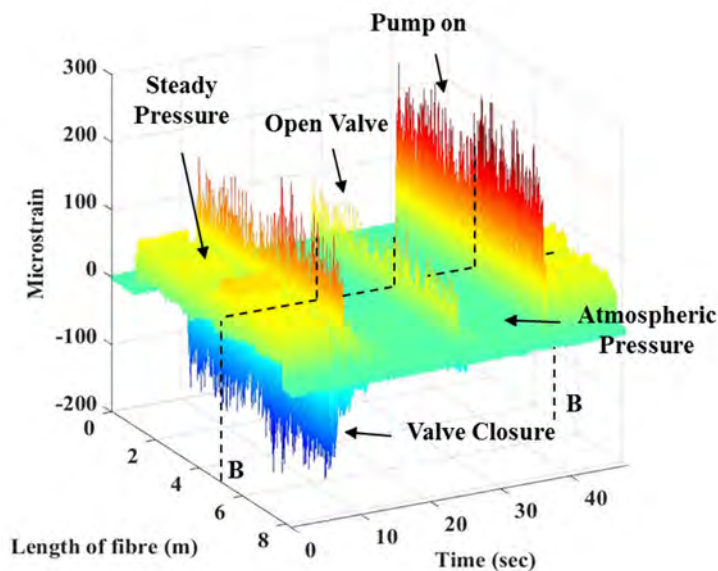


Figure 3.30. Distributed strain measured during transient events (due to valve closure and turning on the pump)

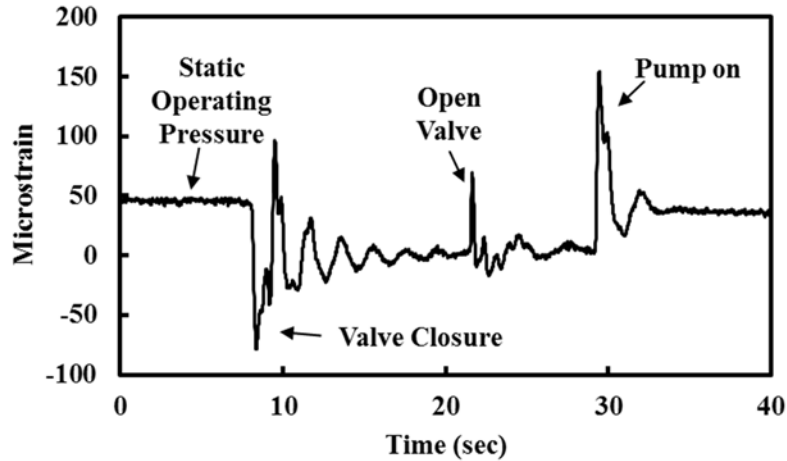


Figure 3.31. Dynamic strain response (time series) measured at section B-B in Figure 3.30

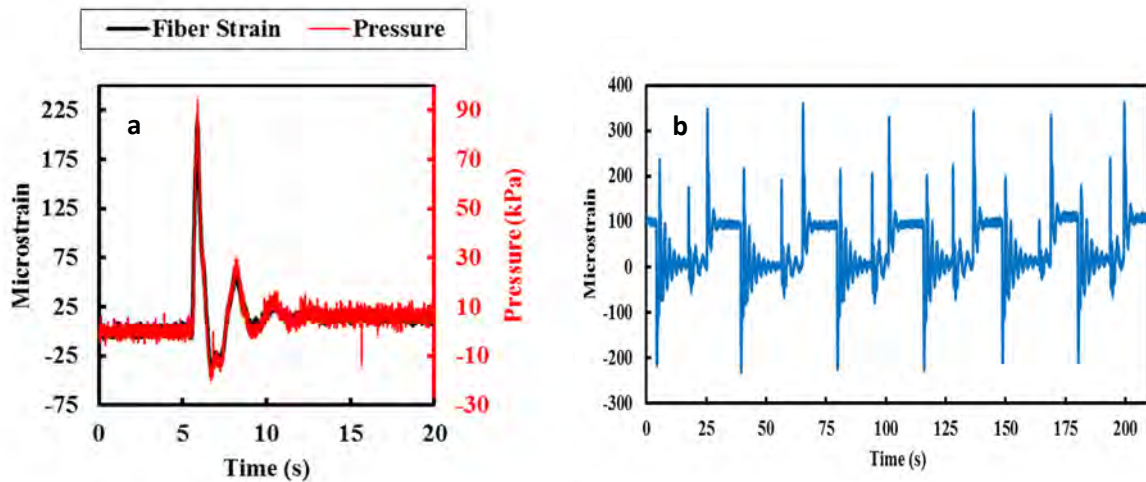


Figure 3.32. (a) Comparison between the dynamic strain measurement with pressure profile measured by pressure transducer during a pressure transient event (due to operating pump), and (b) dynamic strain measurement at location B-B when subjected to multiple sets of pressure transient events

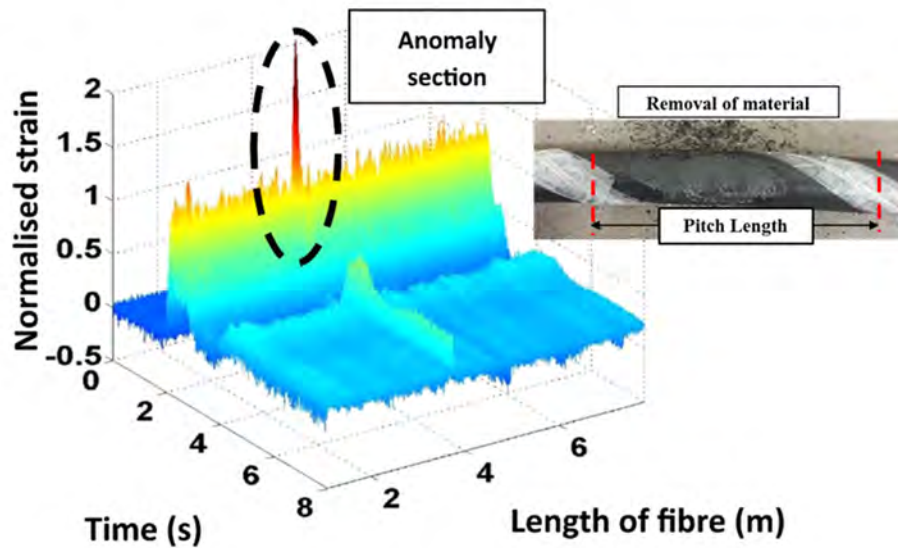


Figure 3.33. Dynamic strain measurement along the monitored pipe with the presence of localised damage

3.11.4 Fatigue Damage Monitoring

Distributed optical fibre sensors were bonded along a specimen that was subjected to fatigue testing using an INSTRON 100kN testing machine. The experiment aimed to show the ability of the distributed optical fibre strain sensors to perform continuous real-time monitoring of fatigue crack growth along the host structure. Figure 3.34 shows the strain measurement at a point along the distributed optical fibre sensors. The result demonstrates the long-term durability, stability and reliability of distributed optical fibre sensors. The failure of the specimen occurred after 254,362 cycles in the fatigue loading test. As highlighted by the dotted region in Figure 3.34, the strain gradually changes in the last 3500 cycles before failure occurs. The results demonstrate the ability of the distributed strain measurement technique for the in-situ monitoring of damage along monitored structures (Wong et al., 2016a).

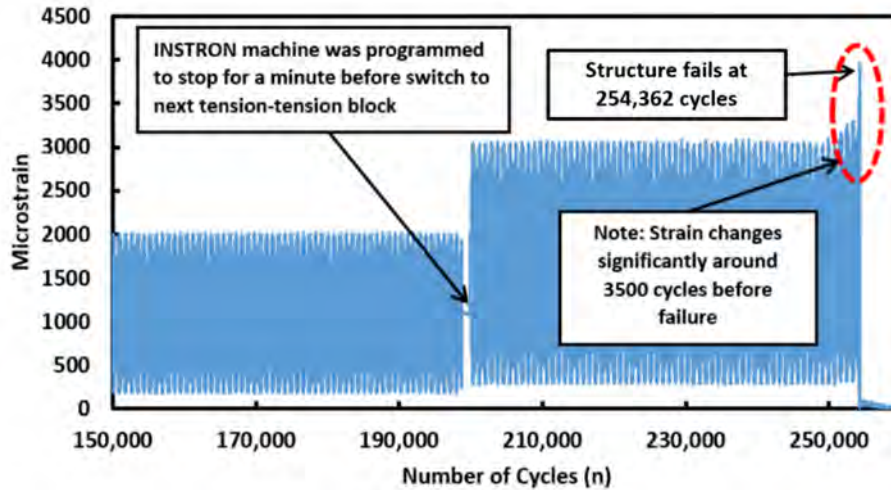


Figure 3.34. Strain measurement at a point along the distributed optical fibre sensor vs. number of cycles

Distributed optical fibre sensors were also used on CI pipe subjected to fatigue internal loading. Figure 3.35 shows the strain measurement along one of the bonded fibres in the hoop direction around a CI pipe with artificial damage. The result show that the measured strain changes significantly as the crack propagates due to fatigue towards the fibre in the last 200 cycles. It was found that the fibre sensor can only detect the change in strain when the distance between the crack tips and the fibre is less than 40 mm. The findings show that the orientation of the deployed fibre is an important parameter, which may depend on the desired detectable damage size.

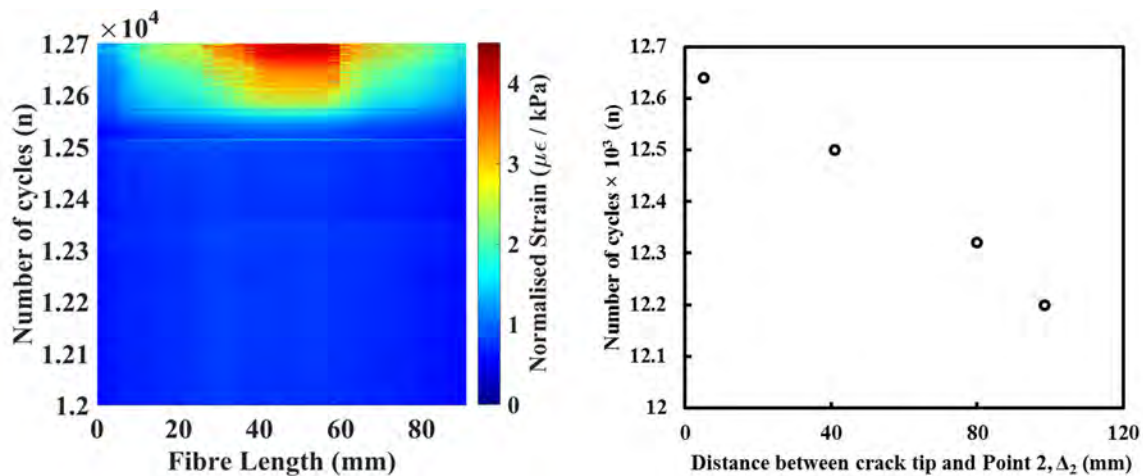


Figure 3.35. Fatigue crack growth monitoring using distributed optical fibre sensors

3.11.5 Summary of Optical Fibre Studies

- The concept of smart pipes for new pipes where fibre optic sensors are deployed to provide information on pipe condition continually was introduced with some proof-of-concept testing.
- Validation: The strain measured by distributed optical fibre sensors corresponded to the fatigue loading profile accurately, whilst also providing real-time structural health

- monitoring capabilities. The durability and dynamic strain response along the length of the test specimen was evident from testing.
- Transient monitoring. The distributed strain responses due to pressure transients were monitored accurately using distributed optical fibre sensors. However, more robust sensing arrangements are necessary for buried pipe line deployments. A concerted research project is needed in this area.
 - Detection of anomalies. The presence of localised damage along the pipe and the features of localised damage are accentuated during pressure transient events recorded by the fibres. This provides evidence that a suitable fibre optic sensor can detect local damage in buried CI pipelines.

More details can be found in the following publications: Rajeev et al. 2013a, Lim et al. 2016, Wong et al. 2016a, Rathnayaka et al. 2016d, Zhang et al. 2017b, Rathnayaka et al. 2013, Shannon et al. 2016c.

3.12 CONCLUSIONS

The results of the Advanced Condition Assessment and Pipe Failure Prediction Project Activity 1 and 2 are given in this document. The Activities are based on historical pipe failure information, pipe traffic loading tests, pressure transient modelling, cohort properties, large diameter burst tests, fatigue mechanisms, finite element modelling, physical modelling for the prediction of failure, and distributed optical fibre sensors. Each section provides final findings, which may be of benefit to our water utility partners who still use a high percentage of CI pipes as water mains.

The major findings of the project are as follows:

- Based on the historical data, corrosion was considered to be the main cause of failure, but it may need to qualify that this is mainly true for pipe barrel. During the project, some case studies were encountered of joint failures, where not much corrosion was evident. However, significant contributions of other factors, such as pressure transients and traffic load, are also evident.
- The pipe strains generated by internal water pressure are about six times bigger than that generated by traffic loads. This highlights the relative importance of these two factors.
- Severe pressure transients from multiple start-ups, shut-downs or automated controls are a major concern for pipe bursting.
- Routine pressure transients do not provide an immediate risk of pipe failure.
- Main sites found to be vulnerable for high-pressure transients are: downstream of main and booster pump stations, upstream and downstream of automated control valves, and reticulation networks that are in close proximity to pump stations and control valves.
- In cohorting CI water mains, the pipe diameter, wall thickness, cement lining condition, pipe coating, and material tensile strength are keys to distinguish the cohort.
- Flaws in the tested cohort pipe samples significantly reduced the material strength.
- For large-diameter CI pipes, a large corrosion patch with significantly deep corrosion that is leaking is needed, along with sufficiently high internal water pressures, before longitudinal splitting occurs.

- Condition assessment for large diameter pipes likely to burst should focus upon locating large corrosion patches running along the pipe with low remaining wall thickness (>80% corrosion depth), rather than small pits with minimum remaining wall thickness.
- It was established that cast iron pipe failures mainly follow Leak Before Break concept, introduced in this project. Hence, leaks can be monitored for condition assessment and possible failure prevention.
- The fatigue damage is severe when the maximum pipe stress is over 90% of material tensile strength. Fatigue analysis is required when the maximum stress is higher than 65% of material tensile strength, and can be neglected if the maximum stress is less than 50% of material tensile strength in CI pipe barrels.
- CI pipelines that experience transient pressures or frequent burst/refill events may be more likely to be influenced by fatigue damage.
- In order to reduce fatigue damage, operational transients should be reduced or dissipated, and dramatic pressure changes need to be controlled.
- The Monash Tool (MT) was created from longitudinal failure analysis of pipe barrels with uniform corrosion or single remaining wall corrosion defects that are idealised into ellipsoids to provide a deterministic approach.
- The MT assesses 1) nominal (hoop) tensile stress, 2) stress concentration factor (SCF) and maximum tensile stress for fracture initiation, 3) critical crack length for pipe burst, and 4) remaining life to initiation of local failure leading to a leak. In addition, the probability calculation of pipe failure prediction and remaining life are also incorporated.
- With appropriate scanning data of a naturally corroded CI pipe, the proposed numerical method with the hyperbolic model can be readily used for structural and mechanical analysis of pipes under various loading conditions.
- Failure probability is greatly affected by the wall thickness, water pressure and corrosion rate.
- The physical modelling results show that the lifetime probability of failure follows a Weibull distribution, and they are reasonably consistent with the observed failure data.
- Optical fibres are validated as a tool to: 1) measure pressure transients, 2) detect pipe anomalies during pressure transient events and 3) monitor fatigue damage in pipes.

PART 2
**ACTIVITIES 2 AND 4A – RESEARCH ACTIVITIES INTO DIRECT
CONDITION ASSESSMENT TECHNOLOGIES AND “ALONG-THE-
PIPE” FRAMEWORK FOR CONDITION ASSESSMENT OF CICL
CRITICAL WATER MAINS**

Project Team (UTS):

Professor Gamini Dissanayake
A/Professor Jaime Valls Miro
A/Professor Sarath Kodagoda
Dr. Alen Alempijevic
Dr. Teresa Vidal-Calleja
Dr. Buddhi Wijerathna
Dr. Nalika Ulapane
Dr. Lei Shi

4 ACTIVITY 2 AND 4E SUMMARY

This report compiles the outcomes from the research activities related to direct condition assessment (CA) tools and an “along-the-pipe” framework for CA led by UTS as part of the ACAPFP project.

The goal of this work was first and foremost to advance the understanding of some of the most widely used technologies currently employed for the CA of critical cast iron (CI) pipes, so as to appreciate their strengths and weaknesses based on their scientific principles of operation, and to investigate their suitability for utilities to better manage their pipeline assets. Moreover, the project was also scoped with the aim to improve the interpretations of the signals acquired by CA tools employed by the water industry utilising modern machine learning algorithms to better capture pipeline wall geometries and reduce, or at the very least quantify, the uncertainty associated to CA interpretations. As such this activity was progressed in partnership with four commercial service providers of different technologies, although the findings are generic to the underlying techniques based on Magnetic Flux Leakage (MFL), Pulsed Eddy Currents (PEC), Remote Field Eddy Currents (RFEC) and acoustic wave propagation.

The UTS team was also tasked with engaging trials of “upcoming technologies,” meaning direct condition assessment techniques developed in more recent times and thus with less market uptake, so as to provide guidelines to asset managers about their abilities under common application scenarios. The technologies are all described as “screening” in that they don’t provide detailed descriptions of pipe geometries but low-resolution indications of the coarse status of a pipe. The technologies tested include pressure wave propagation (PCA-Echologics ePulse™ and Detection Services p-CATTM) and Magnetoelastic sensing (Pure Technologies’ SmartBall® EM PWA).

In addition, a major research effort was undertaken to produce an “along-the-pipe” CA framework whereby predictions about likely remaining pipe thickness geometries at unseen locations are made from limited local inspections.

Recommendations on currently available CA tools studied presented in this report are based on present and future suitability of these towards two of the key contributions of the outcomes of the ACAPFP project:

- the needs of the new models proposed for pipe failure analysis, that requires a thickness map to ascertain the size of the corrosion patches; and
- the needs of the new framework proposed for “along-the-pipe” CA, that requires thickness maps of locally excavated inspections and can further benefit from a screening tool capable of producing average condition of the pipe along its length.

It was found that currently available pulsed eddy current based techniques are able to produce thickness maps that are suitable for failure analysis and the proposed “along-the-pipe” CA prediction framework. Commercial providers of Magnetic Flux Leakage (MFL) and Remote Field Eddy Currents (RFEC) based CA tool currently provide pit depth information only, although data gathered from the sensors contain sufficient information to produce thickness maps. Acoustic technologies evaluated in this project were found to be unsuitable for assessing large diameter cement lined cast iron pipes for identification of patch corrosion or preparation of thickness maps for the tested pipe.

UTS research team has developed algorithms that will make it possible to generate thickness maps from the data acquired by tools based on MFL and RFEC. UTS team has also developed and implemented a data interpretation algorithm to process information from PEC sensors and produce more accurate pipe thickness readings. Furthermore, UTS algorithms can produce readings in real-time as opposed to the relatively long process currently employed by the commercial provider of the PEC technology engaged as research partner.

UTS research outcomes have been communicated to the technology providers who were engaged as research partners. Some of the research has also been published in scientific journals and conferences. Our understanding is that some commercial providers are in the process of incorporating the learning from ACAPFP project into their condition assessment tools.

Of the screening tools evaluated our study has confirmed that signals cannot be analysed to capture continuous thickness maps with detailed geometries and are therefore unsuitable for pipe failure analysis. Given the notable challenge in validating quantities that represent average pipe conditions (in general over 10's or 100's of meters), the project has not been able to ascertain the accuracy of the screening technique studied in probabilistically significant terms.

Extensive research on a framework for “along-the-pipe” interpretations resulted in a suite of software that uses a data-driven statistical model aimed at enriching the information gathered from local inspections. It can take into consideration input from screening tools and/or prior knowledge about the pipe and produces the probability of extreme values in terms of remaining wall thickness and corrosion patch sizes.

4.1 SCOPE

The project is concerned with Critical Water Mains, and has focused on cast iron cement lined (CICL) pipes of sizes > 350mm diameter. The project's aims are:

- Understanding the capabilities in the field of most prevalent CA technologies.
- Enhancement to the raw data interpretation process (i.e., no sensor redesign).
- Development of a framework for “along-the-pipe” interpretations from limited inspections.

In addition, latest results from our colleagues working in this project on pipe failure analysis indicate that over and above pit depths, as traditionally provided to utilities by CA vendors in their inspection reports, the geometry of large corrosion patches are important in failure prediction. This report aims to convey our views about the suitability of the techniques in that regard, both as they stand today but also their potential to be able to provide that information in the future given the acquired signals.

Moreover, given the input needs for an effective “along-the-pipe” CA framework, this report also aims to discuss the suitability of the various CA techniques for that purpose.

This Part of the report compiles the outcomes of the activities referred to as 2, 4a and 4d in the original “Advanced Condition Assessment and Pipe Failure Prediction” project proposal. The part is structured in three chapters:

- Chapter 4 includes a summary of the activities.
- Chapter 5 includes all the information related to the various technologies studied.
- Chapter 6 describes the “along-the-pipe” framework.

4.2 TEST BED AND VERIFICATION

In order to collect data from all the CA technologies studied for the research program, Sydney Water provided a unique live CICL test bed to the project, where provisions were made for pig intrusions and excavations. The test bed has been decommissioned and is therefore no longer part of Sydney Water’s live network. A connection point to an adjacent 600mm water main and various scour valves and hydrants allow for the pipeline to be charged and pressurised as needed. The test bed is 1.5 km, although most inspections and exhumations were carried out in the first contiguous 1 km starting at the charging point. A comprehensive pipe inspection program with strict guidelines for the providers was followed over the duration of the project, effectively carrying out six distinctive “trial” inspection periods, and sporadic inspections with “upcoming technologies.” A list of the extensive activities is collected in Table 4.1.

A longitudinal section of the test bed and a top-down view superimposed on a Google map is shown in Figure 4.1, where blue arrows indicate the location of pits where spot CA inspections were carried out (Figure 4.1).

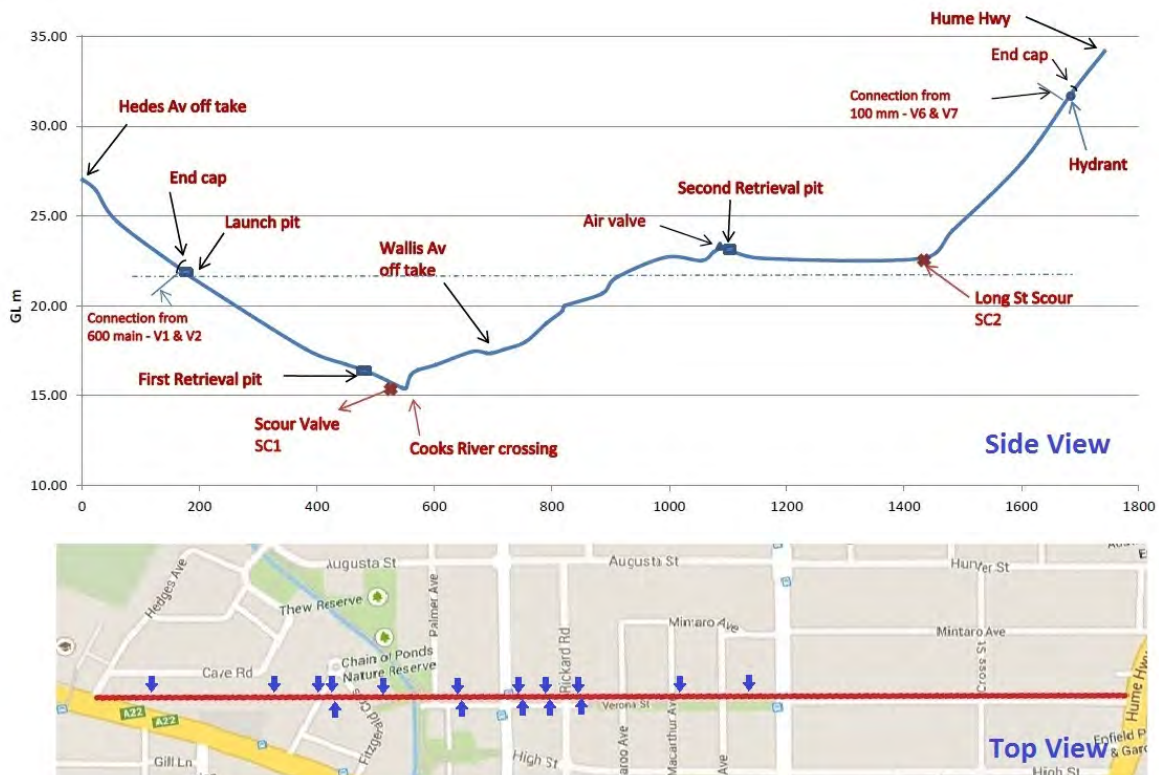


Figure 4.1. Project test bed provided by Sydney Water. Longitudinal section (above) and view on a map (bottom) with spot CA inspections shown in blue

Extensive pipe exhumation was carried out after each trial as a means to verify the condition of the pipe and validate the interpretations against accurate laser profilometry (“3D laser scanners”). All the replacements were made using DN600 Class 35 ductile iron cement lined pipe (DICL) and 600 ‘Vari-Gib’ (Gibault) couplings. Exhumation and ground-truth analysis was done after grit-blasting the CICL pipe sections to AS 1627.4 Class 2.5/NACE 2 standard. The extent of corrosion (remaining wall thickness) could then be measured to an accuracy of 0.8mm using the

methodology presented in Skinner et al. 2014. A user manual documenting the process to generate the ground-truth is one of the project deliverables to utilities – see Appendix Section 11.3.

Critical material property variations and their influence in CA interpretations of metallic pipes were also quantified. A document describing the expected variations and the various procedures readily available to attain the measurements is another deliverable to the utility partners – see Appendix Section 11.4.

Centimetre-accuracy high precision GPS surveying was also carried out by UTS on the test bed to build a 3D profile of the test bed pipeline to aid the research program. The spool level GIS information allowed the establishment of a reliable projection between in-pipe and above-ground locations. The methodology is presented in Shi et al. 2016a.

Table 4.1
List of test bed activities*

Date	Location	Technology Provider	Tool	Type
Jan-12	(Trial 1) Pit A, Pit B, Pit C	AIA / AESL	Smart-CAT™	Local inspection
Jan-12	(Trial 1) Pit A, Pit B, Pit C	Rock Solid Group	HSK BEM™	Local inspection
Feb-12	(Trial 1) Pit A, Pit B, Pit C	PCA-Echologics	RFT Mainscan™	Local inspection
Mar-12	(Trial 1) Pit A to Pit C	Russell NDE	SeeSnake	In-pipe
May-12	(Trial 1) Pit A to Pit C	Russell NDE	SeeSnake	In-pipe
	Pit A, Pit B, Pit C removed from the test bed			
Sep-12	(Trial 2) T2P1, T2P2, T2P3, T2P4, T2P5	AIA / AESL	Smart-CAT™	Local inspection
Sep-12	(Trial 2) T2P1, T2P2, T2P3, T2P4, T2P5	Rock Solid Group	HSK BEM™	Local inspection
	Trial 2 pits removed from the test bed for ground-truth generation			
Mar-13	(Trial 3) Pipe Seg. 1630, 1650	AIA / AESL	Smart-CAT™	Local inspection
Apr-13	(Trial 3) T3P1, T3P2, T3P3, T3P4, T3P5	AIA / AESL	Smart-CAT™	Local inspection
May-13	(Trial 3) T3P1, T3P2, T3P3, T3P4, T3P5	Rock Solid Group	HSK BEM™	Local inspection
	Trial 3 pits removed from the test bed for ground-truth generation			
Nov-13	(Trial 4) non-test bed-pipes	Rock Solid Group	HSK BEM™	Local inspection
Dec-13	(Trial 4) non-test bed-pipes	AIA / AESL	Smart-CAT™	Local inspection
Apr-14	(Trial 4) Pit A to Pit C	Pure Technologies	SaharaII® II PWA SaharaII® II EM PWA	In-pipe

(continued)

Table 4.1 Continued

Date	Location	Technology Provider	Tool	Type
Sep-14	(Trial 5) T5P1, T5P2, non-test bed-pipes	AIA / AESL	Smart-CAT™	Local inspection
Sep-14	Pit A to Pit C	PCA-Echologics	ePulse™	Acoustics Screening
Oct-14	(Trial 5) T5P1, T5P2, non-test bed-pipes	Rock Solid Group	HSK BEM™	Local inspection
Trial 5 pit 1 (2 segments) removed from the test bed for ground-truth generation				
Apr-15	Pit A to Pit C	Detection Services	p-CAT™	Acoustics Screening
Jul-15	Pit A to Pit C	Detection Services	p-CAT™	Acoustics Screening
Trial 6 pit 1 removed from the test bed for inspection and then ground-truth generation				
Aug-15	(Trial 6) T6P1, non-test bed-pipes	AIA / AESL	Smart-CAT™	Local inspection
Aug-15	(Trial 6) T6P1, non-test bed-pipes	Rock Solid Group	HSK BEM™	Local inspection
Aug-15	(Trial 6) T6P1, non-test bed-pipes	PCA-Echologics	RFT Mainscan™	Local inspection
Feb-16	Pit A to Pit C	Detection Services	p-CAT™	Acoustics Screening
Feb-16	Pit A to Pit C	Pure Technologies	SmartBall® EM PWA	In-pipe Screening
Sep-16	not on test bed	Detection Services	p-CAT™	Acoustics Screening

* Soil sampling trials, material properties test, GIS surveying trials, and UTS validation exercise trials on the test bed are not included in the table

More details can be found in the following publications: Valls Miro et al. 2013, Valls Miro et al. 2014, Skinner et al. 2014.

5 RESEARCH ACTIVITIES INTO CONDITION ASSESSMENT TECHNOLOGIES FOR CICL CRITICAL WATER MAINS

5.1 MAGNETIC FLUX LEAKAGE (MFL) TECHNOLOGY

5.1.1 Technical Description

During an inspection with a Magnetic Flux Leakage (MFL) tool, a sample of a ferromagnetic material is placed in a strong magnetic field. This magnetic field is typically generated using excitation coils wound in a “U” shaped yoke as shown in Figure 5.1. An appropriate strength of excitation is used to cause magnetic saturation in the material of interest leading to closely packed flux lines (marked “A” in Figure 5.1). When there is a change in remaining wall thickness due to a defect, the magnetic flux leaks out (marked as “B” in Figure 5.1). The leakage flux can be measured using a pickup coil or a Hall-effect sensor. The remaining wall thickness can be inferred from the strength of the leakage flux.

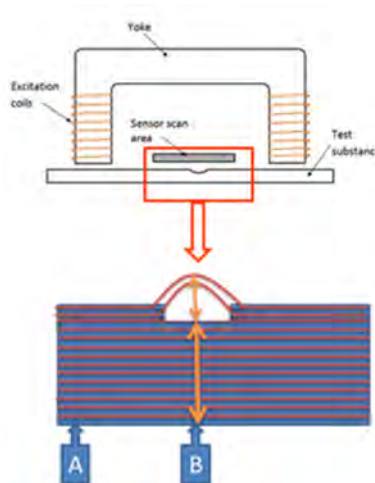


Figure 5.1. Leakage of magnetic flux due to a reduction in wall thickness in area ‘B’ is shown to illustrate the principle of operation of MFL. ‘A’ represents an area without any material losses due to corrosion

To use an MFL tool, the pipe outer surface needs to be exposed through digging, and preparation is required to remove any foreign materials. The tool frame needs to be setup in order to maintain a constant air gap throughout the scanning process as changes to air gap introduces errors in the interpretation. Small air gaps are preferable due to increasing power requirements with larger air gaps. It is also desirable to maintain a slow constant speed to minimise errors due to eddy current effects.

MFL tools measure leakage flux while in motion. Therefore, with an appropriate data interpretation, high resolution remaining wall thickness measurements in the longitudinal direction can be obtained. As Hall effect sensors can be placed close to each other, higher resolution in the circumferential direction can also be achieved. MFL providers generally restrict their analysis to areas of isolated pitting, rather than areas where pitting is embedded in general wall losses. In such situations, an accurate measurement of the remaining wall thickness can be obtained with

appropriate calibration. Nominal pipe thickness is an essential requirement. This is derived either from utility records or from spot measurements using ultrasonic (U/T) probes. Variation in the nominal pipe thickness can introduce errors in the MFL analysis. It is also important to make sure that the pipe material is correctly identified, for example whether it is cast iron or ductile iron. If this is not done, large errors could result. MFL injects high flux to saturate the material which can cause a residual flux in the testing material. Although the residual flux in the material diminishes with time, other magnetic-based CA technologies may be affected at ensuing inspections.

5.1.2 Observations during Trials

UTS engaged Asset Integrity Australasia Pty Ltd (AIA), a joint venture of Advanced Engineering Solutions Limited (UK) - with their Smart-CAT tool as a representative MFL device during the trial program. Cement lined pipe sections of 1 m long, 660 mm diameter gray cast iron from the test bed were inspected. The tool localization around the pipe was manually done while the location along the pipe was automatically determined using a sensor. It takes approximately three hours to completely inspect one meter of exposed 660 mm diameter pipe. In addition to readings from the MFL tool, depending on the pipe diameter, AESL may take up to 120 ultrasonic measurements to provide details of wall thickness variations. AIA reports ten deepest isolated pits they found.



Figure 5.2. AIA Smart-CAT MFL tool used during the trials at Sydney Water test bed. This pipe was later grit blasted to remove corrosion products and its geometry was acquired using a laser scanning process as outlines in Appendix Section 11.3.

Inspected pipes were extracted, grit blasted and remaining wall thickness measured as described in the ground-truth generation document in Appendix Section 11.3 to provide ground truth for comparisons. UTS was able to estimate the remaining wall thickness of isolated 10 worst pits to an accuracy of 4.6 mm.

The impact of changes in the permeability of the pipe material present in the test bed on the thickness estimation was found to be not significant.

5.1.3 Recommendations

The MFL technology provider currently does not provide the shapes of corrosion patches or thickness maps as required by the failure analysis or “along-the-pipe” CA framework developed during ACAPFP project. UTS research has shown that the signals measured by MFL tools can be

processed to capture this information. Furthermore, as MFL measurements are continuous, it may be possible to recover thickness maps with a higher resolution than currently feasible with other technologies. Presently, the recommendation is therefore that utilities intending to use pipe CA using the tools developed by the ACAPFP project to request vendors to deliver shapes of corrosion patches and thickness maps as specified in this report.

It is important to note that algorithms used by technology providers for interpreting information from their tools are continuously evolving. It is, therefore, recommended that utilities develop a regime for validating reports provided by all technology providers. UTS has developed a methodology for this purpose which is explained in detail in the ground-truth generation document in Appendix Section 11.3.

5.1.4 Vendors of MFL Technology in the Market

There are several commercially available MFL inspection tools for CI pipes. A list of providers and relevant information gathered during this project has been compiled in Table 5.1.

Only a small number of vendors have tools that are capable of saturating thick CI pipes. Therefore, this is likely to be the most relevant factor influencing the selection of a provider.

5.1.5 Summary of UTS Research Outcomes

UTS conducted an extensive research program to analyse MFL technology and explore novel strategies for interpreting data from the Smart-CAT MFL tool.

1. New algorithm for interpreting MFL signals: UTS has developed a simulation of MFL tool behaviour based on finite element analysis. This was validated by comparing the model output to the response of the AIA/AESL's MFL. A data driven machine learning technique; Gaussian Process (GP) was developed (Valls Miro et al. 2013) to predict the remaining wall thickness (RWT) as well as its uncertainty from the readings gathered by the MFL tool. Predictions from the new algorithm were compared with the AESL/AIA reported results and the ground truth for eight 1 m long, 660 mm diameter gray cast iron cement lined pipe sections from the test bed. The UTS GP predictions showed better accuracy in terms of predicted pit depths. Although evaluations were limited to pipes on the test bed, the strategy developed is generic. The underlying methodology was demonstrated and explained in detail to an engineer from AIA. A comprehensive report and a specifically designed software module was delivered to AESL/AIA for evaluation and possible future use.
2. Algorithm for extracting ellipsoidal patches from MFL signals: Based on the finding that approximating corrosion patches with a best fitting ellipsoid can be used for failure prediction, feasibility of extracting ellipsoidal patch geometry directly from the MFL signal was investigated. An algorithm based on an optimization strategy (Skinner et al. 2014) was tested in simulation and appeared to be effective with this limited approach.
3. Thickness Maps from MFL signals: Research demonstrated that it is feasible to use readings from the MFL tool to generate thickness maps in a form suitable for both failure analysis and along-the-pipe CA framework. The algorithm developed was published in Valls Miro et al. 2014.
4. Industry take-up: As a result of the UTS developments, the AESL is collaborating with the Newcastle University in the UK to develop analytical algorithms that utilise

machine learning methodologies. AESL is also in the process of developing methods for sizing corrosion patches and estimating wall thickness maps. More details can be found in the following publications: Wijerathna et al. 2013, Wijerathna et al. 2015.

5.2 REMOTE FIELD EDDY CURRENT TECHNOLOGY

5.2.1 Technical Description

The Remote Field Eddy Current (RFEC) technology allows in-line inspection of ferromagnetic pipelines. Tools based on this technology are usually composed of an exciter coil and one or several receivers. The exciter coil, driven by a low frequency alternating current, generates an electromagnetic field as shown in Figure 5.3. A receiver located at a sufficient distance from the exciter is used to measure the remote field. When the electro-magnetic (EM) field flows through the pipe, the amplitude of the field is attenuated, and the phase is delayed. Thus, the measurement from the receiver can be used to infer the pipe wall thickness. RFEC measures the effective remaining pipe wall, independently of whether losses are external or internal. The most important property of the RFEC technology is that phase and log-amplitude show a linear relationship with the wall thickness. However, the fact that the EM field passes twice through the pipe's wall (double-through wall effect) needs to be considered when inferring the wall thickness from the measurements collected by the receiver. The measurement sensitivity reduces when the exciter coil is located at the joints where wall thickness is large. Thus, there is a small region in each spool where the inferred thickness may be inaccurate.

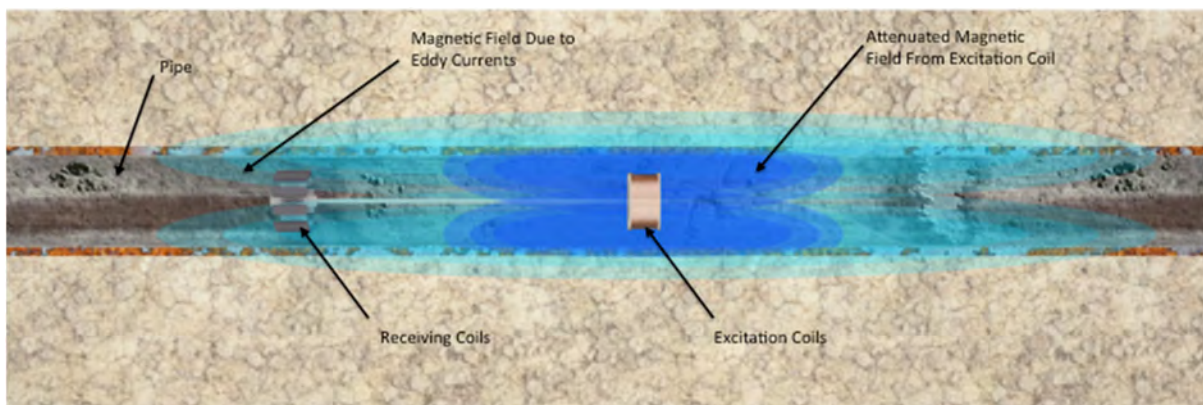


Figure 5.3. Schematic of a RFEC tool showing the path of the electro-magnetic field within a section of a pipe. The amplitude of the direct field is quickly attenuated by the induced Eddy currents flowing in the pipe wall; however, the field that has passed through the wall near the exciter is less attenuated, and is dominant in the remote field zone where it re-enters the pipe.

An in-line tool based on RFEC principles can inspect large sections of a pipeline in a relatively short time (3-4 hr/km). Depending on the diameter of the pipe the civil work required to insert the tool in the pipeline may be significant. In-line tools are commonly driven by the water flow or pulled through the pipe using a tether. Above-ground markers and/or verification steps through the identification of construction features (e.g., joints, elbows) together with encoders on the sensor or the tether are used to determine the location of the sensor measurement. Prior cleaning

of the pipe may be required to guarantee free-flowing of the tool, most notably for unlined CI pipes as often found in UK and North America.

The main advantage of REFC is that it does not require contact with the pipe although near proximity is necessary. RFEC tools can record continuous measurements and infer the thickness of the pipe in the longitudinal direction at a relatively high resolution. However, the number of sensing elements in the circumferential direction as well as the gap between the sensor and the pipe wall can affect the resolution of the technique. High resolution tools have hundreds of sensors; whereas low resolution tools have between 1-20 sensors. RFEC technology is sensitive to the change of material properties, in particular to the product of electrical conductivity and magnetic permeability, thus it is important to correctly identify the material under investigation.

5.2.2 Observations during Trials

Pipeline Inspection and Condition Analysis Corporation (PICA), majority owned by Russell NDE Systems Inc. was engaged with their in-line SeeSnake tool during the trial program carried out at the test bed. Two inspections of the test bed were carried out. Data collected during the first trial in March 2012, was not usable as the rate of flow was found to be outside recommended values. The analysis presented in this section is based on the inspection report provided by PICA in August 2012. CCTV data was collected separately prior to the deployment of the tool and used in the analysis of the inspection results reported. The SeeSnake tool used during the inspections is depicted in Figure 5.4.



Figure 5.4. PICA Corp SeeSnake tool deployed during the trials at Sydney Water test bed

PICA provides a comprehensive document with information collected from the pipeline. Most relevant information was an estimate of the condition of the pipe for each of the 275 spools present in the test bed. The average remaining wall thickness, the minimum and maximum circumferential thickness values and the minimum thickness of three of the worst local defects per spool were reported. PICA indicated that the localisation of the tool is usually within 1% of the length inspected; however, during this trial there was a discrepancy in measurements between the above-ground measurement and the distance recorded by odometers on board the Tool. UTS is of the view that the localisation error of the tool can be improved by combining encoder information with other sensors such as cameras.

A number of sections of the pipe of various length were extracted, grit blasted and remaining wall thickness measured as described in a previous section to provide ground truth for

comparisons. PICA and UTS collaborated to precisely correlate PICA raw data to some of the exhumed and grit blasted sections, using the signatures due to pipe joints and large defects as a guide. There was only one case where a large defect could not be correlated with the ground truth, possibly because it was located under the region of low sensitivity. Some of the 1m ground truth sections could not be exactly located within the raw data (at spool level) as there were no large defects present. Therefore, these sections could not be utilised for UTS' analysis.

From the exactly located sections, a total of seven defects had a match with PICA's data. Based on the reported interpretation of this data, the root mean square error of the minimum thickness point of the seven defects was 5mm. The largest discrepancy was found in the case of a small through-hole that was present in one of the pipe segments, where PICA reported a thickness of 11.8mm. It is probable that the small through hole was below PICA's threshold of detection; however, PICA did report the local defect where the hole was found in, as 44% wall loss. Given that PICA's sensors are approximately 50mm away from the inside of the pipe, it is not surprising that the small through hole was under-called.

As most of the exhumed pipe segments are only about 1m long, the evaluation of the reported average wall thickness of the full spools could only be done for two sections. The results show a root mean square error of 1.7 mm in the estimate of the average wall thickness. In the case of one pipe section the actual thickness was inside the reported min/max circumferential bounds and for the other section the actual thickness was outside these bounds.

5.2.3 Recommendations

PICA's implementation of RFEC currently provides relatively accurate minimum remaining wall thickness estimation of the most significant defects in each spool inspected. It does not provide the shape of corrosion patches or thickness maps as required by the failure analysis tool developed during the ACAPFP project. UTS research has shown using computer simulations that the signals captured by an RFEC Tool can be processed to enhance this information. As precise characteristics of the SeeSnake tool are not available to UTS, this finding has not been verified using experimental results. However, UTS is of the opinion that the RFEC signal measurements as obtained by the SeeSnake tool have the potential to recover the extension of the relevant defects as long as the double-through wall effect is properly considered during the signal analysis. Presently, recommendation is therefore that utilities intending to use pipe CA using the tools developed by ACAFPF project to request vendors to deliver shapes of corrosion patches or more complete information in the form of thickness maps as specified in this report.

5.2.4 Vendors of RFEC Technology in the Market

There are few commercially available RFEC pipe inspection tools. The list of providers and relevant information gathered during this project has been compiled in Table 5.1.

Only PICA Corporation (a subsidiary of Russell NDT Holdings Ltd.) has a tool offering inspections of large diameter thick CI pipes.

5.2.5 Summary of UTS Research Outcomes

UTS conducted an extensive research program to analyse RFEC technology and explore novel strategies for interpreting data from RFEC tools.

1. An algorithm to automatically detect construction features on Remote Field Eddy Current (RFEC) signals. UTS has developed, and shared with Russell NDE, a software package to automatically detect joints using raw data from the SeeSnake inspection on Sydney Water's Test bed in Strathfield. The algorithm was calibrated using data from the test bed inspection only and it may require modifications to be used in other inspections.
2. A new methodology to model RFEC phenomenon (direct and inverse models). UTS has proposed a methodology to model the RFEC phenomenon for 2D axisymmetric pipes. This model allows estimating pipe thickness along the axial direction. First, the parameters of a direct model are calibrated using realistic computer simulations. Later, a least squares optimisation algorithm is used to solve the inverse problem using the calibration from the direct model. This algorithm has the potential to recover thickness maps and its suitability was demonstrated using computer simulations.
3. New algorithm to reduce the effect of the double-through wall phenomena of the RFEC signal. UTS has designed an automated filtering process (called background removal) to account for the well-known double through wall effect of RFEC technology. The aim of this algorithm is to enhance the raw signal for further detection of large defects and for accurate interpretation of remaining wall thickness. The algorithm utilises the calibrated direct model above-mentioned to further remove the influence of the signal passing through wall at the emitter coil region with an optimisation algorithm using all the measurements available along the axial axis.
4. A new framework to automatically recover corrosion patches using RFEC signals. UTS developed the overall framework to detect and segment the most significant defect in a spool. This allows recovering the shape of the corrosion patches automatically from the RFEC signals. Firstly, the direct model needs to be calibrated (as per point 2). Secondly, the contribution of signal passing through the wall at the exciter location has to be removed (as per point 3). Finally, an algorithm for detection, classification and segmentation of the signal minima using signal processing algorithms is used to recover the corrosion patches shape.

All the developments of this methodology will be available as part of the PhD thesis related to RFEC, which is to be completed in 2017.

More details can be found in the following publications: Vidal-Calleja et al. 2014, Falque et al. 2014, Falque et al. 2015, Falque et al. 2016.

5.3 PULSE EDDY CURRENT TECHNOLOGY

5.3.1 Technical Description

A Pulsed eddy current (PEC) probe consists of two electromagnetically coupled coils (exciter and detector). The rising edge and the falling edge of a voltage pulse applied to the exciter coil generates eddy currents in the pipe wall (seen in yellow in Figure 5.5, right). Voltage induced in the detector coil due to the eddy currents is influenced by the volume and the electromagnetic properties of the metal in the vicinity of the sensor unit.

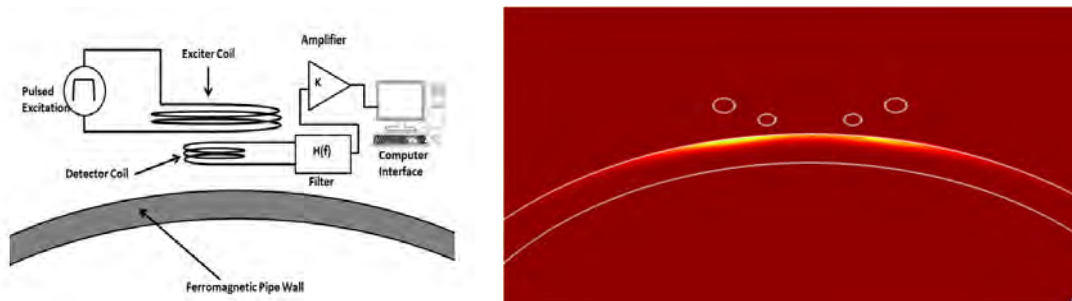


Figure 5.5. Typical sensor design and signal conditioning circuitry (left). Cross view of the PEC sensor coils sitting on top of a pipe. The top two larger circles represent the cross section of the exciter coil, while the bottom, smaller circles represent the detector coils. A cross section of the pipe wall is seen under the sensor, with the induced Eddy currents shown in yellow on the pipe wall (right).

The main strength of this technology is that once calibrated for a particular ferrous material, the average pipe wall thickness under a region of the sensor footprint (notionally the area under the detector coil) can be accurately estimated by analysing the decay of the eddy currents. Furthermore, the thickness estimates can be made largely insensitive to lift-off (i.e., the thickness of non-conducting and non-magnetic coating separating the sensor and the metal). This is advantageous in non-contact applications where the metal is covered by insulation, dirt or internal cement lining if the sensor is to be deployed as an in-line inspection apparatus.

Each measurement takes a finite amount of time as the measurement process involves pulsing the exciter and capturing the waveform of the induced voltage signal in the detector. Typically, the sensor remains stationary during each measurement.

Isolated pits covering an area smaller than the detector coil size cannot be detected as the sensor measures an average thickness of a region under the sensor footprint, unless multiple overlapping measurements are captured.

5.3.2 Observations during Trials

UTS engaged Rock Solid Group (RSG) with their HSK BEM™ kit and a single antenna 2-inch sensor as a representative PEC device during the trial program carried out at the test bed (Figure 5.6). Nine 1 m long, 660 mm diameter gray cast iron cement lined pipe sections from the test bed were inspected. Inspected pipes were extracted, grit blasted and remaining wall thickness measured as described in the ground-truth generation document in Appendix Section 11.3 to provide ground truth for comparisons. The tool was manually placed on a rectangular grid placed on the pipe wall and kept stationary for 30 seconds to take one wall thickness measurement. The resolution of the thickness map is 50 mm as the sensor footprint is a square of 2 inch (~50 mm) long sides. It takes approximately 7 hours to completely inspect one meter of exposed 660 mm diameter pipe.



Figure 5.6. RSG HSK PEC tool with a single antenna used during the trials at Sydney Water test bed

The accuracy of the pipe wall thickness estimated using the RSG single antenna sensor is 89% with a RMSE = 2.9 mm when compared to the ground truth. In the regions where there was a small through holes (approximately a tenth smaller than the receiver coil), the RSG single antenna sensor produced an average thickness measurement of 12 mm. Material property variation among the various pits excavated in the test bed was found to generate an error in the order of $\pm 5\%$. Analysis of material property on CI cohorts beyond the test bed generates an error in the order of $\pm 15\%$.

Limited experiments on the current RSG six-way antenna on a single CI pipe section indicated the average error for the six-way antenna is larger than single antenna sensor. RSG have been developing a new tool consisting of 8 way antenna designs, at the time of writing this report the tool has not been evaluated by UTS.

Lyft PEC tool from Eddyfi International LLC, typically used for steel, is motorised to move automatically and is able to take 1 measurement per second. Limited experiments on one exhumed CI pipe form the test bed indicated the Lyft tool, provided it was calibrated adequately, has similar performance to that of RSG single antenna sensor

5.3.3 Recommendations

Vendors of PEC technology examined are able to provide the shapes of corrosion patches or thickness maps as required by the failure analysis or “along-the-pipe” CA framework developed during ACAPFP project. However, the depth of pits reported is usually an underestimate due to the inherent averaging effect.

It is important to note that algorithms used by technology providers for interpreting information from their tools are continuously evolving. It is, therefore, recommended that utilities develop a regime for validating reports provided by all technology providers. UTS has developed a methodology for this purpose which is explained in detail in the ground-truth generation document in Appendix Section 11.3.

5.3.4 Vendors of PEC Technology in the Market

There are few commercially available PEC pipe inspection tools. The list of providers and relevant information gathered during this project has been compiled in Table 5.1 at the end of this Section.

5.3.5 Summary of UTS Research Outcomes

UTS conducted an extensive research program to analyse PEC technology and explore novel strategies for interpreting data from the RSG single antenna tool.

1. Novel Algorithm for interpreting PEC signals: UTS has identified a PEC signal feature based on the decay-rate which can be automatically extracted from noisy raw signals while being immune to changes in sensor lift-off and tilt. The feature is generic to the detector coil based PEC sensor architecture and is independent of sensor shape and size. UTS has developed algorithms to automatically estimate critical pipe wall thickness using the decay-rate feature that produces results almost instantaneously (estimate of thickness from the raw measurement in 16msec). Accuracy of the thickness estimates from the new algorithm is 92% with an RMSE = 2 mm when compared to the ground truth, in our case study which exploited the RSG single antenna two-inch sensor extensively on the Sydney Water test bed.
2. Strategy for improving the speed of measurement: UTS has developed a strategy to speed up PEC measurements by reducing the time per measurement to 100 msec, whereas RSG usually takes 30 seconds for a measurement. This is also faster than one second per measurement observed in tests with the Eddify Lyft tool.

More details can be found in the following publication: Ulapane et al. 2014.

5.4 PRESSURE WAVE PROPAGATION TECHNOLOGIES

5.4.1 Technical Description

Non-destructive pressure wave propagation inspection is based on the fact that the transmission of a transient pressure wave propagating in a water filled pipeline is affected by the characteristics of the pipe structure (joints, wall anomalies, etc) and its surroundings. Intuitively, the pressure wave causes the pipe to expand and contract, and thicker (thus stiffer) materials tend to flex less, allowing the signal to travel faster, so the remaining pipe wall can be inferred. Hence, by studying the propagation of a sudden transient pressure signal emitted from a given source (e.g., an acoustic exciter, or surge pressures that may accompany sudden changes in the rate of flow in a pipeline such as the start of a pump or the closing of a valve) as picked up by one or multiple pressure sensing devices (e.g., hydrophone receivers, or dynamic pressure transducers), information about the influence of the transmission medium can be inferred based on the physical principles of how the signal travels over it. A typical acoustic pressure signal is shown in Figure 5.7.

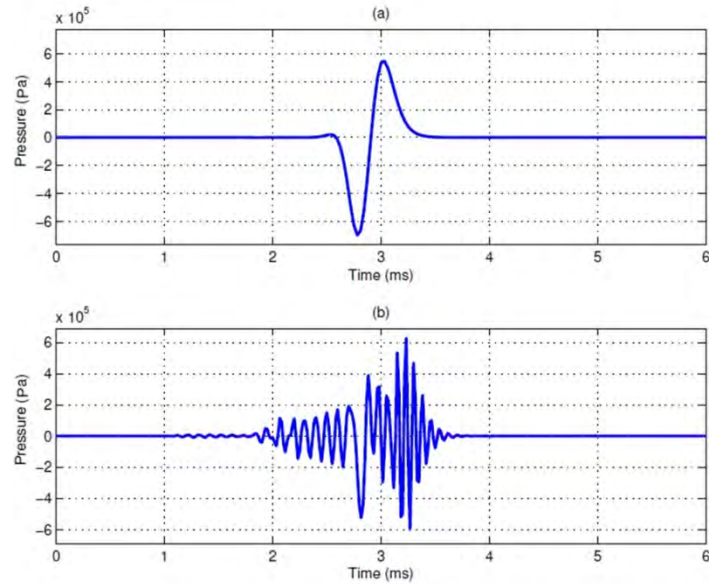


Figure 5.7. Typical acoustic pressure wave signal at the exciter (top) and receiver

Pressure wave propagation looks in one way or another at arrival time differences of the signal between emitter and receiver. As such, interpretations refer to “average quantities” of the pipe structure between measuring points, most notable pipe wall thickness, so longitudinal discrimination is coarse. Likewise, pressure wave propagation techniques are insensitive to features such as pitting defects, patch geometries, cracks, etc. No circumferential discrimination is possible. Pressure wave propagation tool providers do not report distinctive pipe wall losses and cement lining losses.

From a civil works standpoint, pressure wave based inspections are in general easier to deploy than other CA alternatives in the market: signal deployment and measurement is relatively straightforward, particularly for the external case. For the internal case, the extra cost of the related civil works needs to be taken into consideration.

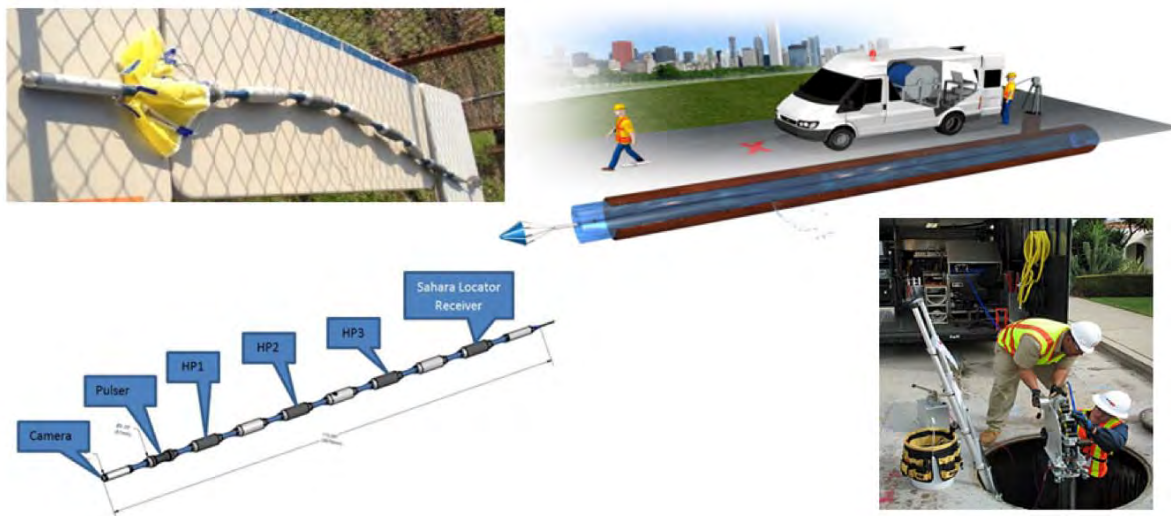
Pressure wave propagation techniques pose notable challenges in validation given the averaging nature of the quantities reported (in general over 10’s or 100’s of meters), and the fact that only limited scientific verification of results has been made publicly available.

5.4.2 Technology Vendors of Pressure Wave Propagation Technology in the Market

Available pressure wave based tools differ to a large extent on how the wave phenomenon is generated (e.g., an acoustic emitter, or through induced surge pressure in the fluid). Moreover they can also be differentiated on how the actual deployment and measurement of the signal takes place, e.g., directly in contact with the external pipe wall (e.g., Echologics ePulse technique), in contact with the water column through external access points such as valves or hydrants (e.g., Detection Services p-CAT™), or deploying the sensors inside the pressurized water-filled pipeline and moving with the flow (e.g., Pure Technologies Pipe Wall Assessment tool deployed on their Sahara II platform).

5.4.2.1 Pure Technologies Ltd – Sahara II Acoustic Pipe Wall Assessment (PWA)

Pure Technologies Ltd Sahara II platform is primarily a leak detection device. With the addition of an Acoustic Pipe Wall Assessment module, the device deploys a cable arrangement terminating with an acoustic sensor head into a pressurized flowing fluid filled pipe using a drogue to generate a pulling force when exposed to flowing water (Figure 5.8). This arrangement is the method used to deploy the acoustic PWA concept instrument into an operating pipeline, with an additional video camera in the sensor head. The Sahara deploys through a 100-mm diameter appurtenance, such as a small valve.



Source: Courtesy of Pure Technologies (top right).

Figure 5.8. Pure Technologies Sahara II acoustic PWA tool as trialled on Sydney Water test bed (top left), a schematic of the actual tool sensor configuration arrangement (bottom left), and an illustration of the deployment mechanism (right)

5.4.2.1.1 Observations from the Trial of Sahara II Acoustic PWA

An inspection of the project's test bed supplied by Sydney Water with the Sahara II PWA tool was conducted from 14 April, 2014 to 17 April, 2014. Personnel from the company's headquarters in Canada and their Australian counterpart worked together in conjunction with SW and UTS personnel to collect data from various inspections over this period. An inspection report and the acoustic raw data was supplied to the project. Extensive technical consultations took place before, during and after the trials.

A summary of the most relevant findings is as follows:

Calculations from the measurements are related to the average hoop stiffness of the pipe walls sitting between emitter and receiver. This, in turn, is related to pipe structure in the form of average pipe wall thickness. However, this association is not straightforward and has not been fully established by the provider.

Analytical validations and convincing simulations using COMSOL Multi-physics FEA solver were conducted and shared with the technology partner indicating that acoustic PWA appears less sensitive for detecting meaningful pipe wall losses/defects in large metallic CI and DI pipes. Preliminary results appear more promising for non-metallic AC pipes.

Validation of the technique is challenging given the “averaging” nature of the technique (even more challenging for AC pipes given the occupational health and safety concerns associated to the asbestos material).

Exhumation and ground-truth analysis was used to analyse a 5-meter pipe section - reported by Pure as a significant unidentified anomaly in their test bed inspection report. No particular features that could explain a noteworthy geometric anomaly could be determined from the ground-truth data. Material property variations of the pipe CI were also quantified and found to be minimal, and within those reported in the literature in relation to gray CI.

5.4.2.1.2 Relevance and Guidelines for Utilities (Sahara II Acoustic PWA)

At this point it is our view that the Sahara II Acoustic PWA CA technique is not promising for large metallic CI or DI pipeline assets, given their lack of sensitivity to detect meaningful pipe wall losses and defects. As mentioned above, preliminary results indicate the technique would appear more feasible in detecting meaningful variations in non-metallic AC pipes, although this has not been extensively tested and further study would need to be undertaken for the technique to be validated prior to adoption in the field.

Our study shows that Acoustic PWA signals in its current form cannot be analysed to capture continuous thickness maps with detailed geometries suitable for pipe failure analysis. It is also our view that given its lack of discriminative abilities, the technique also appears unable to provide meaningful input as a screening tool to the project’s “along-the-pipe” framework for large metallic pipes.

The Acoustic PWA technique is no longer being offered by Pure Technologies. The vendor indicates they have decided to keep the technique in research and development until significant improvements can be made.

More details can be found in the following publication: Su et al. 2015.

5.4.2.2 PCA-Echologics ePulse

Echologics (a Canadian company), supplies the ePulse tool used in the project via their Australian counterpart PCA-Echologics. The ePulse system originated from technology developed by the National Research Council of Canada. ePulse is an external and trenchless pipe CA tool. It needs access to the external pipe wall (e.g., through valves, fire hydrants, or manually created access points to expose the pipe walls). In practice, the signal is generated by banging the wall with a metallic object. A typical deployment scenario, with two examples of receiver placement, is depicted in Figure 5.9.

By measuring arrival time differences of the acoustic waves at locations along the pipe, ePulse is able to calculate the velocity of acoustic waves in the pipe and convert it to the minimum average metal thickness of the pipe between the measuring points. This distance is often set around 100 m or larger. The system is portrayed as applicable to various pipe materials including metal, CCP, AC and PVC, and it claims no specific limitation on the pipe size. The equipment is the same or similar to PCA-Echologics leak finder sensor, so while doing CA leaks can also be detected.

According to PCA-Echologics, ePulse results are directly influenced by the average hoop stiffness of the pipe. The hoop stiffness at any given point along the length of the pipe is assumed controlled primarily (but not exclusively) by the minimum thickness geometry around the pipe circumference. PCA-Echologics describes the ePulse measurement as representing the “average minimum wall thickness,” which is explained as equivalent to: 1) virtually slicing the pipeline in

“rings” 60 cm wide in the longitudinal direction between measurement points; 2) assuming a constant cross section profile per ring take the minimum remaining wall thickness in each of the ring profiles; 3) compute the average of all these minimum values.

PCA-Echologics acknowledges they have only been able to conduct limited field validations themselves and welcomes utility self-reporting information from verifications to enhance the accuracy of their interpretations. Towards the end of the project PCA-Echologics provided a document describing a validation protocol and discussed their validation data with the UTS team.

EPulse results are affected by air pocket in the pipe. The technology requires knowledge of an array of specific parameters related to water and conduit, to be provided by the utility.

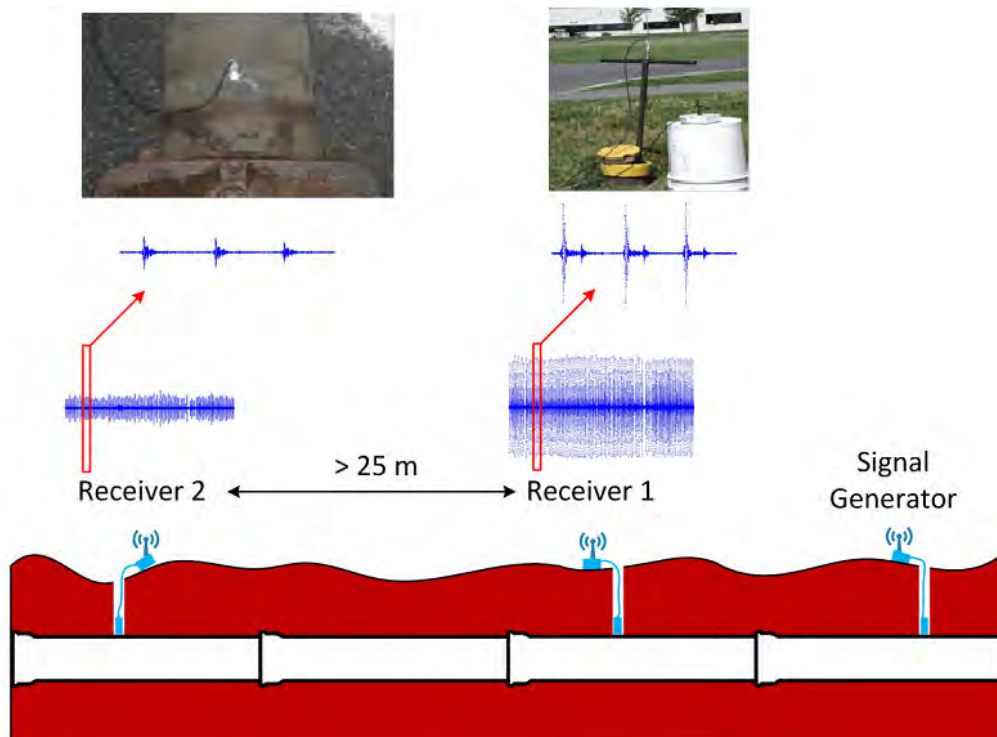


Figure 5.9. PCA-Echologics ePulse typical deployment scenario with two acoustic receivers

5.4.2.2.1 Observations from the Trial of ePulse

An ePulse trial was carried out on the project’s test bed supplied by SW during September 2014. This was planned at varying and higher than usual access point spacing to better assess the influence of spatial resolution. Measurement spacing ranged between 3.6 and 102.6 meters.

A summary of the most relevant findings is as follows:

PCA-Echologics indicated limited confidence on sensor spacing results of less than 25 meters from the tests undertaken, and does not recommend it.

For spacing larger than 25 meters, ePulse test bed trial results do not contradict the averaging remaining wall thickness information gathered during the research project from other sources. As very limited validation of larger pipe section was undertaken given the inherent difficulty in doing so, significantly more extensive testing is required to draw any conclusions from the trials that can be deemed statistically significant.

5.4.2.2.2 Relevance and Guidelines for Utilities (ePulse)

ePulse is not able to provide high confidence actionable information to the utilities at distances between measurements less than 25m (i.e., not at spool level).

Incorporating measurements from a statistically validated ePulse technique into the project's proposed "along-the-pipe" CA framework has been shown able to add value by improving its predictive capability potential.

5.4.2.3 Detection Services p-CAT™

Detection Services is an Australian company. The p-CAT™ system is rooted in the Inverse Transient Pressure Analysis technique (ITA) developed by the University of Adelaide. From a theoretical point of view and its deployment there is a level of resemblance between p-CAT™ and ePulse. p-CAT™ needs direct access the water column, not just the external pipe wall like ePulse. In practice this is done through fire hydrants, bleeding valves, isolation valves and similar appurtenances. A typical deployment scenario, carried out to trial the technology on the project test bed, is depicted in Figure 5.10.

p-CAT™ reports the average pipe wall thickness between two points, thus unlike ePulse the estimates provided by the technology can be directly contrasted by inspection of the asset with no further assumptions on the measurement. Given the length of pipes involved this is however not a trivial exercise. p-CAT™ can report average wall thickness down to a minimum of 10-meter sections. They do this through proprietary analysis of the recorded signal, which is dictated to a very large degree by the availability of suitable access points in the pipeline. Thus, for mains analysis reporting is generally provided at larger spacing between measurement points. Regardless, the study of spatial analysis needs to be carried out on a case-by-case basis prior to the inspection to ascertain the minimum average wall thickness resolution that can be achieved for the given asset.

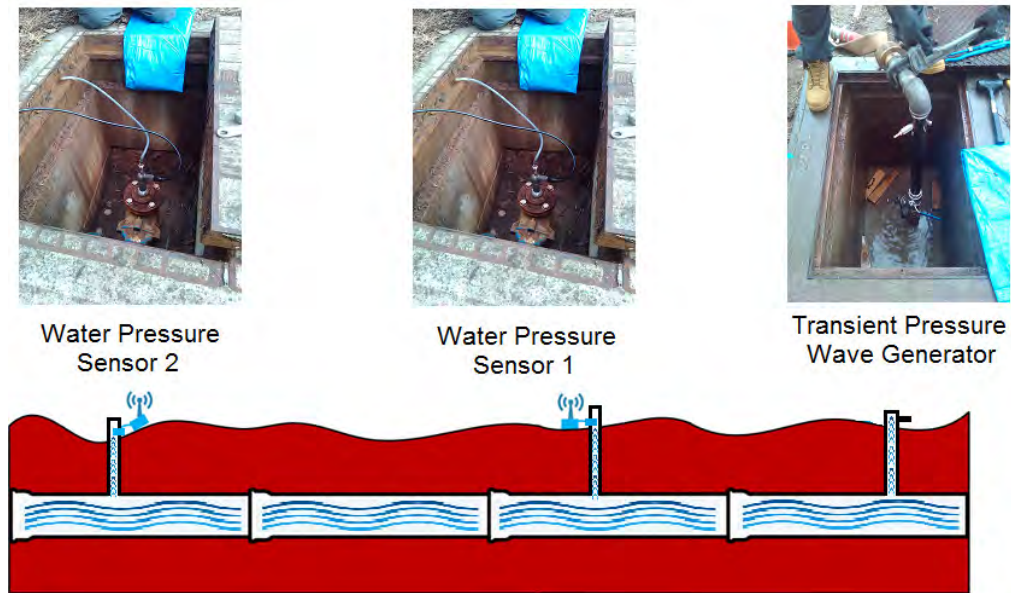


Figure 5.10. Detection Services p-CAT™ typical deployment scenario with two acoustic receivers

5.4.2.3.1 *Observations from the Trial of p-CAT™*

A number of p-CAT™ trials have been carried on the project test bed, all of them unsuccessful. The first one in April 2015 was abandoned due to excessive amounts of dissolved air in water, a requirement unbeknown prior to this project. A second attempt was then carried in July 2015 where considerable steps were taken by Sydney Water, as advised by the technology provider, to minimise the levels of oxygen in the test bed water apparently accumulated during the charging process. The levels of dissolved gas in water were still deemed unacceptably high by the technology provider for reliable reporting of any results. To circumvent the charging issue, a new p-CAT™ trial at a live main in the Sydney Water network (not the project test bed) was planned for February 2016 but later cancelled. The preparation requirements set out by the technology provider to gain access to the water column were deemed by the utility too significant an undertaking (logistically and economically) to be carried out within the available window of opportunity before the main was to be renewed. A trial was eventually carried out in September 2016 on another live main in the Sydney Water network that met the requirements for p-CAT™ to be deployed.

A summary of the most relevant findings is as follows:

p-CAT™ results are affected by air pockets. p-CAT™ does not report on sections where their analysis deems the data to be invalid in being affected by air pockets.

p-CAT™ results are affected by the level of dissolved air in water. Hence it needs to be measured prior to proceeding with the inspection.

Access to the water column is necessary. Since access points in critical water mains are not as readily available, the suitability of a p-CAT™ inspection needs to be investigated by the technology provider on a case-by-case basis.

p-CAT™ analysis treats cement lining as a certain amount of the effective metal wall thickness reported (the percentage depends on the young's modulus of the materials).

Pipe conditions are generally reported for long sections – in the order of 100's of meters or kilometers. The suitability of the tool to discriminate sections of the inspected pipeline down to the minimum claimed of 10m is not guaranteed for all inspections, and needs to be studied on a case-by-case basis.

A validation program of the inspection undertaken in the Sydney Water network in September 2016 is underway but as of writing no conclusions in regards to the accuracy of the technique can be drawn yet.

5.4.2.3.2 *Relevance and Guidelines for Utilities (p-CAT™)*

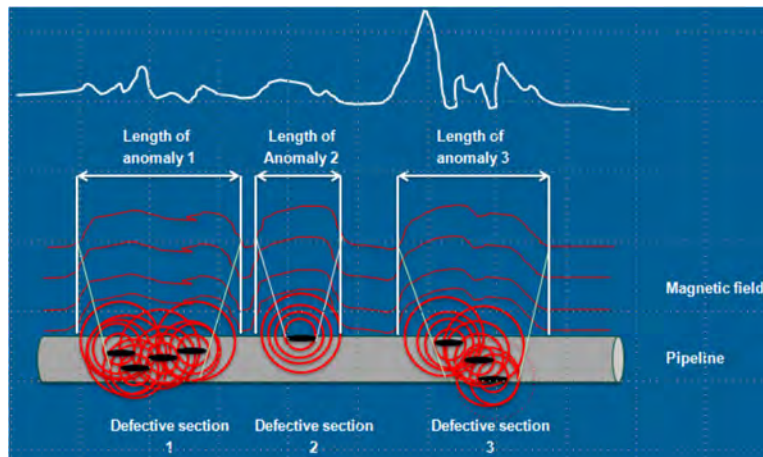
The project has not been able to ascertain the accuracy of the technique as yet from the inspection carried out. Hence as of writing it is not possible to make further judgements, except relating the experiences from the trials program noted above.

As per ePulse comments above, incorporating measurements from a statistically validated p-CAT™ technique into the project's proposed "along-the-pipe" CA framework has been shown able to add value by improving its predictive capability potential.

5.5 MAGNETOELASTIC SENSING TECHNOLOGIES

5.5.1 Technical Description

The essence behind this technique is the observed phenomenon (Villari effect) that when a magnetised ferromagnetic material is subject to elastic changes (e.g., bending), local changes in the material's magnetic permeability occur which lead to measurable changes in magnetisation, thus providing a mechanism for sensing. This can be intuitively explained as stresses in the material producing changes in the magnetic field around it, measurable by magnetometers. A pipeline buried in the ground sits in the earth's magnetic field and as such it will be magnetised. When there are anomalies in a pipeline, such as corrosion, dents, cracks etc., the premise is that there will be variations in the magnetic field due to the increased stress in the region which will appear differently than if the pipe was uniform. An illustration of the principles behind Magnetoelastic sensing in relation to pipeline CA is shown in Figure 5.11.



Source: Courtesy of Speir Hunter Ltd.

Figure 5.11. Illustrative example of the Magnetoelastic principle on a pipeline

5.5.2 Vendors of Magnetoelastic Sensing Technology in the Market

There are two commercially available Magnetoelastic sensing pipe inspection tools, mainly driven by the way they are field deployed:

- Above ground: Detection Services SCT (Stress Concentration Tomography)¹
- In-line: Pure Ltd Smartball® EM PWA (also referred to as Smartball® PWA)

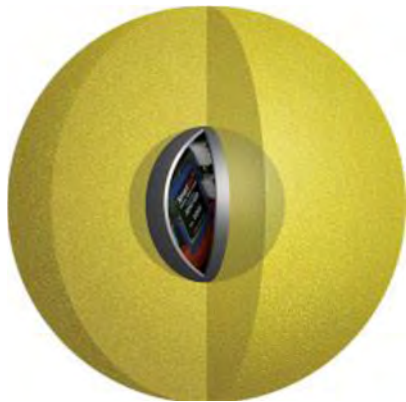
No specific technical details are known about the technology beyond what is available in the public literature and on reports provided by the technology vendor. The Smartball® EM PWA was engaged for trials in this project as it was readily deployable during the project timeline. SCT is reported unsuitable for thick CI pipes and could not be incorporated in the test bed study. Moreover, only recently it was made commercially available through Detection Services.

¹ also available under the banner of Speir Hunter Ltd. SCT, and various incorporations of the Russian company Transkor with the technology branded as Magnetic Tomography Method (MTM).

5.5.2.1 Pure Technologies Ltd Smartball® EM PWA

The EM PWA technology is deployed as part of the Smartball® device, a small suite of sensor the size of a tennis ball, encapsulated inside a foam outer shell deployed via insertion through an existing 100 mm tapping (Figure 5.12). The device is propelled downstream with the flow, and collected via another tapping with a purpose-designed netting. The tool passively collects EM PWA measurements as it traverses the pipeline rolling along the bottom. On-board accelerometers record rotations that are translated to tool locations during the inspection, in combination with external acoustic correlators.

Anomalies are classified by their range of severity as High, Medium or Low. Minimum resolution when reporting the location of an anomaly is one spool.



Source: Courtesy of Pure Technologies (left).

Figure 5.12. An illustration (left) of the Smartball® device hosting the EM PWA sensor and during the test bed trial (right)

5.5.2.1.1 Observations from the Trial of Smartball® EM PWA

The project has carried out two inspections with Pure Ltd EM PWA. Being a tool under development, the initial tests were carried out while the sensor was mounted in the tethered Sahara platform, at the same time as the Acoustic PWA inspection was also undertaken (refer to Section 5.4.2.1). The scope of the initial results appeared too limited for meaningful judgement. The EM PWA sensor was also subsequently installed on the free-flowing Smartball® platform and a trial inspection on the test bed was performed in February 2016. A summary of the key findings to date is as follows:

1. There appear to be significant issues with localization of the tool, so anomalies reported at a given pipe segment could easily be located some pipe spools either side.
2. The tool appears able to discriminate features in the pipe such as joints, clamps, and other appurtenances as part of the anomalies reported.
3. When it comes to condition of the pipe (wall losses, pitting, corrosion etc.) the tool appears to have reasonable true positives but also many false negatives. This is based on limited validation of pipe section and therefore more extensive testing is required to draw the true extent in statistical terms.

4. The tool detects leaks during the same inspection.

5.5.2.1.2 *Relevance and Guidelines for Utilities (Smartball® EM PWA)*

It is not possible to establish a causal effect from EM PWA. The technology vendor acknowledges that the cause of the stress in a pipe, or its magnetic variation footprint, cannot be uniquely identified, and just as it could be due to anomalies in the pipe wall, it could also be due to many other factors (e.g., pipe bending, earth loadings, non-uniform pipe walls, etc). So, the technology's aim is as a low-resolution screening tool indicative of the coarse status of a pipe.

The technology has seen its translation into field deployable tools only in recent times, becoming more widely available for test during the latter development of the project. Based on the experiences from this project, it is our view that the EM PWA CA technique can be validated in practical terms despite the challenges associated to accessing full spools to relate the anomalies reported by EM PWA with the true conditions in the test bed. This process is on-going.

Our study shows that EM PWA signals cannot be analysed to capture continuous thickness maps with detailed geometries suitable for pipe failure analysis. Incorporating measurements from EM PWA into the project's "along-the-pipe" predictive framework for CA has been proven to be theoretically straightforward. It is also our view that should EM PWA be proven statistically significant it would be useful to screen likely pipes in poor condition, a relevant feature for the "along-the-pipe" framework.

The potential for false negatives of the Magnetoelastic PWA technique, in its current form, does not provide high confidence actionable information to the utilities. The technique is currently not being offered commercially by Pure Technologies unless a client specifically requests it.

5.6 SUMMARY TABLE OF TECHNOLOGY CAPABILITIES

The following table contains a summary of the capabilities of the techniques considered. It is not exhaustive but contains tools from some of the most prominent technology vendors on the market, and some form of engagement has been established by the team during the course of the project – if only by exchange of email to ascertain characteristics claimed about the tools for large CICL pipes. As such, not all of these techniques have been studied in depth as part of this project primarily as some tools would appear unsuitable for large CICL pipes on the basis of information supplied by the providers, information was not forthcoming, or the level of readiness in the tool development.

The taxonomy below is targeted at the key objective set out by this project: pipe failure analysis needs in terms of pit depths and the extent of significant corrosion patches. This is examined both, as they stand today, but also given our views about the potential for the technique to be able to provide that information in the future given more sophisticated analysis of the acquired signals is undertaken as revealed by our own research. It might also be the case that the technology vendors feel they are already able to supply that info and only the reporting needs adjusting given the emerging needs revealed by this project.

As with all classifications of this nature there is a certain degree of flexibility built-in to be able to provide useful information for CA from an asset management point of view.

Table 5.1
Summary table of technology capabilities

Technology	Provider	Tool	Type	Pipe Wall Thickness > 27 mm	Cast Iron	Pipe Diameter > 450 mm	Cement Lining > 10 mm	Pitting (sub-cm diameter)	Corrosion Patch Geometry
MFL	Pure Technologies	PureMFL™	Inline			(Claim)	(Claim)		
MFL	AIA / AESL	Smart-CAT™	External			(N/R)	(N/R)		(Potential)
MFL	Silverwing	Pipescan	External			(N/R)	(N/R)		
MFL	ZHONG TE JIAN T&D	ZTJ-MFL-A	External			(N/R)	(N/R)		
MFL	IDEA	IDEAP0702	External	(Claim, on steel)		(N/R)	(N/R)		
RFEC	Russell NDE	SeeSnake	Inline						(Potential)
RFEC	Pure Technologies	PureEM PipeDiver	Inline						
PEC	Rock Solid Group	HSK BEM™	External			(N/R)	(N/R)		(Possible)
PEC	Applus+	RTD INCOTEST™	External	(Claim)		(N/R)	(N/R)		
PEC	TUVRheinland		External	(Claim)		(N/R)	(N/R)		
PEC	Eddyfi Int'l LLC	Lyft	External			(N/R)	(N/R)		(Possible)
PEC	ZHONG TE JIAN T&D	ZTJ-PEC-A	External	(Claim)		(N/R)	(N/R)		
TT	PCA-Echologics	RFT Mainscan™	External			(N/R)	(N/R)		

(continued)

Table 5.1 Continued

Technology	Provider	Tool	Type	Pipe Wall Thickness > 27 mm	Cast Iron	Pipe Diameter > 450 mm	Cement Lining > 10 mm	Pitting (sub-cm diameter)	Corrosion Patch Geometry
MAG	Detection Services	SCT	Above-ground				(N/R)		
MAG	Pure Technologies	SmartBall® EM PWA	Inline						
U/T	JD7 Ltd	Pipescan+™	Inline		(Claim)		(Claim)		
U/T	Breivoll Inspection Technologies	Pipescanner	Inline			(Claim)			
Acoustics	PCA-Echologics	ePulse	External	(Claim)	(Claim)	(N/R)	(N/R)		
Pressure Transients	Detection Services	p-CAT™	External	(Claim)	(Claim)	(N/R)	(N/R)		
Acoustics	Pure Technologies	Sahara II PWA	Inline			(N/R)	(N/R)		

Legend:

MFL - Magnetic flux leakage

RFEC - Remote Field Eddy Current/Remote Field Technology

PEC - Pulsed Eddy Current

TT - Electromagnetic Through Transmission

MAG - Magnetoelastic

U/T - Ultrasounds

(N/R) - Not relevant, i.e., the category applies to tool independently of the sizing stated

Potential - In our view, the category can be asserted by analysing the raw signal

Possible - The category is already contained in the interpreted data (e.g., thickness maps), but not reported

External - Requires access to the exposed external pipe wall

 YES (verified or claimed*)

 Claimed YES but verification related poorly

 NO (verified or communicated by vendor)

 Potential / Possible

Blank - No Information

* claimed also reflects the scenario when tool has been tested but it has not been possible to verify the results

5.7 CONDITION ASSESSMENT TECHNOLOGIES – CONCLUDING REMARKS

The key findings of the project in relation to CA technologies for failure analysis can be summarised as follows:

1. The information required for stress analysis and failure prediction based on outcomes generated by our project colleagues points to the fact that commercial providers of CA tools for large CI pipes based on Magnetic Flux Leakage, Remote Field Eddy Currents and Pressure Wave Propagation do not currently provide information in their reports which can produce thickness maps suitable for failure analysis and the “along-the-pipe” prediction framework. Pulsed Eddy Currents sensing is able to produce thickness maps which are suitable for those purposes.
2. The project has proven that in the case of Magnetic Flux Leakage and Remote Field Eddy Currents the raw signal data contains information fitting for that purpose. In the case of Pressure Wave Propagation techniques that is not possible.
3. The UTS research team has developed advanced signal processing algorithms that make it possible to generate thickness maps from the raw data acquired by tools based on Magnetic Flux Leakage and Remote Field Eddy Currents.
4. The UTS research team has also developed and implemented a data interpretation algorithm to process information from Pulse Eddy Currents sensors and produce more accurate pipe thickness readings. Furthermore, UTS algorithms can produce readings in real-time as opposed to the relatively long process currently employed by the commercial provider of the Pulse Eddy Currents technology engaged as a research partner.

Ancillary findings from the project also include:

1. From a qualitative point of view of CA, most techniques provide some information relevant to the CA processes carried out by utilities – as it is being done today.
2. Some techniques are better suited at representing point measurement of wall thickness, e.g., Magnetic Flux Leakage, Remote Field Eddy Currents, while others represent measures of average volume of material under the sensor antennae, e.g., Pulsed Eddy Currents. A third class of techniques aims to capture average or extreme parameters from the pipeline (e.g., remaining wall thickness) over long distances, e.g., those based on Pressure Wave Propagation.
3. An understanding of the resolution and accuracies at which pipe wall defects can be practically reported has been gained.
4. The influence that pipe ferromagnetic properties (e.g., conductivity, permeability) have on the results of electromagnetic-based techniques has been attested.
5. Some techniques have been shown to lack the necessary sensitivity to be able to detect pipe wall losses/defects in large metallic pipes. This applies most notably to Pressure Wave propagation-based techniques.
6. Provable characterisation during the research work has led to advanced interpretation strategies being produced and shared with the respective CA technology providers engaged in the project. These findings are also being considered as part of the “along-the-pipe” framework for CA, as described in Chapter 2 of this report.

7. The interim results have allowed CA technology vendors to incorporate findings into their future strategies, and to participate more closely in shaping up their interpretations and reporting for the benefit of the utility industry - as specified through many utilities' review of their CA contract specifications. A feedback loop to providers of CA tools appears critical to benefit utilities towards more targeted critical asset management and renewals.
8. Validating CA interpretations is a difficult process for utilities. A current outcome from this work (Appendix Section 11.3) offers utilities a proven metrology solution to attest the suitability of local and direct CA tool advances to be readily incorporated into the failure prediction framework.

More details can be found in the following publications: Liu et al. 2014, Shi et al. 2016a, Valls Miro and Shi 2016, Hadfield 2014, Kodikara et al. 2016.

6 RESEARCH ACTIVITIES INTO AN “ALONG-THE-PIPE” FRAMEWORK FOR CONDITION ASSESSMENT OF CRITICAL WATER MAINS

6.1 INTRODUCTION

Within the water industry, condition assessment (CA) prediction is mostly made by interpreting results between local excavation measurements using statistical estimation of extreme measurements (e.g., maximum pitting) with a considerable high level of uncertainty. Currently, the only feasible alternative is to use significantly more costly internal direct measurement tools, yet the effectiveness of this approach has not been fully established within the industry given the compelling deployment and validation investment needed. The work presented in this report proposes a novel data-driven framework for “along-the-pipe” condition assessment prediction. The strategy proposes the use of pipe condition data from targeted locally excavated inspections (preferably as suggested by screening information if proven statistically significant, but not a requirement), and exploits the information contained in the inspected pipe wall thickness geometries to produce predictions about the remaining pipe thickness at unseen locations, both in terms of minimum thickness and pipe wall geometry (e.g., patches of corrosion), and their associated levels of uncertainty. This represents a marked improvement over the standard statistical analysis practices currently available to the water industry and fulfils the overall objective of this project to provide a reliable mechanism to predict the probability of failure of large critical mains.

The proposed framework:

1. Represents a data-driven statistical model aimed at enriching the information gathered from local inspections.
2. Can take into consideration input from screening tools and/or prior knowledge about the pipe for model training data selection.
3. Assesses the probability of extreme values in terms of remaining wall thickness and corrosion patch sizes.
4. Aims to address gaps of notable relevance to critical asset management undetermined by statistical tools such as Extreme Value Analysis (EVA).

The “along-the-pipe” framework has been investigated and tested with CA data from inspections carried out in the critical pipe networks of the ACAPFP project utility partners, and the engagement from a range of commercial CA vendors.

6.2 “ALONG-THE-PIPE” FRAMEWORK FOR CONDITION ASSESSMENT

A schematic about the overall “along-the-pipe” framework from a CA standpoint is depicted in Figure 6.1. The work hereby proposed effectively encompasses the top 4 layers.

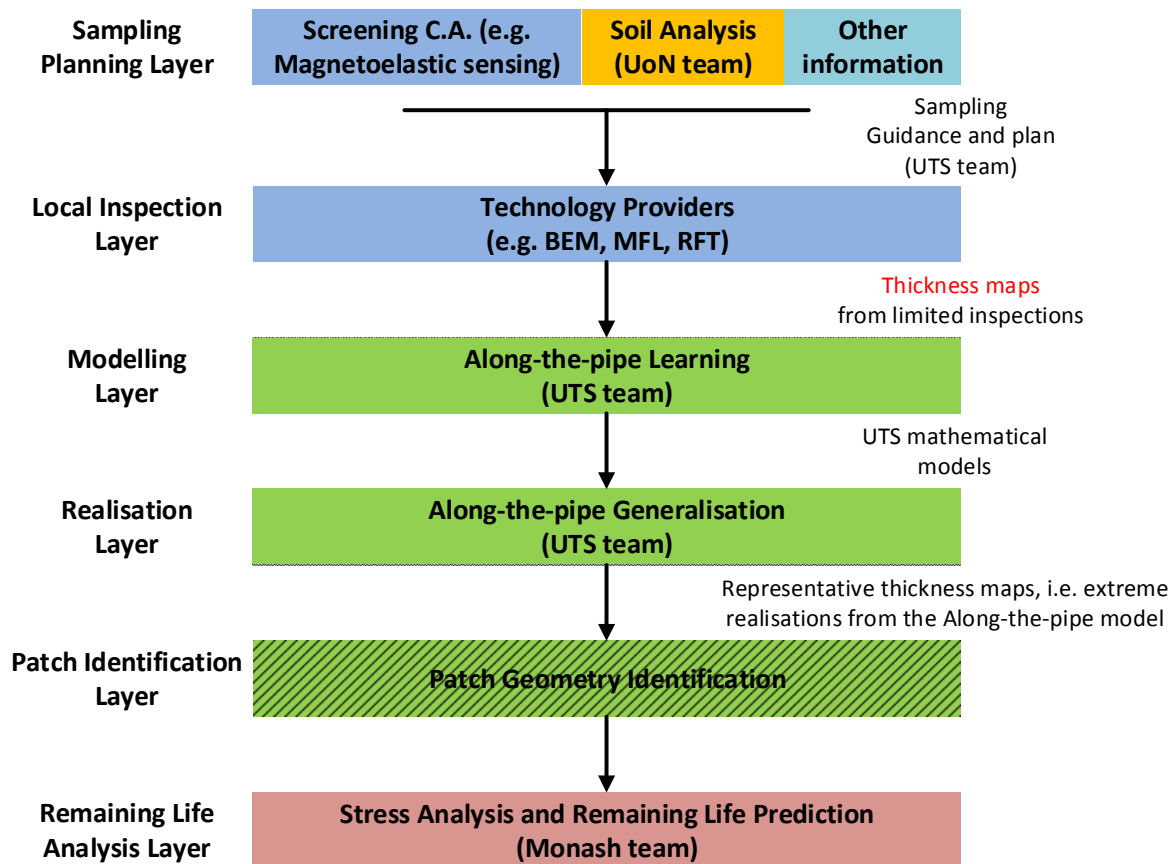


Figure 6.1. Along-the-pipe framework for CA

6.2.1 Screening and Local Inspection Data Gathering

The framework proposes a sampling strategy that can be adapted depending on whether information from a reliable screening tool is available or not.

Insights from anomalies reported by a potentially verified screening tool, or environmental soil indicators demonstrated to correlate to localised pipe degradation can serve as guidance to locate pipe sections that exhibit advanced deteriorating conditions. These targeted pipe sections will then be used to build the proposed data-driven remaining wall thickness models. In doing so the framework seeks to increase the certainty of its prediction with the focus on the most troubling aspects of the asset leading to possible failure.

Screening techniques whose probability of detecting pipe segments in poor condition is reasonably high are thus preferred to minimise costs incurred on the need to undertake additional excavations for potentially uninformative inspections. If that is not available, an asset length-dependent strategy is suggested based on extensive simulation results and test bed verification. This is not yet conclusive and further validations of the proposed sampling strategy on additional live network assets beyond the test bed pipeline are currently underway.

Local detailed CA inspections can then be carried out on the selected sites with a suitable CA inspection tool (as detailed in Chapter 5) able to provide reliable remaining wall thickness maps.

In the extensive experimental work carried out in the test bed (described below in Chapter 6) CA inspections at 3 of the poor condition sites (as guided by a screening tool) were sufficient

to capture the characteristics of a representative remaining wall thickness model of the poor sections in a 1 km pipeline. If no reliable screening tool is assumed, simulation results currently indicate that 4 to 6 local inspections at spaced intervals were found to be needed to gather the required amount of information to build representative probabilistic models of the degraded condition of an asset analogous to the test bed.

For large cast iron pipes, a local inspection should ideally cover a full pipe spool from joint to joint (e.g., 3.66 meters or 12 feet) to safely reveal the full-length of any potential corrosion patches. However, a minimum of 2 meters appears closely representative of the patch geometries found on the test bed pipes inspected in the project.

6.2.2 “Along-the-Pipe” Learning and Generalisation

Assuming local inspection information from a number of pipe sections has been obtained, the overall method becomes a 2-step process: modelling and realisation. As shown in Figure 6.2, the modelling phase extracts information from the specific local inspection data and generalises the knowledge about the parameter of interest (wall thickness) exploiting spatial dependencies in the inspection data. It generates a probabilistic “data correlation model” that represents the inspected pipeline condition. The realisation step provides likely predictions of pipe wall thickness by drawing correlated samples from the model, able to capture the underlying pipe wall thickness correlations at unseen locations whilst accounting for the full length of the pipeline asset in the process. These realisations, in large amount, collectively reflect reasonable variations in the expected condition of the pipe providing adequate generalisation during the learning phase. From all these realisations, the framework is able to focus on the “worst” ones from a failure risk point of view (i.e., those with smaller minimum thickness and larger patch sizes) to build its statistical models.

The framework will be able to capture more closely these “poor” conditions of interest in their models if the local inspections align more closely with the degraded part of the overall pipeline, as potentially singled out by a screening tool, yet it can also generalise if this data is not available.

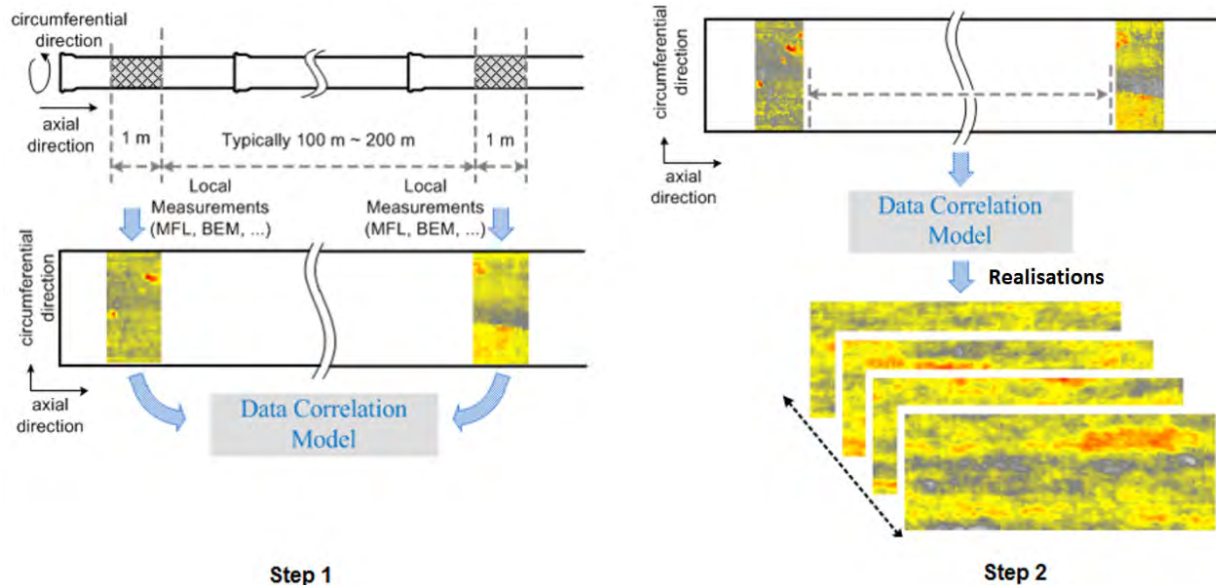


Figure 6.2. Step 1: learn data correlation models from local inspection results. Step 2: sample from the “along-the-pipe” model on area without any additional input.

The correctness and accuracy of the prediction ultimately depend on whether the pipe sections used for training are sufficiently representative so that the learned model correctly captures both the correlation pattern and the thickness distribution.

It is important to note that given the probabilistic nature of the proposed data-driven methodology and the phenomena itself - extreme conditions such as acute pitting are also believed to appear probabilistically - exact inference of the condition of the pipe at arbitrary locations along the length of a pipe is not feasible. However, the strength of the proposed framework lies in its ability to derive likely “poor” conditions (i.e., those with smaller minimum thickness and larger patch sizes) gathered from a large number of sample representations from the learned model. And it is during the realisation step that the framework can generically benefit from incorporating additional regional information about asset geometry (e.g., as supplied by screening techniques such as average wall thickness or minimum circumferential pitting), or from other records (e.g., existence of leaks).

The outcome of the proposed framework is an arbitrary large amount of wall thickness map realisations from the model, where the likely existence of worst-case spoils in the overall targeted pipeline (of known length) may be drawn in probabilistic terms, including a desired confidence level associated to this belief.

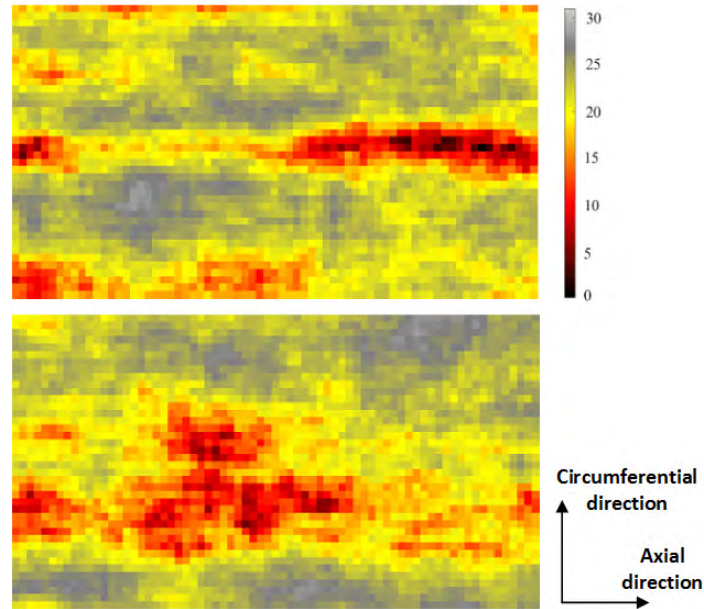


Figure 6.3. Two representative random realisations of a pipe spool generated by the framework (3.6 meters long)

The outcome format in terms of correlated wall thickness maps (as shown in Figure 6.3) represents state-of-the-art practice in data analysis for predictive purposes, and supports a mechanism fitting for subsequent structural stress or any other study reliant on the thickness semblance of a pipe, and not just single-value extrema such as maximum likely pitting.

6.2.3 “Along-the-Pipe” Flow Chart

A flow chart of the proposed “along-the-pipeline” scheme in its current form is given in Figure 6.4.

Indicative results at the conclusion of the project from test bed data would currently suggest $n=3$ when poor condition sites can be reliably identified, and $m= 4$ to 6 equally-space inspections otherwise. It should be noted however that these figures are merely indicate at this stage until more exhaustive trials can be undertaken with a wider selection of pipe cohorts and simulations, most notably with the goal of gaining further insight into a defining sampling strategy of how and where to conduct local inspections, a process currently on-going.

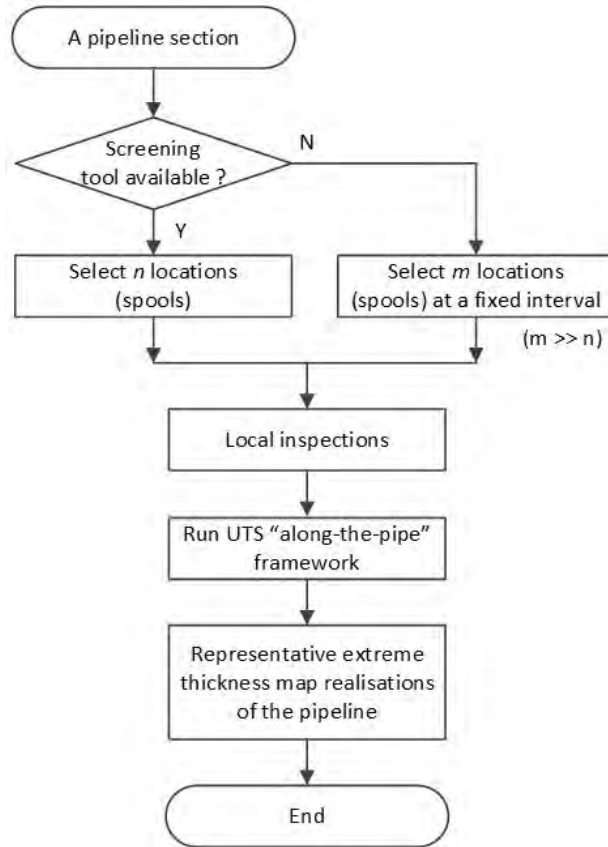


Figure 6.4. Flow chart for the “along-the-pipe” generic framework

6.2.4 Extreme Value Analysis

For comparison purposes results drawn with Extreme Value Analysis (EVA) statistics are also provided. EVA is a standard statistical mechanism to assess the probability of extreme events from sample data, often used by the water utility industry and CA technology providers to extend the local measurement to unseen data. The procedure includes:

1. Data collection – segment the local inspection data into grids of fixed size, and record the maximum pitting or minimum remaining wall thickness in each grid.
2. Distribution fitting – fit an extreme value distribution (e.g., a Gumbel distribution) on the collected data, and check the goodness of the fit to make sure that EVA is applicable.
3. Extrapolation – taking the actual size of the target pipeline area into consideration, extrapolate the prediction of minimum remaining wall thickness or maximum pitting from the fitted distribution.

For predictions of minimum pipe thickness based on local inspection measurements, EVA analysis appears to translate in predictions that tend to be quite conservative – i.e., lower estimates of remaining pipe wall than should exist in reality. Moreover, a relevant shortcoming of the EVA analysis is its inability to capture the spatial dependencies in the thickness measurements, thus predictions do not contain any geometry information (corrosion patch) which this project has revealed of critical importance if stress analysis is to be performed on the expected pipe geometry for pipe failure and remaining life predictions.

6.3 EXPERIMENTAL VALIDATION: A CASE STUDY FROM THE SYDNEY WATER TEST BED

In this section results are presented drawn from thickness maps of 12 exhumed segments (depicted in Figure 6.5) from the test bed to evaluate the proposed framework with real asset data. These 12 segments of 1 meter represent the best existing knowledge from the overall test bed pipeline, and are believed to incorporate the worst sections in the pipeline according to the best knowledge gathered after conducting a methodical program of inspections and verifications.

We apply a metric based on the remaining wall thickness to categorise the 12 pipe segments as being in either good or poor condition:

1. Corrosion patches with any measured thickness lower than 40% of the nominal wall thickness are regarded as a patch geometry of interest in the analysis.
2. Ellipses are fitted in these areas to characterise the spread and width of the patch.
3. A pipe segment with a patch geometry of interest (as above) is regarded as being in poor condition; otherwise is considered in good condition.

Note that other arbitrary intermediate categories can be also studied, but the most interesting aspect of the framework is in targeting the presence of pipes in poor condition, and their likely geometries. Any updates to the current knowledge gathered by our colleagues working in this project on pipe failure analysis can also be readily incorporated.

There are 5 poor condition pipes and 7 good condition pipes in our dataset according to this metric². Pipe G2 represents the worst area seen in the whole test bed pipeline (264 full standard spools x 3.6 meters long each). For this exercise G2 was taken out from the training dataset and only used for evaluation purposes. This represents a realistic scenario where a screening tool may provide a method to identify some pipes in poor condition but not all of them, and not necessarily the worst ones.

To assess the validity of the proposed methodology in capturing likely pipe geometries present in the entire pipe cohort from limited inspections, the remaining pipes in different combinations were then used for training – thus emulating an array of scenarios where different pipes were chosen to build the spatial statistics model, be that driven from a screening tool or otherwise.

The prediction was then carried out on the whole 1 km pipe cohort with the aim to predict extreme low wall thicknesses and largest patch sizes. As a means for comparison, the minimum wall thickness value as predicted (with 95% confidence) by a standard EVA analysis using the same inspection data is also given.

² Please also note that the definition of good or poor condition and what constitutes a corrosion “patch” has not been studied within the scope of this project activity, as its merit relates to stress and failure as that has not been formalised yet. Hence, the condition definitions and the patch characterisation approaches adopted here are for the purposes of evaluating the proposed framework, as the methodology is equally applicable should other characterisations be chosen on the grounds of their relevance to stress and failure analysis.

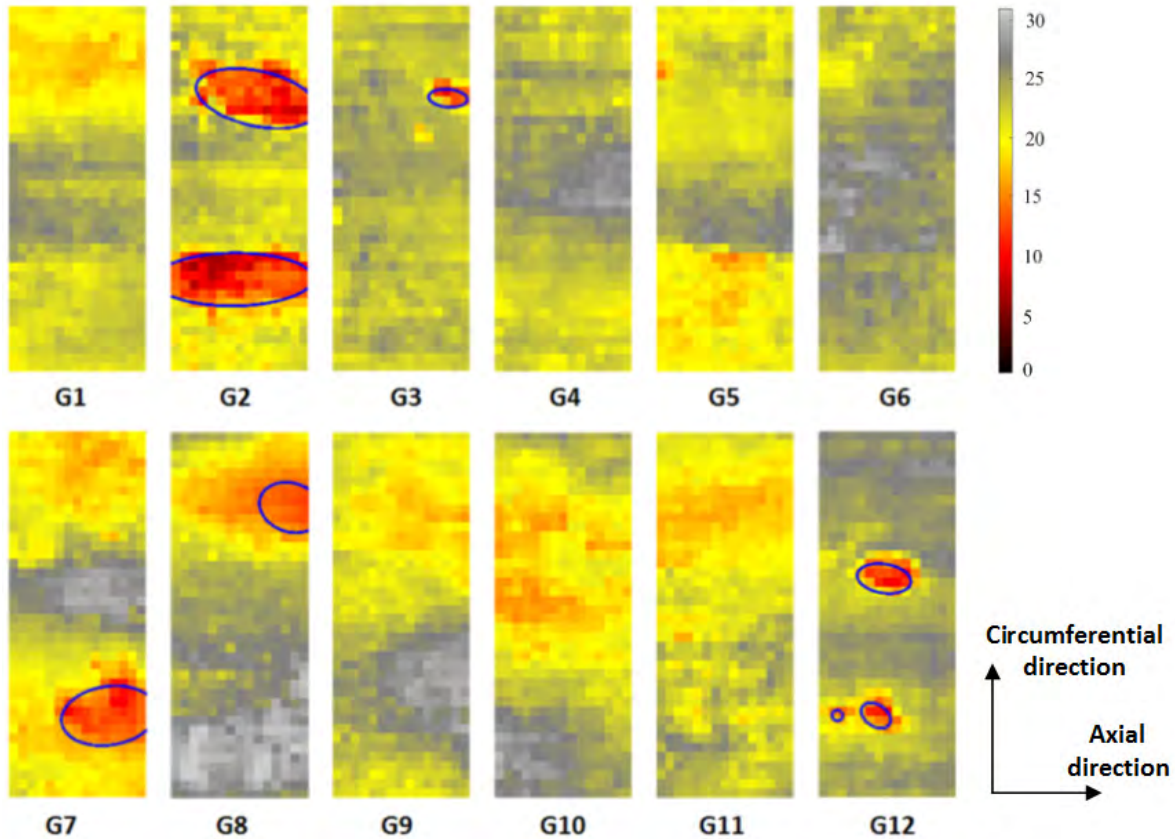


Figure 6.5. Ground truth data obtained from exhumed, grit-blasted, and laser-profiled sections

6.3.1 Results

The benchmark is established based on a summary of the *extreme* geometric values present in G2, as collected in Table 6.1. The framework’s aim is thus to predict the values of *extreme* (low) wall thickness and (large) patch sizes for the whole pipeline (here condensed in the 12 exhumed sections) using the learned models.

Representative results from the various prediction experiments conducted with different combination of pipe sections for training are reported in Table 6.2. For each combination (rows in Table 6.2), the model was learned and then a large number of along-the-pipe predictions made (1000 simulated pipelines of the targeted length, 1 km in the case of the test bed) to infer the distributions of the values of interest, i.e., minimum thickness and maximum patch size major and minor axes.

A description of the terms in Table 6.2 is warranted to better understand its statistical meaning. Table 6.2 collects the results for the minimum wall thickness and maximum patch size produced by the along-the-pipe framework, and the minimum wall thickness produced by EVA, all with a 95% confidence level, with the same input data. In practice, for the proposed framework this means that for the 1000 target pipeline realisations, in 95% of the cases the predicted minimum wall thickness was above the value in the table, and in 95% of the cases the maximum patch size was below the value in the table. Therefore, only in 5% of the realisations the predicted value burst below the minimum wall thickness and above the maximum patch size respectively, i.e., an undesirable yet low-likelihood scenario. Likewise, for EVA, in 95% of the cases the minimum

wall thickness was predicted to be above zero (through-wall). It should be noted that as each parameter studied is a random variable, these can also be reported as a range with a desired confidence level (i.e., “the minimum predicted thickness in the pipeline is between 0 and 5 mm, with e.g., 80% probability”). But in the interest of clarity these have been omitted and only the value with 95% probability is provided.

The experimental results indicate that the proposed “along-the-pipe” prediction is able to provide reasonable extreme geometry information in terms of patches and thicknesses, as long as some of the poor condition pipes are part of the training, even when the actual worst case G2 was unseen during the training process.

It can be observed how the proposed “along-the-pipe” framework produces results which are *closer to reality* while remaining marginally conservative when predicting worst-case scenarios, yet significantly less so than EVA for worst pitting prediction – where through-wall corrosion was forecasted in all instances. As per the needs of asset managers, when dealing with risk analysis it is preferable to assume marginally worst conditions in the pipe than there really exist for a more efficient replacement/repair/rehabilitation strategy, rather than being either too optimistic and hazard an unexpected pipe failure, or overly conservative and replace pipelines before their due time. However, the main advantage of the developed framework is the ability to predict patch sizes together with minimum thickness values, a fitting input to calculations of stress analyses and remaining life predictions, not possible with EVA.

Table 6.1
Lowest thickness and largest patch geometries found in the pipeline (as given by G2)

From Data	Min. Wall Thickness (mm)	Max. Patch Size Major Axis (mm)	Max. Patch Size Minor Axis (mm)
G2	4.8	716	314

Table 6.2

“Along-the-pipe” framework results on predicting extreme conditions in the pipeline (264 spools x 3.6 m each). Results from EVA analysis also shown for comparison.

Training Combinations	EVA Prediction	“Along-the-pipe” Prediction		
	Min. Wall Thickness	Min. Wall Thickness (mm)	Max. Patch Size, Major Axis	Max. Patch Size, Minor Axis
G3, G7, G12	< 0.0	2.0	1444	746
G3, G8, G12	< 0.0	1.2	1411	842
G7, G8, G12	< 0.0	1.4	883	603
G3, G7, G12, G4	< 0.0	2.7	989	572
G8, G12, G4	< 0.0	1.3	1431	817
G3, G7, G12, G5	< 0.0	2.7	713	420
G3, G7, G12, G6	< 0.0	2.5	713	407
G1, G4, G12	< 0.0	3.0	1023	632
G7, G8, G10	< 0.0	2.1	1736	185
G8, G10, G11	< 0.0	1.6	367	204
G3, G7, G12, G4, G5, G6	< 0.0	3.4	503	279
G4, G5, G6	< 0.0	5.6	173	107

Red: poor condition pipes identified by the screening tool and local inspection verification

Green: good condition pipes verified by local inspections

Yellow: failed prediction

6.4 CONCLUSIONS AND RELEVANCE FOR UTILITIES

The “along-the-pipe” framework for CA proposes an innovative interpretative method for critical water pipe condition assessment, aiming at improving and enriching the information gained from local inspections with the objective of making predictions about likely thickness maps present in the overall pipe at unseen locations with severe low remaining wall thickness and maximum patch sizes.

The proposed framework can exploit the guidance from screening tools to select training data to better capture the spatial correlations of remaining wall thickness geometries from poor condition pipes, the ideal scenario. If that is not available, an asset-length dependent strategy is suggested based on extensive simulation results and test bed verification.

The methodology hence proposes a defined strategy of 3 to 6 non-destructive spot inspections with PEC sensing at selected locations (preferably with guidance from a screening tool,

but it also operates effectively without it). This data is then used to build a spatially correlated probabilistic model that is used to define the likelihood of the presence of extreme conditions (low remaining wall thickness and large patch geometries) in the targeted pipeline. Realisations of likely “poor” condition thickness maps can then be gathered for subsequent failure analysis.

Experiments have been carried out with real data from a test pipeline, where the framework has been evaluated against data collected from exhumed pipe sections. Results have been favourably compared with traditional Extreme Value Analysis as the statistical practice widely used by CA providers to the water industry, and utilities themselves, to interpret spot CA measurements and assess remaining life.

Despite the exhaustive in-field validation of the strategy and comprehensive simulation work, the results compiled in this report have been limited to a single pipeline in the network of one of the utility partners in the project. Hence, while the results appear promising, significantly more validation is necessary before its full potential can be conclusively assessed on a larger variety of pipe cohorts and be made readily available as a tool for utilities. Substantial on-going work is currently underway with this objective in mind.

More details can be found in the following publications: Vidal-Calleja et al. 2014a, Sun et al. 2015, Shi et al. 2015, Shi and Valls Miro 2016, Shi et al. 2016b, Sun et al. 2016, Shi et al. 2017, Sun et al. 2017.

PART 3
ACTIVITY 3 – HOW DO WE CALCULATE PIPE DETERIORATION
RATES ACCURATELY WITH RESPECT TO THE PIPE
ENVIRONMENT?

Project Team (The University of Newcastle):

Professor Rob Melchers

Dr. Tony Wells

Dr. Robert Petersen

7 ACTIVITY 3 BACKGROUND, AIMS, AND PROPOSED METHOD

The primary aim for Activity 3 was to develop a model for the prediction of corrosion of cast iron (and other ferrous metal) pipes buried in soil. The main focus was on ageing large diameter cast iron pipes, which are usually unprotected and are known to fail suddenly. Cathodic protection is unusual and experience shows that any coatings applied before installation usually deteriorate relatively quickly. Deterioration of these pipes is mainly the result of corrosion on the external surface of the pipe in contact with soil. Internal corrosion is less of an issue, since a thin interior cement lining is applied during pipe manufacture (or sometimes subsequently), and experience shows that this lining renders interior corrosion negligible.

The original concept for the project was to develop the model from the existing knowledge as represented in the scientific and engineering literature for in-soil corrosion and to add to that understanding from experience in industry. To that would be added the general approach previously used at Newcastle for modelling of corrosion in wet conditions. This general approach included developing a conceptual model for in-soil corrosion, and then calibrating it to data collected from pipes under actual service conditions. It was originally conceived that the model would recognise cases of elevated corrosion in non-homogeneous soils, corrosion under wet conditions, and corrosion influenced by bacterial activity.

The following brief report outlines the main work conducted for this project. It also provides references to relevant papers in the appendices which go into more detail.

7.1 FIELD DATA COLLECTION

To calibrate a corrosion model, good quality data of corrosion losses and the external soil environment surrounding the pipe were required. In the beginning it was expected that 2-4 sets of field data were needed for model calibration. Early in the project discussions commenced with Hunter and Sydney Water staff. Much more data than anticipated became available as a result of in-service inspections of existing pipes, not necessarily those considered to be at risk, being carried out by Matt Dafter for Hunter Water. It consisted of opening-up the site, grit-blasting the pipe in-situ and measuring the corrosion using infra-red scanning. This was a novel approach and provided much more detailed information than previously available or used for research. A total of 20 sets of data, with associated soil conditions, were collected from these sites.

The collection of soil data was based on that reported in the existing literature, principally Romanoff (1957). It places much emphasis on the potential influence of soil parameters on pipe corrosion, even though no correlations had yet been established anywhere in the literature. Since recent research has shown that nutrients necessary for microbiological activity are correlated with additional corrosion in wet conditions, nitrates were included in the soil parameters. A protocol for soil sampling was established and trialled as a part of the Hunter Water data collection work. The protocol was subsequently adopted by Sydney Water and other utilities, including in the UK.

The current version of the data collection protocol is given in Appendix Section 11.5.4 This protocol remains largely unchanged from the protocol used during the Hunter Water data collection trials.

After the Hunter Water pilot trial was successfully completed, a number of pipe sections from failures within the Sydney Water network were received. These pipes were grit-blasted ex-situ and the corrosion was measured using infra-red scanning. Soil data was collected from

undisturbed soil next to the pipeline and adjacent to the pipe failure sites, and following the soil data collection protocol. A total of 7 data sets were collected from these sites.

A number of pipe sections were removed from the test bed as a part of Activity 2's work on condition assessment techniques. The corrosion levels on these pipes were measured also with infra-red as a part of Activity 2 to establish a ground-truth to compare the different condition assessment techniques against. Associated soil conditions were also required for the corrosion modelling work. Soil samples were collected next to the pipe in undisturbed locations surrounding the original excavations. Again, the soil sampling protocol was followed. A total of 8 data sets from these sites were used for model development.

Water Corporation conducted in-service inspections of several sections of pipe within their water main network during the course of the project. As a part of this work they followed the soil data collected protocol, and for a selected couple of sites they also removed pipe sections for visual examination of corrosion losses. These pipes were grit blasted and the corrosion losses were measured by visual examination and using a pit depth gauge. A number of condition assessment reports were received and examined. Data of external corrosion losses and associated soil conditions from 2 sites were deemed of acceptable quality for model calibration and were incorporated into the data set for model development. At these sites maximum external pit depth was measured and recorded from grit-blasted pipes.

In total, 37 sets of data are now available, with associated soil data, for model development and calibration. The pipes in the available data set range from some of the oldest pipes in the water networks (129 years) to much more modern cast iron pipes. The soils were classified mainly as inorganic clays and sands with some classified as loam. All the pipe samples were originally buried under grass easements, except for one sample which was buried under a gravel access road, and another four samples which were buried under road pavements. At most sites the trenches were backfilled with native soil. Some sites showed some visual evidence of the backfill being in part imported sand. Groundwater either was not observed or appeared to reach no higher than half-way up the pipe. This was the case for all sites examined.

More details of the field data collection are covered in Petersen et al. 2013b, and Petersen et al. 2016.

7.2 CONCEPTUAL CORROSION MODEL

It was originally proposed to base the conceptual model on existing knowledge from the literature and also on additional understandings from practical experience. To develop a conceptual model existing knowledge on both the corrosion mechanisms in soils, and the corrosion mechanisms occurring in the long-term under other wet corrosion conditions were considered. Even before this project began it was suspected that the long-term corrosion mechanisms under soil conditions beared similarities with long-term corrosion mechanisms under wet conditions. This idea was based on the discovery that the long-term corrosion versus time behaviour in a soil followed a similar trend to that observed under other wet corrosion conditions, such as immersion and the atmosphere. That trend was the bimodal trend, and this suggested that the underlying corrosion processes in soils is similar in some respects to those in other wet environments. The bimodal trend was used as a basis to develop a preliminary conceptual understanding of the long-term corrosion mechanisms in a soil, and to identify the factors that likely influence the long-term corrosion process. These factors included moisture required for corrosion, nutrients for microbiological corrosion, and backfill quality. This work was presented in Petersen and Melchers (2012).

To support the adopted modelling approach, time was spent analysing a large body of soil corrosion data reported in the historical National Bureau of Standards report on soil corrosion (Romanoff 1957). Corrosion loss and maximum pit depth against time data was examined for a variety of different ferrous metals in a large number of various soils (some 61 soils). It was found that both the maximum pit depth data and weight loss data followed the bimodal trend in the majority of cases that were examined. Roughly 600 cases were examined. It was also found through study of the data that corrosion weight loss and maximum pit depth of ferrous metals (including cast iron) is determined more by soil conditions than by composition/pipe manufacture. This work was presented in Petersen and Melchers (2015).

More recently, further refinements have been made to the conceptual model and understanding of the in-soil corrosion processes and factors. The first is that corrosion only occurs to a significant extent when there is enough moisture next to the corroding surface, and this is regulated more or less by the soil and also by the graphitised layer between the soil and corroding surface (for cast irons). This idea led to the adoption of a time of wetness concept, which is commonly used in atmospheric corrosion. The second refinement is that when there is sufficient moisture at the corroding interface, the corroding conditions are similar to those under immersion conditions. It follows then that the influence of nutrients on corrosion in soil can be modelled in a similar way to how it is modelled under immersion conditions. The third is that corrosion in soils occurs under essentially stagnant conditions and is therefore independent of soil water chemistry. This is based on existing findings in the corrosion science literature on corrosion under stagnant conditions. The fourth is that allowances need to be made to account for increased pit depths in the cases of poor quality backfill. More in-depth discussion of the current understanding of the long-term corrosion processes and factors in soils are presented in Petersen et al. (2016) and Melchers and Petersen (2016).

7.3 ANALYSIS OF THE FIELD DATA IN THE CONTEXT OF THE CONCEPTUAL CORROSION MODEL

The data of corrosion pit depths and associated soil conditions from the 37 field sites were analysed in the context of a simplified version of the conceptual bi-modal model for corrosion. Details of the most recent analysis of this data are contained in Petersen et al. (2016). Some earlier attempts at analysis using preliminary data sets and analysis methods were also conducted at earlier stages of the project (see Petersen et al. (2013a) and Petersen and Melchers (2014)).

Initial analysis of the 37 data sets focused mainly on quantifying the influence of soil moisture on corrosion pit depth development. Quantifying the influence of other factors such as soil nitrates, phosphates, carbonates and chlorides then followed. These preliminary analyses showed that wetness of the metal surface is one of the critical components in the corrosion of buried pipes. In the preliminary study soil moisture was used as a parameter, and some simplifying assumptions about the relationship between wetting of the metal surface and soil moisture were made. These assumptions were found to be a large source of uncertainty in the models derived from the analysis. To resolve this issue, investigation into the wetting of the corroding surface by the soil was conducted and as a result a ‘time of wetness’ concept was developed. This concept was considered a more rational way of accounting for the influence of moisture on the corrosion in a soil. For the purposes of analysing the data a time of wetness of the corroding surface at each site was estimated using a mathematical model. This model included rainfall, evapotranspiration and soil data inputs, and allowed for adjustments to account for local site factors which could

change soil moisture for periods of time. The time of wetness was found to correlate well with the observed corrosion of cast iron pipes.

When conducting the analysis of the data sets a small number of outliers were identified that were inconsistent with the majority of data. A detailed review of the site records for these potential outliers was conducted and unusual conditions were found at each site. From this review of the outlier sites a number of additional factors that could worsen corrosion were identified, including physical damage from poor quality backfill, and prolonged periods of wetness and/or poor drainage.

The following qualitative observations were made from the analysis of the 37 data sets:

1. Sites that may be considered ‘wet’ or which have an elevated chance of the pipe being wet, or which were poorly drained, tend to show greater corrosion, even after only a few decades,
2. Conversely, well- drained sites, such as sandy soils, show little corrosion,
3. Where the back-fill was not homogenous, such as containing gravel, rocks, or clay lumps mixed with sandy or loam soils corrosion tended to be high and localized,
4. Pipes bedded on native soil or having poor or uncertain back-fill usually show greater corrosion along the bottom of the pipe,
5. Soils with elevated nitrate content showed somewhat higher levels of corrosion.

These observations are consistent with findings from a recent analysis of historical data from the National Bureau of Standards study reported in Romanoff (1957); see Melchers and Petersen (2016).

7.4 PRELIMINARY VERSION OF THE CORROSION MODEL

At the present time a preliminary version of the corrosion model, based on the work described in Petersen et al. (2016), is available. This model predicts the maximum corrosion penetration depth p on the exterior surface of a cast iron pipe, for a specified exposure period t . It includes the influence of time of wetness at the surface of the pipe, and the influence of nutrients (nitrates) for microbiological corrosion. Although the homogeneity of backfill has been identified as a main factor, this has yet to be quantified in the current version of the model. Further work is recommended.

7.5 CORROSION AFTER PIPE PERFORATION

To explain why many pipes that have failed through longitudinal cracking show very thin remaining wall thickness over areas much larger than typical for pitting, it was proposed that once a pipe wall is perforated by a corrosion pit, the interior high-pressure freshwater will escape into the interface between the cast iron and the graphitized layer and there cause general corrosion leading to areas of pipe wall thinning. As shown in Activity 1, such thinning over sizeable areas is required for the pipes to burst under internal pressure.

More information on this behaviour was presented at the February 2016 TAC meeting. Work is required to investigate this behaviour in more detail and to quantify it.

7.6 RECOMMENDATIONS FOR FUTURE WORK

Recommendations for future work include the following:

1. Quantify the influence of backfill homogeneity on soil corrosion.
2. Develop a method to predict pitting areas.
3. Investigate and quantify corrosion losses after pipe perforation.
4. Refine the time of wetness analysis. Some assumptions were made in this analysis to develop the preliminary version of the corrosion model, and it is likely that these assumptions contribute to model uncertainty. Additional work to improve time of wetness analysis includes (i) accounting for the influence of the graphitised zone in regulating wetness at the pipe surface, (ii) determining the actual critical moisture content for the clay soils surrounding the pipes under consideration, and (iii) making improvements to the mathematical model used to estimate soil moisture variation at the pipe surface, and from that the time of wetness.

PART 4
ACTIVITY 4B - IMPROVING CONFIDENCE IN CRITICAL PIPE
FAILURE PREDICTION

Project Team (The University of Newcastle):

Professor Rob Melchers

Dr. Tony Wells

8 ACTIVITY 4B SUMMARY

The aim of Activity 4b was to assess the validity of the Linear Polarisation Resistance (LPR) technique as applied to water pipes buried in soils and, if possible, to reduce the uncertainties associated with its use. LPR provides a low cost and rapid assessment of corrosion rates and has been used for many years in some sections of the water industry. However, the level of confidence in the results produced by the LPR technique is still an issue within the water industry. Because LPR as presently used is applied at intervals along a pipe it has the potential to be a useful tool in assessing ‘along the pipe corrosion,’ provided there is a better understanding of the level of confidence that can be placed on the results produced by it. To obtain this, three aspects were considered: (1) the theoretical and practical aspects of the LPR process and associated major sources of uncertainty (2) quantification of the confidence in LPR corrosion predictions and (3) attempt to use a machine learning approach to develop an improved model for LPR prediction of corrosion rates.

A review of the theoretical and practical application of LPR conducted at the University of Newcastle (UoN) concluded that the following factors should be included in any improved LPR-corrosion predictive model: (a) the age and method of pipe manufacture, (b) the soil moisture level and (c) the backfill quality.

An extensive LPR survey undertaken by UoN of several sites showed that variations in soil properties over very short sampling distances may be a significant contributor to uncertainty in LPR-based predictions. In practice this issue is overcome by statistical analyses and by averaging, using many LPR samples. Whether this approach can be improved and so produce more refined predictions remains an open question.

It was identified that an improved model for LPR prediction requires a substantial data set, consisting of LPR readings and soil moisture, age and manufacture method of the pipe, as well as information about the backfill. The machine learning approach proposed by UTS also requires a large amount of data. This is not currently available and could not be generated in the time frame of this activity. Consequently, a data-driven model was not developed.

8.1 INTRODUCTION

The purpose of Activity 4 was to improve current capacities to predict the likelihood of pipe failure along a given length of pipe. A schematic of pipe failure information flow along with the activities involved are shown in Figure 8.1. A necessary part of the failure prediction is the assessment of pipe corrosion rates along the pipe length. The approach adopted in this study involved the use of in-situ measurements at a site together with a corrosion model calibrated to past field observations and integrated with the knowledge available from corrosion fundamentals as well as experience in directly related fields to make informed decisions about the likely present condition and future deterioration of a target pipe along its length. The outcomes could then be used to make informed decisions about the optimal scheduling of pipe renewals in the network with the prediction of failure over space and time.

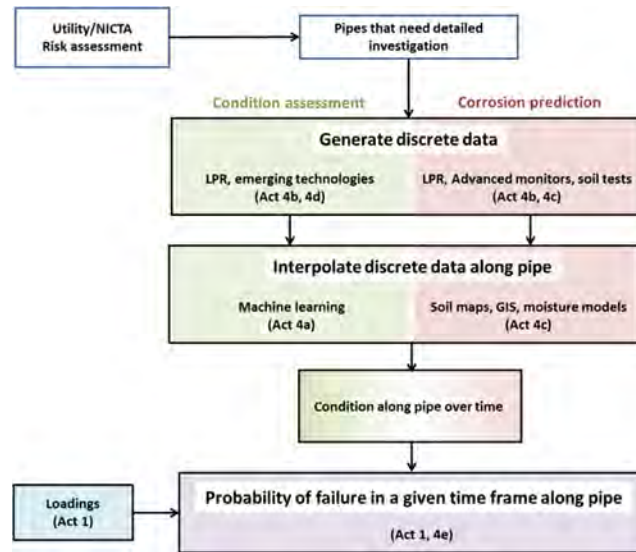


Figure 8.1. Schematic of pipe failure information flow

The findings of Activity 4b are discussed below. A number of appendices (Appendix Section 11.5) are also attached containing data and reports generated during the study.

The aim of Activity 4b was to identify and, if possible, reduce the uncertainties associated with the use of Linear Polarisation Resistance (LPR) technique in estimating the rates of corrosion of buried cast iron water pipes. LPR provides a low cost, rapid, quantitative assessment of corrosion rates and has been used for many years by some sections of the water industry. However, the level of confidence in the results produced by the LPR technique is still an issue within the water industry. To progress this, work discussions were held with a commercial contractor who has supplied LPR services and outcome reports for many years.

Because LPR is applied at intervals along a pipe it has the potential to be a useful tool in assessing ‘along the pipe corrosion,’ provided there is a better understanding of the level of confidence that can be placed on the results produced by the technique. Activity 4b comprised 3 sub-activities: (1) the identification of the major areas of uncertainty in LPR estimates through a better understanding of the theoretical and practical application of the LPR; (2) quantification of the confidence in LPR corrosion predictions; (3) the use a machine learning approach to develop an improved model for LPR prediction of corrosion rates.

8.2 RESULTS

8.2.1 Review of Theoretical and Practical Application of LPR

Two reports were compiled, the first detailing the current knowledge of the theoretical basis of LPR and a second examining the practical application of LPR to the prediction of buried cast iron pipe corrosion rates. The latter was based on discussions with the commercial contractor and on assessments by the project team.

An examination of the theoretical underpinnings of LPR revealed that the LPR test outcomes reflect the rate at which electron processes take place on the metal surface. While it is believed that these processes dominate at the beginning of the corrosion process other external factors are likely to impact the rates of corrosion when corrosion is more advanced. The report concluded that the inclusion of these additional factors may improve LPR predictions of pipe

corrosion rates. A second report examining the practical application of the LPR technique and the manner in which the rate of corrosion is derived from the LPR test reached a similar conclusion. The reports concluded that the following factors should be included in an improved LPR-corrosion predictive model:

- The age of the pipe
 - The available data shows that cast iron pitting rates vary over time as different processes dominate the corrosion reaction. An additional age-related factor in the corrosion rate prediction model would improve model outcomes
- The method of pipe manufacture
 - Comparisons of LPR predictions of corrosion rates with observed values shows that the relationship between LPR test results and observed rates of pitting are different for pipes manufactured by different techniques (for example vertical or horizontally cast, with/without bitumen coating).
- Soil moisture level
 - Soil moisture (in the form of time of wetness) has been identified in the Activity 3 corrosion model as an important factor in the corrosion process however all LPR tests are conducted at a fixed moisture level which does not necessarily reflect moisture levels experienced at the corrosion site. Application of a correction factor to account for the impact of long-term soil moisture levels may be beneficial and should be investigated.
- Backfill quality
 - The contact between the soil surrounds and the pipe surface has been identified in Activity 3 as having an impact on corrosion rates. LPR operators also acknowledge that the LPR technique works best when the backfill is uniform. The incorporation into the predictive model of additional information relating to the backfill quality is recommended to improve corrosion prediction.

8.2.2 Quantification of the Current Level of Confidence in LPR Corrosion Predictions

To quantify the current level of uncertainty in the LPR prediction of corrosion an extensive LPR survey was conducted of the clay soils of the Verona St test bed in Sydney and sandy soils at sites in and around the Perth CBD area. The findings were as follows:

- a) LPR method reproducibility: A number of blind duplicate samples were submitted for analysis. LPR results for duplicate samples were generally in close agreement. Sandy soil samples showed slightly greater variability however as corrosion in such soils is generally lower this was not critical. The uncertainty in maximum pitting rates resulting from the variability in duplicate analysis was equivalent to less than +/- 0.02 mm/yr.
- b) Soil sampling variability: LPR analyses were conducted on soils sampled over a variety of sampling distances in the horizontal and vertical planes. LPR results were highly variable even over very short sampling distances with LPR resistivities varying by up to a factor of 3 over a 2-m distance (Figure 8.2). Again, this was not an issue in sandy soils where corrosion rates are low however the level of variability in clay soils was significant, corresponding to uncertainties up to +/- 0.1 mm/yr in the predicted corrosion rates.

- c) Model accuracy: In practice, LPR results are converted to maximum pit rates using an algorithm (or model) developed by or for the commercial contractor from the analysis of 30 cast iron pipe samples and their surrounding soils. To determine the level of uncertainty in the model prediction access to the original corrosion data was needed. To date, neither the commercial contractor nor the project team, has been able to locate the data.

Assuming that there are no major issues with the model accuracy it can be concluded that variations in soil properties over very short sampling distances may be a significant contributor to uncertainty in LPR-based predictions. In practice this issue is overcome by statistical analyses and by averaging, using many LPR samples. This means that any recommendations based on LPR and its interpretation are for relatively long lengths of pipe cohorts rather than for individual lengths or for short lengths of pipe. Whether this approach can be improved and so produce more refined predictions remains an open question.

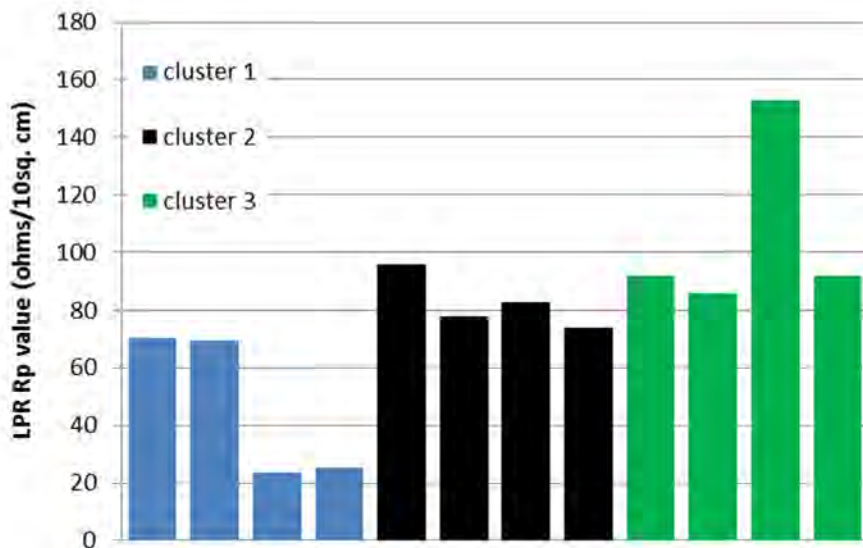


Figure 8.2. Variation of LPR Rp values for 3 clusters of soils sampled along the Verona St test bed. Each cluster consists of 4 soil samples taken at mid-pipe depth over a 2-m distance

8.2.3 Development of an Improved Model for LPR Prediction of Corrosion Rates

Once the relevant factors for model improvement had been identified it was envisaged that an improved model would be developed using the machine learning approach proposed by UTS. It was identified that such an approach would require a large amount of data consisting of LPR readings and soil moisture, age and method of manufacture of the pipe, information about the backfill and finally ground truth corrosion data. Such a data set is currently not available. It could not be generated in the time frame of this activity. Consequently, a data-driven model was not developed.

8.2.3.1 Conclusions and Recommendations for Future Work

Variations in soil properties over short distances are likely to be a significant contributor to uncertainty in corrosion rates predicted using the LPR technique. Consequently, corrosion rates specified at a single location from the analysis of a single soil sample are to be treated with caution. In practice this issue is overcome by statistical analysis and averaging of many LPR samples taken over the region of interest.

The work completed in Activity 4b has clearly indicated the factors that are likely to improve the LPR to corrosion rate predictive model. To progress this work, it will be necessary to assemble a significant data base of soil, pipe and corrosion data discussed above to allow for the model development and validation to take place.

PART 5
ACTIVITY 4C - PREDICTING THE LIKELIHOOD OF PIPE
CORROSION AND ITS SEVERITY ALONG THE PIPE TO FORECAST
FAILURE

Project Team (The University of Newcastle):

Professor Rob Melchers

Dr. Tony Wells

9 ACTIVITY 4C SUMMARY

The principal objective of Activity 4c was to establish a methodology for interpolating soil properties relevant to water pipe corrosion between sites where measurements could be obtained, and thus use the model from Activity 3 to predict current and likely future corrosion along the pipe, i.e., between measured points. Activity 4c also was to consider the feasibility and possible prototype for an advanced monitoring tool.

A considerable number of soil properties were considered at 3 different sites. Almost all showed a significant degree of variability even between samples taken 1m apart. Generally similar findings have been noted in the agricultural literature but for much shallower depths. However, in agricultural settings high variability is not always observed. This suggests that the high variability observed at the Sydney and Perth sites cannot be assumed to hold elsewhere.

To handle the variability issue, a new soil sampling methodology was developed to obtain average of soil properties at a given level of confidence, predicated on the estimated impact a particular soil property has on corrosion. In this approach a pilot survey of the area of interest is undertaken to assess the likely variabilities in the soil properties, from which the minimum number of additional samples required to adequately characterise the soil properties can be estimated.

The feasibility of an advanced soil monitoring tool was also assessed. Based on the corrosion model from Activity 3 a number of soil properties need to be assessed, preferably in-situ. A review of currently available technologies showed that, for example, soil nitrates can be measured in situ, but that the commercially available equipment is insufficiently sensitive. It is suggested that further work is required to assess the immediate and longer-term viability of in-situ monitoring.

9.1 INTRODUCTION

The aim of Activity 4c was to establish a methodology for estimating soil properties relevant to water pipe corrosion between sites where measurements could be obtained (a process known as interpolation). Once this was accomplished the corrosion model formulated in Activity 3 could then be used to predict the current and likely future corrosion along the pipe, i.e., between measured points. Activity 4c also considered the feasibility and possible prototype for an advanced monitoring tool. The findings of Activity 4c are discussed below. A number of appendices are also attached.

9.2 RESULTS

9.2.1 Interpolation of Soil Properties along the Pipe

Work undertaken in Activity 3 points to the following soil properties as being important to the rates at which buried cast iron water pipes corrode:

- Soil moisture
- Nutrient (nitrate) concentration in the soil and possibly other chemical species such as chlorine, sulphate, phosphate and carbonate
- Soil physical properties that impact on soil water holding capacity and moisture transport.

To determine the proper procedure for estimating these properties between measured points it was first necessary to develop an understanding of how the soil properties vary over distance.

To accomplish this a survey of the relevant soil properties was conducted at the Verona St test bed in Sydney and also in the Perth and Fremantle areas. Soil samples were taken at various positions around buried water pipes at these locations and also along the pipe length at mid-pipe depth at separation distances ranging from <1 to 200 m. Analysis of the soil samples so taken revealed that soil chemistries (including soil nutrient (nitrate) levels), soil moisture and wilt point and field capacity levels were highly variable around the pipe circumference (for example see Figure 9.1) and also along the pipe length at pipe (Figure 9.2) even at the highest sampling resolution (<1 m separation between samples). Sand, silt and clay content of soil samples however showed less variation. Similar high variability has been observed in agricultural soils at much shallower depths however, at least in agricultural settings, this level of variability is not always observed. This suggests that the high variability observed at the Sydney and Perth sites cannot automatically be assumed to hold elsewhere.

Soil spatial data was analysed using the semi-variogram technique which characterises the disparity in sample pairs as a function of the distance between them. The results of this technique allow the distance over which soil properties are related (the correlation length) to be determined. Variogram analysis of the key soil variables revealed that there was no correlation between soil properties even at the smallest sampling separation (i.e., <1 m).

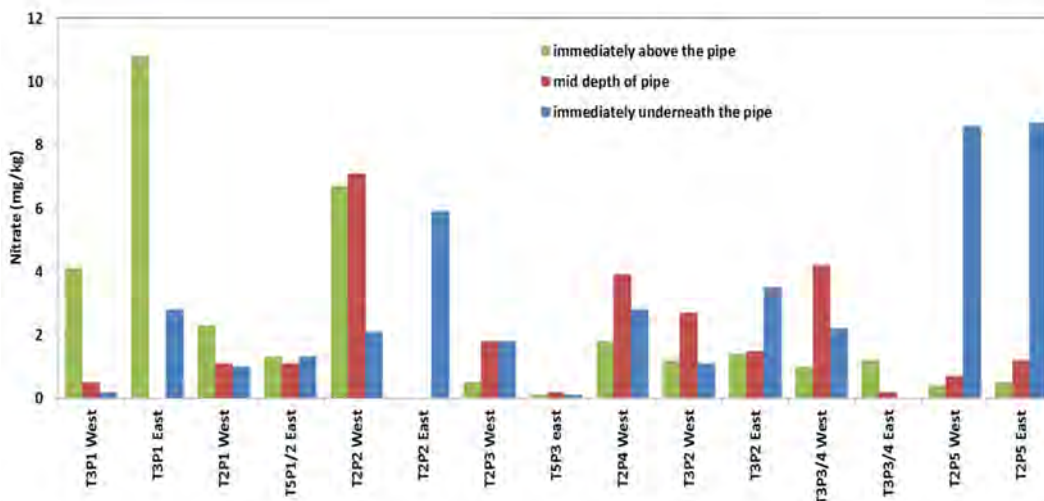


Figure 9.1. The variation in soil nitrate levels observed above the buried pipe, at the mid depth of the pipe, and underneath the pipe

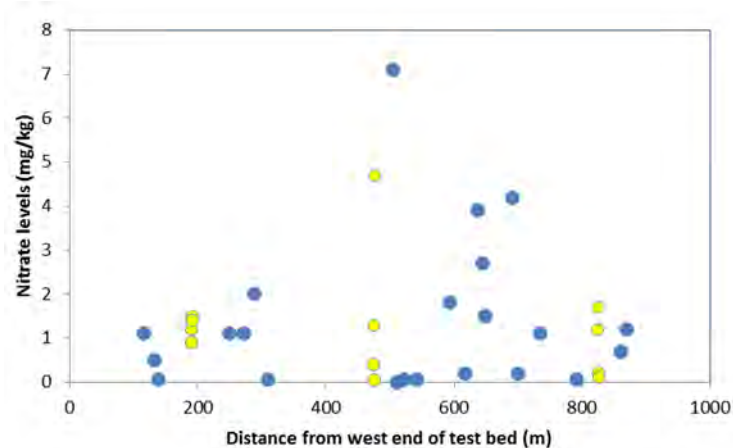


Figure 9.2. Variation in soil nitrate levels along the length of the Verona St test bed. All soils sampled at pipe depth. Yellow points are data from high resolution clusters (4 samples over 2 m)

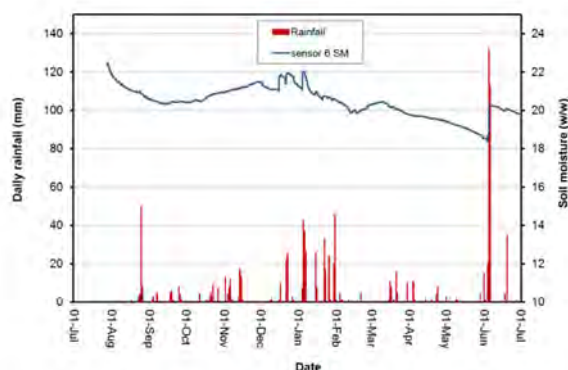


Figure 9.3. Long-term variation in soil moisture at site 6 - Verona St test bed, Sydney. Rainfall is that recorded at Concord golf club (nearby BOM site)

9.2.1.1 Stability of Soil Moisture Levels over Time

Soil moisture is important to the pipe corrosion process. In addition to its spatial variation it is also of interest to know how soil moisture at pipe depth varies over time. As little long-term soil moisture data is available at such depths (typically >1.5 m) a field monitoring program was established along the Verona St test bed to collect long-term soil moisture data. The data revealed that soil moisture levels were relatively constant over time (for example see Figure 9.3). Prolonged periods of above or below average rainfall were required before perceptible shifts in soil moisture content were observed. Comparison of long-term trends at a number of sites however showed that while soil moisture was relatively constant at any one location there remained a considerable spatial variation in soil moisture from point to point (Figure 9.4).

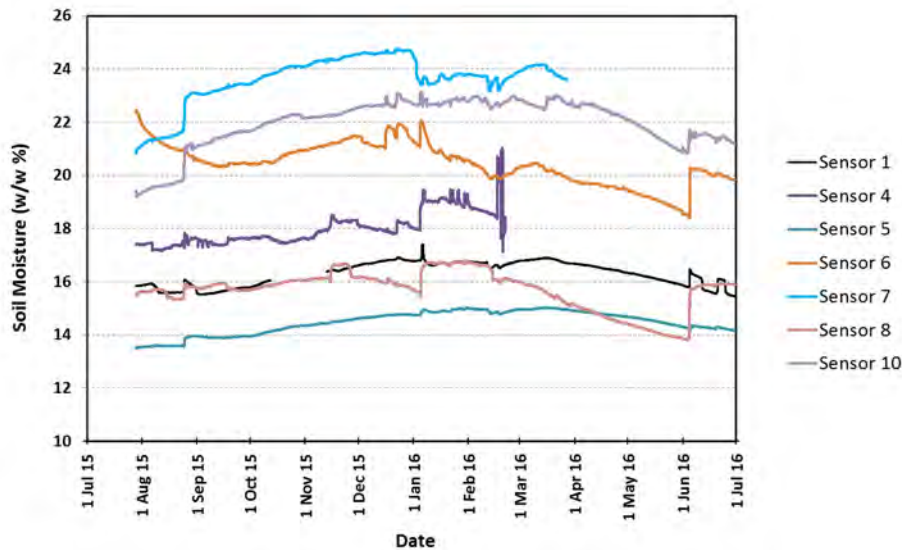


Figure 9.4. Soil moisture recorded at pipe depth along the Verona St test bed at 7 sites

9.2.2 Feasibility Assessment for an Advanced Monitoring Tool

The feasibility of an advanced soil monitoring tool was also assessed for the in situ measurement of the soil properties deemed as important in Activity 3 (see above). A review of currently available technologies showed that of the above listed variables only soil nitrates can be measured in situ, however even for this property commercially available equipment is insufficiently sensitive. It is suggested that further work is required to assess the immediate and longer-term viability of in-situ monitoring.

9.2.3 Method of Soil Property Estimation

The main aim of activity 4c was to develop a methodology for interpolating soil properties relevant to water pipe corrosion between sites where direct measurements are made. The high level of variability coupled with the lack of correlation between soil properties from neighbouring sample sites precludes the use of more classical interpolation techniques (such as polynomial or spline fitting). To accurately characterise soil conditions over any given length of pipe it would be necessary to sample the soil at extremely high resolution (<1 m spacing) which is impractical.

To overcome this issue a new sampling methodology was proposed which allows the average soil property over a given length of pipe to be determined within certain bounds at a given level of confidence. For example, along a given length of pipe it may be determined that... "we are 90% confident that the average soil nitrate level is 2.5 +/- 0.5 mg/kg...."

The number of soil samples required to make such a statement is dependent on the following factors:

- 1) The level of confidence required in the average value
 - a) The greater the required level of confidence the more samples will be needed. Generally, a 90 or 95% confidence is specified.

- b) As the acceptable level of error decreases the number of soil samples required increases.
 - c) The acceptable level of error for a given soil property is dependent on how sensitive the corrosion model is to the parameter. If, for example, the corrosion model is relatively insensitive to a given soil property then the acceptable level of error can be increased with relatively little impact on the predicted level of corrosion and consequently fewer samples are needed to specify the average soil property value.
- 2) The spread (or standard deviation) of the soil property along the pipe length
- a) The spread or standard deviation of the soil property along the pipe length can be estimated by undertaking a small pilot survey of the area of interest and calculating the standard deviation of the samples taken. In practice a minimum of 30 samples are recommended for such pilot surveys.

The strategy proposed is to first conduct a 30 sample pilot survey of the area of interest.

Once the soil properties of the initial survey sample have been analysed an estimate of the spread of the data, (S), for that area can be made. The acceptable level of error, (E), and the required level of confidence, ($CI\%$), are then determined after consideration of the impact of that soil property on the corrosion predictions made via the Activity 3 corrosion model.

The number of samples required for future surveys of the area can then be estimated from the following relationship:

$$n = \left(\frac{t_{df, \alpha/2} \times S}{E} \right)^2 \quad [9.1]$$

where n is the number of samples required, S is the standard deviation of the pilot survey, E is the acceptable level of error in the soil property and $t_{df, \alpha/2}$ is the student t factor for a given degree of freedom (df) and value α ($=1-CI\%$). This student t factor can be looked up in statistical tables or calculated in excel as follows $t=T.INV(\alpha/2,df)$.

The degrees of freedom, df , is calculated from n which is initially unknown. To calculate n therefore an iterative procedure is used. Initially n is estimated via the following:

$$n_{initial} = \left(\frac{z_{\alpha/2} \times S}{E} \right)^2 \quad [9.2]$$

where $Z_{\alpha/2}$ is the Z score for a confidence factor $\alpha/2$ (which can be looked up in any conventional statistics book or calculated in excel via $Z=-NORMSINV(\alpha/2)$) and all other factors are as defined previously. Once $n_{initial}$ is known the degrees of freedom, df , can be calculated ($df=n-1$) and equation [9.1] can be solved for n . The new value of n is then used to calculate the new value of df and equation [9.1] re-evaluated. The process is repeated until n is unchanged from one iteration to the next.

9.2.3.1 Example

A 30 sample pilot survey of the Verona St test bed is conducted. Analysis of soil nitrate levels for the 30 samples reveals a standard deviation of **0.2 mg/kg** in nitrate concentrations. After consideration of the activity 3 corrosion model it is decided that we are comfortable with an error of **+/- 0.05 mg/kg** error in the average nitrate level which we want to know to a **90% level** of confidence.

$$\alpha = 1 - \frac{90\%}{100} = 0.1$$

$$S = 0.2$$

$$E = 0.05$$

To make the initial estimate for n:

$$Z_{\alpha/2} = Z_{0.1/2} = Z_{0.05} = 1.6449$$

Using equation [9.2] then:

$$n_{initial} = \left(\frac{Z_{\alpha/2} \times S}{E} \right)^2 = \left(\frac{1.6449 \times 0.2}{0.05} \right)^2 = 43.3 \approx 44 \quad [9.3]$$

So, our initial estimate is that we require 44 samples (always round up to be conservative). The initial estimate for the degrees of freedom therefore is 43. The refined estimate for the number of samples required can now be calculated from equation [9.1].

first iteration:

$$df = 43$$

$$t_{df, \alpha/2} = t_{43, 0.05} = 1.681$$

$$n = \left(\frac{t_{df, \alpha/2} \times S}{E} \right)^2 = \left(\frac{1.681 \times 0.2}{0.05} \right)^2 = 45 \text{ samples}$$

second iteration:

$$df = 45 - 1 = 44$$

$$n = \left(\frac{t_{df, \alpha/2} \times S}{E} \right)^2 = \left(\frac{1.680 \times 0.2}{0.05} \right)^2 = 45 \text{ samples}$$

A 90% confident prediction of the soil nitrate average to +/- 0.05mg/kg will require 45 samples to be taken.

9.3 CONCLUSIONS AND RECOMMENDATIONS FOR FUTURE WORK

The highly uncorrelated nature of the soil properties observed at the Verona St test bed and at the Perth sites suggest that a classical interpolation procedure is not appropriate for estimating soil properties and hence corrosion behaviour along the pipe. Instead a procedure has been proposed which enable an estimate of the average soil property to be estimated for a given level of confidence within certain bounds.

The findings of this study are based on soil surveys conducted at a limited number of sites and will need to be verified at future locations as similar studies reported in the scientific literature, albeit for shallower soils, indicate that the high level of variability observed in this work may not be universal.

It is also important that the approach to estimating soil property averages outlined here be verified at a number of future sites.

10 ACKNOWLEDGEMENTS

Advanced Condition Assessment and Pipe Failure Prediction Project (ACAPFP), or Critical Pipes Project, is a collaborative project funded by Sydney Water Corporation (Lead), The Water Research Foundation, Melbourne Water, Water Corporation (WA), UK Water Industry Research Ltd, South Australia Water Corporation, South East Water, Hunter Water Corporation, City West Water, Queensland Urban Utilities, and Yarra Valley Water. Research Partners are Monash University (Lead), University Technology Sydney (UTS), and the University of Newcastle Australia.

The research project was led by Professor Jayantha Kodikara, Monash University, and he was also the leader of Activities 1 and 4e. Professors Jamie Valls Miro and Gamini Disanayake of UTS led Activities 2, 4a, and 4d. Professor Rob Melchers of The University of Newcastle led Activities 3, 4b, and 4c.

11 APPENDICES

11.1 APPENDIX 1A: EXPLANATORY NOTES FOR MONASH TOOL

11.1.1 Introduction to Monash Tool

As per the requirements of the Advanced Condition Assessment and Pipe Failure Prediction (ACAPFP) project, the Monash Tool (MT) was developed by Monash water pipeline researchers. This tool is intended for the purpose of providing guidance to the structural analysis associated with the condition assessment of pressurised cast iron (CI) pipelines. The MT is applicable for the conduct of longitudinal failure analysis of pipe barrels with uniform corrosion or single remaining wall corrosion defects that are idealised into ellipsoids. The emphasis of the tool development was on CI pipes.

The MT for assessing the pipe structural condition is based on the following estimates:

1. Nominal (hoop) tensile stress
2. Stress concentration factor (SCF) and maximum tensile stress for fracture initiation
3. Critical crack length for pipe burst
4. Remaining life to initiation of local failure leading to a leak

11.1.2 Evaluation Methods

11.1.2.1 Nominal (Hoop) Tensile Stress Calculation

11.1.2.1.1 Input Variables

The snapshot below shows the general input variables that are required in the MT. Their physical meanings are illustrated in Figure 11.1.

Pipe properties		
Pipe elastic modulus (GPa)	E_p	100
Poisson's ratio	ν_p	0.3
Pipe wall thickness allowing for uniform corrosion(mm)	T	20
Pipe outside diameter (mm)	D	660
Burial depth (mm)	H	950
Ultimate tensile strength (MPa)	σ_t	157
Soil properties		
Soil modulus (MPa)	E_s	25
Lateral earth pressure coefficient	k	0.4
Soil density (kN/m ³)	γ	19
Loading		
Traffic load (kN)	W	20
Internal pressure (kPa)	P	1000

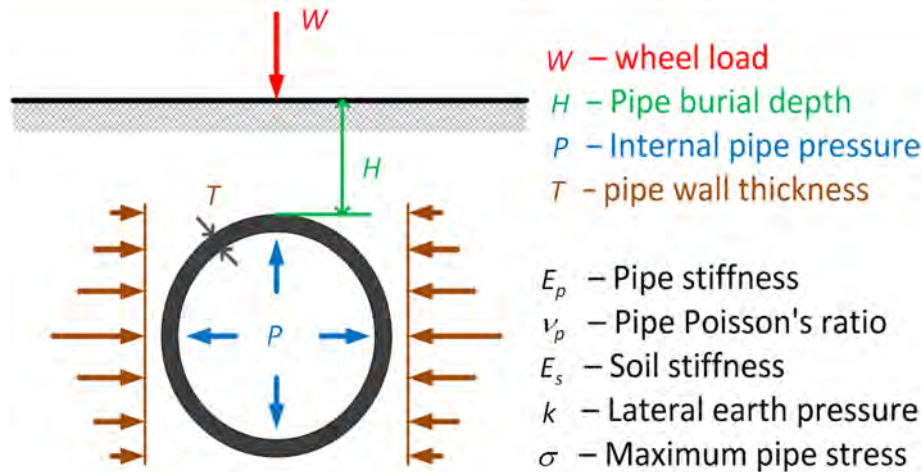


Figure 11.1. General variables for pipe and soil

- The current MT undertakes longitudinal failure analysis of the pipe barrel subject to uniform and (or) patch corrosion.
- The current MT is valid only within the range of variables listed in Table 11.1, where the units for each input variable are given. However, it may be applied outside these limits, although the results have not been checked.
- Thermal stress due to temperature changes is not considered in the current tool.
- The wheel load represents a single tyre load from traffic if applicable (e.g., steering axle). For other axles with multiple tyres, it is necessary to estimate an appropriate single tyre load. See Table 11.1 for recommendations.
- Burial depth is from the road surface to the crown of the pipe. Conservatively, the pavement structure is not specifically represented. It may be possible to use a height-weighted average soil modulus, if the influence of pavement is essential.
- Internal pressure includes steady-state pressure plus any transient pressure increase giving maximum possible operational pressure, i.e., internal pressure = maximum steady- state pressure + maximum transient pressure increase.

- Pipe wall thickness is equal to the current equivalent uniform wall thickness, as illustrated in Figure 11.2. Therefore, it is possible to allow for any uniform corrosion by reducing this amount from nominal (as constructed) wall thickness. If the pipe was cement lined in-situ after some years of operation, the nominal wall thickness may be reduced by the amount of internal wall corrosion during the period from the construction date to the date of in-situ lining.

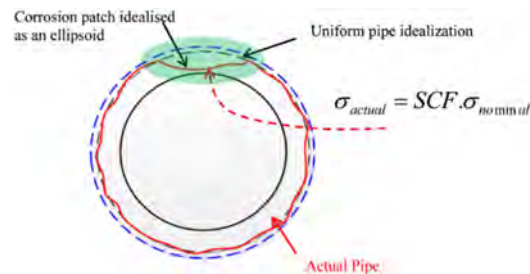


Figure 11.2. Sketch of wall thickness as an input in the Tool

In general, current wall thickness = As constructed wall thickness – uniform remaining wall external corrosion - reduction in wall thickness due to remaining wall internal corrosion.

- The input variables, such as the pipe stiffness, pipe Poisson’s ratio, soil stiffness, soil Poisson’s ratio (not mentioned here, but a value of 0.3 was used by default) have less effect on the solution. Therefore, the nominal values given in Table 11.1 may be used.

**Table 11.1
Physical properties for large-diameter cast iron buried pipes**

Description of physical parameters		Symbol	Unit	Value for NLR
Location	Burial depth	h	mm	300, 800, 1300, 2000
Backfill soil surrounding pipelines	Elastic modulus	E_s	MPa	2, 4, 10, 25, 50
	Unit weight	γ	kN/m ³	18.5
	Lateral earth pressure coefficient	k		0.1, 0.25, 0.4
	Poisson’s ratio	ν_s		0.3
Pipe physical properties (cast iron)	Elastic modulus	E_p	GPa	100
	Poisson’s ratio	ν_p		0.3
	Wall thickness	T	mm	4, 8, 10, 15, 27
	Pipe diameter	D	mm	300, 660, 1000
Load	Surface load (traffic)	W	kN	0 to 75
	Operating water pressure	P	kPa	0, 300, 500, 800, 1000, 1300, 1500

11.1.2.1.2 Output

Based on the above-mentioned input variables, the nominal tensile stress can be calculated:

Nominal (hoop) tensile stress (MPa)	σ_{nom}	21.0
--	----------------	-------------

For a uniformly corroded pipe or a new pipe, this is the maximum tensile stress within the pipe.

The technical details of the development of equations for the nominal stress calculation may be found in Robert et al. (2016b).

11.1.2.2 Calculation of Stress Concentration Factor (SCF) and Maximum Tensile Stress for Fracture Initiation

When there is a corrosion patch (or pit), the stress at that location is higher than the nominal stress computed in 11.1.2.1.1. This is calculated by using a stress concentration factor (SCF), which depends on the geometry of the corrosion patch. For MT, this patch is idealised by an ellipsoid.

11.1.2.2.1 Input Variables

The inputs shown in Figure 11.1 are required. In addition, the dimensions of the ellipsoid defect are needed:

Corroded patch geometry (set $a=0$ for uniform corrosion)			
Major (longitudinal) radius (mm)	a	50	b_{max} 50.00
Minor (circumferential) radius (mm)	b	40	
Corroded depth (mm)	c	18	

Note that a is the major axis and b is the minor axis, which should not be longer than b_{max} . When $a=b$, a spherical shape patch is simulated. The dimension c is the depth of corrosion at the middle of the patch (see Figure 11.3). Approximation of irregular corrosion pattern by equivalent ellipsoid shape), which should be less than the pipe wall thickness allowing for uniform corrosion input earlier.

In the case of a uniform corrosion, simply set $a = 0$.

11.1.2.2.2 Output

SCF will be calculated, and subsequently the actual tensile stress, which is the product of SCF and nominal tensile stress (maximum tensile stress = nominal tensile stress \times SCF). The actual tensile stress is then compared with the tensile strength of the CI pipe to assess if the pipe base starts to fail or not (i.e., fracture initiation or a LEAK). These outputs are illustrated below:

Stress concentration factor	SCF	5.9
Actual (hoop) tensile stress (MPa)	σ	124.7
Local failure or Initiation of a LEAK?		No

11.1.2.2.3 Notes

- Please note that an in-situ irregular remaining wall corrosion defect needs to be idealised into an equivalent ellipsoid (or crater) shape, and the corrosion depth, c , is the maximum corroded depth within the corrosion defect, as shown in Figure 11.3. This methodology is similar to the procedure given in ASME B31G (ASME 2012), but has been checked by Monash researchers for applicability to water pipes.

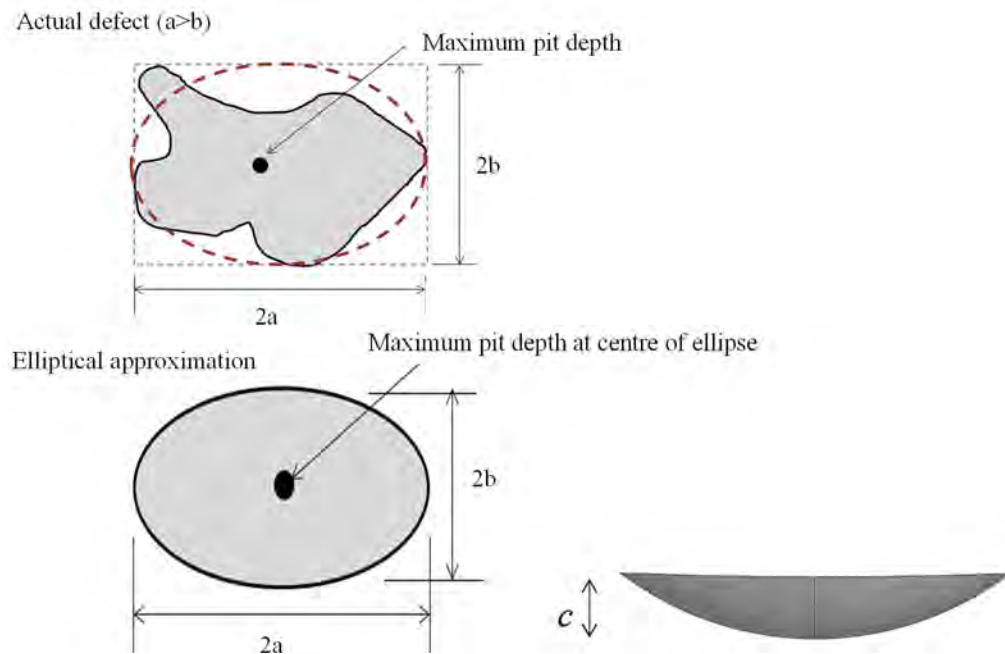


Figure 11.3. Approximation of irregular corrosion pattern by equivalent ellipsoid shape

- The other note is for an oriented corrosion defect, the length, $2a$, varies as per the changes of the orientation angle, θ , as indicated in Figure 11.4. This methodology was adapted from ASME B31G (2012), but has been checked by Monash researchers for applicability.

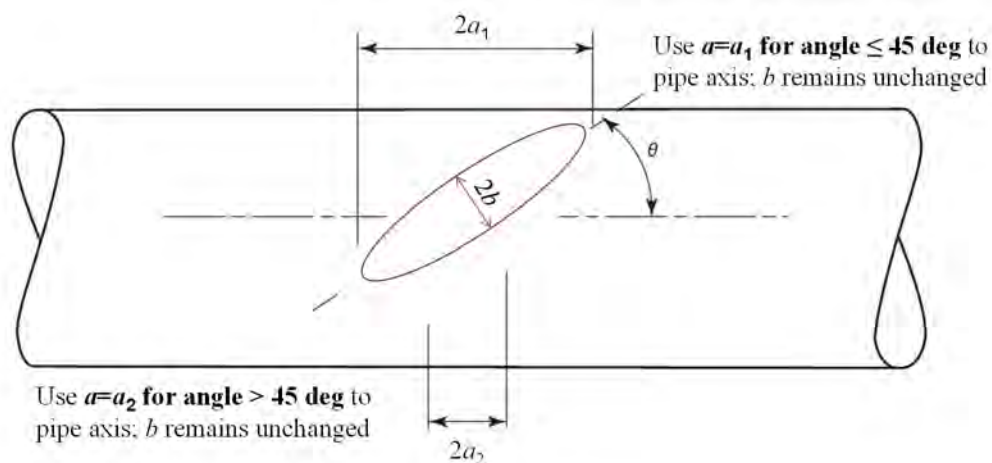


Figure 11.4. Change of length, $2a$, for an oriented corrosion defect

It is expected that fracture initiation may lead to a leak. However, in reality, whether a leak occurs or not depends on the length of the crack generated by the initial failure. For small pits, pit basal failure means the creation of a through-wall hole eventually and some of these may not leak due to the cement lining bridging them and/or graphitisation plugging the pit. However, for larger patches a larger crack may be generated which could with time lead to leakage.

The technical details of the development of equations for the maximum stress calculation incorporating patches will be detailed in a forthcoming technical paper by the Monash research team.

11.1.2.3 Calculation of Critical Crack Length for Pipe Burst

Once a fracture is formed through basal failure of a patch (and possibly a leak), whether this can cause a pipe to burst is approximately evaluated here. Please note that this calculation is approximate at this stage since it does not use the actual crack length generated in the initial failure, but the length of the corrosion patch (i.e., $2a$) as the reference crack length. Therefore, it provides a conservative assessment. It is considered that a burst will occur, when the stress intensity factor (SIF) equals the fracture toughness of the pipe material.

11.1.2.3.1 Input Variables

The inputs shown in Figure 11.1 and the dimensions of the ellipsoid defect shown in Section 11.1.2.2.1 and Section 11.1.2.2 are needed.

In addition, pipe fracture toughness, Kc is required:

Critical (longitudinal) crack length		
Pipe fracture toughness ($\text{MPa} \cdot \text{m}^{1/2}$)	Kc	15

11.1.2.3.2 Output

Click the “Critical Crack Length” button to calculate the critical crack length, Lc that is followed by the possibility (Yes or No) of pipe burst along the longitudinal direction of the pipe.

Critical crack length (mm)	Critical Crack Length	Lc	153.5
Possible to BURST?			No

11.1.2.4 Remaining Life

In cases where a corrosion patch has not progressed to a sufficient size to form initial failure (or a leak), the remaining life to cause a leak can be evaluated using normal and lateral corrosion rates. If a pipe burst does not occur with the leak, the time to burst from a leak cannot be evaluated at this stage. This window of time is referred to as the leak-before-break window (LBBW) of time. The LBBW depends on the transient loads, such as transient pressures, traffic and their frequency.

11.1.2.4.1 Input Variables

The inputs shown in Figure 11.1 and the dimensions of the ellipsoid defect shown in Figure 11.3 are needed.

Remaining life		
Vertical corrosion rate (mm/year)	r_{sv}	0.1
Horizontal corrosion rate (mm/year)	r_{sh}	0.5

11.1.2.4.2 Output

Click the “Remaining Life” button to calculate the estimated remaining life of the pipe. Note that the appearance of “over 100y” indicates the pipe life may be extended to at least another 100 years based on the current input, while “0” implies that the pipe already leaks or is broken.

Remaining life (year)	Remaining Life	5
-----------------------	----------------	---

11.1.3 Disclaimer

1. Use of the information and data contained within this tool is at your sole risk.
2. If you rely on the information in this tool, you are responsible for ensuring by independent verification its accuracy, currency or completeness.
3. The information and data in this tool are subject to change without notice.
4. The tool developers listed at the top of the tool may revise this disclaimer at any time by updating this tool.
5. Monash University and the developers accept no liability whatsoever arising for any loss resulting from the use of the tool including any information and data.

11.2 APPENDIX 1A: DEFINITIONS OF STATISTICAL FUNCTIONS AND FAILURE DATA

11.2.1 PDF

For any given pipe failure data, the histogram is first exploited. For example, the Sydney Water failure data (2000 to 2012) give a CI failure histogram as shown in Figure 11.5. The failure population is 1556. Each bar indicates the number of failure pipes falling in the specified age interval. For example, there are around 500 pipes failure between 30 and 45 years old. By normalizing the histogram, the probability mass function (PMF) is obtained. If the data are continuous, the PMF is known to be a probability density function (PDF), as shown in Figure 11.6. The PDF simply gives the percentage of the interval data. The total area under PDF is unity.

11.2.2 CDF

The cumulative distribution function (CDF), describes the probability that a real-valued random variable X with a given probability distribution will be found to have a value less than or equal to x. The time-dependent failure probability of pipes can be regarded as the CDF of a

particular type of distribution. The CDF of Sydney Water can be computed by integration/summation of the PDF result, as shown in Figure 11.7:

$$\text{CDF}_{xi} = \text{Sum} (\text{PDF}_{xj} * \text{Age_Interval}) \quad j \leq i.$$

11.2.3 Hazard Rate

Hazard rate is a conditional probability of the failure density function. The condition is that the failure has not occurred at time t. It is the ratio of the probability density function PDF to the survival function or reliability function $R(t) = (1 - \text{CDF})$, given by

$$\text{Hazard rate} = \text{PDF} / (1 - \text{CDF})$$

It denotes the instantaneous failure rate as the time interval tends to zero. The hazard rate for Sydney Water failure data is computed as shown in Figure 11.8.

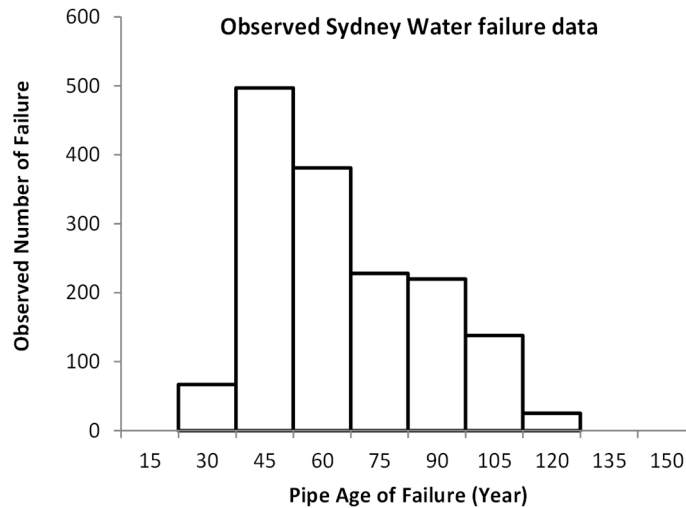


Figure 11.5. Histogram of SW failure data (2000 – 2012)

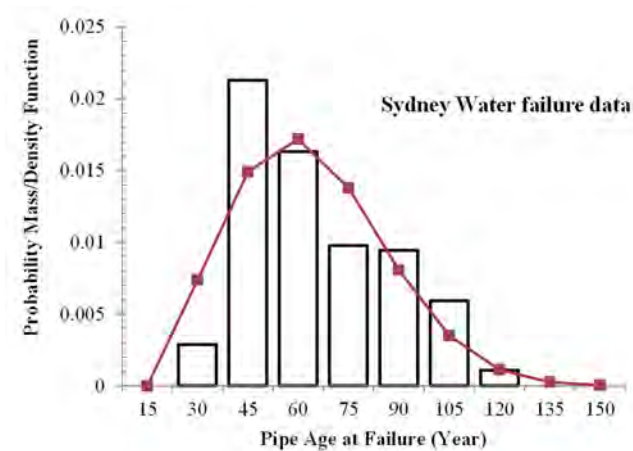


Figure 11.6. PMF/PDF of SW failure data

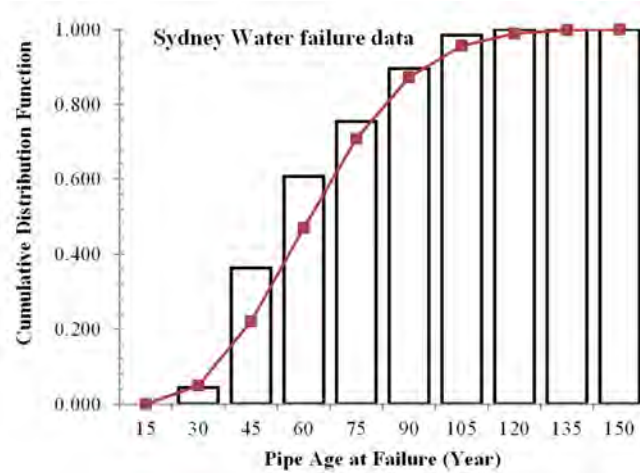


Figure 11.7. CDF of SW failure data

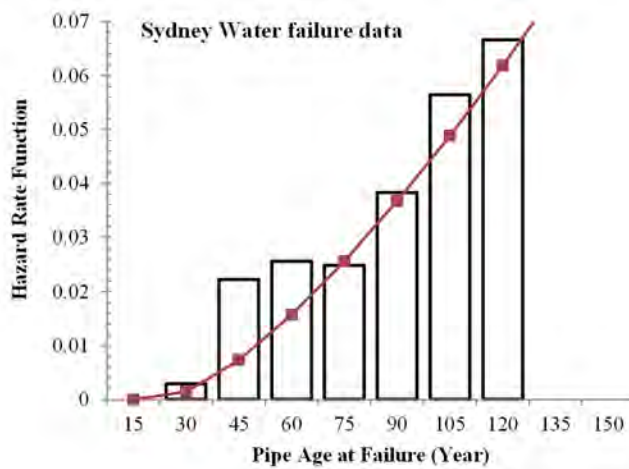


Figure 11.8. Hazard rate of SW failure data

11.3 ACTIVITY 2 APPENDIX 1: PROCEDURE FOR OBTAINING GROUND TRUTH OF REMAINING WALL THICKNESS OF CRITICAL PIPES

11.3.1 Preface

This is a procedure manual detailing the sequential procedure for obtaining ground truth (i.e., 2.5D Thickness Maps) of remaining wall thickness of critical pipes. This document is an outcome of the Advanced Condition Assessment and Pipe Failure Prediction Project (<http://www.criticalpipes.com/>).

11.3.2 Introduction

The ground truth or the best estimate of remaining wall thickness of critical water pipes is computed by means of ray-tracing performed on 3D point clouds of pipes. Point clouds are obtained using the EXAscan 3D Scanner provided by Creaform© (<http://www.creaform3d.com/en>, date of last visit: 04/05/2016) shown in Figure 11.9. It is operated using the VXelements© software. Current practice involves using VXelements© version 4 under the ‘Super User’ license. Sydney Water Laptop (Barcode Number: 10660571) has the software installed providing ‘Super User’ rights to users.



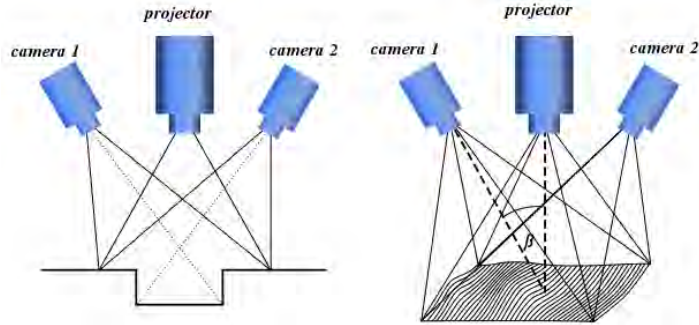
Figure 11.9. EXAscan 3D Scanner by Creaform©

11.3.3 EXAscan 3D Scanner - Operating Principle

The EXAscan 3D Scanner operates by means of projecting a narrow band of light onto a surface of a 3D object and capturing distorted forms (views) of the illuminated surface area (light section) via two cameras viewing the illuminated area from perspectives different than that of the projector (see Figure 11.10). These distorted forms of projected light are transformed to exact geometric reconstruction of the illuminated surface section, whereby the surface section is captured and saved in the form of a 3D point cloud.

Geometric reconstruction of 3D surfaces is carried out by recognizing and recording local patterns generated by ACC-H3D-PTBC Positioning Targets (see Figure 11.11) affixed on the surface being scanned (see Figure 11.12). Scanning is carried out in two steps:

1. Scanning the targets.
2. Scanning the surface.



Source: Wikipedia 2008.

Figure 11.10 Operating principle of the EXAscan 3D scanner



Figure 11.11. A box of positioning targets

First, scanning targets is done. When scanning targets, local patterns generated by targets are recognized and recorded. Secondly when the surface is scanned, previously recorder target patterns are used as location references and the surface is scanned and recorded at a high resolution. Due to the aforementioned operating principle, it is extremely important to follow the three steps below in order to avoid errors.

1. Whenever a scan is paused at any time, begin the scan from a previously scanned location since continuation of surface reconstruction is based on recognizing previously recorded target patterns.
2. Once a section of targets has been scanned during the process of scanning targets, the scanned targets must not be touched, removed or moved until scanning the surface associated with those targets has been completed since any displacement of targets may result in errors when scanning the surface. After targets have been scanned, target density can be increased by placing more targets before scanning the surface, however, scanned targets cannot be moved.
3. Loop closure (i.e., returning to the position or target pattern at the location where the scan was begun). This is necessary to minimize errors in the point cloud through a target location optimization performed by the scanning software (VXelements©).



Figure 11.12. Targets affixed on a surface being scanned

11.3.4 Recommendations for Best Practices

11.3.4.1 Always arrange for a person operating the scanner to be trained by an experienced scanner operator and closely study the VXelements© user manual in addition to reading this guide.

11.3.4.2 Perform 3D scanning in low light (no more than 200 lux).

11.3.4.3 Closer the targets, the better. Baseline is any target having at least four nearest neighbours within 4~5 cm radius.

11.3.4.4 3D scanning of pipes is likely to cause fatigue and/or muscular strain to scanner operators. Avoid making operators crawl into pipe sections as it fatigues operators, put them at risk of injury and may also cause errors due to operators rushing due to fatigue. Best practice would be to slice long pipes and make operators scan sections no longer than 0.75~1 m.

11.3.4.5 Only pipes of 475 mm or more internal diameter should be scanned in whole. In case a pipe of lesser internal diameter has to be scanned, they must be split along the axial direction as shown in Figure 11.13 to make two segments and the two segments must be scanned separately following the procedure described in this guideline.

11.3.5 Safety Precautions

11.3.5.1 Always support pipes with wedges to avoid rolling (see Figure 11.14).

11.3.5.2 Use personal protective equipment, i.e., steel capped boots, long sleeved tops, and goggles (when cleaning dust/dirt off pipe surfaces and scanning internal surfaces).

11.3.5.3 Execute manual handling (e.g., rolling pipes) with caution and seek support where necessary.

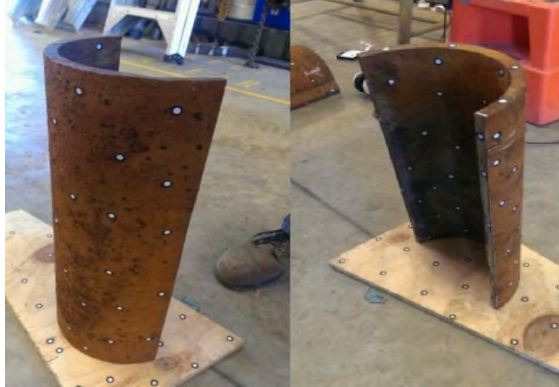


Figure 11.13. A split section of a pipe having less than 475 mm internal diameter



Wedge

Figure 11.14. A wedge supporting the pipe to avoid rolling

11.3.5.4 Internal surfaces of pipe sections no longer than 1 m can easily be scanned without operators having to crawl in. Therefore, cutting pipe sections of 1 m in length is recommended.

11.3.6 Obtaining Point Clouds

The steps of obtaining point clouds include preparation of pipes, affixing targets, scanner configuration, scanning the target model and scanning the surface.

11.3.6.1 Preparation of Pipes

11.3.6.1.1 Exhume the pipe section required to be scanned.

11.3.6.1.2 Clean the external surface to remove soil and dirt (best practice would be washing).

11.3.6.1.3 Remove internal cement lining if prevalent.

11.3.6.1.4 Sandblast both internal and external surfaces to remove rust and graphite/graphitisation.
Blasting Standard: SP5, Abrasive Material: Silica Sand.

11.3.6.1.5 In case one or more calibration defects as shown in Figure 11.15 are not already marked on the pipe section, they need to be mark at this stage. A minimum of one circular cylindrical

calibration defects of 1 cm or more diameter and 5 mm deep needs to be marked on the crown of the pipe. This is done to have as a visible reference to relate a generated ground truth plot to an actual pipe.

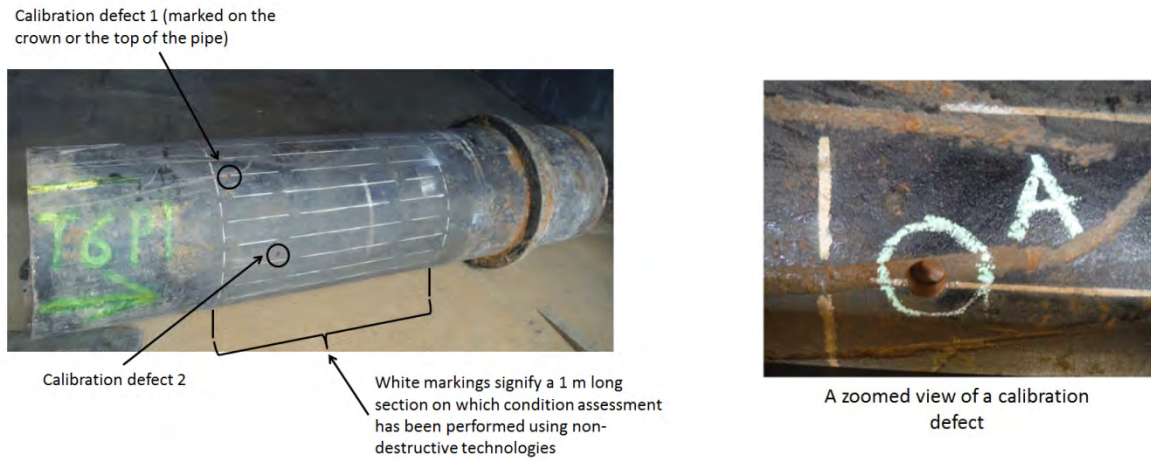


Figure 11.15. Calibration defects marked on a pipe

11.3.6.2 Suitable Environment for Scanning Pipes

Scanning pipes should be done in a low-light (or dark) environment to avoid surface localization errors caused by noise resulting from external light. It is recommended to scan pipes in an enclosed indoor environment lit by reflected sunlight. An illuminance less than 200 lux on the top centre of the pipe external surface is preferred. There is no minimum lux value requirement. Figure 11.16 shows an example of how a suitable location appears to the human eye along with a lux reading. Best practice to measure light condition will be a well calibrated lux meter. Alternatively, the Luxi For All/Luxi[©] iphone application or any other suitable smartphone application which can perform a lux reading can be used.



Figure 11.16. A suitable environment for pipe scanning

11.3.6.3 Affixing Targets

11.3.6.3.1 Dust off both internal and external pipe surfaces.

11.3.6.3.2 Affix ACC-H3D-PTBC Positioning Targets (as in Section 11.3.6.4) to cover both internal and external surfaces. Figure 11.11 appeared before showed a box of targets.

11.3.6.4 A Suitable Method for Affixing Targets

11.3.6.4.1 Place the pipe on parallel wooden planks placed on the floor as shown in Figure 11.17. The pipe axis should be perpendicular to the planks. The length of wooden planks should be greater than the pipe circumference to be able to conveniently roll the full circumference of the pipe without the pipe falling off the planks. The planks should be placed about 50% of the pipe length apart and a plank width should not exceed one eighth of the pipe length approximately.

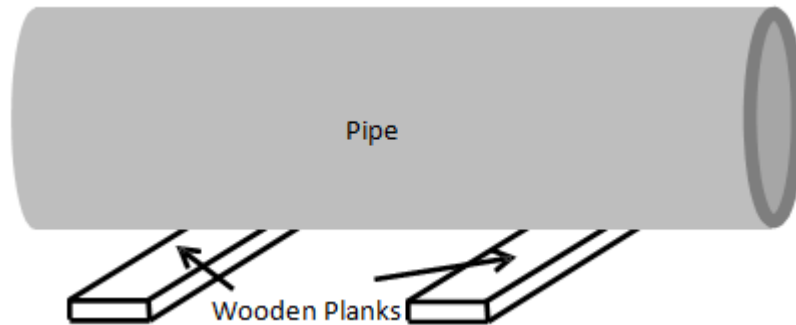


Figure 11.17. Pipe placed on wooden planks (Not drawn to scale)

11.3.6.4.2 Target locations must be random and be placed in such a way that the distance between any two adjacent targets is not more than 5 cm as shown in Figure 11.18.



Figure 11.18. Placement of targets on pipe wall

11.3.6.4.3 Cover the full circumference of the external surface as shown in Figure 11.19 with targets. Leave two bands with no targets as shown in Figure 11.19 as targets should not come to contact with the planks when the pipe is being rolled.

Dimensions of the bands with no targets should be:

- a) Width = Plank Width + 2 inches approximately.
- b) Length = Approximately 75% of the pipe circumference.

See Figure 11.20 for details.

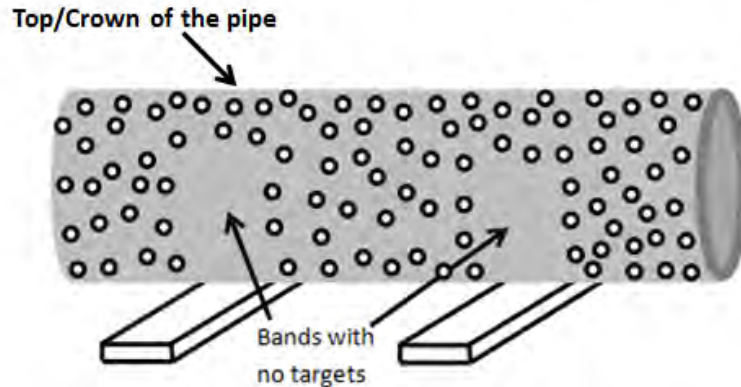


Figure 11.19. Targets affixed on external surface (not drawn to scale)

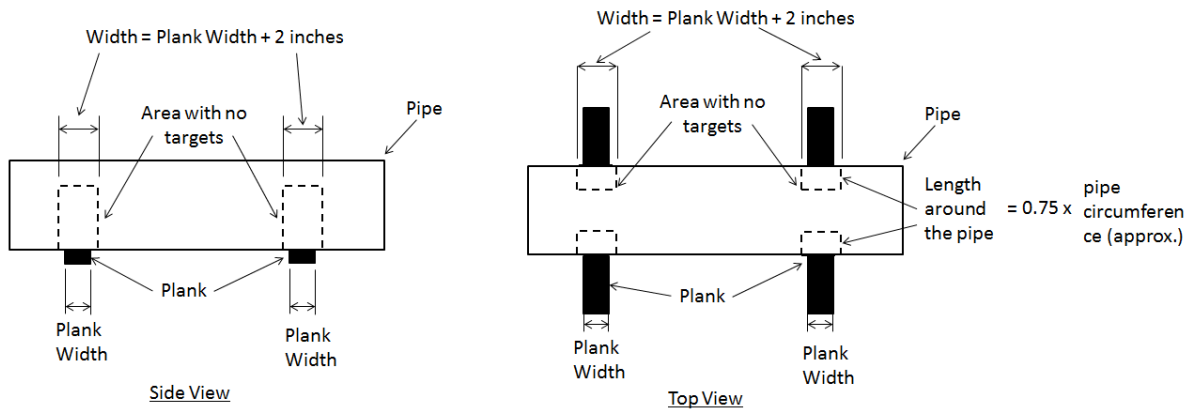


Figure 11.20. Side and top views of a pipe placed on planks showing dimensions of bands with no targets (not drawn to scale)

11.3.6.4.4 Cover the entire internal surface of the pipe in targets as shown in Figure 11.21(a). If the pipe is too long to physically reach the entire internal section, apply targets on the internal surface as shown in Figure 11.21 (b). Cover the top half with targets. In the bottom half, cover only a band having a width of 25% of pipe length approximately. The band should be located at the centre of the pipe to enable a human to move into the pipe to scan without coming to contact with targets.

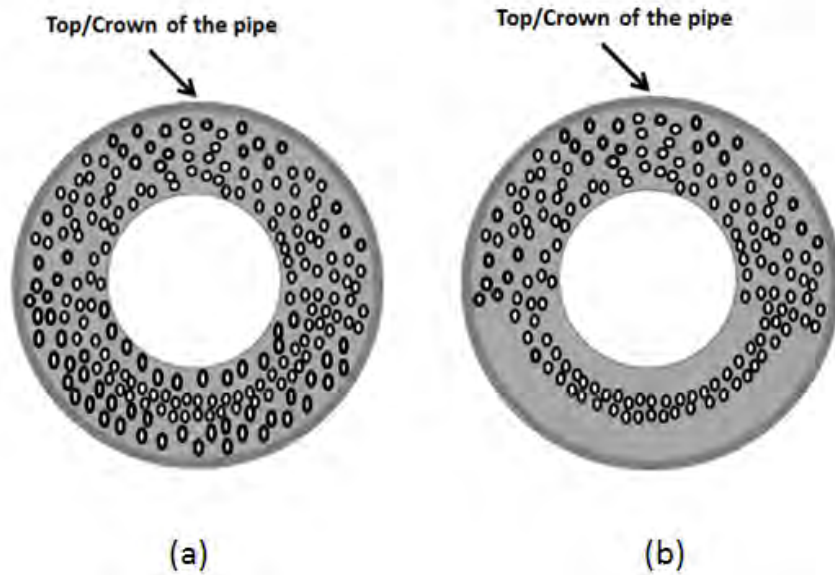


Figure 11.21. (a) Full internal surface covered by targets when looking towards the inside of the pipe; (b) Internal surface partially covered by targets in a long pipe to enable an operator to move into the pipe to scan the internal surface

11.3.6.5 Setting up the Scanner

11.3.6.5.1 Components of the scanner setup are shown in Figure 11.22.



Figure 11.22. Components of the scanner setup

11.3.6.5.2 Turn on the Sydney Water laptop (Barcode Number: 10660571) and connect the FireWire adapter (ExpressCard/34 IEEE 1394a 2 Ports) and cables as shown in Figure 11.23 and turn on power.

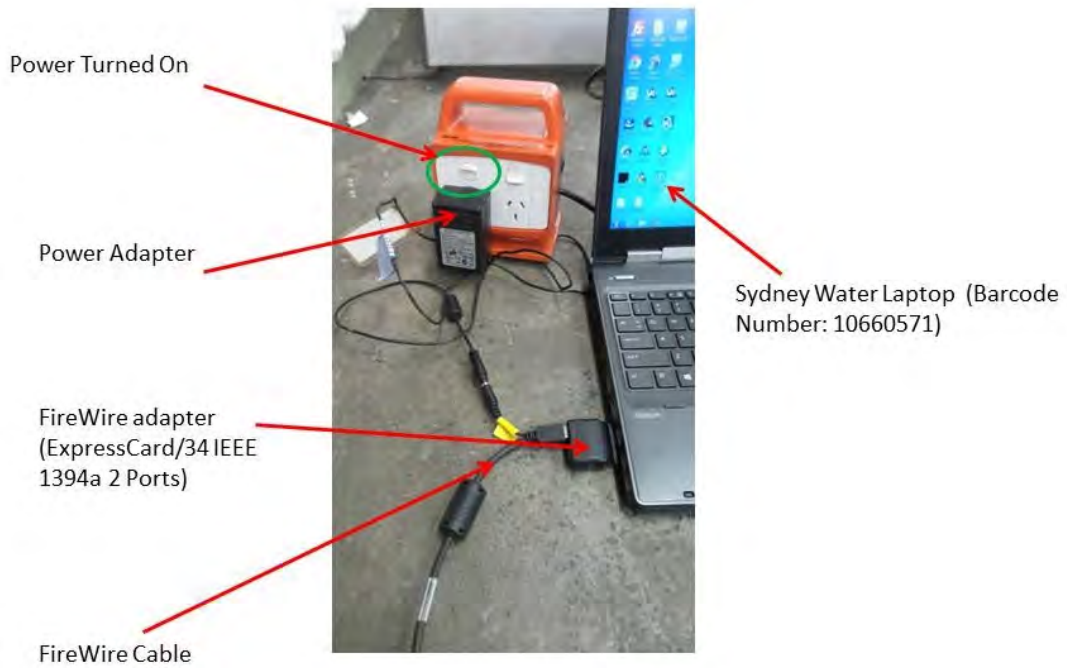


Figure 11.23. Cables connected to the Sydney Water laptop

11.3.6.5.3 Connect the other end of the FireWire cable to the scanner as shown in Figure 11.24 and the scanner will turn on automatically.



Figure 11.24. Cable connected to the scanner

11.3.6.5.4 Open the VXelements version 4 software interface (see Figure 11.25).

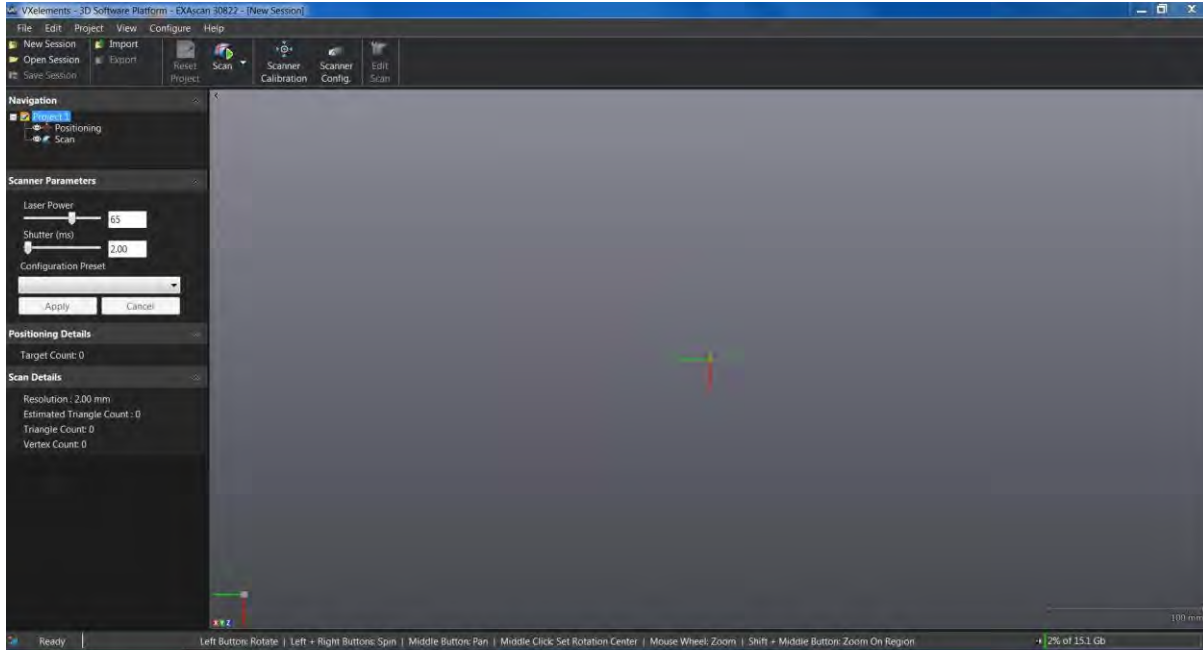


Figure 11.25. VXelements© version 4 user interface

11.3.6.6 Scanner Configuration

11.3.6.6.1 Set up the scanner as in Section 11.3.6.5 and open VXelements version 4 software.

11.3.6.6.2 Click on 'Scan' under 'Project 1' on the left side pane and locate the 'Scan Parameters' section (see Figure 11.26).

11.3.6.6.3 Do the following in the 'Scan Parameters' section:

- a) Set the 'Resolution' to 2.00 mm.
- b) Drag 'Boundary Optimization' slider to 50%.
- c) Drag all other sliders to 0%.
- d) Tick the 'Fill Positioning Targets' box, and
- e) Click 'Apply.'

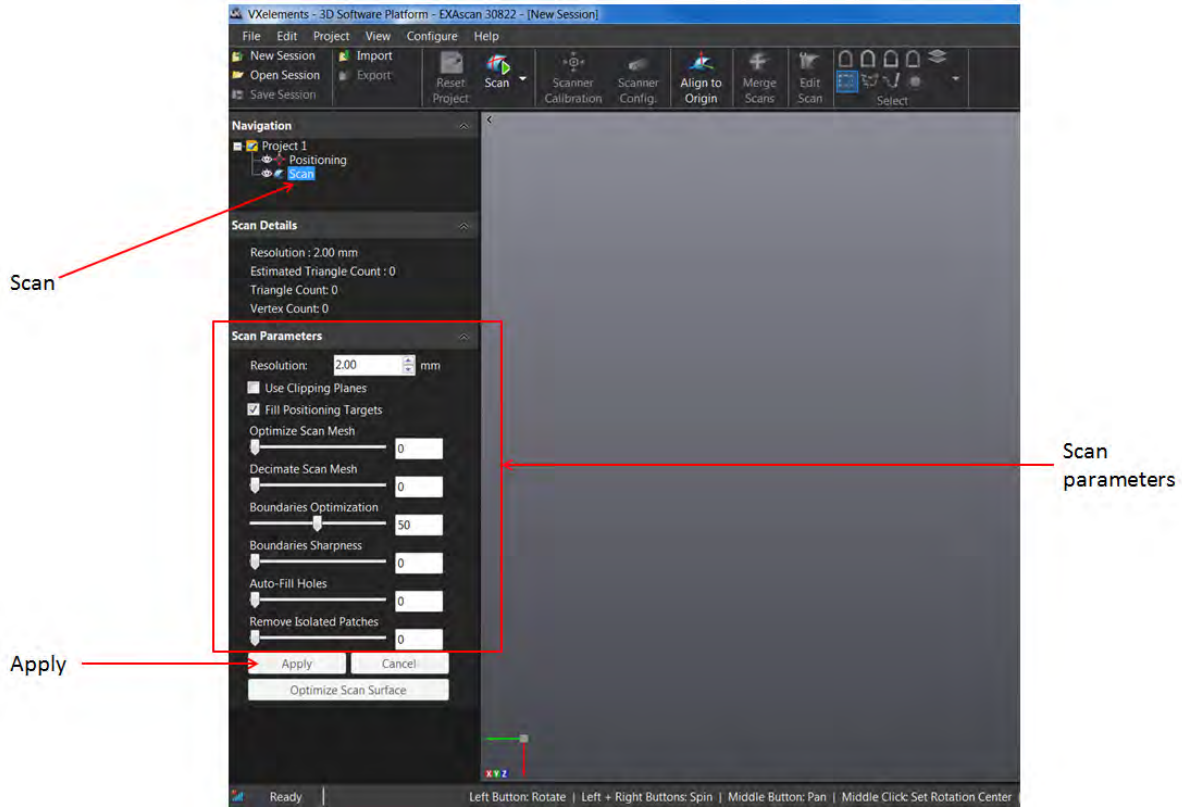


Figure 11.26. Adjusting scanner parameters

11.3.6.6.4 Then click on 'Project 1' and then 'Scanner Configure' as shown in Figure 11.27.

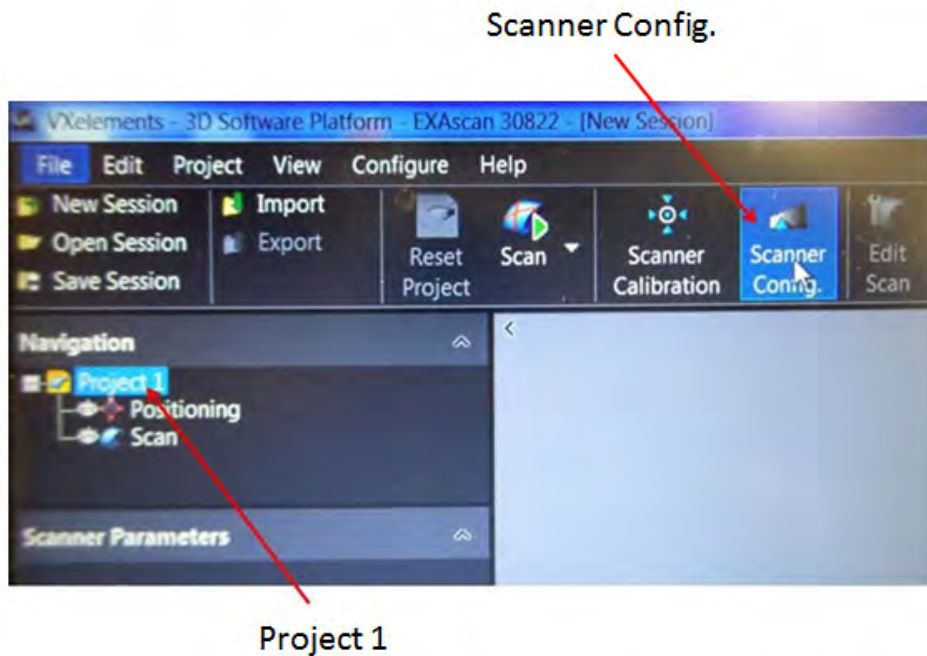


Figure 11.27. Setting up scanner configuration mode

11.3.6.6.5 The screen shown in Figure 11.28 will appear.

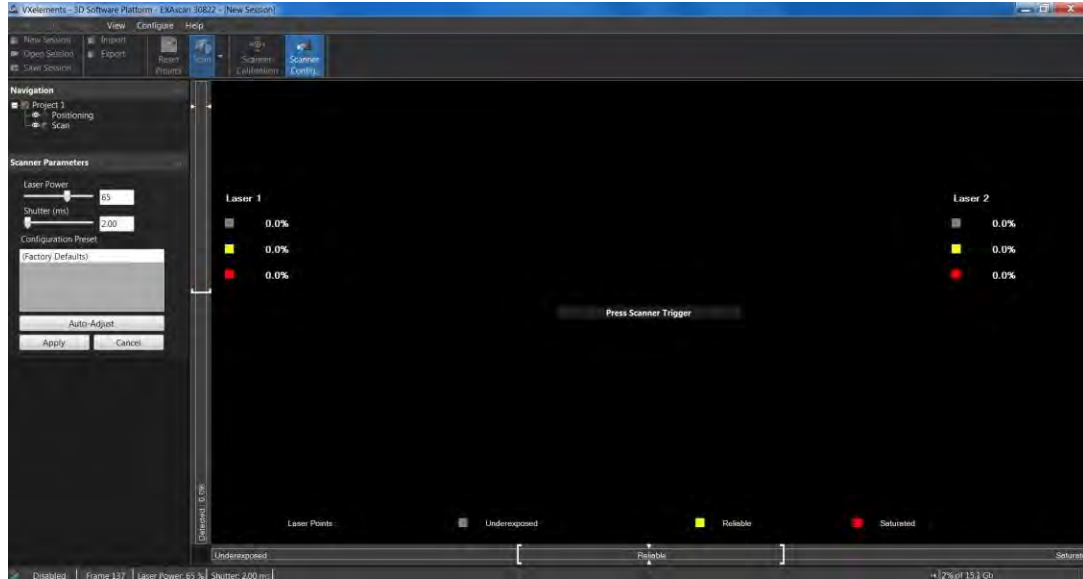


Figure 11.28. Scanner configuration screen

11.3.6.6.6 Hold the scanner with the laser emitter pointing towards the external pipe wall and remaining approximately 30 cm away from the wall as shown in Figure 11.29. The scanner should be perpendicular to the surface being scanned.



Figure 11.29. Scanner placement for configuration

11.3.6.6.7 Press the scanner trigger (see Figure 11.30).



Figure 11.30. Scanner trigger button

11.3.6.6.8 Attempt to achieve a reliability of 90~100% on the external pipe surface for both lasers by increasing the ‘Laser Power’ and ‘Shutter (ms)’ as in Figure 11.31.

11.3.6.6.9 Once the suitable reliability is achieved on the external surface, release the scanner trigger and place the scanner in a position suitable to scan the internal surface and press the trigger.

11.3.6.6.10 Likewise, alternate internal and external surfaces and attempt to find a common setting, i.e., a ‘Laser Power’ level and a ‘Shutter (ms)’ speed, which gives highest reliabilities (90~100% will be best) for both surfaces. Once a suitable reliability is reached click “Apply” (see Figure 11.31).

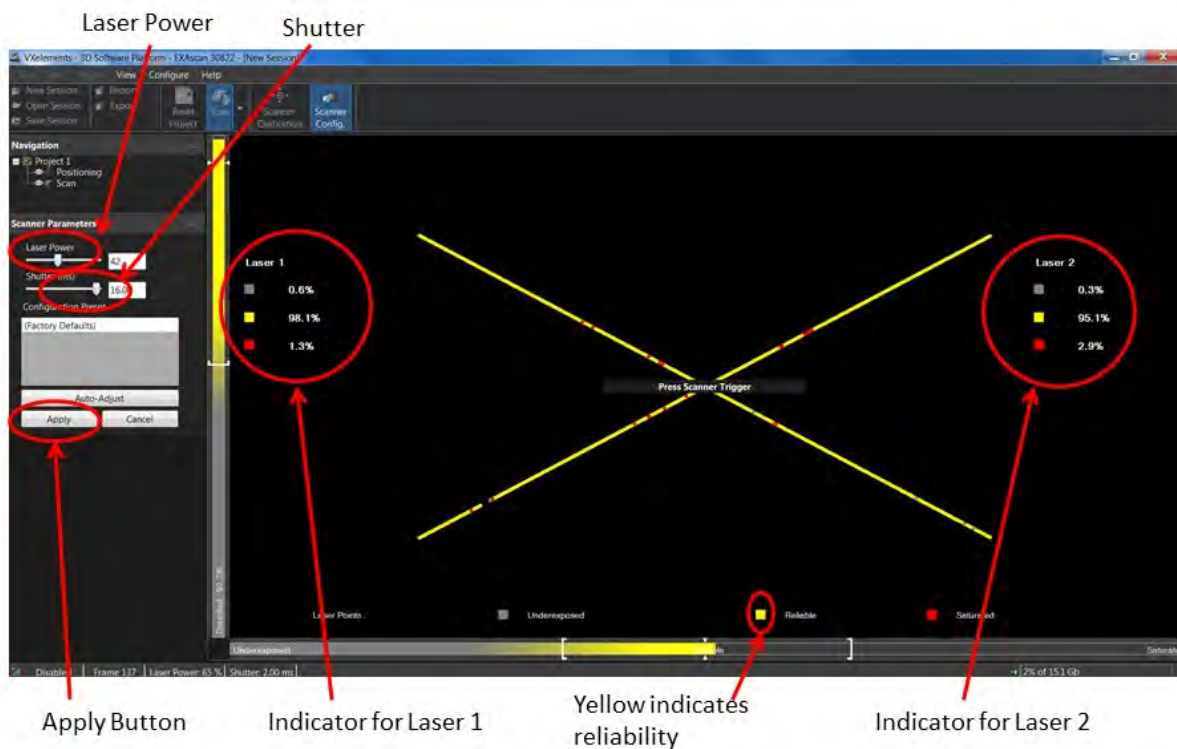


Figure 11.31. Scanner reliability indicators

11.3.6.7 Scanning the Targets

11.3.6.7.1 Configure the scanner as explained in Section 11.3.6.6.

11.3.6.7.2 Click 'Scan Positioning Targets' as shown in Figure 11.32. Then hit the space bar for the software to be ready to scan targets.

Space Bar

Space bar performs a soft connection and a disconnection between the scanner and the laptop. If at any time the scanner does not capture targets when the scanner trigger is pressed as in step 6.7.4, the space bar must be pressed for the soft connection to happen. Similarly, if at any time editing or saving a model is not allowed, the space bar must be pressed for the soft disconnection to happen.

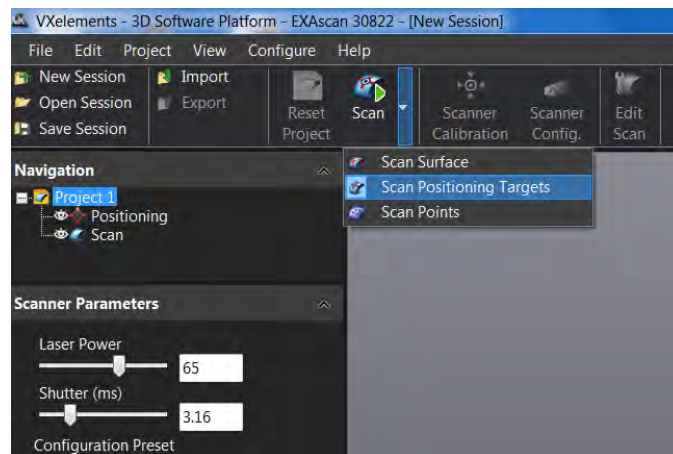


Figure 11.32. Click 'Scan Positioning Targets'

11.3.6.7.3 Hold the scanner with the laser emitter pointing towards the targets on the external pipe wall and remaining about 30 cm away from the wall as shown in Figure 11.33.



Figure 11.33. Scanner placement for scanning targets

11.3.6.7.4 Press the scanner trigger to start scanning.

The colour of the bar towards the left of the screen (see Figure 11.34) indicates the distance between the scanner and the pipe surface. The colours indicate the following:

 or  indicates the scanner is too far from the surface

 or  indicates the scanner is too close to the surface.

 indicates ideal distance

Similarly, for convenience the operator may also use the **three lights** on the **top of the scanner** (see Figure 11.37) as indicators of distance. The scanner should remain in the **green zone** as much as possible.

Important: Once scanning has begun, if scanning is paused at any stage, resumption must occur at an already scanned location before advancing to new locations. This is to enable error free localization as the software relies on previously scanned targets to register the location of new targets.

Scanning Errors

The most recently scanned **targets** will appear in **red** as shown in Figure 11.34 and Figure 11.35 while any previously scanned **targets** will appear in **white** on the laptop screen. **Targets** appearing in **any other colour (light blue for example)** (Figure 11.35) at any time while scanning indicate an **error** in the model and scanning must be paused immediately by releasing the scanner trigger. After pausing, hit the space bar, and then press “Edit Scan” located on the top pane (see Figure 11.36). This enables manual deleting of bad targets. Use the mouse to select bad targets by clicking on them. When erroneous targets have been selected, press the “Delete” on the keyboard to delete bad targets. Deleting results in the software perceiving as if the erroneous targets were not scanned and the bad locations can be scanned again.

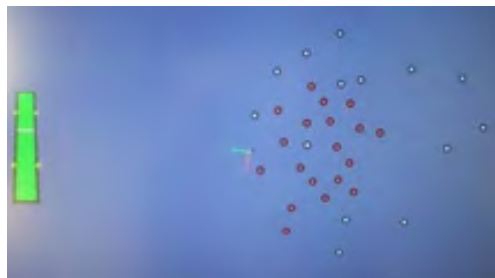


Figure 11.34. A set of well scanned targets

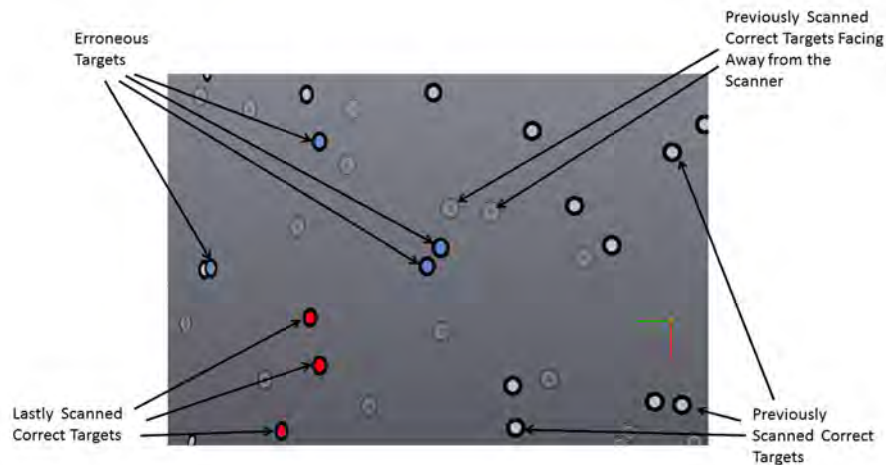


Figure 11.35. Erroneous targets appearing in light blue

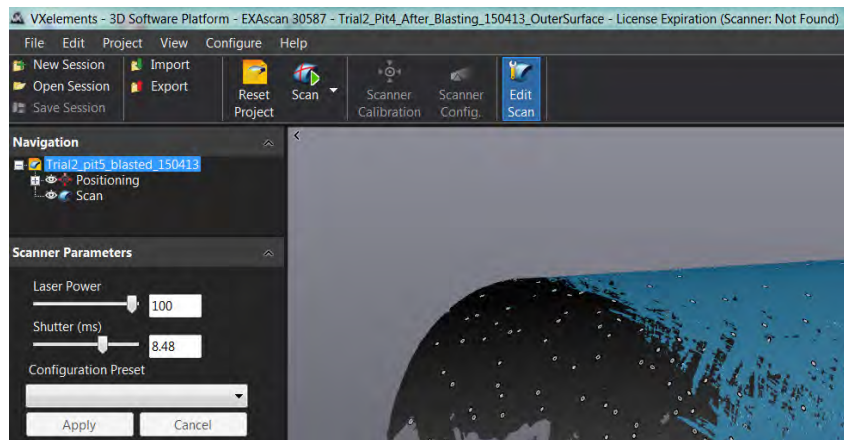


Figure 11.36. Edit Scan button on the top pane

11.3.6.7.5 Once the first few error-free (Red and White) targets appear on screen, release the scanner trigger to pause scanning.

11.3.6.7.6 Hit the space bar to disconnect the scanner from the laptop.

11.3.6.7.7 Then save the captured target model using File → Save Session As (or keyboard shortcut Ctrl+Shift+S). Provide a suitable filename and save as a Session File with the .csf extension at a desired folder. Saving regularly hereafter when proceeding with scanning is recommended.

11.3.6.7.8 Hit the space bar again to reconnect the scanner to proceed scanning.

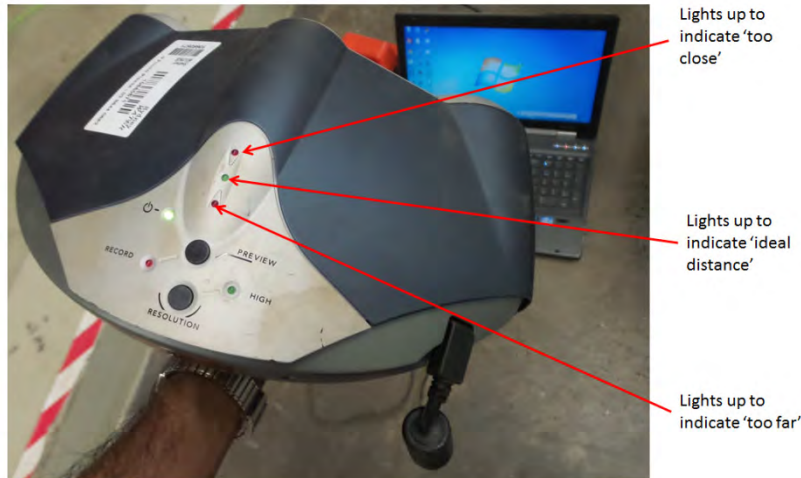


Figure 11.37. Lights on the scanner to indicate distance

11.3.6.7.9 Scan a ring having a width of approximately 25% of the pipe length covering the full circumference of the external wall at the centre of the pipe (see Figure 11.38). Rotation of the pipe is necessary for this task and it should be ensured only the blank (target-less) areas come to contact with the planks.

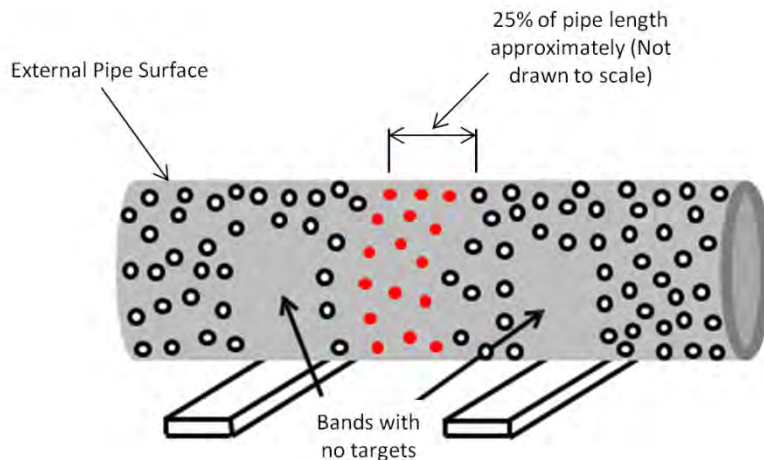


Figure 11.38. Scanning an external circumferential band (not drawn to scale)

11.3.6.7.10 Scan a straight line having a width of about one eighth of the pipe circumference, starting from the centre and scanning towards the edge (see Figure 11.39).

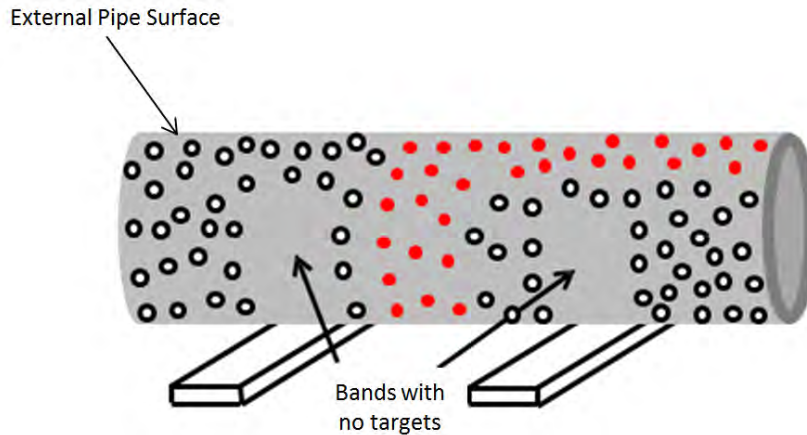


Figure 11.39. Scan a straight band towards an edge (not drawn to scale)

Bridging is the process of localizing the internal surface with respect to the already localized external surface. To achieve this, the scanner needs a path to follow from external targets to the internal targets. Place a **Bridge** with targets affixed, touching the lastly scanned pipe edge (see **Figure 11.40**). The **Bridge** “must” be stationary during the process for accurate localization. The exterior of the scanner casing shown in **Figure 11.22** can be used as a **Bridge** after placing targets with appropriate spacing (5 cm), see **Figure 11.41**. It is a good idea to save the model once the **Bridge** is captured with no errors.

11.3.6.7.11 Now start from the already scanned external edge and continue to capture the targets on the **Bridge** so that the **Bridge** will be localized with respect to the external surface. Now continue to capture targets on the internal edge so that they will be localized with respect to the **Bridge**. To perform this, there should be continuity from the Bridge to the internal surface as shown in **Figure 11.40** and **Figure 11.41**. If continuity is not available at this point after placing targets as explained in Step 6.4, placing additional targets on the internal edge, or slightly rotating the pipe will be necessary to provide continuity.

The **Bridge** will be used for a second time later (**Figure 11.45**). However, the currently used side of the **Bridge** (**Side A in Figure 11.40**) cannot be used again. The side used on the second occasion will be denoted as **Side B**, see **Figure 11.45**.

11.3.6.7.12 Once some internal targets are captured, save the model again, remove the bridge and continue scanning the internal surface.

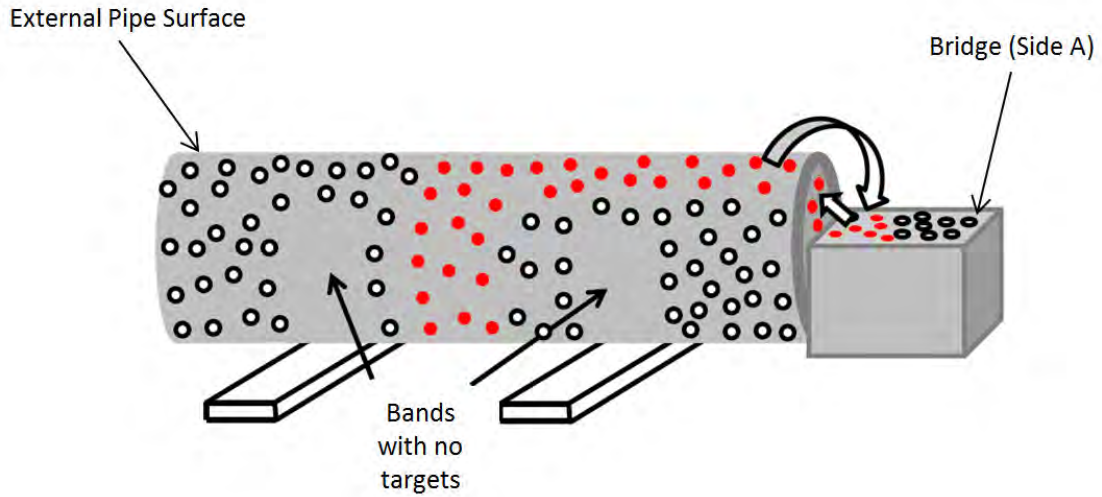


Figure 11.40. Bridging (not drawn to scale)



Figure 11.41. The scanner casing being used as a bridge

11.3.6.7.13 Once the internal targets at the edge are captured, scan a straight line towards the centre of the pipe as shown in Figure 11.42. The band should have a width of about one eighth of the pipe internal circumference. Avoid touching or moving targets during this process.

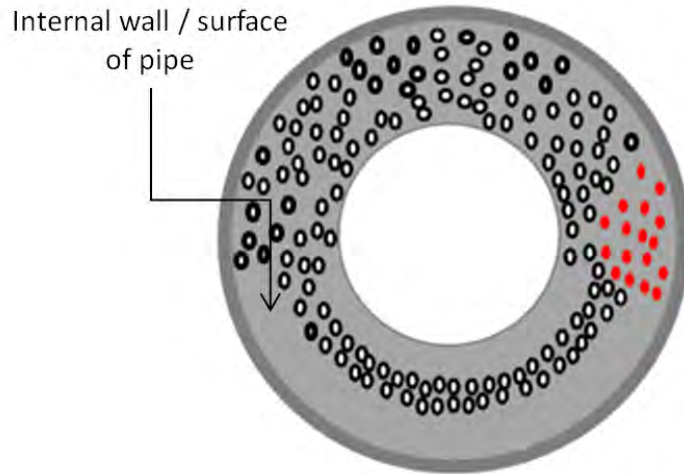


Figure 11.42. Scanning towards the centre of the pipe (not drawn to scale)

11.3.6.7.14 Then complete a circumferential loop in the central region as shown in Figure 11.42. The loop width should be approximately 25% of the pipe length.

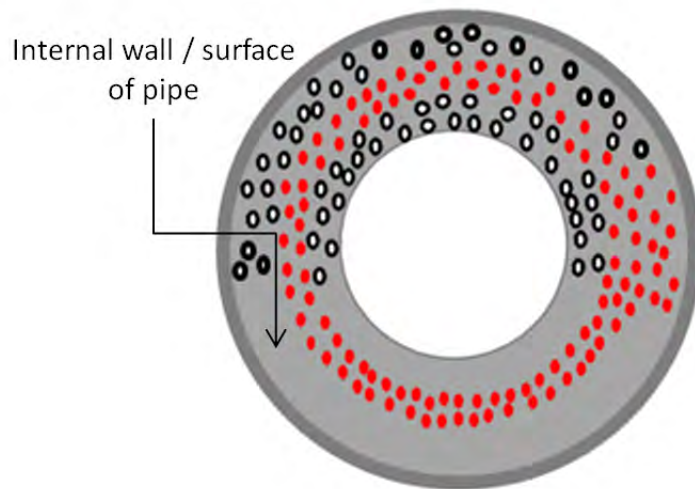


Figure 11.43. Scanning a circumferential loop (not drawn to scale)

11.3.6.7.15 Then continue the straight band towards the other end of the pipe as shown in Figure 11.44.

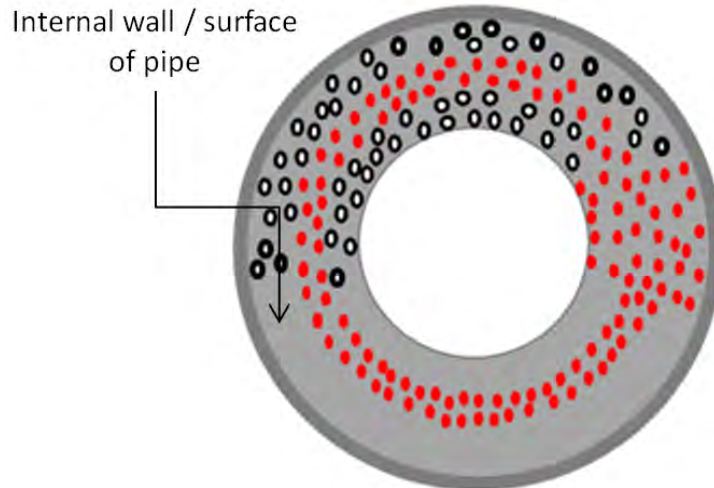


Figure 11.44. Continuing the linear band to the other end (not drawn to scale)

11.3.6.7.16 **Bridge** from the lastly scanned internal edge to the external edge and continue the external straight line towards the centre as shown in Figure 11.45. The **Bridge** used at this point must be different from the previous one, i.e., the target pattern must be different to avoid the software being confused about location. If one surface (**Side A**) of the scanner casing was used before, another surface (**Side B**) with a different target pattern must be used as the second **Bridge**.

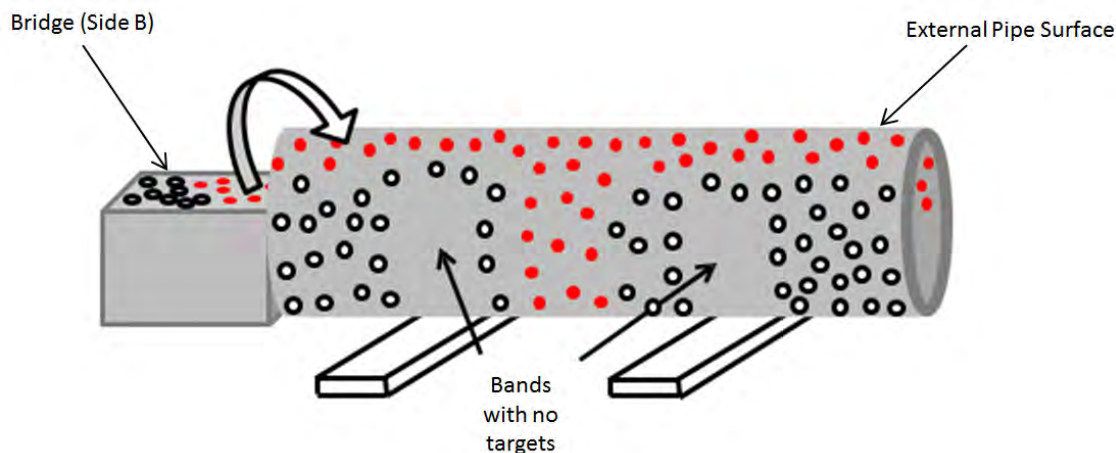


Figure 11.45. Bridging to the external targets and continuing towards the centre (not drawn to scale)

11.3.6.7.17 Now complete scanning the remaining external targets (see Figure 11.46). This requires rotating the pipe and it must be ensured that only the blank (target-less) areas come to contact with the planks. It is not mandatory to capture all the targets at this stage since targets will be reregistered when scanning the surface. However, it is recommended to scan most of the targets which are conveniently accessible.

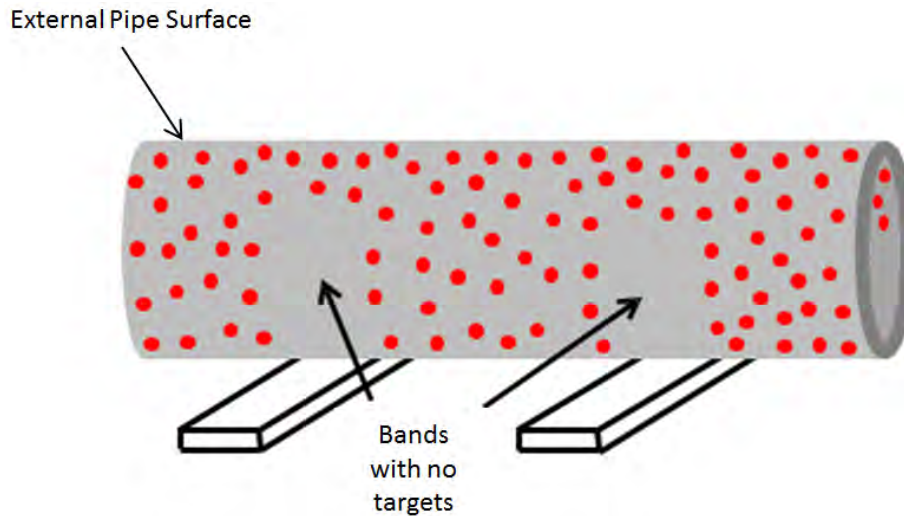


Figure 11.46. Completing scanning the external targets (not drawn to scale)

11.3.6.7.18 Complete scanning the internal targets (see Figure 11.47). It is not mandatory to capture all the targets at this stage since targets will be reregistered when scanning the surface. However, it is recommended to scan most of the targets which are conveniently accessible.

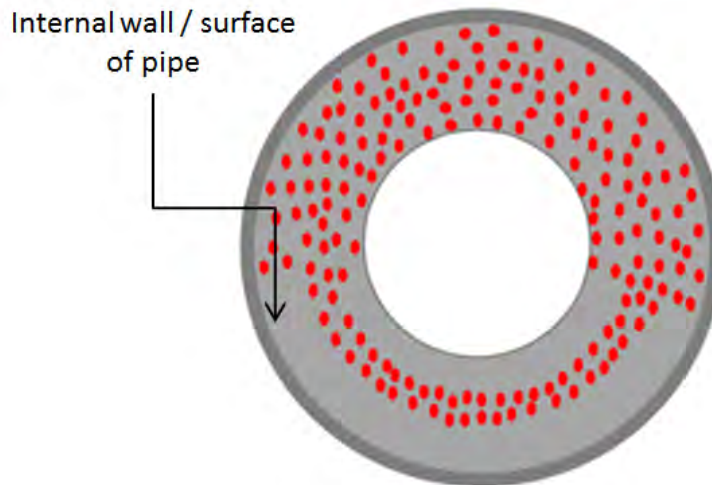


Figure 11.47. Completing scanning the internal targets (not drawn to scale)

11.3.6.7.19 Scanning of the target model is now complete. Hit the space bar to disconnect the scanner. Now click 'Optimize Positioning Model' at the bottom of the left side pane (see Figure 11.48). If the target model was saved before, the 'Optimize Positioning Model' option may remain disabled at this point. Ignore optimization if the option remains disabled and proceed to save the final target model.

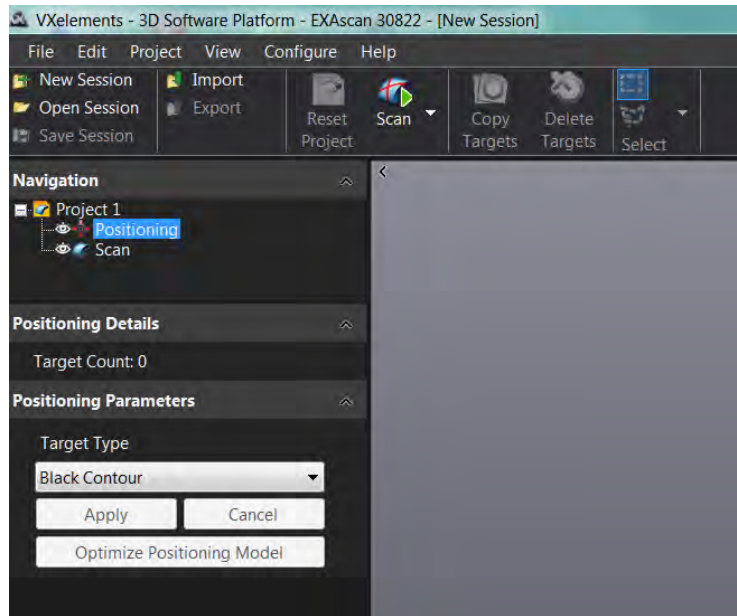


Figure 11.48. “Optimize Positioning Model” option

11.3.6.8. Scanning the Surface

11.3.6.8.1 Click ‘Scan Surface’ as shown in Figure 11.49. Then hit the space bar for the software to connect with the scanner.

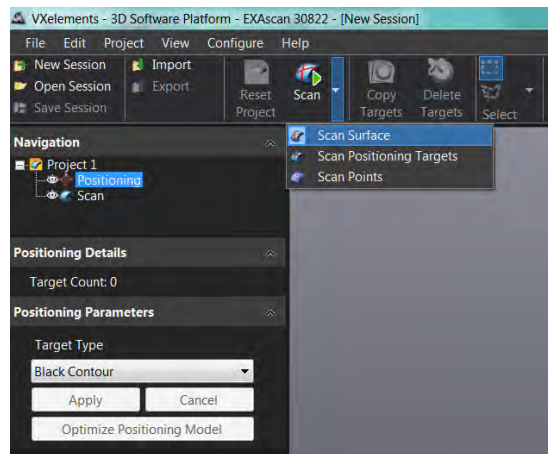


Figure 11.49. Click 'Scan Surface'

11.3.6.8.2 Hold the scanner with the laser emitter pointing towards the targets on the external pipe wall and remaining approximately 30 cm away from the wall as shown in Figure 11.33. The scanner should approximately be perpendicular to the surface being scanned.

11.3.6.8.3 Press the scanner trigger (Figure 11.30) to start scanning. After starting scanning the surface, release the trigger to pause, hit the space bar to disconnect the scanner and save the surface model using File → Save Session As (or keyboard shortcut Ctrl+Shift+S). Provide a suitable

filename and save as a Session File with the .csf extension at a desired folder. Saving regularly hereafter is recommended.

11.3.6.8.4 The same colourbar convention shown under step 5.7.4 applies to scanning the surface as well. The operator should try to hold the scanner in the Green Zone as much as possible.

11.3.6.8.5 Move the scanner at about a speed of 2 cm per second when scanning surfaces. Take extra care and move the scanner slower when scanning edges to ensure the scanner captures a sufficient number of targets to capture edges accurately.

11.3.6.8.6 First scan the whole external surface. Start with the area already covered with targets and place new targets in the blank areas as the process goes. This requires the pipe to be rolled. Ensure an area covered with targets touches the planks only after the corresponding surface has been scanned. Take extra care when scanning edges (move the scanner slower).

11.3.6.8.7 Now scan the whole internal surface. Start with the area already covered with targets and place new targets in the blank areas as the process goes. Scanning the whole surface may require the operator to crawl into the pipe if the pipe section is long. It will also make the operator come to contact with targets. Therefore, ensure the operator comes to contact with targets only after the corresponding surface has been scanned.

11.3.7 Computing Ground Truth

Computing the Ground Truth to generate 2.5D thickness maps from 3D models involves exporting point clouds of pipe surfaces from VXelements, outlier removal, filling missing data, aligning axes, up-sampling, ray-tracing and post processing. A person performing this task requires competence in Geomagic, Meshlab, Visual Studio and Matlab software, and also requires programming skills (C++ and Matlab) and a background in one of the suitable fields including but not limited to Engineering, Mathematics, or IT in order to learn concepts underpinning the process. The Ground Truth Computation process can be carried out by the Critical Pipes Project team of University of Technology Sydney (UTS) and training can be provided if necessary.

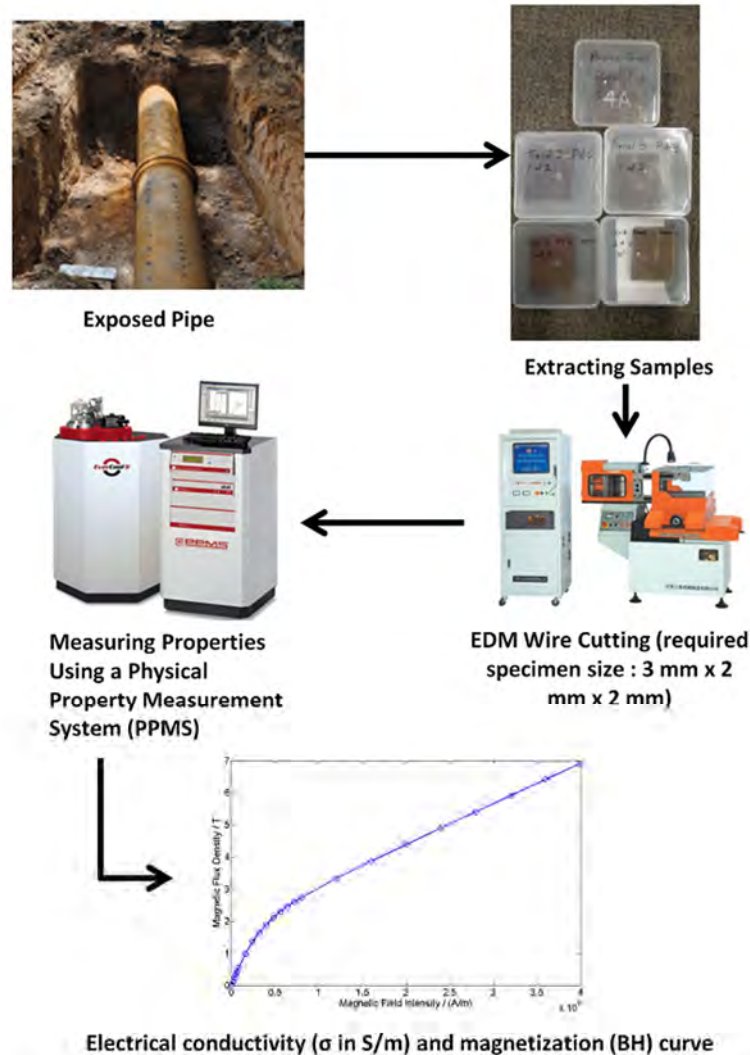
11.4 ACTIVITY 2 APPENDIX 2: INFLUENCE OF MATERIAL PROPERTIES ON CRITICAL PIPE NON-DESTRUCTIVE EVALUATION TECHNIQUES

11.4.1 Preamble

This document specifies the recommended procedures for measuring certain critical pipe material properties for modelling and analytical purposes of the Advanced Condition Assessment and Pipe Failure Prediction Project (ACAPFPP), and presents the effect of material properties on selected critical pipe Nondestructive Evaluation (NDE) Techniques.

11.4.2 Measuring Electrical and Magnetic Properties of Pipe Materials

The procedure for measuring electrical and magnetic properties of critical pipe materials is presented in Figure 11.50.



Source: Courtesy of Quantum Design Inc. © 2018 (middle left) and <http://www.diytrade.com> (middle right).

Figure 11.50. Steps for measuring electrical and magnetic properties of critical pipe materials

First, high thickness regions of a pipe wall are required to be qualitatively identified first since that enables extracting samples from those regions while causing minimal physical destruction to the structural integrity of pipes. This can be done by performing Pulsed Eddy Current (PEC) scans first and visualizing its decay rate feature values since they are proportional to the thickness of remaining ferromagnetic material. Usual mechanical cutting tools can be used for the process and extracting relatively large samples is necessary in order to avoid heating the interior of samples from which specimens of size 3 mm x 2 mm x 2 mm are eventually cut using an Electric Discharge Machining (EDM) wire cutter. The key when wire cutting specimens is to pay strict consideration towards minimizing heating by using cooling liquids since heat may adversely affect electrical and magnetic properties which are intended to be measured. Alternatively, filing the specimens too is an option with the capability of controlling heating given a significant availability

of time and manual labour. A machine cut sample obtained from a grey cast iron pipe along with two wire cut test specimens of different sizes extracted from that sample are shown in Figure 11.51.

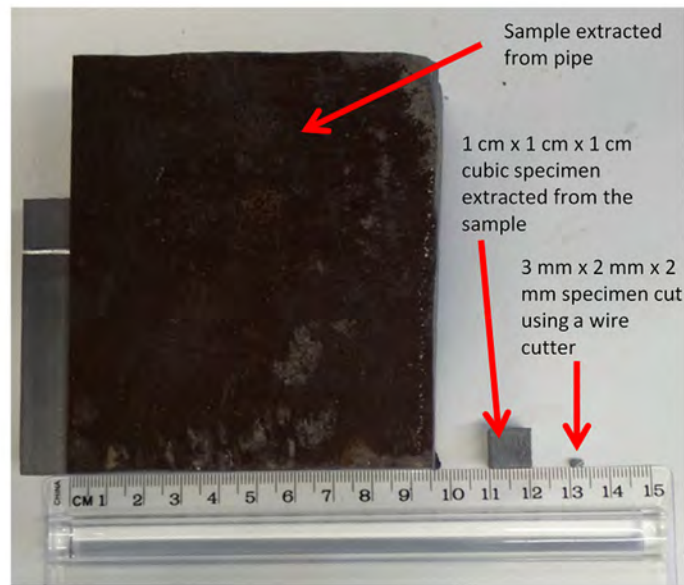


Figure 11.51. Extracted specimens for testing material properties

The original sample in Figure 11.51 was deliberately made to have about 10 cm x 10 cm surface area to enable extracting multiple specimens if required. Obtaining samples of such size causes significant partial destruction to in situ pipe walls, in actual practice therefore, the original sample can be much smaller if only one specimen is intended to be extracted as long as adequate cooling liquid is used to avoid over heating while machine cutting.

As done for this project, the state of the art mechanism for measuring such intrinsic physical properties is using a Physical Property Measurement System (PPMS). Cutting specimens of size 3 mm x 2 mm x 2 mm is usually necessary to allow optimal fitting into the specimen holders and performing accurate measurements. The aforementioned specimen size is not global however should be decided upon after referring to the specifications of the PPMS being used. Using powder particles instead of solid specimens is also possible with a PPMS to measure magnetization curves although not recommended due to the chances of powder being contaminated by foreign materials as a result of the process of extraction.

A set of magnetization curves measured in the form of magnetic flux density variation against magnetic field intensity from specimens extracted from grey cast iron pipe segments is shown in Figure 11.52. Sampling intervals of 10 Oe or less (lower the better) for magnetic field intensity is recommended for the nonlinear region (i.e., region below 2 T magnetic flux density). For the linear region (i.e., region above 2 T magnetic flux density), larger sampling intervals for magnetic field intensity of around 2.5×10^5 A/m will be adequate.

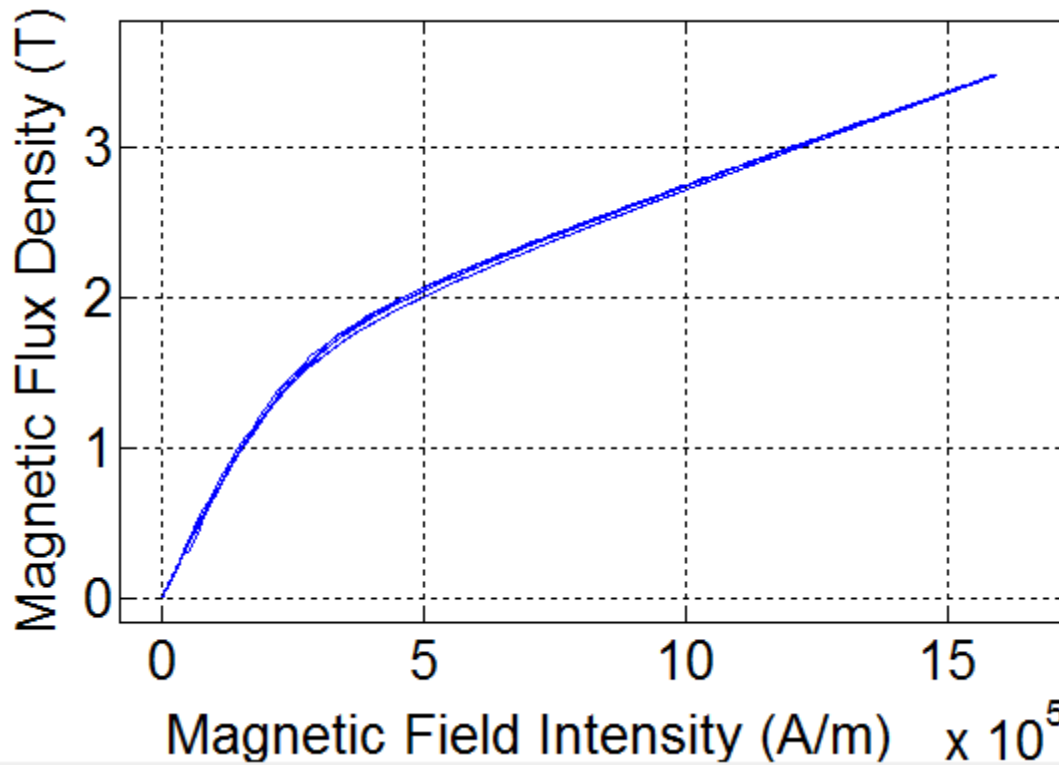


Figure 11.52. A set of magnetization curves measured from specimen taken from a grey cast iron pipes

Four Probe Method may be used to perform resistivity measurements, this is usually how a PPMS measures electrical conductivity of a material. An alternative method based on X-ray fluorescence (XRF) devices may also be used to approximate a range for electrical conductivity of pipe materials. State of the art portable XRF devices are available for in situ applications at present as shown in Figure 11.53 and these devices can be used to analyse emission characteristics of materials to non-destructively determine a material's composition. Despite subtle variations, all critical pipe materials are usually composed of about 93 % Fe, 3 % C, 2 % Si in mass percentages and the rest usually include elements such as P, Mn, S, Ti and Cr.



Source: Courtesy of Skyray XRF.

Figure 11.53. In situ application of an XRF device for material analysis

Pipe surfaces require to be cleaned to remove rust and graphitization in order to expose ferromagnetic material to enable X-rays to make contact to determine correct composition. Physical properties including electrical conductivity of elements and certain composite materials are known and are available in standard texts and online resources. These properties can be used to apply the rule of mixtures to calculate a range for effective material properties such as electrical conductivity of a composite material. Once mass percentages on elements are found, the excel sheet at SVN\field_trials\XRF can be used as shown in Figure 11.54 to estimate an approximate mid-range electrical conductivity. Since this method allows only approximating the electrical conductivity, the four probe facility available with the PPMS is the recommended method to be used.

Conductivities (S/m)	Density (kg/m3)	Element	Mass Percentage				
2.20E+06	7874	Fe	92.92	0.011800864	80.33924872	1.77E+06	
1.00E+05	2260	C	3	0.001327434	9.037052204	9.04E+03	
0	2330	Si	1.85	0.000793991	5.405424215	0	
0.00E+00	1823	P	1.12	0.000614372	4.182590334	0.00E+00	
6.20E+05	7470	Mn	0.791	0.00010589	0.720891421	4.47E+03	
1.00E-15	1960	S	0.072	3.67347E-05	0.250086588	2.50E-18	
2.50E+06	4507	Ti	0.034	7.54382E-06	0.051357673	1.28E+03	
7.90E+06	7140	Cr	0.014	1.96078E-06	0.013348848	3.34E+02	
					0.01468879	100	
						1.78E+06	

Substitute mass percentage of elements

Approximate mid-range electrical conductivity in S/m will automatically be calculated

Figure 11.54. UTS generated excel sheet to approximate electrical conductivity of critical pipe materials through XRF measurements

The PPMS can measure electrical conductivity variation against temperature. It is recommended that this variation is measured for a temperature range of 280 K to 320 K to understand how electrical conductivity of a critical pipe material may vary due to the impact of ambient temperature.

11.4.3 Typical Variation of Critical Pipe Electrical and Magnetic Properties

The typical variation of magnetization curves is shown in Figure 11.55 and Figure 11.56, while the variation of electrical conductivity is shown in Figure 11.57 and Figure 11.58.

As per a variety of samples tested by UTS, any selected magnetization curve does not vary more than $\pm 5\%$ from a median magnetization curve of the same material.

Similarly, electrical conductivity of any material does not vary more than $\pm 30\%$ from a median electrical conductivity for the selected material, for temperatures between 280 K and 320 K. More specifically, cast iron may exhibit variations up to $\pm 30\%$ while steel and ductile iron exhibited lesser variations as per the tested samples. Median electrical conductivity values for each material can be presented as: cast iron = 2×10^6 S/m, ductile iron = 4.9×10^6 S/m and mild steel = 1.42×10^7 S/m.

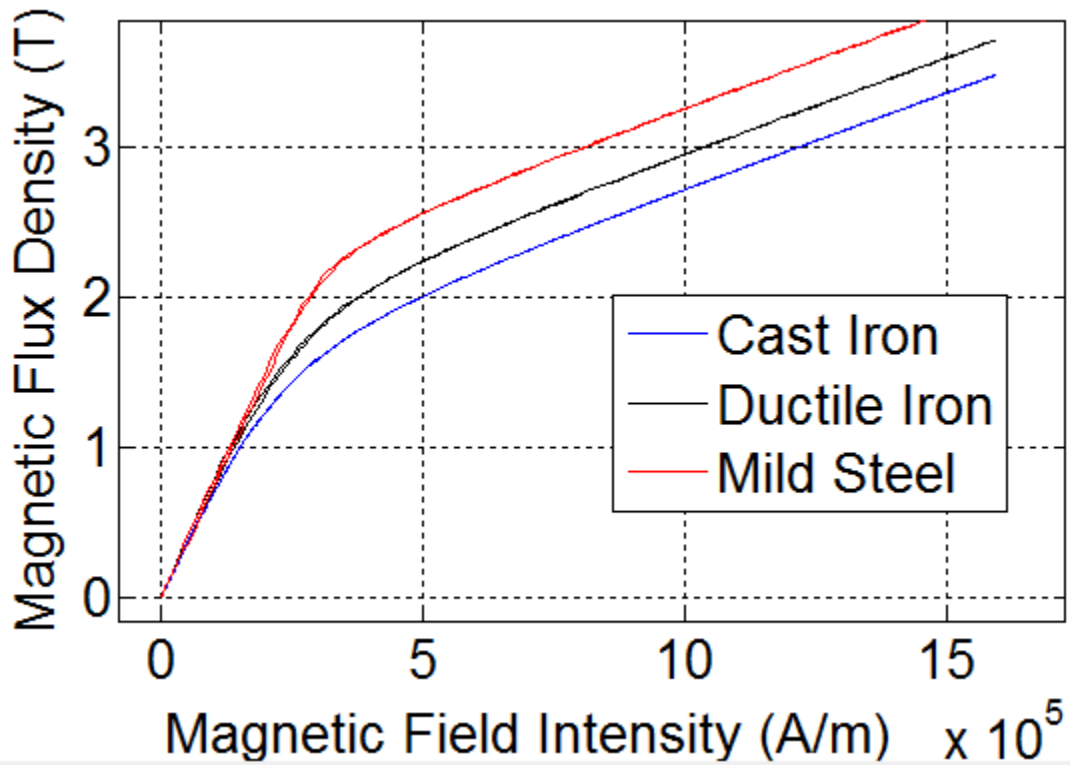


Figure 11.55. Variation of magnetization curve for different materials

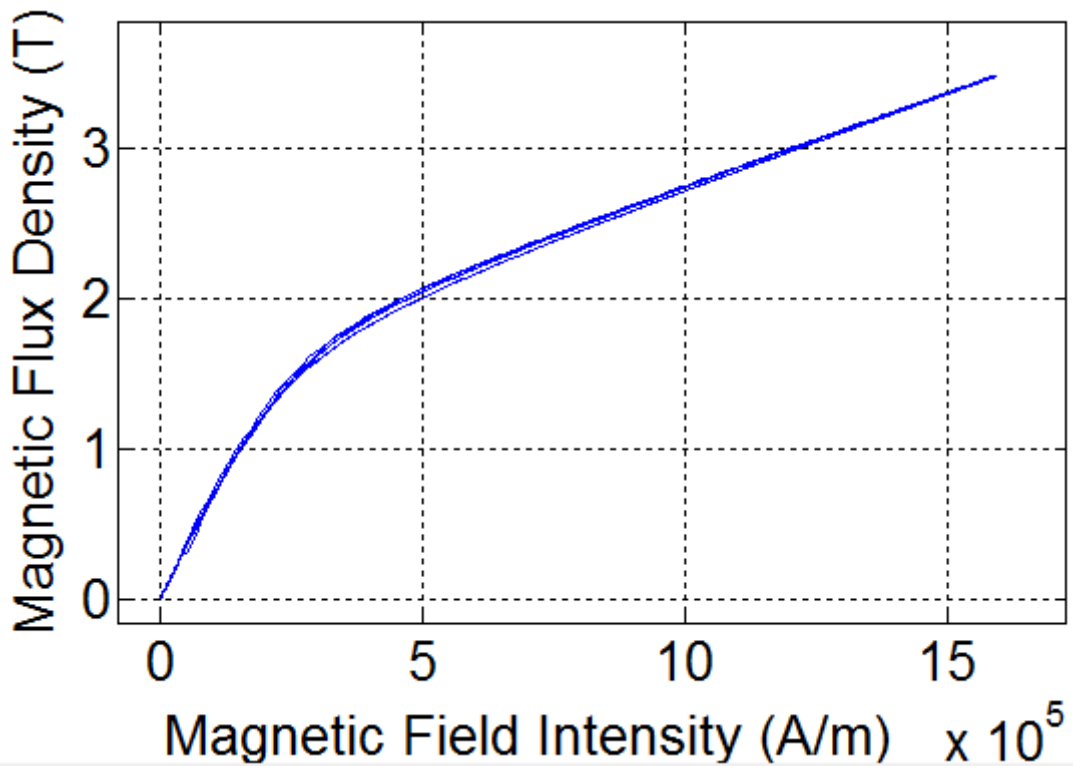


Figure 11.56. Variation of magnetization curve within cast iron

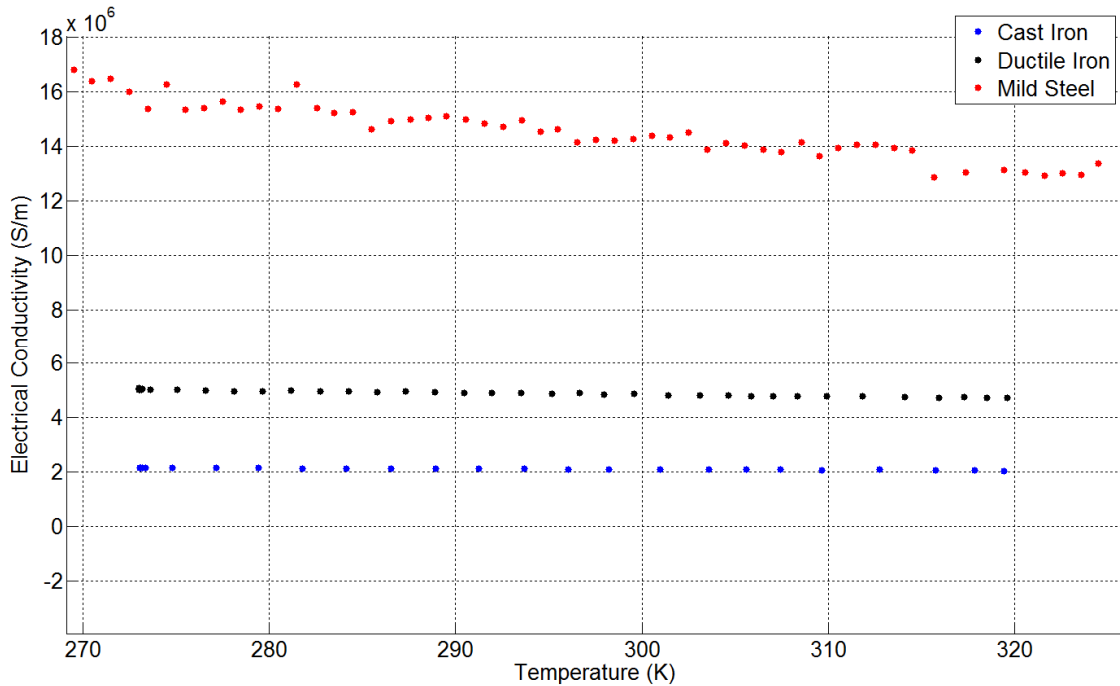


Figure 11.57. Variation of electrical conductivity for different materials

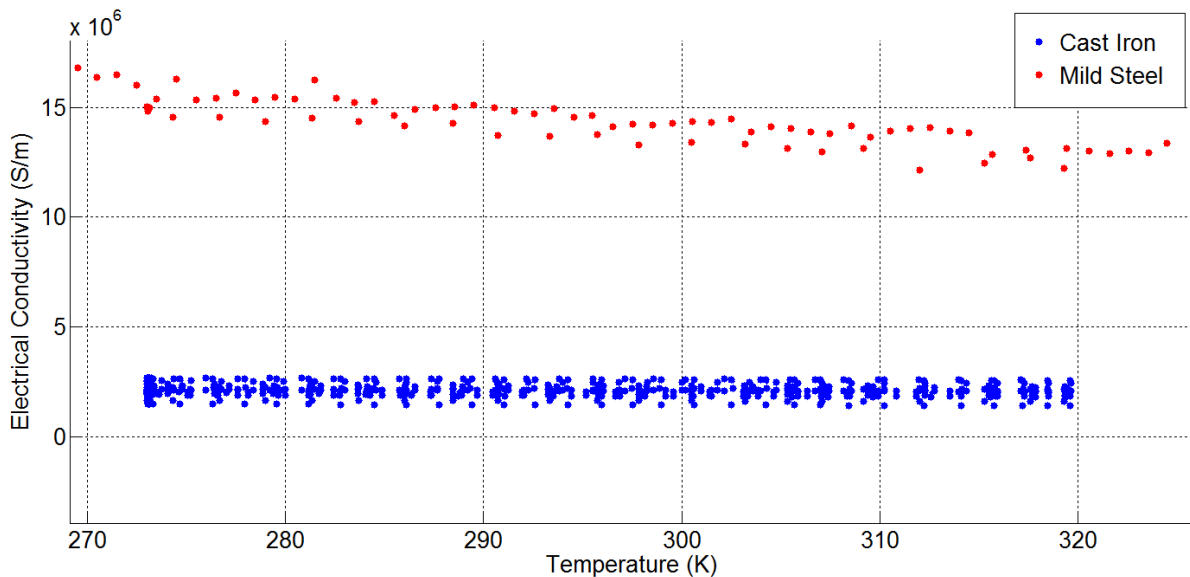


Figure 11.58. Variation of electrical conductivity within cast iron and mild steel

11.4.4 Effect of Critical Pipe Electrical and Magnetic Properties on the Accuracy of a Defect Depth Predicted by MFL

MFL is immune to electrical conductivity variations and is susceptible only to variations in the magnetization curve. Therefore, the effective impact on a predicted defect depth will be less than 3% for any critical pipe material.

11.4.5 Effect of Critical Pipe Electrical and Magnetic Properties on the Accuracy of Average Wall Thickness Predicted by PEC (BEM)

BEM is susceptible to the combined effect of electrical and magnetic properties (i.e., the $\mu\sigma$ multiplication, where μ is the magnetic permeability and σ is electrical conductivity). Table 11.2 summarises the effective variation of BEM predicted average wall thickness of critical pipe materials.

Table 11.2
Effect of material electrical and magnetic properties of BEM estimated thicknesses

Material	Variation of $\mu\sigma$ Mean [Range]	Variation (Percentage) of UTS Thickness Estimates
Cast Iron	150 [109 ~ 205]	$\pm 15\%$
Ductile Iron	406 [362 ~ 457]	$\pm 6\%$
Mild Steel	1000 [889 ~ 1123]	$\pm 6\%$

Note: The most generically accurate thickness estimates tend to result when the statistical mean of material properties calculated from multiple measurements is used (e.g., $\mu\sigma \approx 150 \text{ S.H.m}^{-2}$ for the test bed, $\mu \approx 7.54 \times 10^{-5} \text{ H/m}$ and $\sigma \approx 1.98 \times 10^6 \text{ S/m}$). Therefore, $\mu\sigma \approx 150 \text{ S.H.m}^{-2}$ is considered as the best estimate of cast iron material properties to determine the BEM sensor model.

11.4.6 Effect of Critical Pipe Electrical and Magnetic Properties on the Accuracy of Wall Loss and Local Thickness Estimates Predicted by RFT

RFEC is susceptible to the combined effect of electrical and magnetic properties (i.e., the $\mu\sigma$ multiplication, where μ is the magnetic permeability and σ is electrical conductivity). Due to the double-through wall property of the technology, the sensor readings are twice more sensitive to the modification of the magnetic properties. However, the relative analysis used by the industrial partner on the analysis of local defects, greatly reduce this susceptibility. The effective variation of the RFT predicted average wall thickness of critical pipe materials is summarised in Table 11.3 for the average wall thickness (full pipe), and local analysis (corrosion patch analysis). The susceptibility has been measured with Finite Element Analysis.

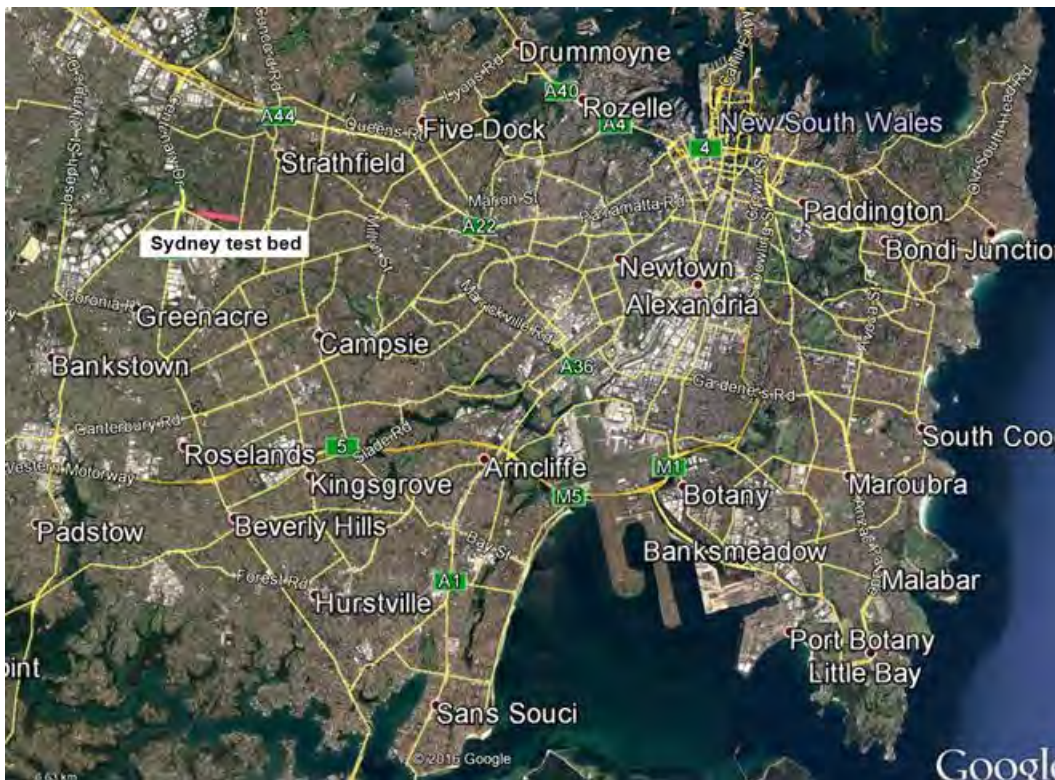
Table 11.3

Effect of material electrical and magnetic properties of RFEC estimated thicknesses

Material	Variation of $\mu\sigma$	Variation (percentage) of UTS Wall loss Estimates	Variation (percentage) of UTS Local Thickness Estimates
Cast Iron	150 [109 ~ 205]	$\pm 16.57\%$	$\pm 38.73\%$ / $\pm 5.93\%$
Ductile Iron	406 [362 ~ 457]	$\pm 4.20\%$	$\pm 11.31\%$ / $\pm 2.99\%$
Mild Steel	1000 [889 ~ 1123]	$\pm 5.66\%$	$\pm 15.63\%$ / $\pm 4.41\%$

11.5 ACTIVITY 4B AND 4C APPENDICES

11.5.1 Activity 4b: LPR Data for Verona St Test Bed Site (Sydney)



Source: Map data © 2016 Google.

Figure 11.59. Location of the Verona St test bed

The Verona St test consists of one and a half kilometres of pipeline that Sydney Water decommissioned in 2010 due to its poor condition. Figure 11.59 shows the map of the area in Strathfield, Sydney where the test bed lies. Cement lined cast iron pipes of approximately 665 mm OD were laid along the bed in 1922. The soil along the test bed is generally heavy clay – particularly at pipe depth (general 1.5 to 2 m below the ground surface). The general layout of the test bed and sampling locations are shown in Figure 11.60.

Soil samples were taken at various locations along the test bed. Initial samples were taken to coincide with pipe exhumation to enable soil properties to be directly compared with corrosion behaviour. Later samples were taken when soil moisture sensors were installed along the bed. Samples were mainly taken at the mid depth of the pipe immediately adjacent to the pipe. However, samples were also taken above and below the pipe to enable the level of local variability to be assessed (Figure 11.61).

Spacing between samples generally ranged from 5 to 50 m however three high density sampling locations were also sampled (Figure 11.62) to help determine the level of local variability in soil Rp values. At these points samples were taken ~0.5 m apart.

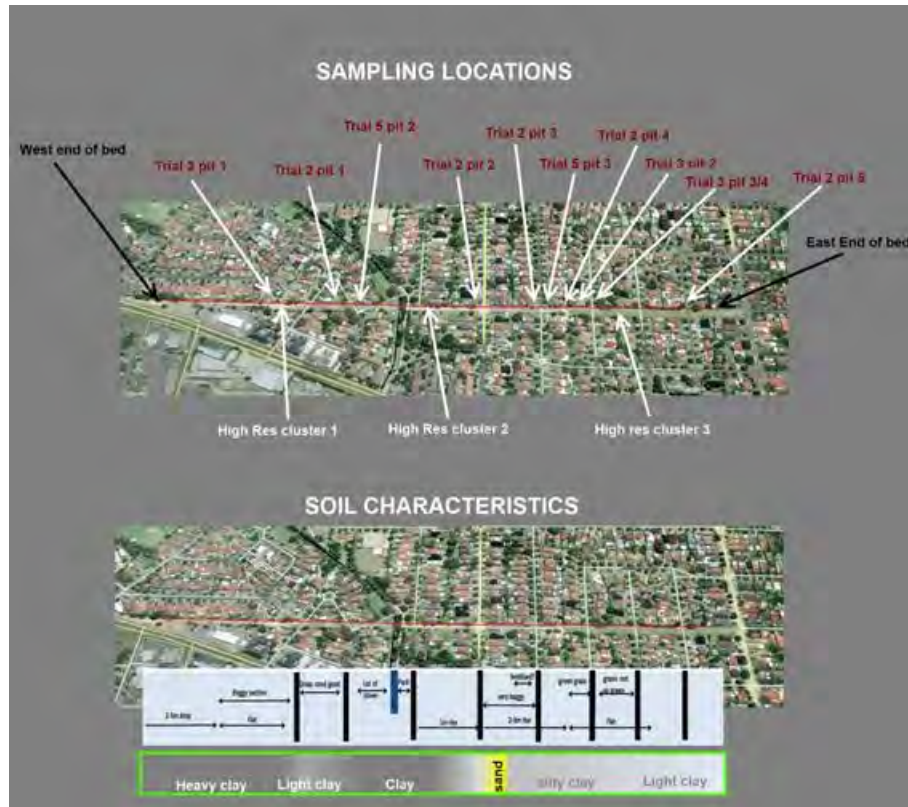


Figure 11.60. General layout of Verona St test bed

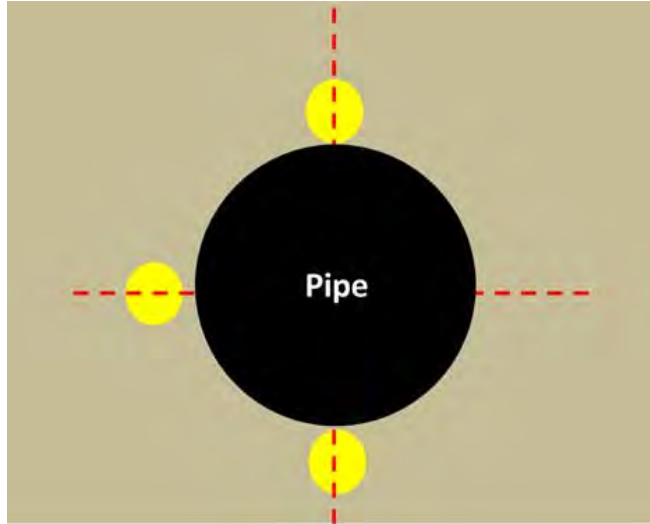


Figure 11.61. Sampling above and below the water pipe

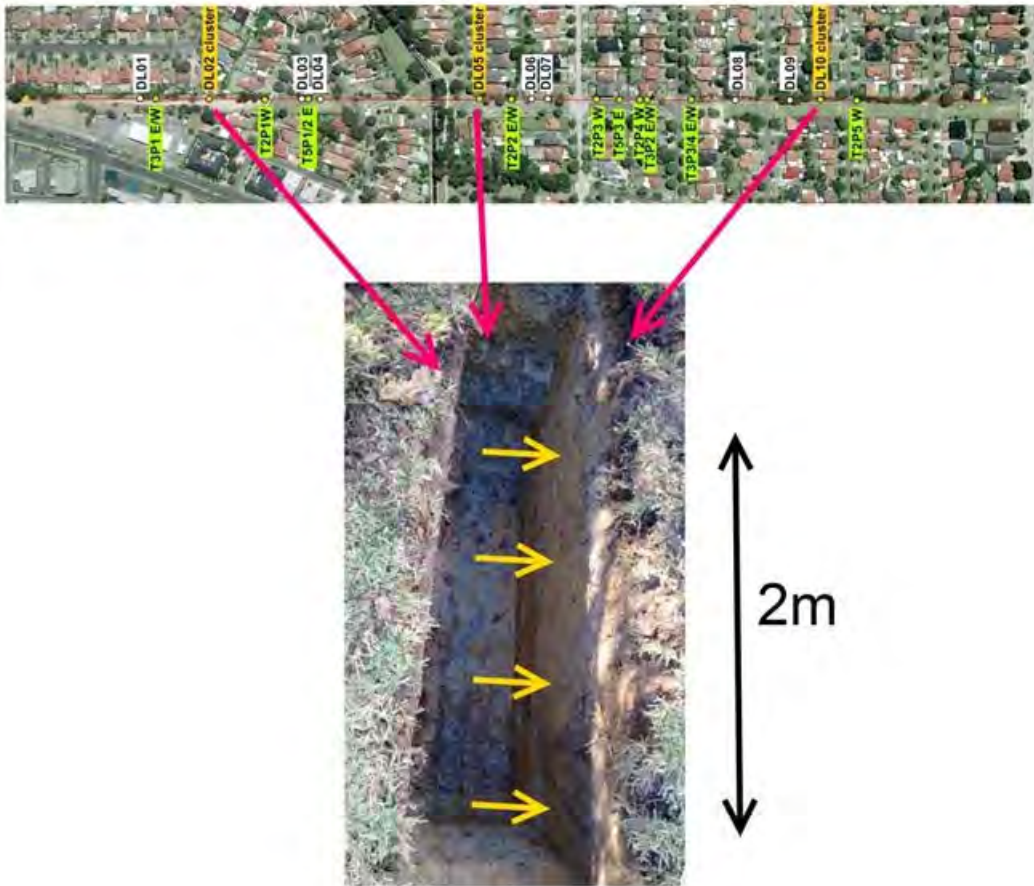


Figure 11.62. Location of high sample density clusters and remaining soil sampling sites

Soil samples were analysed by PCA Echologics using their standard testing procedure. The test assigns a resistance value, R_p , to each soil sample from which the maximum pitting rate

for pipe in contact with that soil can be estimated. LPR data and trends for samples retrieved from the Sydney test bed are shown in Table 11.4 and Figure 11.63 to Figure 11.67.

As was evident from the soil chemistry surveys conducted in the same area (see Activity 4c report) little or no spatial trends were observed in the distribution of Rp values along the test bed (Figure 11.63). Repeated sampling over very short horizontal (Figure 11.64) and vertical distances (Figure 11.65) also showed a significant degree of variability (in the order of 40-50% variation in Rp value). Again, this behaviour was similar to that observed for other soil properties in the area.

This variation incorporates any inherent variability in the testing procedure (i.e., the variance due to variations in the testing method when testing identical samples). Testing of blind duplicate and triplicate samples showed variation in Rp values of up to 30%. Given the nature of the soil samples however (very cohesive clays) it may be argued that true replicate samples are hard to produce and thus this variance may still reflect a level of non-uniformity in the samples submitted. Never the less in practice it can be concluded that there is a significant degree of variability to be expected when analysing samples from clay soils such as present at the Sydney test bed for Rp values. The high degree of spatial variability and lack of spatial structure in the soil RP property is reinforced by a semi variogram analysis which showed no spatial correlation between samples (Figure 11.67) even those samples taken 50 cm apart.

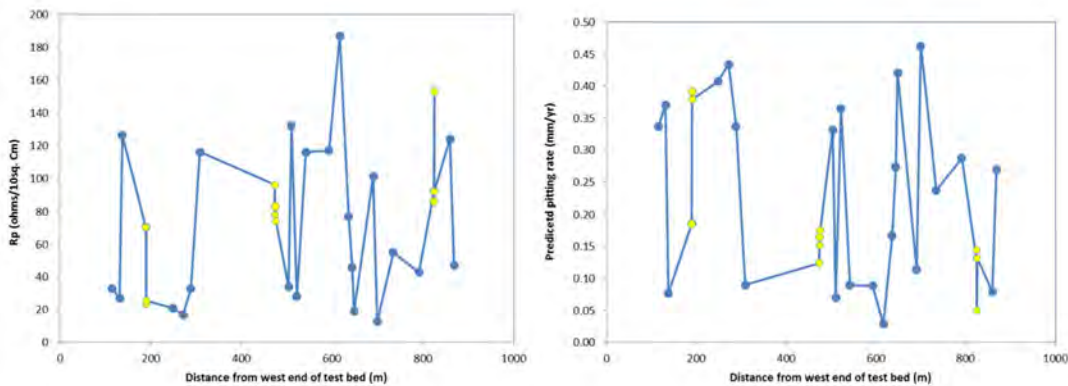


Figure 11.63. Variation in Linear Polarised Resistance Rp values and predicted maximum pitting rates at mid-pipe depth along the length of the test bed

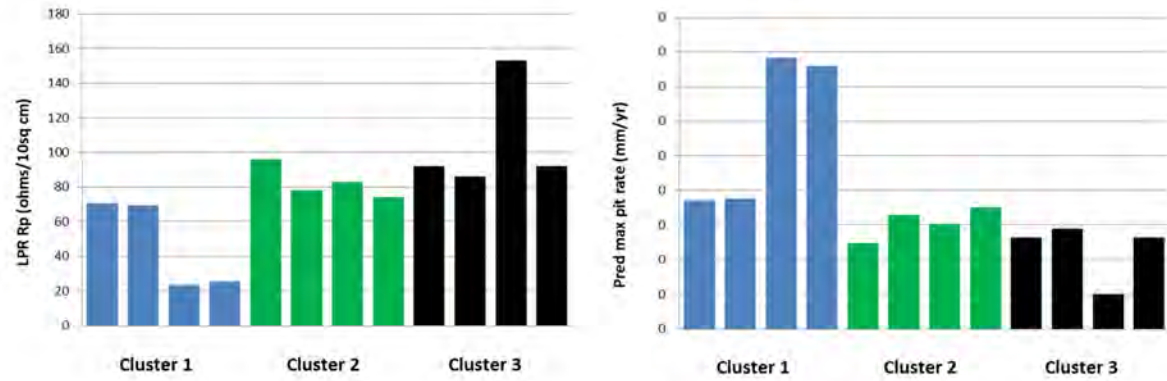


Figure 11.64. Horizontal variation of LPR Rp values (left) and corresponding predicted max pitting rates (right) observed for the three clusters of high resolution samples, (samples spaced 50 cm apart)

Table 11.4
LPR Rp values recorded for soils at mid-pipe depth along the Verona St test bed

Sample ID	Easting	Northing	Distance from West end	Rp (ohms/10sq cm)
DL01	321908.6	6248702.4	115.3	33
T3P1 West M	321924.1	6248698.6	131.8	27
T3P1 East M	321930.1	6248698.6	137.8	126
DL02+500mm to west	321981.4	6248692.6	189.4	70.5
DL02	321981.9	6248692.5	189.9	70.5
DL02+1m to east	321982.8	6248692.4	190.9	23.5
DL02+1.6m to east	321983.5	6248692.3	191.5	25.5
T2P1 West M	322039.6	6248683.4	248.5	21
T5P1/2 East M	322081.0	6248680.6	272	17
DL03	322079.7	6248678.7	288.6	33
DL04	322099.9	6248675.9	309	116
DL05 +500mm to West	322263.3	6248654.7	473.9	96
DL05	322263.9	6248654.7	474.5	78
DL05 + 1m to east	322264.9	6248654.5	475.5	83
DL05 + 1.5m to east	322265.4	6248654.4	476	74
T2P2 West M	322293.0	6248648.8	504.1	34
T2P2 east M	322299.5	6248648.8	510.5	132
DL06	322310.8	6248648.2	522	28
DL07	322330.5	6248645.8	542.1	116
T2P3 West M	322381.3	6248637.4	593.1	117
T5P3 East M	322405.3	6248634.8	617.2	187
T2P4 West M	322424.2	6248632.1	636.4	77
T3P2 West M	322431.7	6248630.9	644	46
T3P2 East M	322436.2	6248630.9	648.6	19
T3P3/4 West M	322477.4	6248624.7	690.6	101
T3P3/4 East M	322487.6	6248621.3	700.1	13
DL08	322521.5	6248619.0	734.6	55
DL09	322578.0	6248611.4	791.6	43
DL10 +500mm West	322610.0	6248606.8	823.9	92
DL10	322610.5	6248606.7	824.4	86
DL10+800mm East	322611.3	6248606.7	825.2	153
DL10+1.3m East	322611.7	6248606.5	825.7	92
T2P5 West M	322645.4	6248600.7	859.9	124
T2P5 East M	322655.0	6248599.1	869.1	47

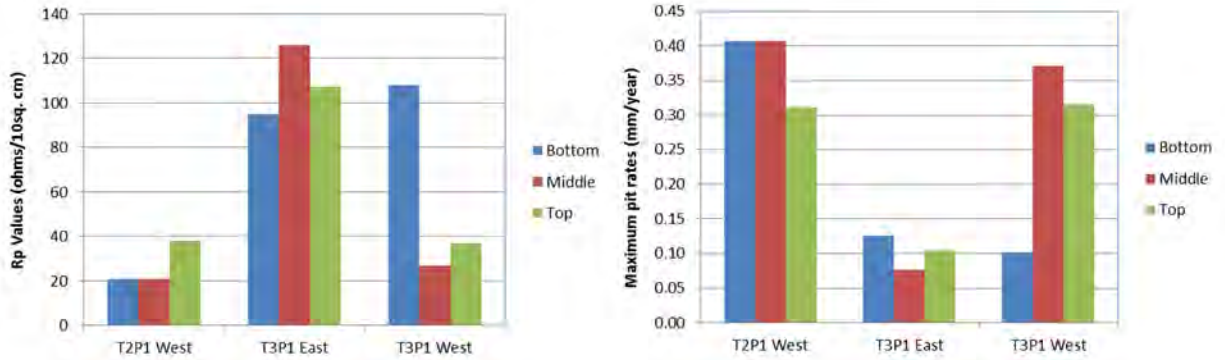


Figure 11.65 Vertical variation of LPR Rp values (left) and corresponding predicted max pitting rates (right) observed at three sites

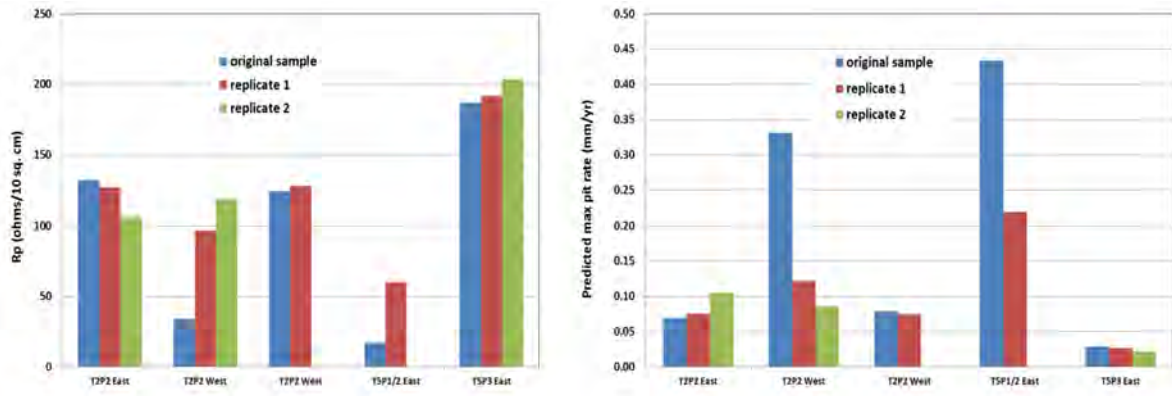


Figure 11.66. Variation in reported Rp values (left) and max predicted pit rates (right) for duplicate and triplicate samples

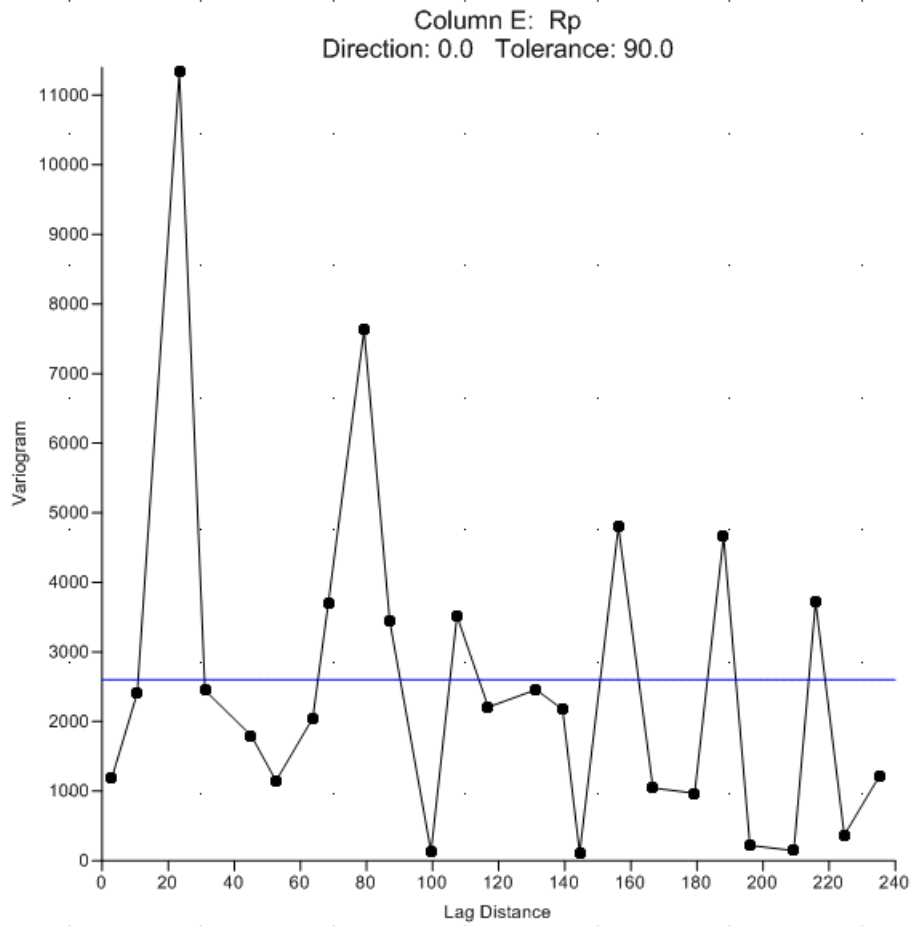


Figure 11.67. Semi variogram for LPR Rp values recorded along the Sydney test bed. The random fluctuations around a flat trend indicates that there was no spatial correlation between soil Rp values.

11.5.2 Activity 4b: LPR Field Data for Perth Subiaco and Fremantle Sites



Source: Map data © 2016 Google.

Figure 11.68. Location of the Perth soil sampling sites

A LPR soil sampling campaign was also conducted in the Perth CBD area (Figure 11.68). Perth soils are predominantly sandy and so offer a contrast to the clay rich, more corrosive soils of the Sydney test bed. All samples were taken at pipe depth with the distance between adjacent samples ranging from 2 m to 3 km.

Soil Rp and wilt point properties for the Perth samples are listed in Table 11.5. A diagram showing the spatial distribution of LPR Rp values recorded for the Perth sites is shown in Figure 11.69 and the semi variogram for the Rp data is shown in Figure 11.69. The distribution of Rp values again showed no distinct spatial trends (Figure 11.69 left) however Perth soils, being quite sandy, are not believed to not be so corrosive as the clay soils of the Sydney test bed area. When Rp values are replotted in terms of corrosion potential (as defined by PCA Echologics) the variance is less pronounced principally because much of the soil is non-corrosive (Figure 11.69 right). A semi variogram of the Perth CBD LPR Rp values (Figure 11.69) reinforces the conclusion that there is no spatial correlation between soil samples collected in this area (as already observed for the clay soils of the Sydney test bed).

Table 11.5
Perth soil sample site locations, appearance, texture, wilt point and LPR Rp values

Sample ID	Eastings (m)	Northings (m)	Colour	Texture	Rp value (1) ohms/10sq. cm	Rp value (rpt) ohms/10sq. cm	Wilt pt (%)
1	389470.373	6465326.82	Yellowish Brown	Sand	239		1.69
2	390070.609	6465375.746	Dark Yellowish Brown	Sand	273		1.47
3	390011.979	6465377.555	Dark Yellowish Brown	Sand	203		1.8
4	388916.453	6464825.922	Brown	Sand	238	164	1.435
5	389348.697	6464820.738	Dark Yellowish Brown	Sand	166		1.43
6	389676.753	6464825.833	Dark Yellowish Brown	Sand	173		1.61
7	388846.247	6464562.188	Dark Yellowish Brown	Sand	146		1.72
8	388851.443	6463866.422	Dark Yellowish Brown	Sand	215		1.55
9	388849.225	6463696.475	Dark Yellowish Brown	Sand	201		1.48
11	389270.035	6464263.013	Dark Brown	Sand	94	115	2.94
12	389269.707	6464048.852	Dark Yellowish Brown	Sand	220		1.42
13	388056.184	6464242.819	Dark Yellowish Brown	Sand	199		1.65
14	388453.204	6464241.279	Dark Brown	Sand	177		1.94
15	388452.055	6464242.597	Yellowish Brown	Sand	153		1.38
16	387447.014	6463800.987	Brown	Sand	110		2.17
17	388159.899	6463799.937	Dark Yellowish Brown	Sand	96		2.27
18	388197.161	6463798.016	Dark Greyish Brown	Sand	147		1.32
19	388849.476	6463864.771	Dark Yellowish Brown	Sand	208	281	1.325

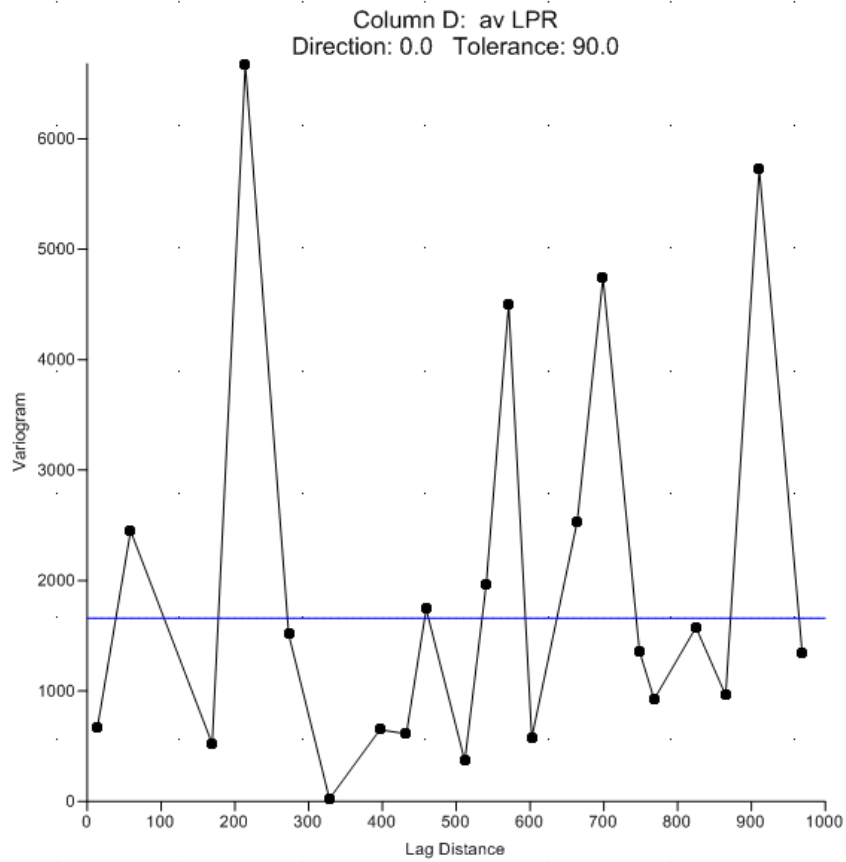


Figure 11.69. Semi variogram for Perth CBD LPR Rp values. The random fluctuations around a flat trend indicates that there was no spatial correlation between soil Rp values.

11.5.3 Activity 4b: Report on the Current Knowledge of the Theoretical Basis of Linear Polarisation Resistance

**REPORT ON CURRENT KNOWLEDGE OF THEORETICAL BASIS OF
LINEAR POLARISATION RESISTANCE:
ACTIVITY 4B.1**

Prepared by:
Tony Wells
University of Newcastle

SUMMARY

This report details the current knowledge of the theoretical basis of Linear Polarisation Resistance (LPR) and is the first output from activity 4b (Reducing the uncertainty in the use of non-destructive, indirect measurement with LPR) which in turn is part of the Advanced Condition Assessment and Pipe Failure Prediction Project. The aim of studying the theoretical underpinnings of the LPR process is to:

- Build up a conceptual understanding of the LPR process and
- Identify possible features of the LPR process that may impact on the uncertainty of cast iron corrosion rates predicted by this method. The identified areas will be investigated in the next stage of Activity 4b.

To this end the theory of ferrous corrosion is set out in detail with special relevance to buried cast iron pipe corrosion. The theory is developed from the basic chemical reactions taking place to the thermodynamic and kinetic equations which form the basis of the LPR assessment of soil corrosivity. The environmental factors affecting the rate of corrosion and how corrosion of cast iron pipes evolves over time is then discussed.

The following possible sources of uncertainty have been identified and will be the subject of further investigation:

- (1) The non-linearity in cast iron corrosion rate trends over time
- (2) The changing rate limiting processes that occur over time
- (3) Soil moisture levels
- (4) Differential aeration

A database of relevant literature is also attached.

INTRODUCTION

In August 2011 international water research organisations, Australian water utilities and three Australian universities came together through a collaborative research agreement, and committed overall funding of \$16 million (including \$4 million cash) over five years to undertake research into the assessment of the lifespan of water pipes. This project entitled the “Advanced Condition Assessment and Pipe Failure Prediction Project” initially comprised 3 activities which are now briefly described:

Activity 1 - Failure Prediction

The principle aim of activity 1 is to determine how, when and where critical pipes will fail within the water supply network. Expected outcomes include:

1. Development of data and models for pipe stresses due to internal and external factors, for pipes with varying deterioration levels (with a particular focus on pressure transients)
2. Conceptual development of optical fibre technology for monitoring new pipes

3. Establishing pipe failure states for various pipe materials
4. Development of a model for failure mechanisms

Activity 2 - Condition Assessment

The aim of this activity is to advance knowledge and improve levels of confidence of direct methods for condition assessment using advanced data interpretation techniques which have already been successfully employed in fields such as aerospace, cargo handling, undersea ecology, land vehicles and mining. The key outcome of this activity is expected to be:

1. Improved interpretation with higher levels of confidence for the researched condition assessment tools (MFL, BEM, RFEC and acoustic).

Activity 3 – Corrosion Modelling

One of the foremost requirements of pipe failure prediction is the accurate estimation of pipe deterioration rates. Methods currently available for estimation of pipeline deterioration are purely empirical, insufficiently accurate and limited in application. The purpose of Activity 3 is to develop calibrated theoretical models to predict significant deterioration in the structural strength of buried pipelines on the basis of established scientific principles. Key outcomes for Activity 3 will be:

2. Development and calibration of scientifically validated theoretical models for rate of corrosion loss on cast iron (maximum pit depth and area).
3. Development of a model for estimating the corrosion of pipe wall thickness under different environmental conditions.

The interaction between Activities 1, 2 and 3 are summarised in Figure 1. Activity 2 provides methodologies that allow the current condition (pipe wall thickness) of the water pipe to be determined. Activity 3 provides a model of the corrosion process operating at the site. This allows a determination of how the pipe wall thickness changes over time. This in turn allows the strength of the pipe at a specific location over time to be assessed (Activity 1). Comparing the failing strength of the pipe against the expected loadings on the pipe allows the time of failure (or the probability of failure at any given time) to be determined.

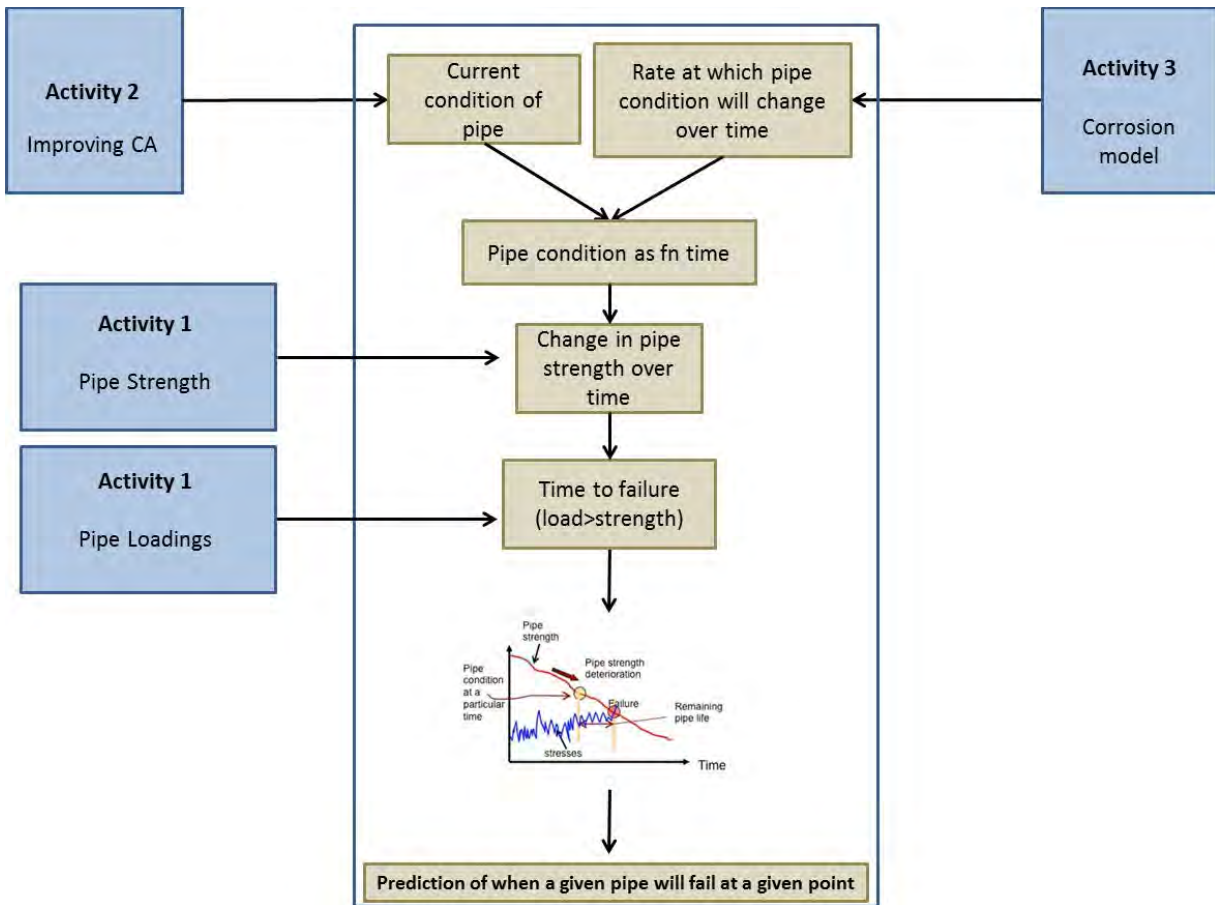


Figure 1. Interaction of Activities 1, 2 and 3

The principle outcome of Activities 1, 2 and 3 is to determine the probability of pipe failure at a specified time at a specified location (i.e., the location where the condition assessment is undertaken and where the rate of corrosion is determined (i.e., as a function of the soil analysis undertaken at that location)). At the start of 2014 a further activity (Activity 4) was initiated which seeks to extend the work undertaken in Activities 1, 2 and 3. The purpose of Activity 4 is to improve current capacities to predict the likelihood of pipe corrosion and its severity and thus the likelihood of pipe failure along a given length of pipe, i.e., interpolating between the discrete location predictions of Activities 1, 2 and 3 (see Figure 2).

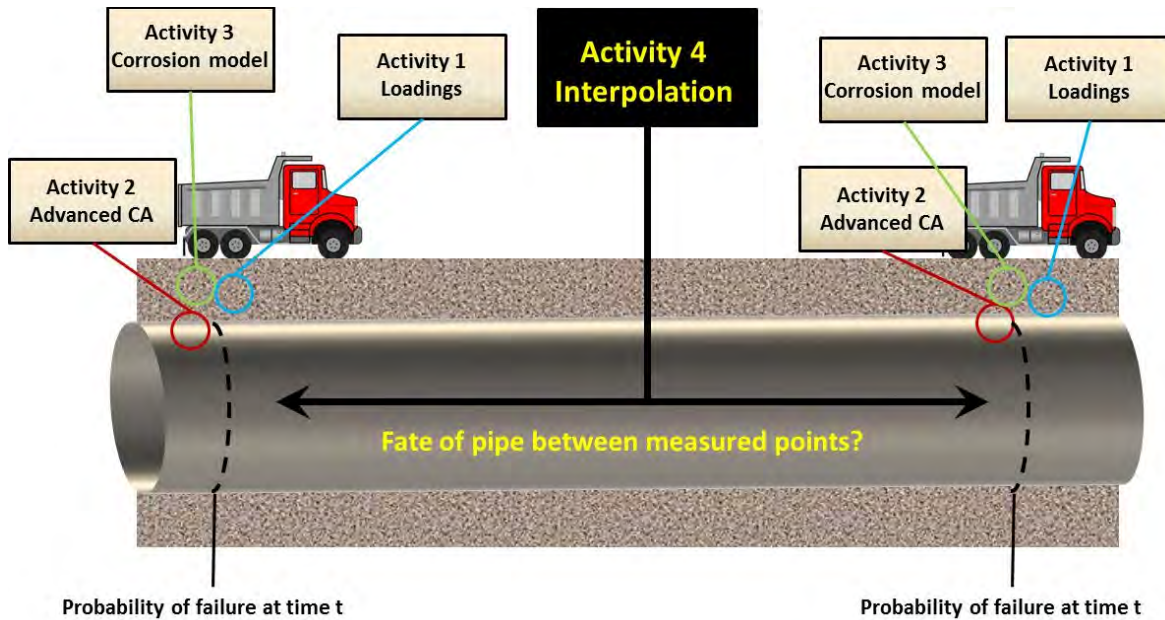


Figure 2. How Activity 4 fits in

The approach proposed is to use in-situ measurements at a site together with a corrosion model calibrated to past field observations and integrated with the knowledge available from corrosion fundamentals as well as experience in directly related fields. The intent is to use the model to interpret field observations, to make informed decisions about the likely condition of a target pipe along its length. The outcomes could then be used to make informed decisions about the optimal scheduling of pipe renewals in the network with the prediction of failure over space and time.

Activity 4 comprises a number of sub-activities:

- Activity 4a. Enhanced reliability of condition assessment of buried large diameter water mains
- Activity 4b. Understanding and Reducing uncertainty in the use of LPR
- Activity 4c. Enhanced ability to predict the likelihood of pipe corrosion along the length of a pipe
- Activity 4d. Enhanced reliability of emerging technologies not yet incorporated into current project
- Activity 4e. Enhanced ability to predict failure probability

Activity 4b is tasked to look at uncertainties surrounding the use of the LPR (Linear Polarisation Resistance) technique. LPR is a tool commonly used by the water industry to quickly estimate the soil corrosivity and hence the likely rate of corrosion at a specific location. The LPR technique provides a low cost and rapid assessment of corrosion rates and consequently has the potential to be used in interpolating corrosion behaviour between points already characterised through more intense soil chemistry analysis (such as used as input into Activity 3 corrosion models). Thus, it is seen as a possible tool in the corrosion interpolation which is a vital part of Activity 4's aim of interpolating corrosion behaviour (and hence failure behaviour) along the length of a pipe.

Activity 4b comprises the following actions:

- 4b.1 A review of the existing conceptual knowledge of LPR theory.
- 4b.2 Examination of the LPR approach in current practice.
- 4b.3 Development of an improved electrochemical model of the LPR process.

This document reports the findings of activity 4b.1, namely the review of the existing conceptual knowledge of LPR theory. The aim of 4b.1 is to understand the LPR process from a theoretical point of view and from this knowledge propose the likely areas of uncertainty of the application of LPR to assess corrosion behaviour. This knowledge will then be used in activity 4b.2 to focus the areas of investigation into the practical application of the LPR measurement process.

This report will discuss the theoretical principles behind LPR measurements and any insights gained into likely areas of uncertainty in corrosion rates predicted from LPR measurements. Firstly, a general discussion of ferrous corrosion will be given with special focus given to thermodynamics and kinetics of the corrosion process and the concept of polarisation. This will be followed by a more detailed look at cast iron pipe corrosion. Finally, the likely sources of uncertainty when using LPR to predict cast iron water pipe corrosion will be highlighted.

THEORETICAL BASIS FOR LPR MEASUREMENTS

Basics of Ferrous Metal Corrosion Reactions

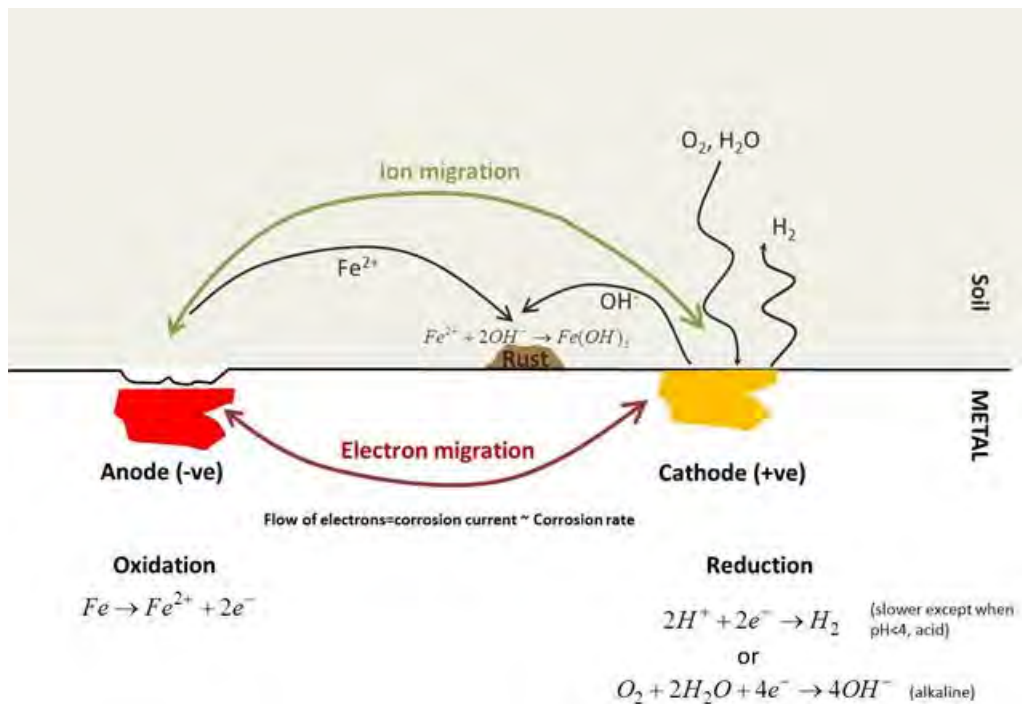


Figure 3. Schematic of the corrosion of ferrous metal

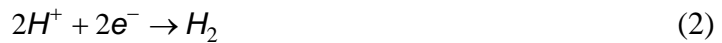
A simplified diagram of the corrosion of ferrous metal is shown in Figure 1. The corrosion reactions are occurring at two sites: the anode and the cathode. At the anodic site Fe atoms are

stripped of electrons and the resulting positive ion (Fe^{2+}) moves into the adjacent electrolyte (in this case the aqueous liquid in the soil pores). The reaction taking place at the anode is as follows:



The process of raising the valence of the atom or ion, (in this case Fe is oxidised from zero to a valence of +2), is called oxidation. Oxidation reactions occur at the anode.

The electrons released by reaction (1) at the anodic site flow to the cathodic site where they are consumed in the cathodic reaction. This will generally involve either of the following reactions:



Both reactions are examples of reduction reactions (i.e., the valence of the atom is reduced). Reduction reactions occur at the cathode. The reduction of the hydrogen ion (2) is generally much slower than the oxygen reduction reaction (3) except in acid conditions ($\text{pH} < 4$) consequently reaction (3) dominates at the cathodic site in all but acidic conditions if oxygen is available. Rust is formed when the Fe ions and liberated OH^{-} ions react to form iron hydroxide ($\text{Fe}(\text{OH})_2$).

Thermodynamics of the Corrosion Process

When reactions occur, there is a change in the free energy of the system. The free energy is known as the Gibbs free energy (G). For reactions to proceed spontaneously the change in G must be negative, i.e., the system loses energy ($\Delta G = G_{\text{final}} - G_{\text{initial}} < 0$), as systems naturally tend towards their lowest energy state. If the value of ΔG is positive energy must be added to the system (greater than or equal to ΔG) before the reaction can proceed. The change in free energy depends on the initial and final state of the system and is not affected by the path taken between the two states (i.e., ΔG is a “state function”).

In Figure 3, the two halves of the corrosion reaction are shown which together make up what is known as the electrochemical cell. Each half cell has a characteristic potential. In practice we can't measure this potential except in relation to another half-cell. It is common practice to determine the half-cell potential relative to the standard hydrogen electrode ($\text{SHE} - \text{H}_{2(\text{p}=1\text{atm})} \rightarrow 2\text{H}^{+} + 2e^{-}$) which is assigned a value of zero. (Note that as it is impossible to construct an electrode out of hydrogen gas an inert electrode is used instead – normally platinum).

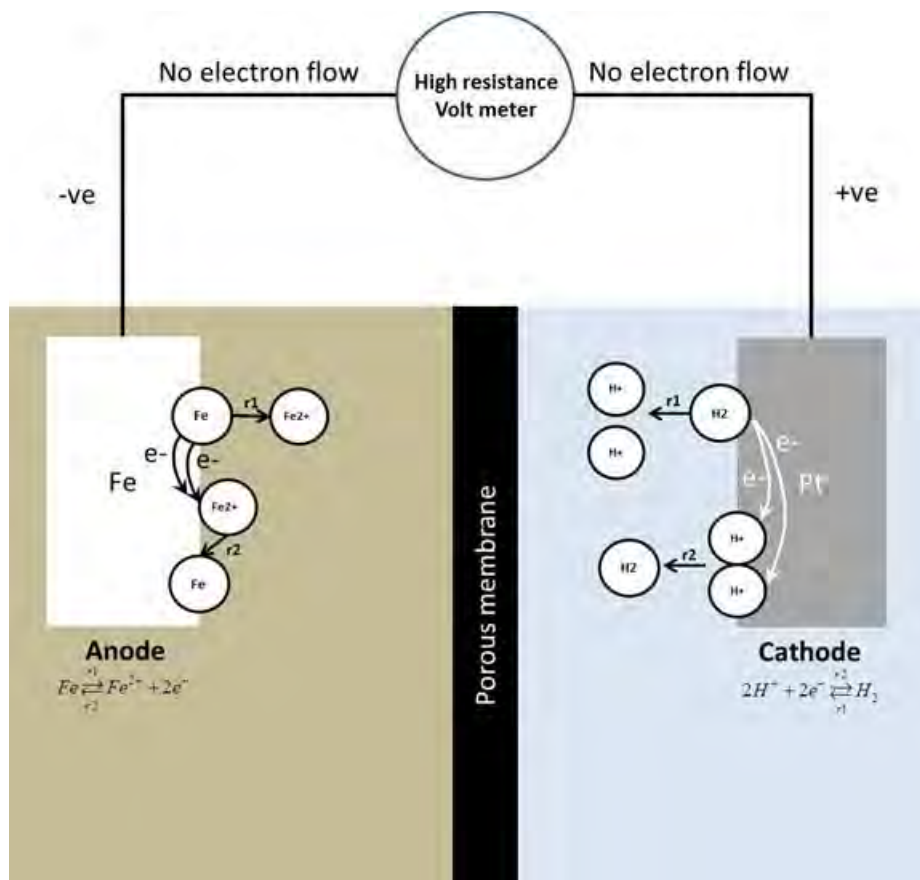


Figure 4. An electrochemical cell with iron dissolution at the anode and hydrogen generation at the cathode

For example, consider the two half-cell reactions as shown in Figure 4. On the anode side of the cell an iron electrode is immersed in a standard solution of iron ions ($[Fe^{2+}] = 1M$) with which it is in equilibrium. On the cathodic side of the cell an inert Platinum electrode is immersed in a $1M H^+$ solution saturated through which H_2 is bubbled at $1atm$ pressure, $T=25C$ (i.e., a standard hydrogen electrode). The forward and backwards reactions at the anode (i.e., the formation of Fe^{2+} and deposition of Fe) are proceeding at equal rates so no net reaction is observed. At the cathode the formation of H^+ ions and H_2 is also in equilibrium (no net forward or backward reactions there either). The high resistance volt meter ensures that no electrons are flowing between the electrodes.

In this case the voltmeter will show a potential difference between the two electrodes of $0.44V$ (with the Fe electrode negative with respect to the hydrogen electrode – hence the potential of the Fe half-cell is $-0.44V$).

Any number of reactions can be studied in this fashion and a table of half-cell potentials constructed. Reactions in this table are always written as reduction (cathodic) reactions and as such are referred to as standard reduction potentials (see Table 1, the table is also referred to as the EMF series, half-cell or oxidation reduction potential (redox) table).

As you go down the table the species is less likely to gain electrons (or can more easily lose them). A few equivalent ways to look at these numbers are:

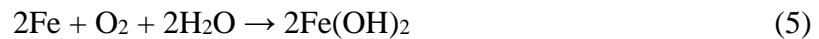
- As you go down the table the species involved can more easily lose electrons

- The more negative the E° value, the further the reaction equilibrium naturally lies to the left.
- Species further up the table are nobler
- Species lower down on the table will corrode in preference to species further up

The table can be used to calculate the whole cell voltage by looking at the half cell reactions and adding together. For example, for our iron corrosion reaction where OH^- is formed at the cathode, i.e.:



where the overall reaction is therefore:



The total cell voltage is equal to $0.4 - (-0.44) = 0.84\text{V}$

Table 1
Standard electrochemical potentials

Standard Reduction Potentials in Aqueous Solution at 25⁰C

Reduction Half-Reaction	E° (V)
$F_2(g) + 2 e^{-}$	$\rightarrow 2 F^{-}(aq)$ +2.87
$H_2O_2(aq) + 2 H_3O^{+}(aq) + 2 e^{-}$	$\rightarrow 4 H_2O(\ell)$ +1.77
$PbO_2(s) + SO_4^{2-}(aq) + 4 H_3O^{+}(aq) + 2 e^{-}$	$\rightarrow PbSO_4(s) + 6 H_2O(\ell)$ +1.685
$MnO_4^{-}(aq) + 8 H_3O^{+}(aq) + 5 e^{-}$	$\rightarrow Mn^{2+}(aq) + 12 H_2O(\ell)$ +1.52
$Au^{3+}(aq) + 3 e^{-}$	$\rightarrow Au(s)$ +1.50
$Cl_2(g) + 2 e^{-}$	$\rightarrow 2 Cl^{-}(aq)$ +1.360
$Cr_2O_7^{2-}(aq) + 14 H_3O^{+}(aq) + 6 e^{-}$	$\rightarrow 2 Cr^{3+}(aq) + 21 H_2O(\ell)$ +1.33
$O_2(g) + 4 H_3O^{+}(aq) + 4 e^{-}$	$\rightarrow 6 H_2O(\ell)$ +1.229
$Br_2(\ell) + 2 e^{-}$	$\rightarrow 2 Br^{-}(aq)$ +1.08
$NO_3^{-}(aq) + 4 H_3O^{+}(aq) + 3 e^{-}$	$\rightarrow NO(g) + 6 H_2O(\ell)$ +0.96
$OCl^{-}(aq) + H_2O(\ell) + 2 e^{-}$	$\rightarrow Cl^{-}(aq) + 2 OH^{-}(aq)$ +0.89
$Hg_2^{2+}(aq) + 2 e^{-}$	$\rightarrow Hg(\ell)$ +0.855
$Ag^{+}(aq) + e^{-}$	$\rightarrow Ag(s)$ +0.80
$Hg_2^{2+}(aq) + 2 e^{-}$	$\rightarrow 2 Hg(\ell)$ +0.789
$Fe^{3+}(aq) + e^{-}$	$\rightarrow Fe^{2+}(aq)$ +0.771
$I_2(s) + 2 e^{-}$	$\rightarrow 2 I^{-}(aq)$ +0.535
$O_2(g) + 2 H_2O(\ell) + 4 e^{-}$	$\rightarrow 4 OH^{-}(aq)$ +0.40
$Cu^{2+}(aq) + 2 e^{-}$	$\rightarrow Cu(s)$ +0.337
$Sn^{4+}(aq) + 2 e^{-}$	$\rightarrow Sn^{2+}(aq)$ +0.15
$2 H_3O^{+}(aq) + 2 e^{-}$	$\rightarrow H_2(g) + 2 H_2O(\ell)$ 0.00
$Sn^{2+}(aq) + 2 e^{-}$	$\rightarrow Sn(s)$ -0.14
$Ni^{2+}(aq) + 2 e^{-}$	$\rightarrow Ni(s)$ -0.25
$V^{3+}(aq) + e^{-}$	$\rightarrow V^{2+}(aq)$ -0.255
$PbSO_4(s) + 2 e^{-}$	$\rightarrow Pb(s) + SO_4^{2-}(aq)$ -0.356
$Cd^{2+}(aq) + 2 e^{-}$	$\rightarrow Cd(s)$ -0.40
$Fe^{2+}(aq) + 2 e^{-}$	$\rightarrow Fe(s)$ -0.44
$Zn^{2+}(aq) + 2 e^{-}$	$\rightarrow Zn(s)$ -0.763
$2 H_2O(\ell) + 2 e^{-}$	$\rightarrow H_2(g) + 2 OH^{-}(aq)$ -0.8277
$Al^{3+}(aq) + 3 e^{-}$	$\rightarrow Al(s)$ -1.66
$Mg^{2+}(aq) + 2 e^{-}$	$\rightarrow Mg(s)$ -2.37
$Na^{+}(aq) + e^{-}$	$\rightarrow Na(s)$ -2.714
$K^{+}(aq) + e^{-}$	$\rightarrow K(s)$ -2.925
$Li^{+}(aq) + e^{-}$	$\rightarrow Li(s)$ -3.045

The Gibbs free energy change (ΔG) (or the thermodynamic driving force) for the overall reaction can be subsequently calculated using the following relationship:

$$\Delta G^0 = -nFE^0 \quad (6)$$

where ΔG^0 is the change in Gibbs Free energy at standard conditions, n is the number of electrons transferred in the reaction, F is the Faraday constant (96485 C/mol) and E is the cell potential (voltage). In our example:

$$\Delta G^0 = -nFE^0 = -2 \times 96485 \times 0.84 = -162094 \text{ J/mol Fe} = -162 \text{ kJ/mol Fe}$$

Note that if the cell voltage is positive the change in Gibbs free energy is negative so the reaction can occur spontaneously however there is no guarantee as to how fast it will occur – it could for example proceed at such a slow rate as to be for all practical purposes not proceeding at all. This is an important consideration in studying corrosion reactions. It should also be noted that in the above example all of the reactions are occurring at standard conditions (1M concentrations etc.). In practice this is unlikely and therefore non ideality must be accounted for

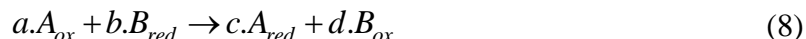
The Nernst Equation

To account for non-standard conditions the standard cell potential, E^0 is modified as follows via the Nernst equation:

$$E = E^0 - \frac{RT}{nF} \ln Q \quad (7)$$

where E is the cell (or half-cell) potential at non-standard conditions, E^0 is the standard half-cell potential (as listed for example in Table 1), R is the universal gas constant, T is temperature (K), n is the number of electrons involved in the reaction, F is Faraday's constant, Q is the reaction quotient which is the ratio of products over reactants with values raised to a power equivalent to the species' stoichiometric coefficient.

For a complete cell reaction with a balanced reaction of the form



where A_{ox} is the species being oxidised and B_{red} is the species being reduced. The reaction quotient becomes:

$$Q = \left(\frac{[A_{red}]^c [B_{ox}]^d}{[A_{ox}]^a [B_{red}]^b} \right) \quad (9)$$

And therefore

$$E = E_0 - \frac{RT}{nF} \ln \left(\frac{[A_{red}]^c [B_{ox}]^d}{[A_{ox}]^a [B_{red}]^b} \right) \quad (10)$$

*Note: (1) All pure liquids and solids have an activity of one and can be omitted. (2) In dilute solutions the activity of a species is virtually equivalent to the species concentration however this may not be the case as concentration increases.

So, for example for the half-cell reactions:



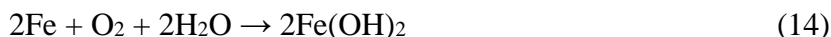
From Table 1 the cell potential is 0.84V at standard conditions (when the concentration of Fe^{2+} ions and OH^- ions are 1M, O_2 pressure is at 1 atm). If for example the concentration of Fe^{2+} is 0.1M then for the iron half cell:

$$Q = \left(\frac{a_{\text{Fe}(s)}}{a_{\text{Fe}^{2+}}} \right) = \left(\frac{1}{0.1} \right) = 10 \quad (12)$$

And therefore

$$E = E^0 - \frac{RT}{nF} \ln Q = -0.44 - \frac{8.314 \times 293}{2 \times 96485} \ln(10) = -0.44 - 0.03 = -0.47V \quad (13)$$

Consequently, lowering the concentration of Fe^{2+} ions from 1M to 0.1M has made the half-cell voltage more negative. This is akin to decreasing the driving force of the reaction in the forward direction (as you would expect from Le Chatelier's principle). The overall cell voltage (assuming all other species are at standard conditions is therefore $E = 0.4 - (-0.47) = 0.87V$ and the driving force changes from -162 kJ/mol Fe to 167 kJ/mol Fe. In other words, the driving force for the overall forward reaction (14) is increased by lowering the Fe concentration on the product side.



Kinetics of the Corrosion Process

Electrodes at Equilibrium

Thermodynamics allows us to determine if a reaction will proceed or not – it tells us nothing about how fast the reaction proceeds. In the study of corrosion, we are usually more interested in how fast the corrosion reactions proceed as this will govern the serviceable life of the infrastructure in question (in our case the water pipe). Consequently, we are interested in the kinetics of the corrosion reactions.

To best understand the kinetics of the corrosion process, consider the half-cell reactions occurring when a piece of iron is contacted with water (Figure 5). When the electrode is first placed into the water Fe atoms dissolve into the solution surrounding the electrode leaving the electrode surface slightly negatively charged. As time goes on more metal atoms dissolve releasing more cations and further increasing the charge on the electrode. At the same time cations are attracted back to the slightly negative electrode surface where they combine with excess electrons to reform iron. Eventually equilibrium is reached such that for any Fe^{2+} ion leaving the electrode surface another is returning to the electrode to form Fe.

When an electrode is at equilibrium with its surrounds the oxidation and reduction reactions are still taking place but are proceeding in opposite directions at the same rates. For example, the formation of Fe^{2+} via r_1 is exactly matched by the reduction of Fe^{2+} occurring as a result of r_2 , i.e., $r_1 = r_2$. A finite interchange between Fe and Fe^{2+} is taking place producing a stream of electrons between the sites where Fe^{2+} is being formed and where Fe^{2+} is being converted back to Fe leaving the electrode and an equivalent stream of electrons arriving at the electrode. The flow of electrons

is called the exchange current and when expressed in relation to the surface area of the electrode is called the exchange current density (A/m²). The relationship between the forward and backward reaction rates and the exchange current density is as follows:

$$r_1 = r_2 = \frac{i_o}{nF} \quad (15)$$

where i_o is the exchange current density (A/m²), n is the number of e- taking part in the reaction (i.e., $n=2$ in this case) and F is again the faraday constant (96485 C/mol).

The exchange current density varies depending on not only the system under investigation (for example $\text{Fe} \leftrightarrow \text{Fe}^{2+}$ or $\text{H}_2 \leftrightarrow 2\text{H}^+$) but also the electrode material used (for example hydrogen oxidation/reduction on a Pt electrode $i_o=10\text{A/m}^2$ while $i_o=2 \times 10^{-9}\text{A/m}^2$ for a lead electrode). Like reversible potentials the exchange current densities are influenced by the ratio of oxidised and reduced species that are present and the temperature of the system. Exchange current density is also usually expressed in terms of the projected or geometric surface area of the electrode and consequently varies depending on the surface roughness of the electrode.

The rate at which any chemical reaction occurs is normally limited by barriers or obstacles that lie between the reactants and the formation of the products. These barriers may take the form of an intermediate energy state that must be obtained before the reactants can combine to form the product (Figure 6) or may be of a more physical nature, for example, may be the result of difficulties experienced in one or more reactants diffusing to the reaction site.

As a result, even though there may be a decrease in the overall system energy in moving from the reactants to the products and hence the reaction is favoured from a thermodynamic point of view (i.e., ΔG is negative) the reactants still require some energy (the activation energy) to make it over the obstacle before the reaction can proceed. In any chemical system some atoms will be more energetic than others thus it is likely that some will possess enough inherent energy to cross the barrier. The higher the activation energy the fewer the number of reactant atoms that can cross over the energy barrier at any one time and hence the reaction is slower. As the temperature of the system increases more reactants are likely to possess enough energy to overcome the barrier or conversely if the system is altered to reduce the height of the barrier (e.g., by the introduction of a catalyst) more reactant atoms can cross over. In either case the rate of reaction increases.

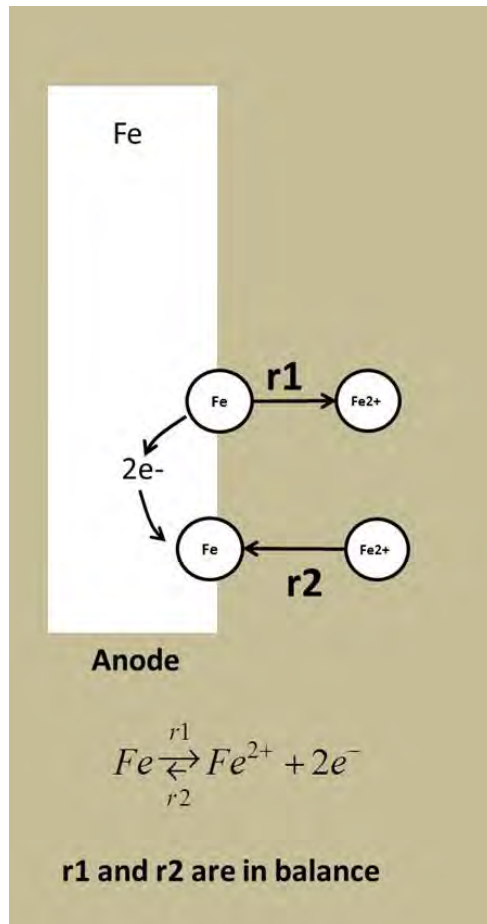


Figure 5. Iron in equilibrium with surrounding water

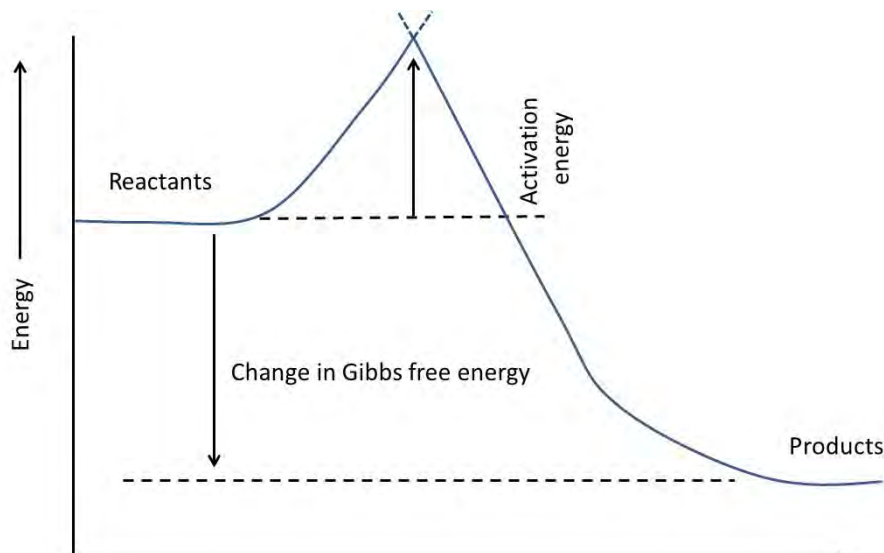


Figure 6. Energy barrier that must be overcome for reaction to proceed

Typically, the reaction rate is expressed as follows:

$$r = k_0 \times \exp\left(\frac{-G^{act}}{RT}\right) \quad (16)$$

where r is the reaction rate, k_0 is a fundamental rate constant, G^{act} is the activation energy and R and T are the universal gas constant and the temperature (in Kelvin) respectively. The expression is a commonly used to express the rate of any chemical reaction taking place where an activation energy must also be surmounted and flows on from a consideration of the energy distribution of atoms at a given temperature (the Boltzmann distribution). The exponential term in reaction (16) represents the probability that the energy barrier will be overcome.

Again, looking at the example of the iron electrode placed in water (Figure 7). As the Fe atoms dissolve into the aqueous phase the electrode surface gains a negative charge. In response the water molecules near the electrode surface align themselves so that their positive ends are toward the electrode surface. The exact nature of this electrically charged layer can be quite complex and many layer geometries have been proposed. For simplicities sake, only the simplest arrangement as shown in Figure 7 is considered here. Once the system reaches equilibrium for any further dissolution to take a Fe^{2+} ion must detach itself from the electrode surface and pass through the positively charged solvent layer before it enters the bulk solution consequently the ion must have enough energy to overcome the natural repulsion of the positively charged layer before the reaction is completed (i.e., they must pass over the energy barrier – shown in red. Similarly, Fe^{2+} ions migrating from the bulk solution to the electrode to complete the reverse reaction must also somehow pass through this barrier. At reaction equilibrium the distance from the base energy level to the peak energy value (E_a) needed to pass through the charged layer is the same no matter which direction the ion is heading (i.e., to or from the electrode) consequently equation (16) suggests that the rates of reaction are the same in either direction, i.e.:

$$r_1 = r_2 = k_0 \times \exp\left(\frac{-G^{act}}{RT}\right) \quad (17)$$

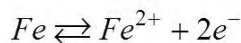
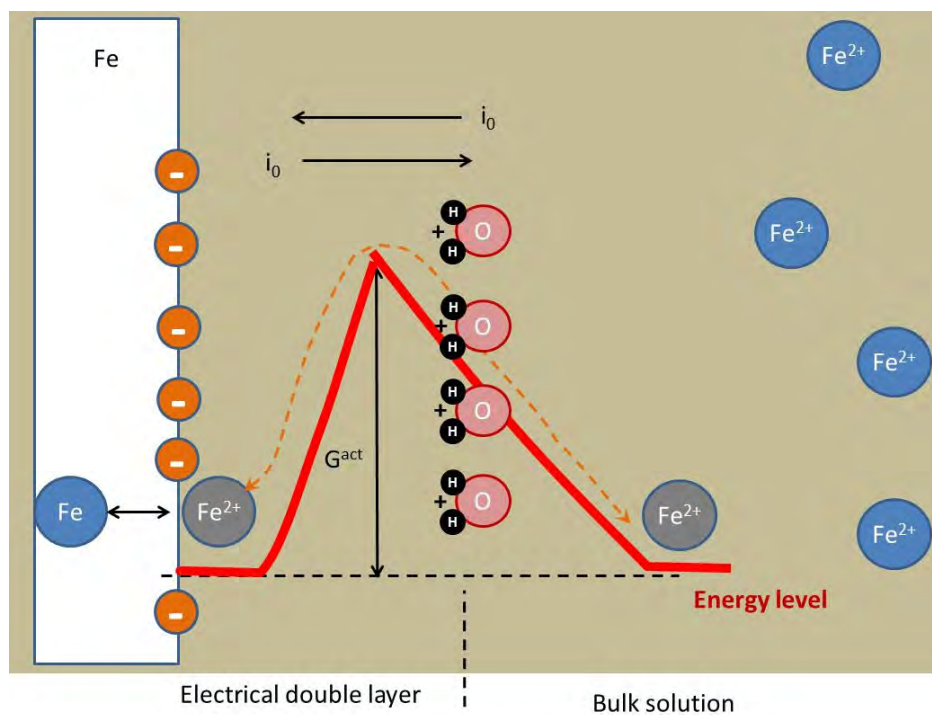


Figure 7. Energy diagram for the dissolution of iron in water

Electrodes Not at Equilibrium - Polarisation

So far, we have considered the kinetics of the half-cell at equilibrium. In this case electrons generated on the electrode surface when the Fe is converted to Fe²⁺ are trapped on the electrode surface because no current is allowed to flow from the electrode. In more realistic corrosion cells such as shown in Figure 3 electrons are drawn away from the anode to the cathode where they take part in the cathodic reaction. When the cell is “short circuited” in this fashion net oxidation and reduction processes occur at the electrode interfaces and the processes are no longer at their equilibrium potential values. The deviation from the equilibrium potential values is termed “polarisation” (or overpotential = η). Polarisation can be defined as the displacement of an electrode potential resulting from a net current.

Drawing electrons away from the anode raises the potential at the anode making it easier for Fe²⁺ ions entering the solution to cross over the energy barrier (see Figure 8). With a reduced energy barrier, the forward reaction (dissolution of Fe) becomes more rapid compared to the reverse reaction (deposition of Fe) consequently there is a net dissolution process occurring.

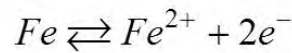
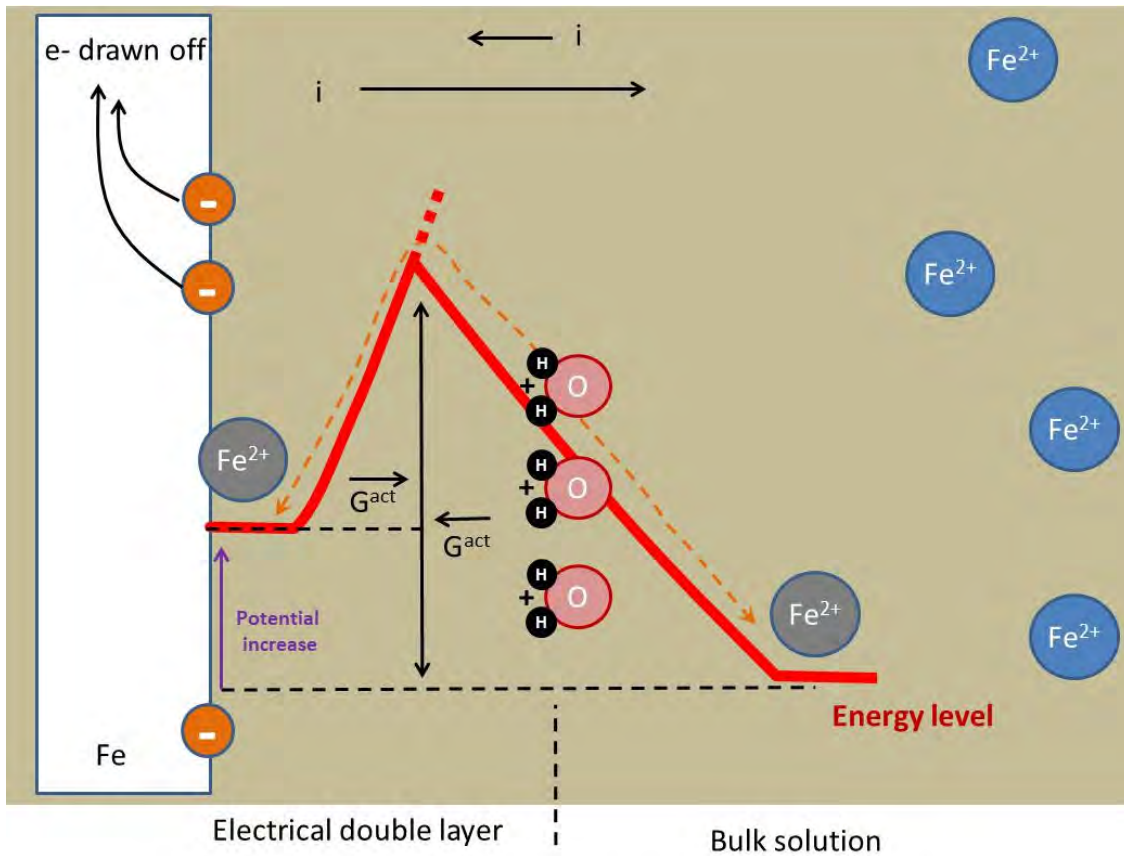


Figure 8. Energy diagram when electrons are drawn away from anode (i.e., the potential at the anode is raised)

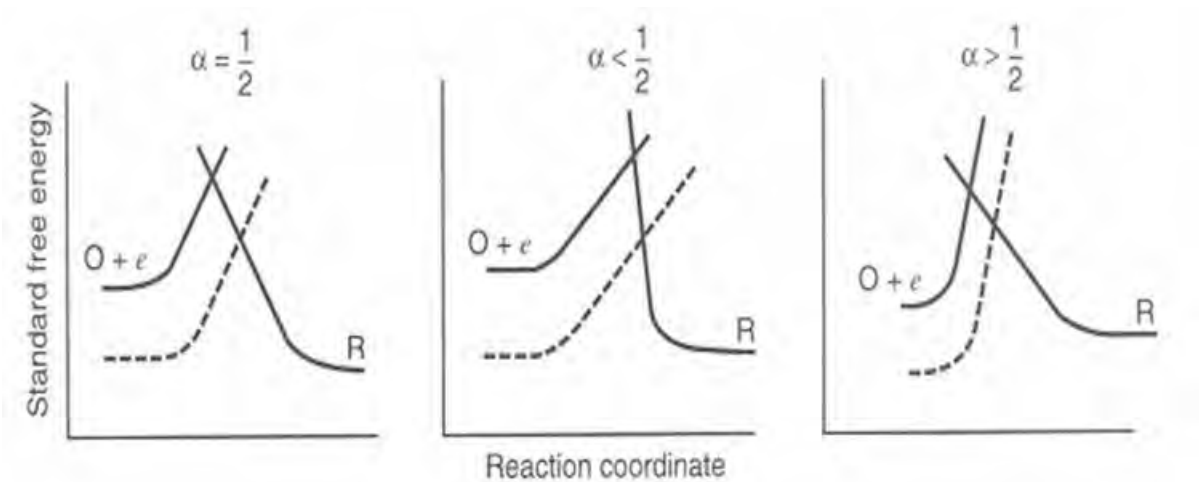


Figure 9. Energy barrier changes depending on geometry factor, alpha

If the potential at the electrode is raised by an overpotential = η , then the starting energy of the Fe atoms is raised by (see equation 6):

$$\text{new electrode energy level} = \text{Original} + n \times F \times \eta \quad (18)$$

The energy barrier to be overcome is dropped by some fraction of that amount (α) where the fraction value is dependent on the geometry of the energy barrier profile (see Figure 9). For simple electron transfer processes operating on metallic electrodes α is normally close to 0.5. In the forward (anodic, dissolution) direction the energy barrier that needs to be overcome is lowered to:

$$\Delta G_{\rightarrow, \text{new}}^{\text{act}} = \Delta G_{\rightarrow, \text{equ}}^{\text{act}} - (1 - \alpha)nF\eta \quad (19)$$

In the reverse (cathodic, deposition direction) the energy barrier is now higher:

$$\Delta G_{\leftarrow, \text{new}}^{\text{act}} = \Delta G_{\leftarrow, \text{equ}}^{\text{act}} + \alpha nF\eta \quad (20)$$

Remembering that for the equilibrium reaction (17), that:

$$r_{\eta=0} = r_0 = k_0 \times \exp\left(\frac{-G_{\text{equ}}^{\text{act}}}{RT}\right) \quad (21)$$

With an overpotential, η , the new reaction rate in the anodic direction, \bar{r}_η , is:

$$\bar{r}_\eta = k_0 \times \exp\left(\frac{-\bar{G}_{\text{new}}^{\text{act}}}{RT}\right) = k_0 \times \exp\left(\frac{-\bar{G}_{\text{equ}}^{\text{act}} + (1 - \alpha)nF\eta}{RT}\right) = k_0 \times \exp\left(\frac{-\bar{G}_{\text{equ}}^{\text{act}}}{RT}\right) \exp\left(\frac{(1 - \alpha)nF\eta}{RT}\right) \quad (22)$$

And in the reverse direction, \bar{r}_η , is:

$$\bar{r}_\eta = k_0 \times \exp\left(\frac{-\bar{G}_{\text{new}}^{\text{act}}}{RT}\right) = k_0 \times \exp\left(\frac{-\bar{G}_{\text{equ}}^{\text{act}} - \alpha nF\eta}{RT}\right) = k_0 \times \exp\left(\frac{-\bar{G}_{\text{equ}}^{\text{act}}}{RT}\right) \exp\left(\frac{-\alpha nF\eta}{RT}\right) \quad (23)$$

Altogether the net reaction ($r_\eta = \bar{r}_\eta - \bar{r}_\eta$) is:

$$r_\eta = k_0 \times \exp\left(\frac{-G_{\text{equ}}^{\text{act}}}{RT}\right) \left[\exp\left(\frac{(1 - \alpha)nF\eta}{RT}\right) - \exp\left(\frac{-\alpha nF\eta}{RT}\right) \right] \quad (24)$$

Therefore:

$$r_{\eta} = r_0 \times \left[\exp\left(\frac{(1-\alpha)nF\eta}{RT}\right) - \exp\left(\frac{-\alpha nF\eta}{RT}\right) \right] \quad (25)$$

From equation (15) we know that the exchange current density is:

$$i_{\eta=0} = i_0 = r_0 nF \quad (26)$$

and

$$i_{\eta} = r_{\eta} nF \quad (27)$$

Combining the above we arrive at the Butler-Volmer equation:

$$i_{\eta} = i_0 \left[\exp\left(\frac{(1-\alpha)nF\eta}{RT}\right) - \exp\left(\frac{-\alpha nF\eta}{RT}\right) \right] \quad (28)$$

Plotting of the Butler Volmer equation for one reaction (see Figure 10) illustrates the effect of changing the electrode potential on the reactions taking place. Application of the anodic and cathodic sections of equation (28) allows us to graph the current being produced by the forward and backward reactions (red dashed lines). By adding the two currents together we get the overall current (blue line). At the equilibrium voltage, E_0 , (here set to -0.44V) there is no applied external potential so the cathodic and anodic reactions are proceeding at equal and opposite rates (with a current = i_0). When the voltage is decreased (negative overpotential) the anodic process is greatly retarded and the cathodic reaction aided so that very quickly the overall current is dominated by the cathodic reaction (see where red dashed line and blue line merge in the pale pink sector). At voltages greater than E_0 the situation is reversed and the anodic reaction (metal dissolution) dominates.

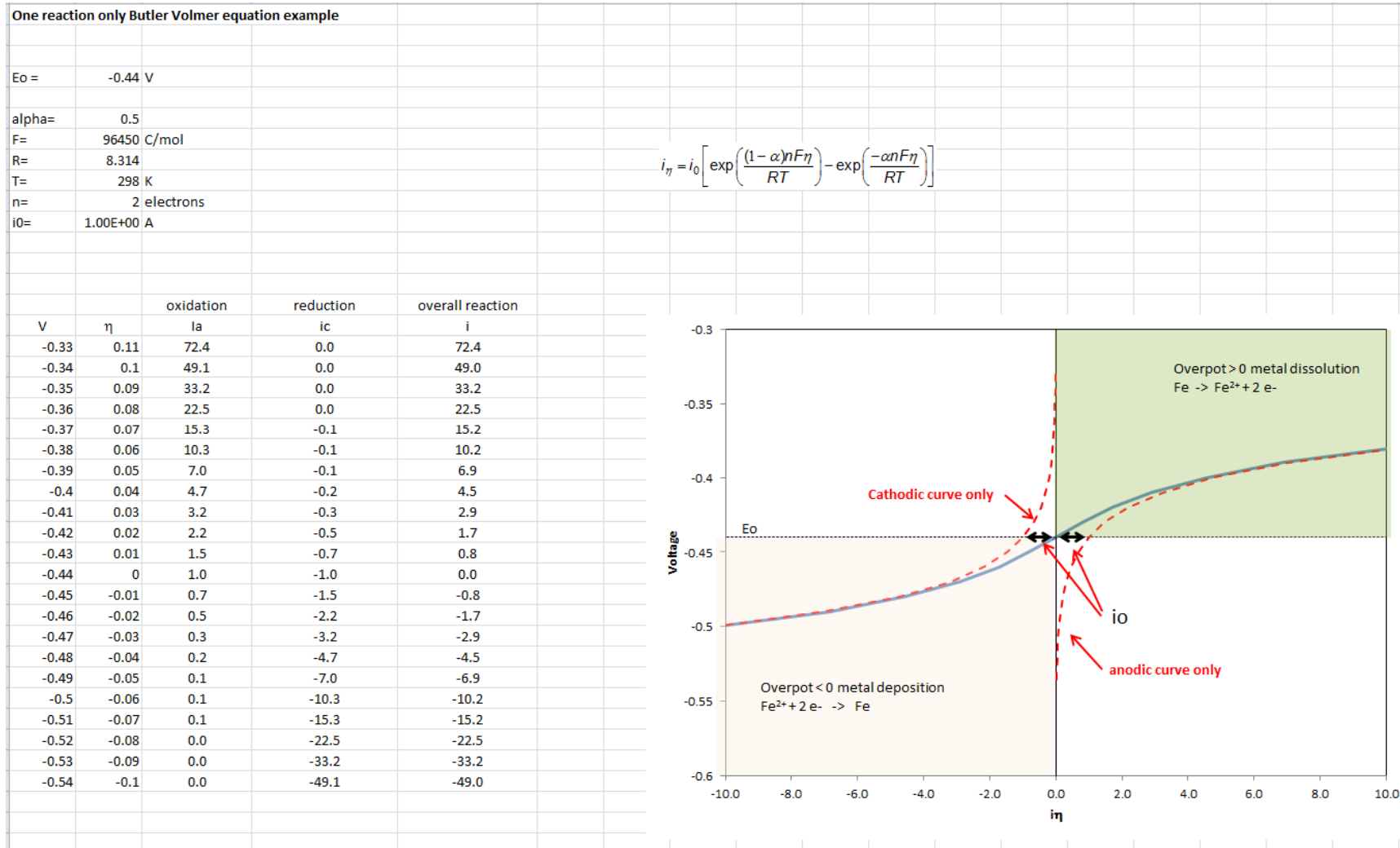


Figure 10. A one reaction example of the Butler Volmer equation

Tafel Equations

If the overpotential is large (>50mV) and positive the second term in equation (28) can be neglected and the equation is reduced to:

$$\eta_{anode} = a + b \log(i_{\eta}) \quad (29)$$

If the overpotential is large and negative equation (28) reduces to:

$$\eta_{cathode} = a - b \log(i_{\eta}) \quad (30)$$

Equations (29) and (30) are the anodic and cathodic forms of the Tafel equation where

$$a = \frac{2.303RT}{\alpha nF} \log(i_0) \text{ and } b = \frac{2.303RT}{\alpha nF} \text{ (the Tafel slope).}$$

What Happens When There Are Two Reactions Taking Place

The corrosion of cast iron pipe involves the reduction/oxidation of iron and the reduction/oxidation of either hydrogen or oxygen taking place at various points on the same metal surface (Figure 3). Consequently, two pairs of reactions (the forward and reverse version at the anode and cathode sites), each of which can be plotted on the same potential versus current diagram using the same procedure listed above for a single reaction (Figure 11). The overall system voltage will represent a negative overpotential (i.e., under-potential) for the oxygen reduction reaction (the cathodic reaction) but at the same time represents an over-potential for the Fe oxidation reaction (i.e., the anodic reaction). This produces a cathodic current (i_c) and an anodic current (i_a). The system as a whole will gravitate to the point where the two currents are equal (and so overall there is no net current ($i_a=i_c$)). The voltage at which this occurs is the corrosion voltage, E_{corr} (Figure 11). The value of E_{corr} lies between the E_0 values for the anode and cathode reactions.

Many analogies exist between the one and two reaction systems. E_{corr} (two reaction system) is analogous to E_0 (single reaction system) and i_{corr} is akin to i_0 (however it should always be remembered that there are different values of i_0 and I_{corr} in the two reaction systems). It is also possible to examine what happens to i_a and i_c when we vary the voltage of the 2 reaction system around the equilibrium value (E_{corr}) in much the same way as we did for the one reaction system. A form of the Butler-Volmer equation can also be written to apply to 2 reaction systems which is analogous to equation (28):

$$i_{applied} = i_{corr} \left[\exp\left(\frac{(1-\alpha)nF\eta_{corr}}{RT}\right) - \exp\left(\frac{-\alpha nF\eta_{corr}}{RT}\right) \right] \quad (31)$$

where $\eta_{corr} = (E_{applied} - E_{corr})$

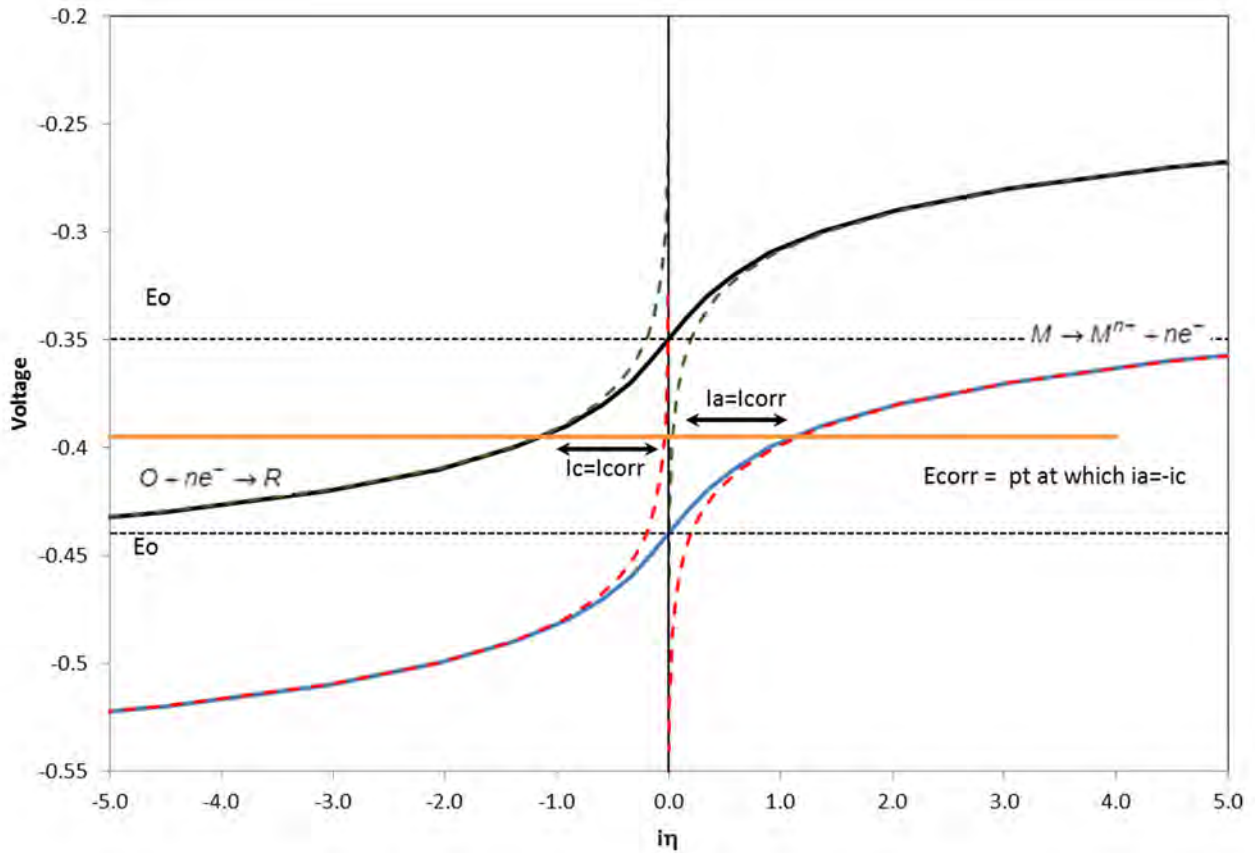


Figure 11. Potential versus current diagram when two reactions are taking place

Linear Polarised Resistance

Of immediate interest to this project and the application of LPR is the case where the applied overpotential is small, ($\eta_{corr} < \sim 20\text{mV}$). In this case equation (31) can be simplified by using the Taylor series expansion approximation for the exponential terms ($e^x = 1 + x + \frac{x^2}{2!} + \frac{x^3}{3!} + \dots$)

For small values of x the exponential term can be approximated by the first two terms of the expansion, that is $e^x \approx 1+x$. Applying the approximation to equation (31) the following approximation for $i_{applied}$ is obtained for sufficiently small values of η_{corr} :

$$\begin{aligned}
 i_{applied} &= i_{corr} \left[1 + \left(\frac{(1-\alpha)nF\eta_{corr}}{RT} \right) - 1 - \left(\frac{-\alpha nF\eta_{corr}}{RT} \right) \right] \\
 &= i_{corr} \left[\eta_{corr} \left(\frac{(1-\alpha)nF}{RT} \right) + \left(\frac{\alpha nF}{RT} \right) \right] \\
 &= i_{corr} \left[\frac{\eta_{corr} nF}{RT} \right]
 \end{aligned} \tag{32}$$

re-arranging:

$$\eta_{corr} = \frac{i_{applied}}{i_{corr}} \times \frac{RT}{nF} \quad \text{therefore} \quad (33)$$

$$E_{applied} = i_{applied} \times \frac{RT}{i_{corr} nF} - E_{corr}$$

A linear polarised resistance term (R_p) that is analogous to ohmic resistance (where $R=V/I$) can be defined such that:

$$R_p = \frac{\partial E_{applied}}{\partial i_{applied}} \quad (34)$$

then

$$R_p = \frac{RT}{i_{corr} nF} \quad (35)$$

therefore

$$i_{corr} = \frac{B}{R_p} \quad (36)$$

By observing the current response to small application of small amounts of overpotential it is possible to estimate the linear polarised resistance value, R_p (equation (34)). If we knew the value of B then we could calculate the corrosion current for the systems however in the current application of LPR measurements in this project this is not necessary. Rather the aim is to determine the corrosivity of the soil surrounding the pipe. Equation (36) tells us that the corrosion current (and hence the soil corrosivity) will be proportional to the inverse of R_p , thus if we can calculate the value of R_p for a variety of soils it should be possible to use reciprocal R_p values to rank different soils in terms of the corrosion current they are likely to generate. The corrosion current is the number of electrons being generated by the dissolution of Fe per second and thus is a good proxy for the corrosion rate. Consequently, determining R_p from an LPR test should allow the relative corrosion rate for our pipe in a particular soil to be estimated and with proper calibration we can then develop a function relating R_p to a corrosion rate.

The major caveat to this argument is that the above discussion assumes that the corrosion reaction rate is dictated by the rate at which the electron transfer processes take place on the surface of the electrode (the phenomena from which equations (15) onwards are derived).

It should also be noted that, as noted by Phil Ferguson in a personal communication, that corrosion pitting rates can only be estimated from an empirically derived relationship between observed pit rates and observed R_p values. It is not possible to predict pitting rates from Tafel slopes with any reliability.

NATURE OF CAST IRON PIPE CORROSION

In order to identify the possible areas of uncertainty in the LPR based prediction of cast iron pipe corrosion rates it is not only necessary to understand the nature of the LPR measurement but also the nature of the cast iron pipe corrosion process as it occurs in the field. The following discussion examines some of the features of the pipe corrosion process.

Corrosion Reaction Rates and Rate Limiting Processes

In situations where corrosion is taking place there can be a number of factors/processes which can act as rate limiting steps in the corrosion process and hence ultimately dictate the rate at which the overall corrosion process takes place. The following section briefly discusses the two rate limiting processes most applicable to pipe corrosion in the soil. In the field of electrochemistry, they are referred to as “polarisation” processes.

Activation Polarisation

Activation polarisation refers to the processes outlined above, i.e., the electron transfer processes occurring at the anode and cathode surface (Figure 12). At the anode the oxidation process is fairly simple requiring only the removal of the electrons from a Fe atom on the electrode surface.

In the case where oxygen reduction is taking place at the cathode, oxygen and water must absorb onto the metal surface (step 1), then absorb the electrons (step 2), combine with each other to form the OH⁻ ions (step 3) before finally the OH⁻ ions finally detach from the metal (step 4). If any of these processes are slow enough to control the rate of the overall corrosion process the reaction is said to be subject to “Activation polarisation.” Importantly, the LPR measurement essentially measures the kinetics of these electron transfer processes.

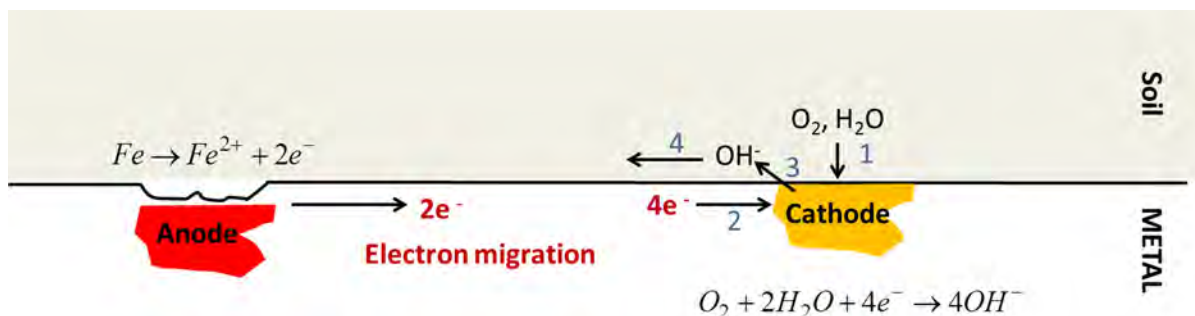


Figure 12. Activation polarisation

Concentration Polarisation

Concentration polarisation refers to diffusion limitation of the corrosion reaction (see for example Figure 13). Consider again the environment shown in Figure 12 in and around the cathode. Once the oxygen and water present in the immediate surrounds of the cathodic site is consumed by the reduction reaction it is necessary for additional oxygen and water to diffuse through the soil matrix to the cathodic site before the reaction can proceed further. At the anodic site while the supply of Fe is always going to be plentiful a build-up of Fe²⁺ in the surrounding soil moisture may hinder the forward progress of the iron dissolution reaction (via adverse concentration gradients). If the diffusion of oxygen/water to the cathodic site or diffusion of iron ions from the anodic site is sufficiently slow (compared to the activation processes discussed previously) the rate of diffusion of these species can act as the rate limiting step in the corrosion process. In cases where the (slow) transport of reactants or products to or from the corrosion site controls the rate of the overall corrosion reaction the corrosion process is said to be diffusion limited. Of relevance to this project is the fact that LPR tests do not take this scenario into account.

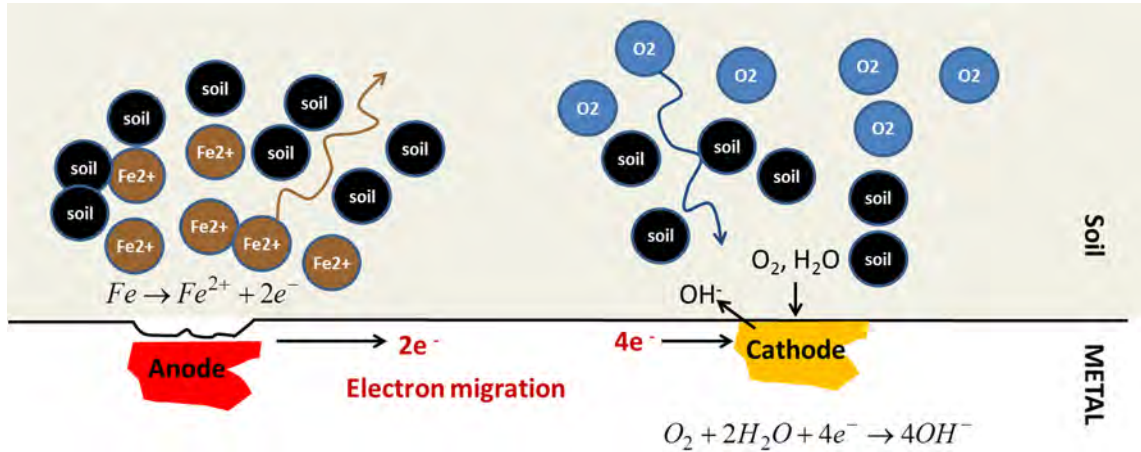
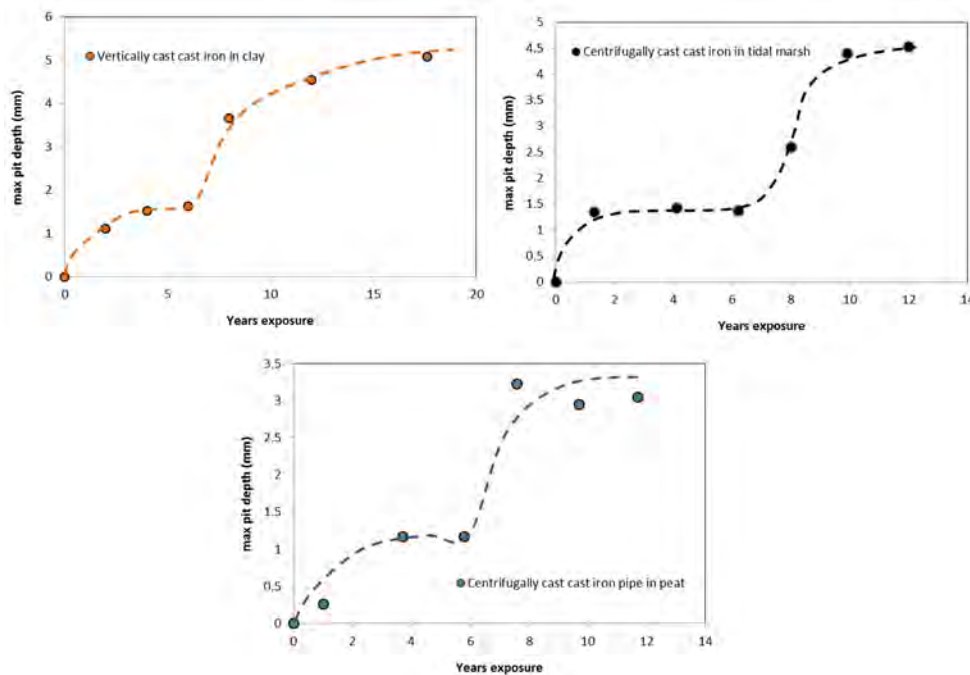


Figure 13. Concentration polarisation (diffusion limited corrosion)

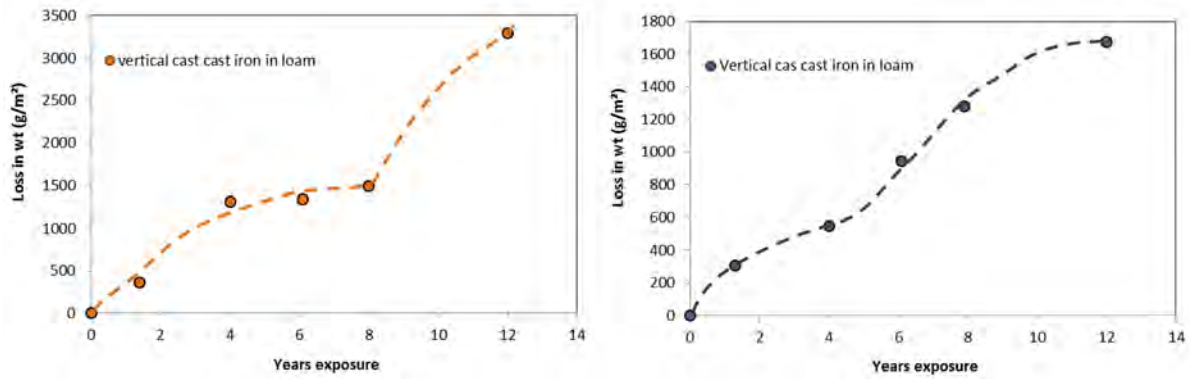
Cast Iron Corrosion Trends over Time

The long-term corrosion trends of ferrous metals have been examined by Melchers (e.g., Melchers and Wells (2006) and Melchers (2014)), and reviewed recently by Petersen and Melchers (2012). Melchers has observed that the corrosion of ferrous metals appears to follow a monotonic bi-modal trend with time (cast iron examples are shown in Figure 14 and Figure 15) with overall corrosion rates driven by different factors at different stages (phase 0 to 4 in Figure 16).



Source: Romanoff 1957.

Figure 14. Some examples of bimodal corrosion behaviour for buried cast iron pipe – extent of maximum pit depth



Source: Romanoff 1957.

Figure 15. Some examples of bimodal corrosion behaviour for buried cast iron pipe – extent of mass loss

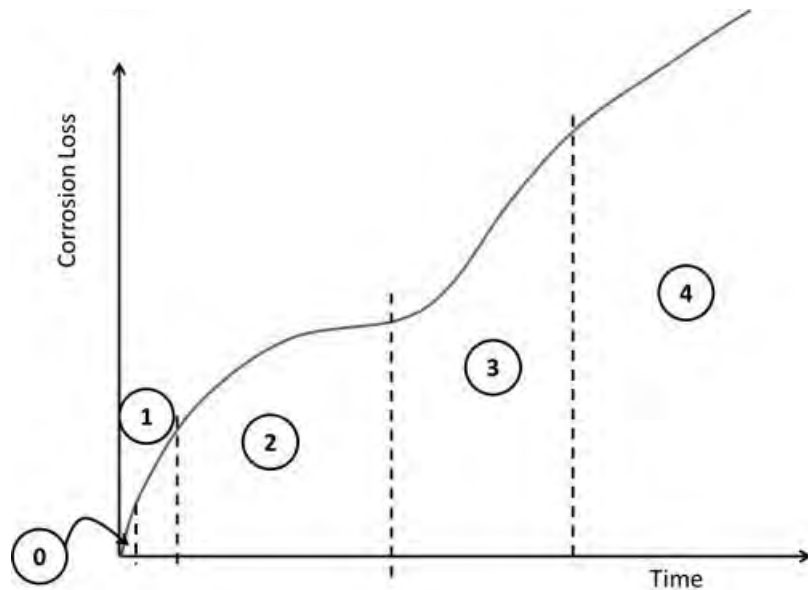


Figure 16. Schematic representation of bimodal behaviour of ferrous corrosion showing the five corrosion phases

In a moist soil environment, the corrosion of cast iron can be characterised as the wet corrosion of the iron component with reactions as listed earlier for iron oxidation (equation (1)) and oxygen reduction (equation (3)). Following the oxidation/reduction reactions the ferrous and hydroxide ion react to form various iron oxide corrosion products which are either deposited within the graphitised zone of the cast iron, on the external surface of the pipe, or diffuse away into the surrounding soil. The build-up of corrosion products however affects how the corrosion process proceeds.

Initially (and most likely for a very short period of time) corrosion is governed by the rates at which electron transfer reactions take place on the metal surface (activation polarisation as discussed earlier and represented as phase 0 in Figure 16). This is the realm that the LPR process examines.

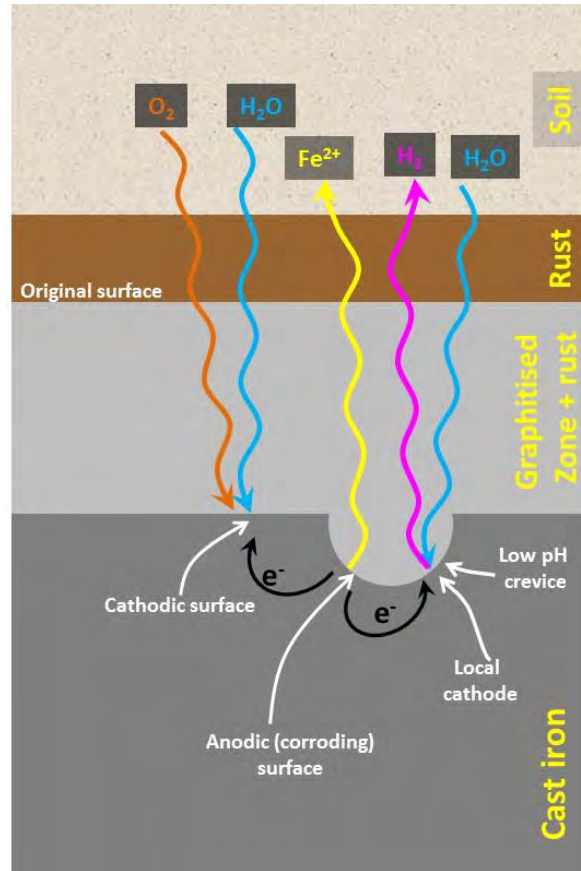
After a short period of time oxygen is depleted in the immediate area of the cathodic sites and corrosion progresses onto phase 1. During phase 1, the rate of corrosion is controlled by the rate of diffusion of oxygen to the surface of the metal from the surrounding environment. As the reaction sites are still at this stage fairly accessible the rate of diffusion is governed by the permeability of the soil adjacent to the pipe, the moisture content of the soil and the depth of burial.

In Phase 2 a build-up of rust products on the external surfaces and the increasing depth of the graphitised zone provide an additional obstruction to the inward diffusion of oxygen to the surface of the metal. As oxygen diffusion rates decrease so does the rate of corrosion.

In Phase 3, the rate of corrosion increases initially, but then gradually declines in time. The initial increase is attributed to a change in the corrosion process from one involving oxygen reduction (controlled by oxygen diffusion), to one involving hydrogen reduction (controlled by hydrogen diffusion) in anoxic (oxygen restricted) niches that form in crevices and pits as a result of non-uniform oxygen access. This behaviour has been described for steel, and may occur during the corrosion of cast iron. The mechanisms involved at the end of phase 2 and the start of phase 3 (surrounding the changeover) are currently under investigation however it is thought that the corrosion rate at this point is controlled by diffusion across a thin layer of magnetite (iron oxide rust product) at the surface of the metal.

By Phase 4, steady-state conditions (i.e., a steady rate of loss = constant rate of corrosion) are established. This phase is the most important for the prediction of the long-term corrosion rate of cast iron in soil. For buried pipes it is believed that Phase 4 may commence as late as 10-20 years after the pipe is installed. It has been suggested (Petersen and Melchers, 2012) that corrosion at this stage may be governed by the rate at which ferrous ions can diffuse out from the corroding surface.

Figure 17 shows a conceptual diagram of the phase 4 process. At this point the corroding surface has retreated into the cast iron component leaving behind a rust impregnated graphitised zone and an external layer of rust products that has built up on the external surface of the metal in contact with the external environment. On the corroding surface a crevice-type formation has developed due to non-uniform oxygen access to the corroding surface (developed during Phase 3).



Source: Adapted from Petersen and Melchers, 2012.

Figure 17. Conceptual view of the diffusion processes active during the corrosion of cast iron in a moist, neutral aerated soil (phase 4)

Environmental Factors Which May Impact on the Cast Iron Pipe Corrosion Rate

A number of environmental factors have been identified that are believed to impact on ferrous pipe corrosion rates. They include soil moisture, soil texture, soil resistivity, soil water chemistry and the ease at which oxygen can diffuse through the soil structure.

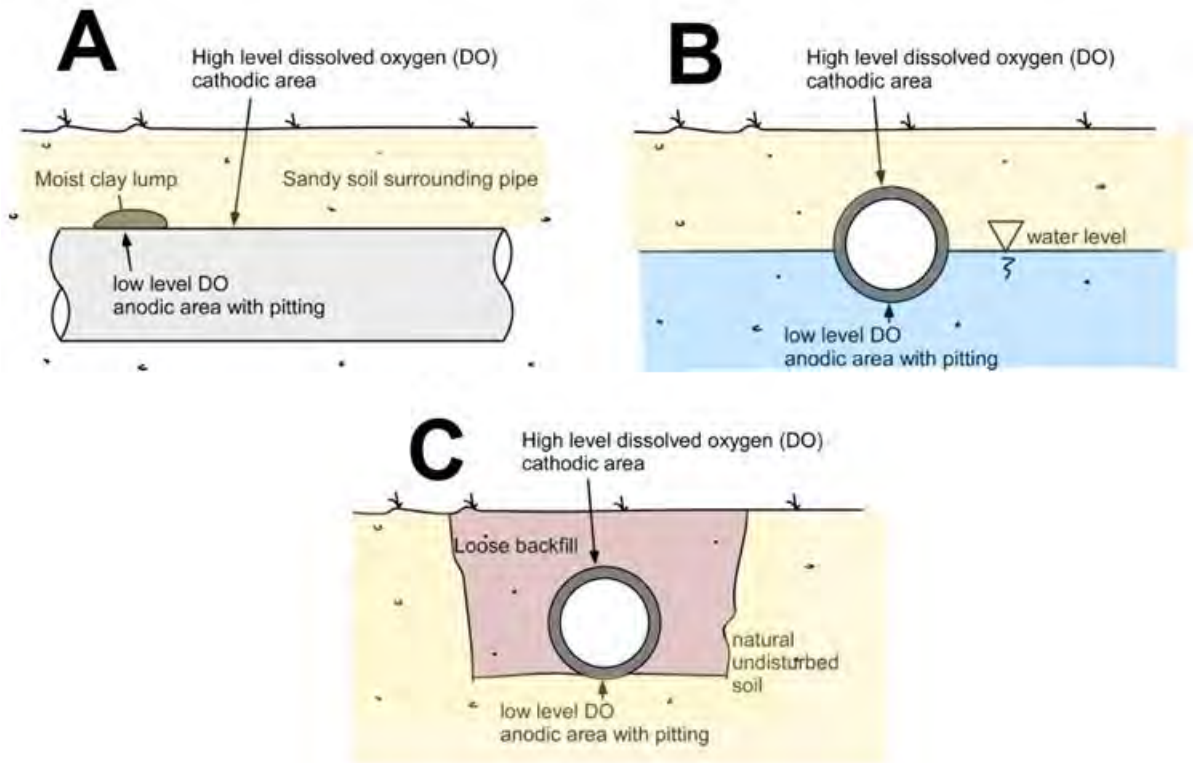
Water is the essential electrolyte required to support the electrochemical corrosion process (Roberge, 2008). The influence of soil moisture on the underground corrosion of mild steel has been examined by Gupta and Gupta (1979) who observed that the corrosivity of soils towards mild steel is low at small soil moisture levels but increases as the soil becomes wetter until a maximum is reached when the soil moisture is at ~65% of the soil's water holding capacity. Wetting the soil beyond this level reduces the corrosiveness of the soil. It is believed that the decrease in corrosion activity in very wet soils is a result of the slowdown in the transport of oxygen through the soil as the more of the pore structure is filled with water. Consequently, it is not the absolute soil moisture content that is important as much as the percent saturation and thus will be dependent on soil texture. As noted by Cole and Marney (2012) the moisture content at the point where the pipe is buried will also be influenced by the surrounding terrain, climatic parameters and the proximity of the water table.

Phil Ferguson in a personal communication observes in regards to soil moisture that from first principles there would be an optimum water/moisture content of the soil that would allow

sufficient oxygen diffusion but still allow effective conductivity of the electrolyte. Phil has observed with desert soils where bulk soil moisture content is very low (and hence air content is high) that a thin film of moisture (usually on the under-side of the pipe) is sufficient to raise the electrical conductivity of the soil to enable significant corrosion to take place. It might therefore be more important to consider moisture conditions adjacent to the pipe rather than the bulk soil moisture content.

Soil resistivity, a measure of how well the soil opposes the flow of electric current, has also been flagged as a corrosion driver. Doyle et al., (2003) for example reports that resistivity is the soil property that most closely related to the maximum external average pitting rate of water mains in the city of Toronto, Canada. However, a study on the influence of soil properties on the performance of underground pipelines conducted by Hay (1984) found only a poor correlation between soil resistivity and average pitting rate ($r^2=0.28$). Soil resistivity is influenced by a variety of factors including: solution ionic content, soil type, degree of compaction, temperature and importantly soil moisture levels (Doyle et al. 2003, Roberge 2008). Perhaps as a result of the interrelated nature of soil resistivity and moisture content Cole and Marney (2012) notes that there exists in the literature a good deal of ambiguity on whether correlations exist between soil resistivity and corrosion rate independent of variations in soil moisture.

Petersen and Melchers (2012) and Gupta and Gupta (1979) also report that differential aeration and/or soil oxygen transport issues can also have an important bearing on corrosion rates of buried ferrous pipes. Differential aeration creates an oxygen concentration cell, where the surfaces with access to the greatest amount of oxygen become cathodic and the surfaces with restricted oxygen access become anodic (with associated metal loss). As noted earlier the link between soil moisture and oxygen transport is important. Neale et al., (2000) showed that soil water content provides the greatest resistance to oxygen transport in the unsaturated zone with significant decreases in oxygen movement in a soil as the moisture content approaches saturation. In their review of pipeline corrosion Petersen and Melchers (2012) highlight three typical cases in which differential aeration of a pipe surface may arise (see Figure 18). Phil Ferguson in a series of personal communications has offered the following observations in regards to differential aeration cells. Firstly, that differential aeration (DA) cells where sand is depicted as the cathode would only apply for a small area of sand (at best) as dryness would prevent it being an effective cathode. Secondly that while rubble, rags, ropes etc. may be responsible for creating a more corrosive backfill by creating DA cells and/or holding moisture for long periods of time this has, in his experience, not been a major cause of pipe failures.



Source: Adapted from Petersen and Melchers 2012.

Figure 18. Three possible scenarios which induce differential aeration. A: Different soils in contact with the pipe. B: Installation of a pipe near the level of the water table. C: Laying a pipe in a ditch and surrounding it with loose backfill.

ASPECTS OF LPR USE IDENTIFIED FOR FURTHER INVESTIGATION

The purpose of this document to report on the existing knowledge of LPR theory and from this knowledge identify aspects of the LPR measurement process which may contribute to uncertainty in the LPR based prediction of buried cast iron pipe rates of corrosion. In the following work (*Activity 4b.2 Examination of the LPR approach in current practice*) data related to the areas identified here will be examined to see if an estimation of the level of uncertainty can be made.

The above discussion of the corrosion of cast iron pipe highlights the following aspects of the process which may be important in this regard:

- The bimodal nature of the trend in the occurrence of corrosion losses over time
- The relative importance of different rate limiting processes over the course of the life of the water pipe
- The impact of soil moisture on corrosion activity
- The impact of differential aeration on corrosion activity

The issues surrounding these aspects of the corrosion process will now be discussed.

The Bimodal Nature of the Trend in Corrosion Losses over Time

Within the Advanced Condition Assessment and Pipe Failure Prediction Project LPR technology will be used to estimate:

- (i) The current condition of the pipe – in effect an estimate of the cumulative corrosion of the pipe from time of installation up to the present day and
- (ii) The manner in which the pipe will deteriorate in the future – i.e., the future rate of corrosion of the buried pipe.

If a constant pipe corrosion rate is assumed over the life-time of the pipe the above two estimations (effectively past and future rates of corrosion) are equivalent however if the rate of corrosion changes over time this complicates the issue and will most likely increase the amount of uncertainty in the LPR based corrosion predictions. The exact extent of the uncertainty however will depend on the extent of the non-linearity in the corrosion behaviour of the pipe over time and what, if any, correlation exists between early rates of loss and rates of loss experienced later in the life of the pipe.

To this end any available field data showing losses over time for buried cast iron pipe (such as reported in Romanoff, 1957) will be examined. Other possible sources of data may include industry data from the projects industry partners (i.e., the water authorities and PCA Echologics). The effectiveness (or otherwise) of LPR based estimations of corrosion rates for older compared to newer pipes may also shed some light on this matter.

The Changes in the Corrosion Rate Limiting Processes over the Course of the Pipe's Life

As we have seen in the above discussion the LPR technique examines corrosion under conditions where the corrosion process is rate limited by electron transfer processes occurring at the metal surface. Based on the current understanding of the corrosion process this scenario is likely to be most relevant only during the very early stages of pipe corrosion process (i.e., phase 0, as discussed above in the Cast Iron Corrosion Trends over Time section). As the pipe corrodes over time other factors, revolving around mass transfer limitations, are likely to have a more significant impact on the rate at which losses occur.

The question that therefore presents itself is whether the LPR measurement can provide an indication of the rate of corrosion at later stages of the life of the pipe when the rate of electron transfer processes no longer dictates the overall rate of corrosion. This issue is not completely independent of the issue of linearity of rates over time discussed above (if for example the rate of corrosion does not vary appreciably over time or there is a significant correlation between early and corrosion rates experienced later in the life of the pipe then a technique that reliably estimates phase 0 corrosion rates will also reliably predict later rates of corrosion). Examination of the accuracy of LPR based corrosion prediction for different aged pipes should also shed some light on this issue.

The Impact of Soil Moisture on Corrosion Activity

As has been noted earlier soil moisture content is suspected of having a large impact on corrosion rates. Currently Activity 3 is examining this issue. LPR measurements conducted by

PCA Echologies are currently conducted on soil samples after their soil moisture has been set at the permanent wilt point (Ferguson and Nicholas, 1992). The question that naturally arises is if this procedure increases the level of uncertainty or not.

The answer to this to some extent will depend on whether the long-term average soil moisture level at the pipe depth is well represented by the wilt point moisture level. If it is as argued by Hay (1984) then fixing the soil sample moisture content to this level will improve the corrosion prediction and reduce the uncertainty that would arise if soils are on the off chance sampled during abnormal soil moisture conditions. If, however this is not the case then fixing the soil moisture at the permanent wilt point level may add to the model uncertainty.

The Impact of Differential Aeration on Corrosion Activity

The impact of differential aeration is by its nature a difficult phenomenon to quantify or predict particularly if it arises from irregular contact between the pipe surface and the surrounding soil (for example arising from a stray lump of clay against the pipe in an otherwise sandy backfill). Most likely the best approach in evaluating the possible impact of differential aeration on the uncertainty in model prediction is to look at how increased soil sampling frequency can influence the prediction confidence intervals.

Consequently, corrosion rate predictions made with multiple samplings at different spatial scales will be examined (if available) to determine the effect of spatial sampling scale on corrosion prediction uncertainty.

SUMMARY

This report details the current knowledge of the theoretical basis of Linear Polarisation Resistance (LPR) and is the first output from activity 4b (Reducing the uncertainty in the use of non-destructive, indirect measurement with LPR) which in turn is part of the Advanced Condition Assessment and Pipe Failure Prediction Project. The aim of studying the theoretical underpinnings of the LPR process is to:

- Build up a conceptual understanding of the LPR process and
- Identify possible features of the LPR process that may impact on the uncertainty of cast iron corrosion rates predicted by this method. The identified areas will be investigated in the next stage of Activity 4b.

To this end the theory of ferrous corrosion is set out in detail with special relevance to buried cast iron pipe corrosion. The theory is developed from the basic chemical reactions taking place to the thermodynamic and kinetic equations which form the basis of the LPR assessment of soil corrosivity. The environmental factors affecting the rate of corrosion and how corrosion of cast iron pipes evolves over time is then discussed.

The following possible sources of uncertainty have been identified and will be the subject of further investigation:

- (1) The non-linearity in cast iron corrosion rate trends over time
- (2) The changing rate limiting processes that occur over time
- (3) Soil moisture levels

(4) Differential aeration

A database of relevant literature is also attached.

REFERENCES

- Cole, I.S., Marney, D., 2012. The science of pipe corrosion: A review of the literature on the corrosion of ferrous metals in soils. *Corrosion Science* 56(0), 5-16.
- Doyle, G., Seica, M.V., Grabinsky, M.W.F., 2003. The role of soil in the external corrosion of cast iron water mains in Toronto, Canada. *Canadian Geotechnical Journal* 40(2), 225-236.
- Ferguson, P.H., Nicholas, D.M.F., 1992. External corrosion of buried iron and steel water mains. *Corrosion Australasia* 17(4), 7-10.
- Gupta, S.K., Gupta, B.K., 1979. The critical soil moisture content in the underground corrosion of mild steel. *Corrosion Science* 19(3), 171-178.
- Hay, L., 1984. The Influence of soil properties on the performance of underground pipelines., The University of Sydney.
- Melchers, R.E., 2014. Microbiological and abiotic processes in modelling longer-term marine corrosion of steel. *Bioelectrochemistry* 97(0), 89-96.
- Melchers, R.E., Wells, T., 2006. Models for the anaerobic phases of marine immersion corrosion. *Corrosion Science* 48, 1791-1811.
- Neale, C.N., Hughes, J.B., Ward, C.H., 2000. Impacts of unsaturated zone properties on oxygen transport and aquifer reaeration. *Ground Water* 38(5), 784-794.
- Petersen, R.B., Melchers, R.E., 2012. Long-term corrosion of cast iron cement lined pipes, *Corrosion and Prevention* 2012, 11-14 Nov 2012, Melbourne, Australia
- Roberge, P., 2008. *Corrosion Engineering : Principles and Practice: Principles and Practice*. Mcgraw-Hill (publishers). New York.
- Romanoff, M., 1957. *Underground Corrosion*. National Bureau of Standards Circular 579.

SUGGESTED READING LIST

For Basic Electrochemistry and Corrosion Theory

1. Z. Ahmad, *Principles of Corrosion Engineering and Corrosion Control*, Butterworth-Heinemann, Jordan Hill, GBR, 2006. ISBN 0080480330, 9780080480336.
2. V. Chaker, J.D. Palmer, *Effects of Soil Characteristics on Corrosion*, ASTM, 1989. ISBN 0-8031-1189-4
3. M.G. Fontana, *Corrosion Engineering*, Tata McGraw-Hill, 2005. ISBN 0070607443, 9780070607446.
4. N. Perez, *Electrochemistry and Corrosion Science*, Kluwer Academic Publishers, Hingham, MA, USA, 2004. ISBN 1402077440, 9781402077449.
5. E.E. Stanbury, R.A. Buchanan, *Fundamentals of Electrochemical Corrosion*, ASM International, Materials Park, OH, USA, 2000. ISBN 1615030670.
6. N.D. Tomashov, *Theory of Corrosion and Protection of Metals: The Science of Corrosion*, Macmillan, 1966.

7. P. Zanello, *Inorganic Electrochemistry: Theory, Practice and Applications*, Royal Society of Chemistry, 2003. ISBN 0854046615, 9780854046614.

LPR Related Literature

1. G.E. Badea, A. Caraban, M. Sebesan, S. Dzitac, P. Cret, A. Setel, Polarisation measurements used for corrosion rates determination, *Journal of Sustainable Energy*, 1 (2101).
2. K. Farrag, Evaluation of External Corrosion-Rate Using Polarization Resistance and Soil Properties. Final report, gas Technology Institute DOT project No: 256, 2010.
3. P.H. Ferguson, Condition assessment of pressure water mains - is it worth doing? Abstract ID 60., in: *ASCE Pipelines Conference 2010, Keystone, Colorado August 28-September 1, 2010*, 2010.
4. P.H. Ferguson, Smoke and mirrors. Which condition assessment techniques work, in: *North American Society for Trenchless technology (NASTT) No-dig Show, Chicago, Illinois May 2-7, 2010*.
5. P.H. Ferguson, D.M.F. Nicholas, External corrosion of buried iron and steel water mains, *Corrosion Australasia*, 17 (1992) 7-10.
6. G. Kear, I. Flatley, S. Jones, Application of polarisation resistance measurements for the estimation of corrosion rates of galvanised steel structures in soils, in: *Corrosion and Protection 06 Conference, Grand Chancellor Hotel, Hobart Australia, 19–22 November 2006 Paper No 127*, 2006.
7. L. Hay, The Influence of soil properties on the performance of underground pipelines., *Masters Degree in Agricultural Science Thesis, Department of soil science, The Faculty of Agriculture, The University of Sydney*, 1984.
8. E. Kalantzis, Prediction of soil corrosivity using linear polarization, in: *Master of Engineering Thesis, Department of Civil Engineering and applied Mechanics, McGill University, Montreal*, 1997.
9. M. Norin, T.G. Vinka, Corrosion of carbon steel in filling material in an urban environment, *Materials and Corrosion*, 54 (2003) 641-651.
10. P.V. Nygaard, M.R. Geiker, Measuring the corrosion rate of steel in concrete – effect of measurement technique, polarisation time and current, *Materials and Corrosion*, 63 (2012) 200-214.

Cast Iron Pipe Corrosion and More General Corrosion Literature of Relevance

1. M. Ahammed, R. Melchers, Reliability of Underground Pipelines Subject to Corrosion, *Journal of Transportation Engineering*, 120 (1994) 989-1002.
2. Baracos, W.D. Hurst, R.F. Legget, Effects of Physical Environment on Cast-Iron Pipe, *Journal (American Water Works Association)*, 47 (1955) 1195-1206.
3. F.E. Brooks, A.G. Fuller, D.L. Crews, Corrosion Behavior of Ductile Cast-Iron Pipe in Soil Environments, *Journal (American Water Works Association)*, 69 (1977) 110-114.
4. I.S. Cole, D. Marney, The science of pipe corrosion: A review of the literature on the corrosion of ferrous metals in soils, *Corrosion Science*, 56 (2012) 5-16.

5. M. Dafter, Long term corrosion of buried water mains compared with short term electrochemical testing, in: Corrosion and Prevention 2013, 10-13 Nov 2013, Brisbane, Australia 2013.
6. M. Dafter, Electrochemical testing of soils for long-term prediction of corrosion of ferrous pipes. Ph.D. Thesis, Department of Civil Engineering, University of Newcastle, 2014.
7. G. Doyle, M.V. Seica, M.W.F. Grabinsky, The role of soil in the external corrosion of cast iron water mains in Toronto, Canada, Canadian Geotechnical Journal, 40 (2003) 225-236.
8. G. Doyle, The role of soil in the external corrosion of cast-iron water mains in Toronto, Canada. Master of Applied Science, Graduate Department of Civil Engineering, University of Toronto, Canada, 2000.
9. S. Duchesne, N. Chahid, N. Bouzida, B. Toumbou, Probabilistic modeling of cast iron water distribution pipe corrosion, Journal of Water Supply: Research & Technology-AQUA, 62 (2013) 279-287.
10. W.F. Gerhold, Corrosion Behavior of Ductile Cast-Iron Pipe in Soil Environments, Journal (American Water Works Association), 68 (1976) 674-678.
11. H.L. Hamilton, Effects of Soil Corrosion on Cast-Iron Pipe, Journal (American Water Works Association), 52 (1960) 638-650.
12. M. Heathcote, D. Nicholas, Life assessment of large cast iron water mains. UWRAA report no. 146, 1998.
13. B.B. Hodgman, Cast Iron Pipe 260 Years Old in France, Journal (American Water Works Association), 23 (1931) 673-677.
14. Y. Katano, K. Miyata, H. Shimizu, T. Isogai, Predictive Model for Pit Growth on Underground Pipes, Corrosion, 59 (2003) 155-161.
15. K.H. Logan, Exterior Corrosion of Cast Iron Pipe, Sewage Works Journal, 20 (1948) 133-137.
16. R.E. Melchers, Microbiological and abiotic processes in modelling longer-term marine corrosion of steel, Bioelectrochemistry, 97 (2014) 89-96.
17. R.E. Melchers, T. Wells, Models for the anaerobic phases of marine immersion corrosion., Corrosion Science, 48 (2006) 1791-1811.
18. H. Mohebbi, C.Q. Li, Experimental Investigation on Corrosion of Cast Iron Pipes, International Journal of Corrosion, (2011) 1-17.
19. H. Najjaran, R. Sadiq, B. Rajani, Fuzzy Expert System to Assess Corrosion of Cast/Ductile Iron Pipes from Backfill Properties, Computer-Aided Civil and Infrastructure Engineering, 21 (2006) 67-77.
20. R.B. Petersen, R.E. Melchers, Long-term corrosion of cast iron cement lined pipes, in: Corrosion and Prevention 2012, 11-14 Nov 2012, Melbourne, Australia 2012.
21. R.B. Petersen, R.E. Melchers, Modelling the long-term corrosion of cast iron pipes, in: Corrosion and Prevention 2013, 10-13 Nov 2013, Brisbane, Australia 2013.
22. B. Rajani, Y. Kleiner, External and Internal Corrosion of Large-Diameter Cast Iron Mains, Journal of Infrastructure Systems, 19 (2013) 486-495.
23. R.E. Ricker, Analysis of Pipeline Steel Corrosion Data from NBS (NIST) Studies Conducted Between 1922-1940 and Relevance to Pipeline Management, Journal of Research of the National Institute of Standards and Technology, 115 (2010) 373-392.
24. M. Romanoff, Exterior Corrosion of Cast-Iron Pipe, Journal American Water Works Association, 56 (1964) 1129-1143.

25. M. Sancy, Y. Goubeyre, E.M.M. Sutter, B. Tribollet, Mechanism of corrosion of cast iron covered by aged corrosion products: Application of electrochemical impedance spectrometry, *Corrosion Science*, 52 (2010) 1222-1227.
26. M. Seica, J. Packer, Mechanical Properties and Strength of Aged Cast Iron Water Pipes, *Journal of Materials in Civil Engineering*, 16 (2004) 69-77.
27. M.V. Seica, J.A. Packer, M.W. Grabinsky, B.J. Adams, Evaluation of the properties of Toronto iron water mains and surrounding soil, *Canadian Journal of Civil Engineering*, 29 (2002) 222-237.
28. W.H. Smith, Soil Evaluation in Relation to Cast-Iron Pipe, *Journal (American Water Works Association)*, 60 (1968) 221-227.
29. W.H. Smith, J.H. F, Corrosion and Cast-Iron Main Breaks [with Reply], *Journal (American Water Works Association)*, 61 (1969) 617-618.
30. E.L. Thurston, R.V. Skold, Current Research on Corrosion and Tuberculation of Cast Iron, *Journal (American Water Works Association)*, 50 (1958) 1429-1432.

11.5.4 Activity 4b: Report on the Relationship between the Theoretical Basis and Practical Application of Linear Polarisation Resistance Technology

**REPORT ON THE RELATIONSHIP BETWEEN THE THEORETICAL
BASIS AND PRACTICAL APPLICATION OF LINEAR POLARISATION
RESISTANCE TECHNOLOGY**

Prepared by:
Tony Wells
University of Newcastle

SUMMARY

The purpose of this report is to examine the practical application of the linear polarisation resistance (LPR) technique to the prediction of corrosion rates of buried cast iron pipes and, in conjunction with the theoretical analysis carried out previously, identify features of the LPR process that impact on prediction uncertainties. In doing so the aim is to define additional factors that can be incorporated into the corrosion prediction algorithm that can improve prediction accuracy. It is not the intention of this report to suggest modifications to the methodology by which the LPR result is obtained. Instead, the focus of this exercise is how best to predict the rate of cast iron pipe corrosion once the LPR test has been carried out and the R_p value obtained, (i.e., ultimately, we are concerned with the model relating corrosion rate to the R_p value and less about the process by which the R_p value was obtained). Once areas of uncertainty have been identified, a list of possible factors to be included in the model will be drawn up. Additional data will then be sought and tested to see if inclusion of that data improves the LPR based corrosion rate prediction model.

An examination of the LPR process suggests that corrosion rates predicted from LPR measurements may benefit from the inclusion of the following additional factors:

1. The method of pipe manufacture: An analysis carried out by Dafter (2014a, 2014c) indicates that the relationship between LPR R_p value and the max pit depth may be different for pipes manufactured by different techniques (for example vertically or horizontally cast). Dafter (2014c) speculated that this may be, (at least in part), due to differences in the original bitumen coating applied to the pipes however there is no direct evidence to support this. By considering a separate calibration equation for each pipe class it may be possible to improve the accuracy of the corrosion prediction.
2. The age of the pipe: The available data indicates that cast iron pitting rates decrease over time. This decrease may be due to the changing nature of the corrosion process itself – moving from corrosion limited by the kinetics of the corrosion reaction to a system where mass transport limitations are the rate limiting step. The LPR test is fundamentally an examination of corrosion processes that are dominant at the beginning of the corrosion process and consequently there is a possibility that LPR results may need some adjustment to account for the slow-down in pitting rates over time. It is important to note however that there may not be a clear distinction between the effects of pipe age, pipe manufacturing method and other factors that impact on the corrosion process which have changed over time (for example the methods used to bury the pipe). To improve the model predictions the strategy should ideally be to account for both the age of pipe and the means of manufacture in the formulation of an improved predictive model. However, the limitations in the data currently available may mean that a single combined correction factor to account for both the effect of pipe age and manufacturing method may be the used in the improved predictive model.
3. Soil moisture level: Soil moisture (or more accurately the level of saturation) is an important factor in determining rates of cast iron pipe corrosion however LPR tests are always conducted at the wilt point soil moisture level regardless of the soil moisture conditions at the pipe site. Analysis of soil moisture data suggests that in many cases the wilt point may not be representative of the average long-term soil moisture content of the soil in many cases and hence running the test at the wilt point may lead to

- inaccuracies in the level of corrosion predicted. The inclusion of a long-term average soil moisture correction factor in the $R_p \rightarrow$ Corrosion rate algorithm is recommended.
4. Backfill type and quality: The use of the LPR test to predict corrosion rates works best when the pipe is buried in native soils. A non-uniform soil environment (due to for example the presence of lumps of clay/rocky material or native soil intrusion into imported sandy fill) has the potential to produce extremely localised corrosion phenomena. In such cases any corrosion prediction made from an analysis of the properties of a limited number of soil samples (including LPR testing) may not be correct. Because of the likely random nature of this problem it will be the most difficult to address in a quantitative sense. Possible strategies for addressing this issue include the use of more intense sampling or the inclusion of an additional risk factor for areas in which this type of backfill is known to be in place. The sampling strategy approach will be investigated as a part of Activity 4c while the risk factor approach is recommended for Activity 4b.3 which is focused on the improvement of the $R_p \rightarrow$ Corrosion model.

INTRODUCTION

This document reports the findings of activity 4b.2, namely the review of the practical application of the Linear Polarisation Resistance (LPR) technique in the estimation of the corrosivity of soils. For a more general introduction to the overall water pipes corrosion project and Activity 4 in particular readers are directed to the earlier report prepared for activity 4b.1 (Wells, 2014) and the water pipes corrosion website (<http://www.criticalpipes.com/>).

In using the LPR test to estimate the rate of corrosion being experienced by a buried cast iron pipe it is important to make the distinction between the LPR test method (i.e., the field + lab procedure which generates the R_p value for the soil) and the subsequent algorithm which converts the R_p value to a corrosion rate. It is important to note that it is not the intention of this report to suggest modifications to the LPR test method. This would be impractical as (1) different companies employ different methodologies and (2) the ability to test the veracity of any new methodology suggested is extremely limited in the time frame set aside for this task. In any case studies such as that recently conducted by Dafer (2014c) conclude that the testing methodology is basically sound. Rather the focus of this exercise is how best to estimate the corrosion rate once the R_p value is known (i.e., we are concerned with the model rather than the method). Changes to the $R_p \rightarrow$ Corrosion rate algorithm can be more easily verified by looking at historical data (provided all additional factors are known) and can thereby can be more easily validated in the time frame assigned to this activity.

In order to identify possible areas in which modifications to the $R_p \rightarrow$ Corrosion rate model can be made it is necessary to examine the theoretical (Activity 4b.1) and practical aspects (Activity 4b.2) of the LPR process to identify current areas of uncertainty and what (if any) additional factors might be included in the prediction model to improve its accuracy. Once areas of uncertainty have been identified, a list of possible factors to be included in the new $R_p \rightarrow$ Corrosion rate model will be drawn up, and additional data (historical where possible and new field data – also where possible) will be gathered. If sufficient data can be assembled personnel at UTS will conduct a machine learning analysis of the data (activity 4b.3) to determine if inclusion of the additional factors improves the accuracy of corrosion rate prediction.

The report into the theoretical background to the LPR process (Wells, 2014) identified the following possible areas of uncertainty in the use of LPR to predict the rate of corrosion of buried cast iron pipes:

1. Variations in corrosion behavior brought about by non-uniformity in the soil surrounding the pipe
2. Variations in corrosion behavior brought about by differing levels of soil moisture level
3. Changes in cast iron pipe corrosion trends over time (including non-linearity of corrosion behavior and changes in rate controlling mechanisms)

This report will examine the practical application of the LPR process in light of these issues. Other practical issues in regards to the application of LPR (for example electrochemical cell design, electrode materials etc.) while important are considered to be outside the scope of this document as the primary aim here is to work with the currently practiced LPR methodology and reduce levels of corrosion prediction uncertainty through the application of an improved corrosion prediction model. For a detailed discussion of the LPR testing methodology readers are directed to Dafter (2014b).

The following report is structured in the following manner. Firstly, a brief description of the LPR current practice is given. Then the practical issues relating to age of the pipe, manner of pipe manufacture, impacts of soil moisture and non-uniformity of the soil environment surrounding the pipe are presented. Finally, a summary of the recommendations for model improvement are presented.

BRIEF DESCRIPTION OF THE LPR ANALYSIS PROCESS

A schematic representation of the LPR test method as practised at PCA Echologics is shown in Figure 1. Once a site for investigation has been identified soil samples are taken (generally by hand auger) in an area adjacent to the buried pipe. Ideally the point of sampling is approximately 300-600 mm from the pipe and at mid-pipe depth. Sometimes however sampling close to the pipe is not possible (due for example to access or safety issues). In such cases samples can be taken as far as 1.5m from the pipe. Soil samples of approximately 400 g mass are used in the following testing.

Once the soil sample is returned to the laboratory they are dried at 50°C to constant weight (generally overnight) before being crushed to enable the gravel fraction (>2mm) to be removed by sieving. A small subsample of the soil mass is then wetted with a small amount of water and allowed to equilibrate for 12 to 24 hours before being placed in a membrane unit which delivers a suction pressure of 15 bar. This suction is held overnight allowing the soil is dried to what is known as the wilt point (WP, the meaning of which will be explained shortly). The wilt point soil moisture content of the soil sample is then determined gravimetrically by heating the sample and recording the drop in mass after all remaining moisture has been removed. In preparation for the LPR test the remaining soil is then wetted to the wilt point by addition of the appropriate mass of water (i.e., as determined from the above discussed wilt point test).

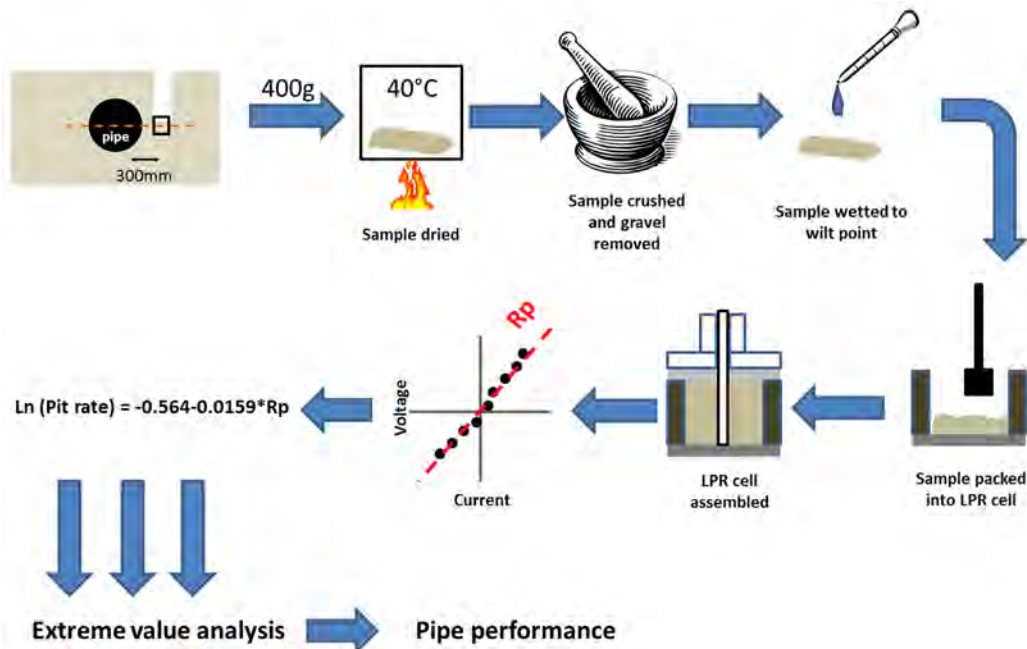


Figure 1. Schematic of the soil sampling and analysis procedure employed by PCA Echologics

The moistened soil is then packed into the LPR cell. A small amount of soil is first added to the open LPR cell and gently tamped down with a few taps of a metal bar before a new layer of soil is added and the tamping repeated. When the soil level is just below the mid-point of the cell the reference electrode is inserted. The reference electrode is positioned so that the end of the electrode finishes flush with the face of the working electrode. The reference electrode used is a standard calomel electrode, while the working electrode is constructed from mild steel and the counter electrode from 316 stainless steel. Once the reference electrode is inserted the remainder of the soil is tapped into the remaining cell volume before the cell is sealed off and the electrodes are connected to the power supply and monitoring equipment.

Once the cell is filled and connected the LPR testing can commence. First the open circuit voltage (E_{corr}) is determined over a 5-10 minute period (to allow system to stabilise). To minimise the effect of IR drop through the cell the potential between the reference electrode and the working electrode is measured. After the open circuit voltage for the cell is determined the current through the cell is manipulated in such a way as to produce a voltage range of $E_{\text{corr}} \pm 10$ mV. In this potential range the voltage-current relationship is normally close to linear (Figure 2).

Not accounting for the iR drop can lead to a significant level of error ($\gg 100\%$, Phil Ferguson, personal communication). Only techniques such as that employed by PCA Echologics and Matt Dafter (for example see Dafter, 2014c) which explicitly account for the iR drop are suitable for assessing corrosion of buried pipelines.

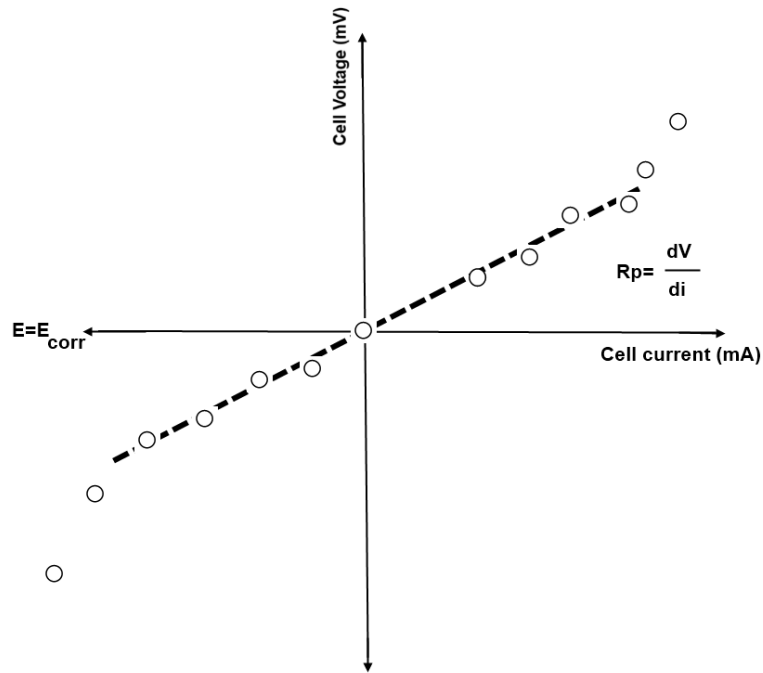


Figure 2. The relationship between current and voltage near the open circuit voltage

A line of best fit (with zero intercept) is then passed through the data (as per the dashed line in Figure 2) and the slope of the line determined. This slope is known as the linear polarised resistance value, R_p . A number of relationships between corrosion rates and the linear polarised resistance value have been reported in the literature however the expression of most interest in this study is that put forward by Ferguson and Nicholas (1992) which is employed by PCA Echologics to relate corrosion rate to the R_p value:

$$\ln(\text{Corrosion Rate}) = -0.564 - 0.0159R_p \quad (1)$$

where CR is the rate of corrosion expressed as the maximum rate of pitting (mm/yr) and R_p is the linear polarised resistance value expressed as Ohms/10sqcm.

R_p values are determined for 3 subsamples of the total soil sample retrieved from each site. If the coefficient of variance (COV) of R_p is less than 10% the average of the three values is used as the representative value of R_p to be used in Eqn. (1). If the COV is >10% the LPR tests are repeated until the overall COV < 10%. Eqn. (1) is then used to determine the maximum rate of pitting per pipe length (either a 3.6m or 5.5m length). This exercise is then repeated along the pipe over the length of interest to generate a set of maximum pitting rates along the pipe. Extreme value statistics are then applied to the maximum pitting rate data to eventually predict pipe performance.

Between each test the cells are cleaned before being refilled with fresh soil. The faces of the working (and to a lesser extent) the counter electrodes are inspected between runs and are polished to maintain a flat surface devoid of corrosion product. Each run takes between approximately 25 to 45 minutes to complete.

PRACTICAL ISSUES THAT MAY AFFECT IMPACT ON THE LPR PREDICTION OF RATES OF BURIED PIPE CORROSION

Some General Notes

As noted by Farrag (2010) and later Dafter (2104a, 2014b) there are a number of scenarios in which the determination of corrosion rates via LPR analysis of soils may be less than ideal. Amongst the scenarios listed by Farrag are:

1. When there is a significant change in the nature of the soil environment surrounding the pipe (for example changing of fill when additional pipes are installed or when a spillage of corrosive materials into the soil occur) and
2. When corrosion is caused by stray direct current (DC) or alternating current (AC). However, this effect is likely to be limited in the case where cast iron pipe sections are separated by rubber ring joints.

Dafter (2014c) notes in his study of the LPR technique that maximum pit depth was found to have no correlation with short-term electrochemical tests in the following scenarios:

1. If the pipe is partially submerged under the water table
2. If pipe is buried in sandy backfill/sandy soils (however it is noted that the rate of corrosion is likely to be quite low in these cases (<0.05mm/yr))
3. If pipe is buried in poor quality bedding (i.e., a mixture of sandy and native soils in contact with the pipe)

It is also recognised at PCA Echologics that LPR cannot account for extrinsic factors that may have a bearing on buried pipe corrosion, in particular the impact of property service connections on corrosion rates. Phil Ferguson in a personal communication also notes that LPR is not suitable to assess/estimate corrosion of loose polyethylene sleeved ductile iron pipe as the corrosion mechanism that operates in these circumstances is not purely "soil" corrosion.

While there are some limitations to the application of the LPR technique it has been shown that as long as its limitations are recognised LPR provides a low cost, easily applied, quantifiable technique for estimating the rate of corrosion of buried cast iron pipes. And as such it shows great potential for mapping out the corrosivity of selected sites previously identified by other strategies (for example prioritisation work carried out by NICTA).

There are some aspects to the current practice of LPR based corrosion prediction however which may contribute to a level of uncertainty in the prediction of corrosion which are now be discussed from the point of view of the practical application of the LPR technique. As mentioned previously the aim here is to identify additional data that, upon its inclusion in the modelling process, will produce a better prediction of corrosion behaviour. Phil Ferguson (pers. communication) notes however that the LPR prediction algorithm is based on the analysis of corrosion occurring under a wide range of conditions and hence some (or all) of these factors may already be accounted for.

Issues Relating the Age of the Pipe

Slowing Down of Pitting Rates over Time

As was noted in the previous report on the theoretical basis of LPR (Wells, 2014) the pitting rate for cast iron is not constant over time. Rather theoretical analysis (for example see Rossum, 1969) and empirical evidence from extended field trails (although variable see Romanoff, 1957) suggests that maximum pit depth growth slows over time (e.g., Figure 3). Also, as noted by Hay (Hay, 1984), “it has commonly been observed that corrosion of buried metals is initially rapid but soon slows down to a more constant rate”.

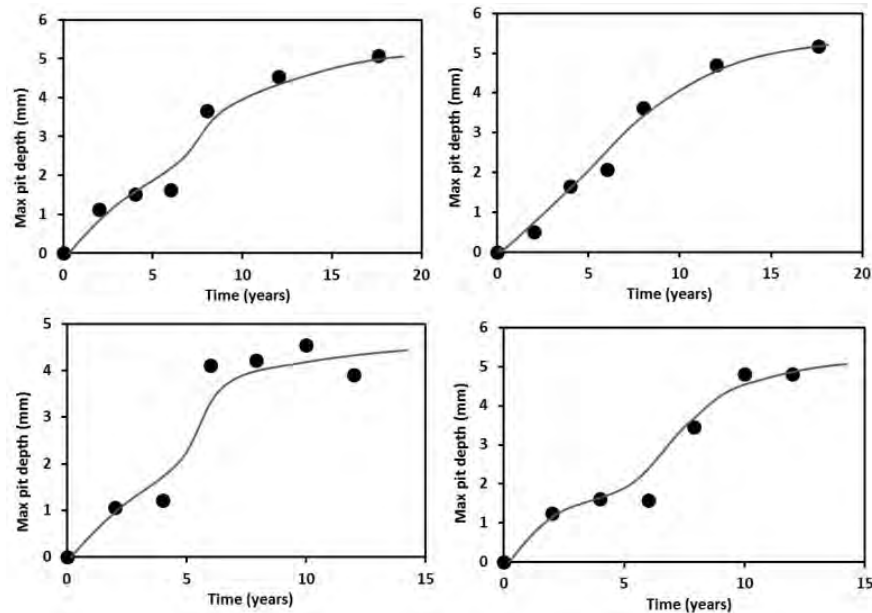


Figure 3. Examples suggesting that pitting rates slow over time (data obtained from Romanoff, 1957). Maximum pit depth as a function of time for cast iron samples buried in Clay (top graphs) and sandy loam (bottom graphs)

The non-linearity of the corrosion process comes about because there are a number of different factors/activities which act as rate limiting steps in the corrosion process and hence ultimately dictate the pace at which the overall corrosion process takes place (Figure 4). As different processes become more important the overall corrosion kinetics change. For example based on our current understanding of the corrosion of cast iron pipes (Petersen and Melchers, 2012; Petersen and Melchers, 2013; Melchers, 2014, see Figure 5) electron transfer and reaction kinetics are likely to be most relevant to the overall rate of corrosion during the early stages of pipe’s life (i.e., phase 0 in Figure 5) however over time other processes, likely involving mass transfer limitations, are expected to have a more significant impact on the rate at which losses occur.

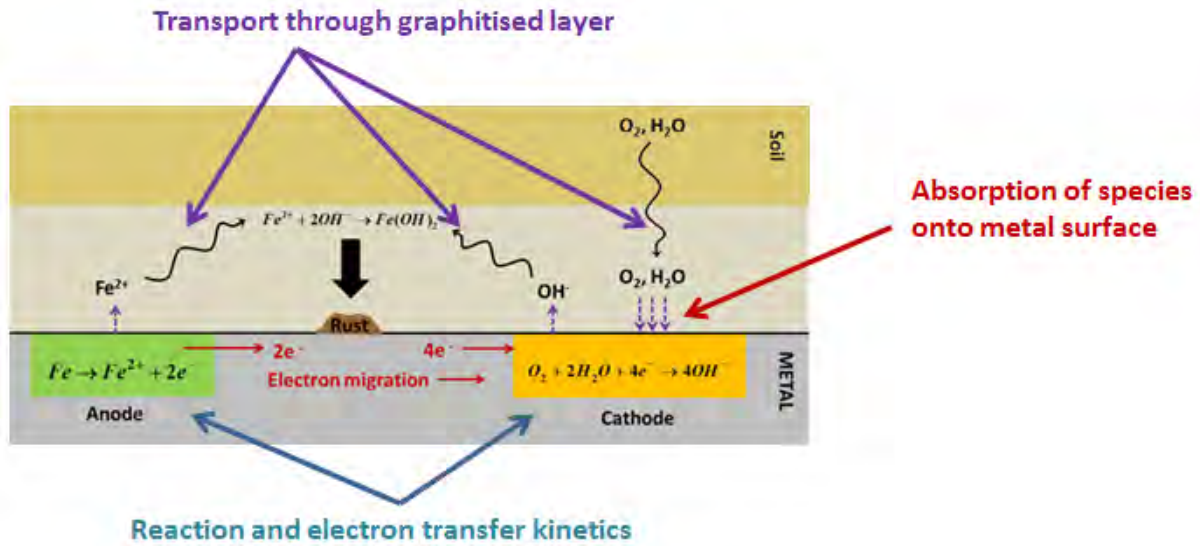
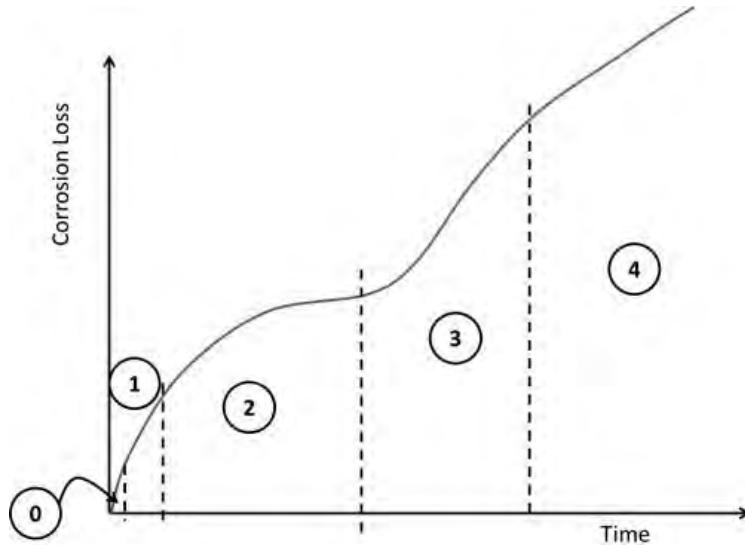


Figure 4. The possible rate limiting processes which dictate the corrosion of buried cast iron pipe

As discussed previously in the theoretical study of the LPR process (Wells, 2014) the LPR technique involves the manipulation of the electron transfer processes on, and immediately surrounding, the metal electrode surface. In a more practical sense LPR testing is always carried out on pristine, polished metal surfaces characteristic of a newly laid pipe. The LPR test therefore most accurately reflects corrosion processes that dominate early on in life of the buried cast iron pipe when the rate of electron transfer is the activity that controls the overall corrosion process (i.e., phase 0, Figure 5). The LPR test most likely therefore does not fully encompass all of the factors (especially mass transport limitations) which control the corrosion rate later in the pipe's life and consequently there is a potential for uncertainties in the rate of corrosion predicted for older pipes to be higher as the short term electrochemical test becomes less representative of processes controlling rates of corrosion in those older pipes.

When constructing the equation relating the LPR R_p value with the pitting rate (Eqn. (1)) the pitting rate often is calculated from a one off inspection of the pipe in question following which the pitting rate is determined by dividing the maximum pit depth by the age of the pipe. For example, if the maximum pit depth is 20 mm and the pipe is 100 years old the pitting rate is deemed to be $20/100 = 0.2$ mm/yr. It is important to note that this is the average pitting rate over the last 100 years and may not represent the current (or future) rate of pitting. If for example the maximum pit depth is growing with time as illustrated in Figure 6 it is clear that the current rate of corrosion as represented by the slope of the tangent to the corrosion loss curve (dashed green line) is considerably less than the average rate of corrosion calculated from the one-off inspection of the pipe (represented by the slope of the blue dashed line). It is also clear that future rates of corrosion (slope of the purple line) are also likely to be lower still.



Source: Adapted from Petersen and Melchers 2012 and Melchers 2014.

Figure 5. A generalised conceptual representation of the time dependent behaviour of the corrosion process). [Phase 0 dominated by electron transfer and reaction kinetics, Phases 1-4 dominated by mass transfer limitations]

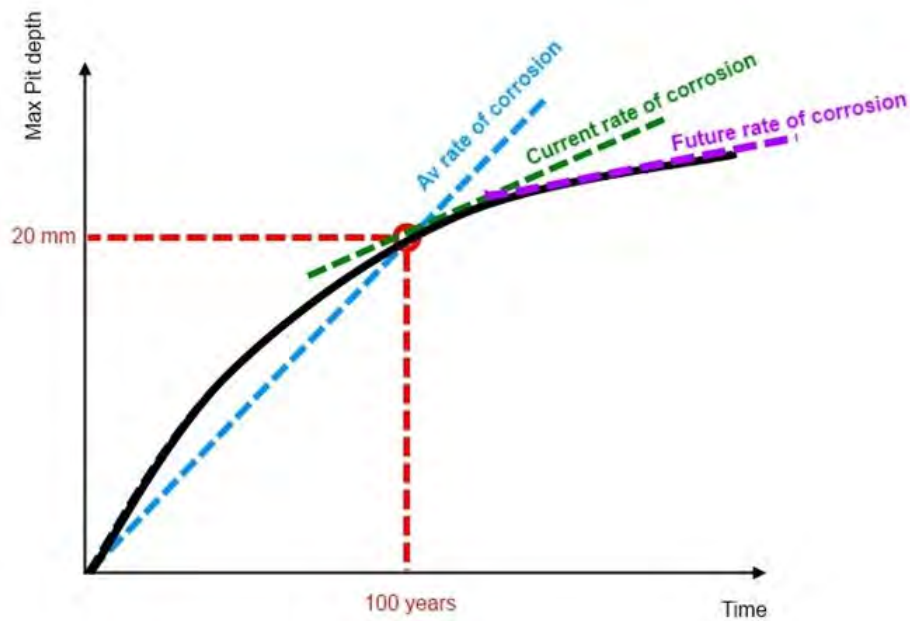


Figure 6. Relationship between average past rates of corrosion (blue), current rate of corrosion (green) and future rates (purple) when rate is not linear over time

The result is that while Eqn. (1) may be a good predictor of the max pit depth of a pipe and hence the average past rate of corrosion some modification is likely to be necessary if the technique

is to be used to predict the current or future rates of corrosion (for instance if the current pipe condition is known and an estimate of the remaining life of the pipe is needed). As it stands it is possible that Eqn. (1) may over predict the future rate of corrosion and consequently return a lower than realistic estimate of the remaining life of the pipe.

The extent to which the rate of corrosion slows down is difficult to determine as data showing the progression of cast iron corrosion over time is limited with the main source of data (Romanoff, 1957) showing a considerable degree of variability in the loss data presented. Nevertheless, by examining the entire body of cast iron corrosion data presented in this study it is possible to get an indication of the relationship between the initial rate of corrosion (experienced by coupons during the first year of burial) and corrosion rates later in the life of the pipe (between 8 and 12 to 17 years exposure, (the end of the study)).

Here the initial rate of corrosion, CR_{init} (mm/yr), is simply defined as:

$$CR_{init} \approx \frac{loss(t_1)}{t_1} \quad (2)$$

where $loss(t_1)$, (mm), is the maximum penetration of corrosion observed at the first retrieval of samples (t_1 = approximately 1 year after burial).

And the rate of corrosion experienced by the pipe later on in its life when corrosion is well established, CR_{mature} (mm/yr), is defined as follows:

$$CR_{mature} = \frac{1}{n} \times \sum_{j=1}^n CR(t_j) \text{ for } 8 \leq t_j \leq 17 \text{ years} \quad (3)$$

Put simply the value of CR_{mature} is the average rate of corrosion calculated for all coupons at the site buried for between 8 to 17 years.

Graphs of initial pitting rates versus the average 8-17 year average pitting rates are shown in Figures 7, 8, 9, and 10. Given the variability in the data presented by Romanoff it was expected that there would be a considerable variability in the rates of corrosion predicted from the loss data and this proved to be the case. In particular some of the average 8-17 year corrosion rates calculated were less than zero (i.e., pit depths in older coupons were smaller than younger coupons). As discussed in Ricker (2010) this level of variability is most likely due to the inherent variability of the corrosion process (an effect not helped by the small coupon sizes and small number of samples retrieved) as well as variability in the local site conditions (e.g., soil chemistry/ texture variability at each site).

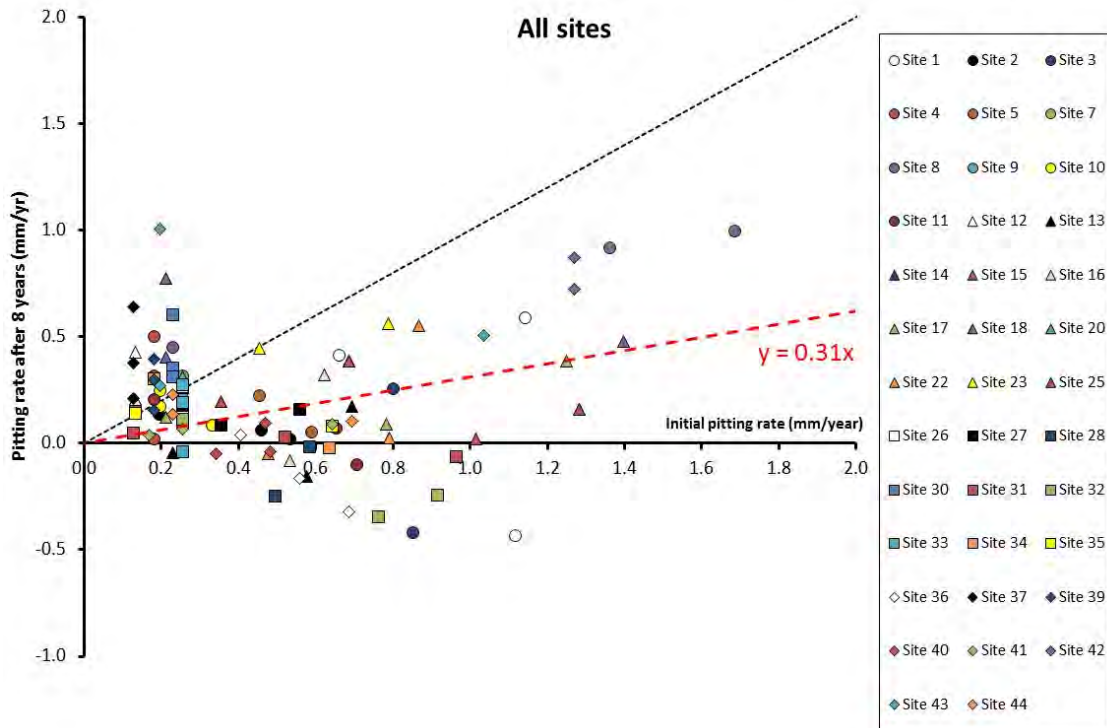


Figure 7. Comparing initial pitting rates with pitting rates after 8 years (data from Romanoff, 1957). The dashed black line represents where initial and 8 to 17 year average pitting rates are equal. Red dashed line is the line of best fit.

Despite the variation in the loss data some aspects of the relationship between the initial and mature corrosion rates are clear from Figure 7 which compares the initial and average 8-17 year rates of corrosion for all of the Romanoff sites. Generally, in keeping with the rate trends over time discussed earlier, it was found that initial rates exceeded rates observed after 8 years (much of the data in Figure 7 falls below the dashed line). The main exceptions to this appear to be at low corrosion rates where data is clustered fairly evenly above and below the dashed line. Given the variability in the data this most likely suggests that pitting rates remain relatively constant under these (relatively benign) conditions. The slope of the regression line (which has been forced through the axes intercept) suggests that on average 8-17 year pitting rate is approximately 31% of the initial pitting rate.

Figures 8, 9, and 10 show the data from Figure 7 subdivided according to soil texture (sandy sites have >50% sand fraction, clay sites >50% clay fraction and silty sites >50% silt fraction). Subdividing the data according to soil texture showed a similar relationship between initial and mature rates of corrosion irrespective of soil type (the average ratio between 8-17 year and initial pitting rates being 28% at sandy sites, 38% at clay sites and 38% at silt sites). Given the spread in the data in each case the differences observed in the slopes of the regression lines is most likely not significant suggesting that the rate of slowdown may be independent of the soil type.

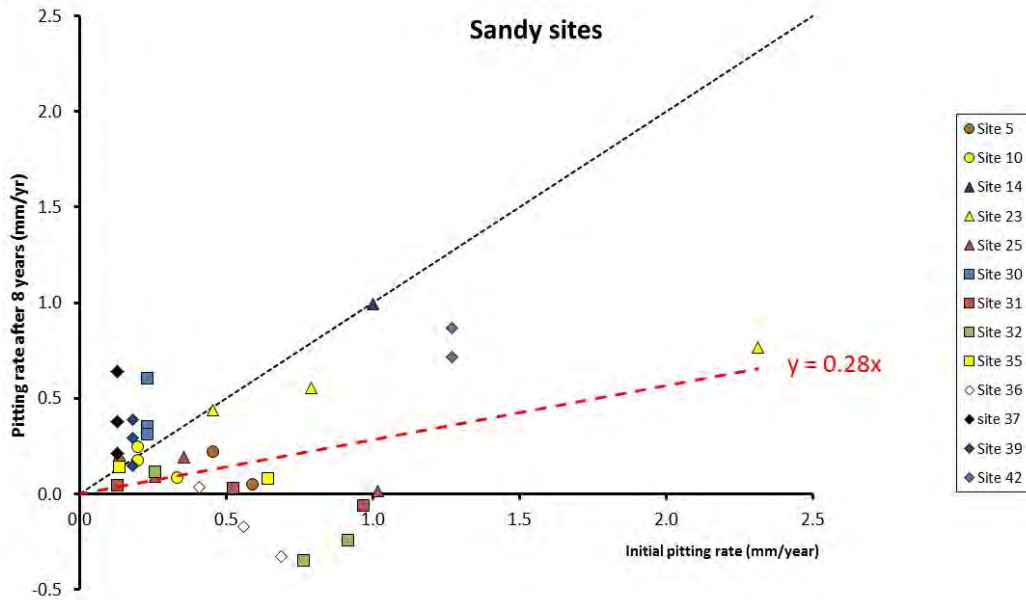


Figure 8. Comparing initial pitting rates with pitting rates after 8 years for sites with sandy soils (sand>50%, data from Romanoff, 1957). Black dashed lines represent where initial and >8year pitting rates are equal. Red dashed line is the line of best fit.

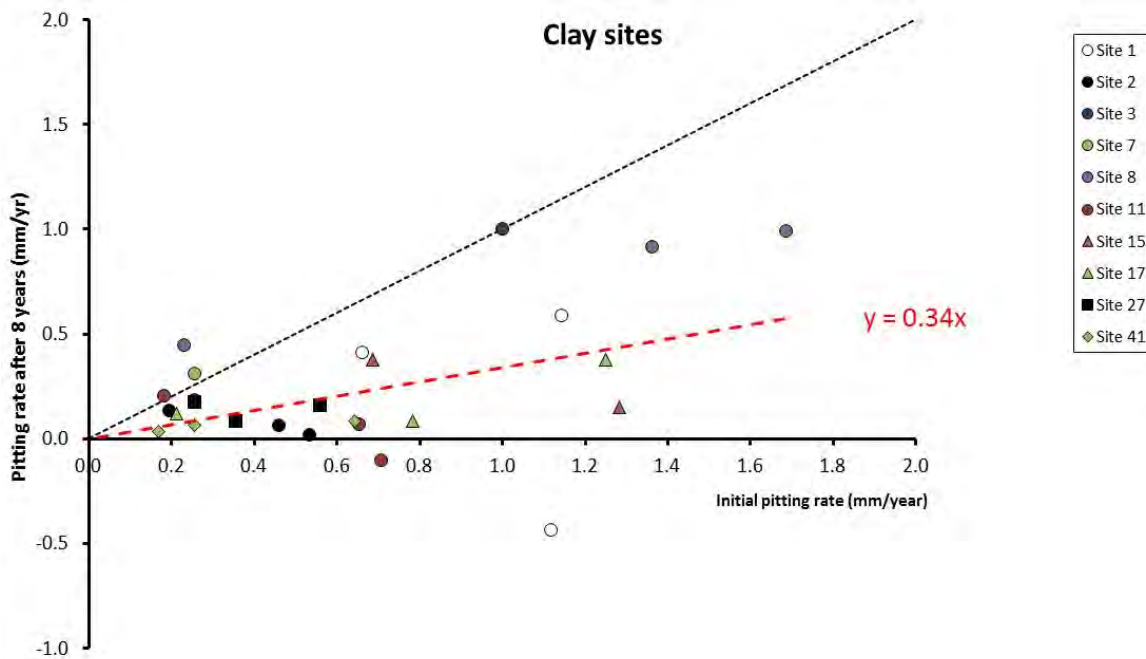


Figure 9. Comparing initial pitting rates with pitting rates after 8 years for sites with clay soils (>50% clay, data from Romanoff, 1957). Black dashed lines represent where initial and >8year pitting rates are equal. Red dashed line is the line of best fit.

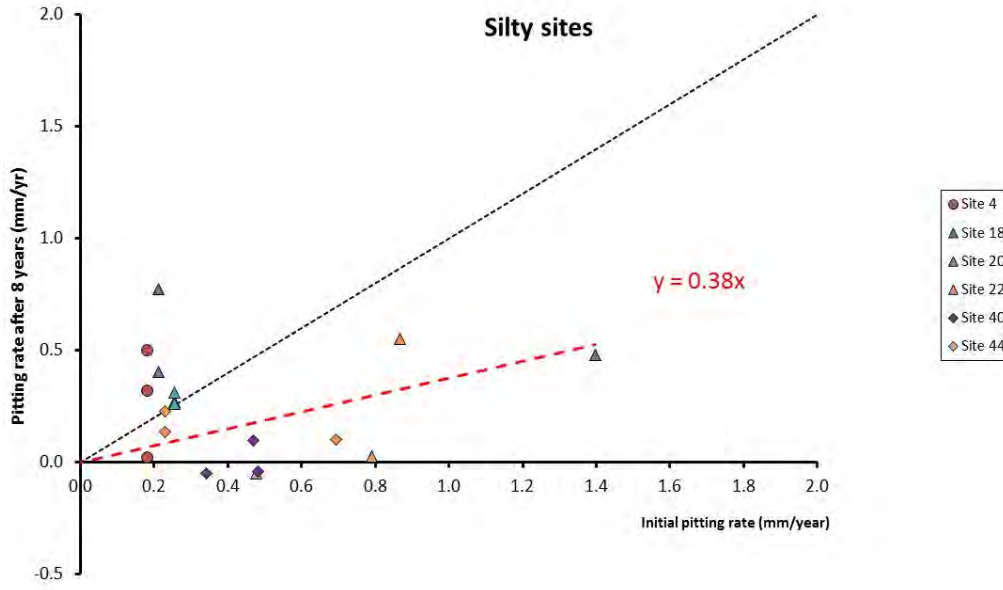


Figure 10 Comparing initial pitting rates with pitting rates after 8 years for sites with silty soils (>50% silt, data from Romanoff, 1957). Black dashed lines represent where initial and >8year pitting rates are equal. Red dashed line is the line of best fit.

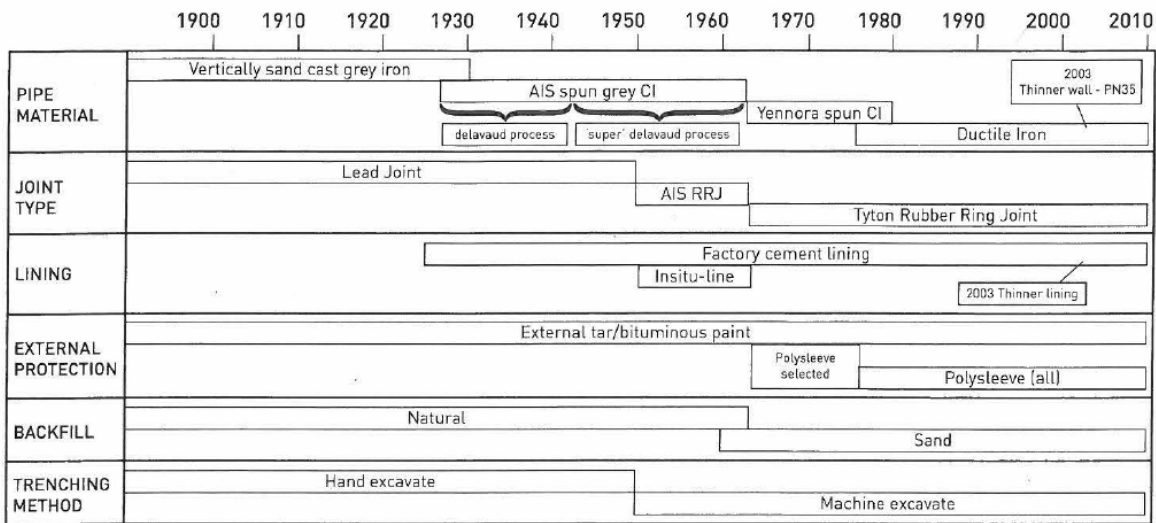
When considering the growth of pits over time Rossum (1969) suggest the following relationship:

$$p = Kt^n \quad (4)$$

where p is the pit depth (mm), K is a proportionality constant, t is time (yrs) and n is the time exponent. Rossum proposed that the value of n ranged from 0.17 to 0.67 depending on soil type. Also reported are the (averaged) exponents derived from field observations (Romanoff, 1957) which fell into roughly the same range of values (again depending on soil type). Values of $n < 1$ suggest that pit rates are slowing over time.

It should be noted that the impact of pipe age is complicated by other factors which may impact on the rate of corrosion that have also changed over time. For example, Nicholas and Moore (2009) (Figure 11) note that in the 1950's manual excavation and backfilling around pipes was replaced largely by the use of mechanical digging equipment. The subsequent changes to the structure, compaction and degree of aeration of the soil surrounds that resulted from the use of mechanical excavation may have had a significant impact on the corrosion activity taking place. Dafter (2014) also notes that post 1960 pipes are often surrounded by partial or poor backfill which would push up corrosion rates for pipes laid during this period.

One other important factor that may impact on corrosion behaviour which has changed over time is the method of pipe manufacture. This will now be discussed in greater detail.



Source: Nicholas and Moore, 2009.

Figure 11. How pipe installation and manufacturing methods have changed over time)

Pipe Manufacture

Another relevant factor that has changed over time is the means by which the cast iron pipe has been manufactured. In his study of cast iron pipe corrosion in the Hunter valley area Dafter (2014a, 2014b) identified four main methods of pipe casting that have been used in Australia over time (Table 1, and Figure 11).

**Table 1
Means of cast iron pipe manufacture**

Years (approximate)	Method
1890-1929	Vertically (statically) sand cast (VC)
1929-1942	De Levauud Horizontally cast (DLHC)
1942-1962	Super “De Levauud” horizontally cast (SDLHC)
1963-1976	Horizontally cast (HC)

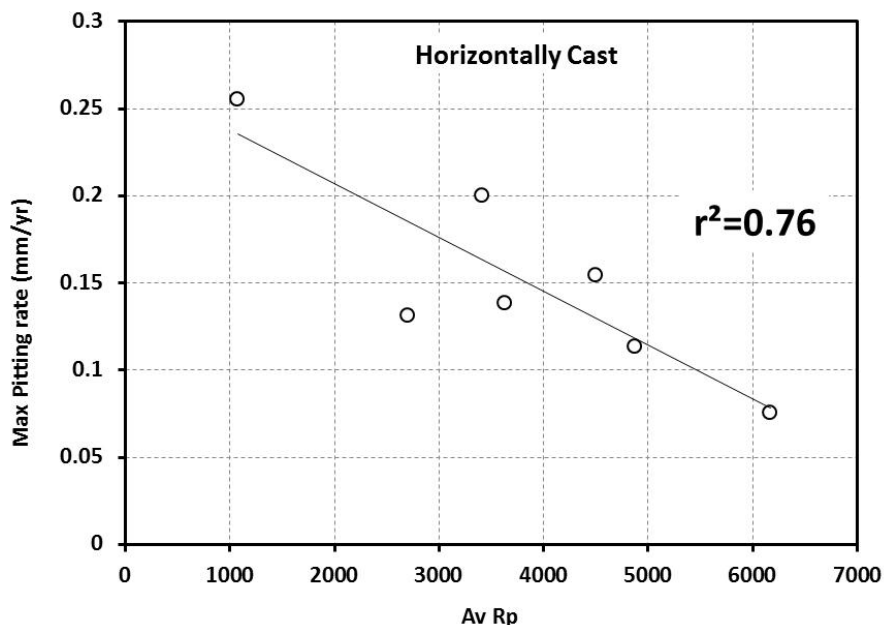
Some of the impacts that different casting methods may have on the corrosion rate are as follows (Dafter 2004; Nicholas and Moore 2007, Makar and Rajani 2000):

- Vertically sand cast pipe was relatively thick and often eccentric in wall thickness around the pipe diameter. This increased thickness may affect long-term diffusion pathways and hence corrosion rates.
- Sand cast pipes had an external chill surface that was affected by segregation of elements such as silica and phosphorus – this property is often considered to enhance corrosion resistance.
- In general, spun pipes have a more uniform wall thickness, less porosity and a less segregated microstructure

- ‘Super De Levaud’ pipes were treated with a mold release agent and it is thought that this affected corrosion resistance by modifying the chill layer (Nicholas and Moore 2007)
- Variation in wall thickness between sand cast and spun pipes could be more than 100% for the same diameter
- The means of the application of a bitumen coating has also evolved with some early (c. 1885) vertically cast iron pipes simply dipped in hot bitumen upon removal from casting while in later years tar or bitumen was simply brushed on.

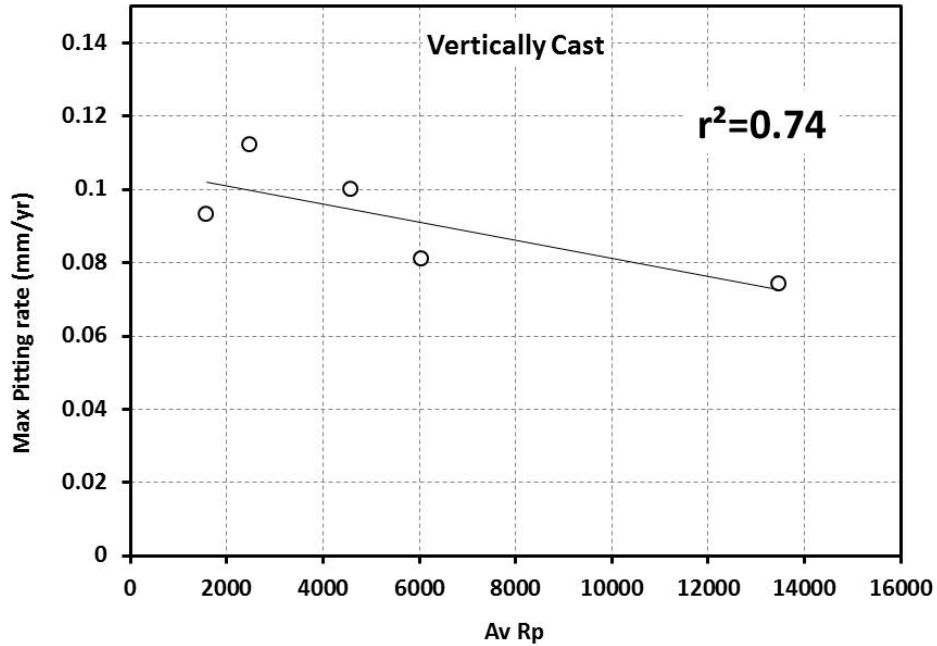
In his analysis of LPR corrosion prediction Dafter (2014) found that correlations between R_p values and the maximum pitting rate were significantly improved when the data was subdivided into cohorts that reflected the method of pipe manufacture. For example, Figures 12 and 13 show the correlation between R_p values (generated using his LPR cell) and the maximum pit depth growth rates for vertically and horizontally cast iron pipe. While the number of data points is limited the regression r^2 values are quite good ($r^2 \sim 0.75$ in both cases). It should be noted however that the data shown in these two figures relates only to (non-sandy) native soil sites.

A comparison of the two regression lines (Figure 14) shows that for the same R_p value vertically cast pipes show a substantially lower rate of corrosion. This may be due to the manufacturing method however there is the possibility that as the data for each pipe type covers a limited number of years (vertically (statically) cast from 1884-1930 and horizontally cast from 1947 to 1962) that the lower corrosion rates observed for the vertically cast pipe may be due to the additional age of the pipe (and the slowdown of corrosion rate discussed above) rather than the result of the manufacturing method. An analysis of the LPR data presented by Hay (1984) along the same lines (Figure 15) shows a similar trend.



Source: Adapted from Dafter 2014c.

Figure 12. Correlation between LPR R_p values and measured pitting rates for horizontally cast iron pipe buried in native soil



Source: Adapted from Dafter 2014c.

Figure 13. Correlation between LPR Rp values and measured pitting rates for vertically cast iron pipe buried in native soil

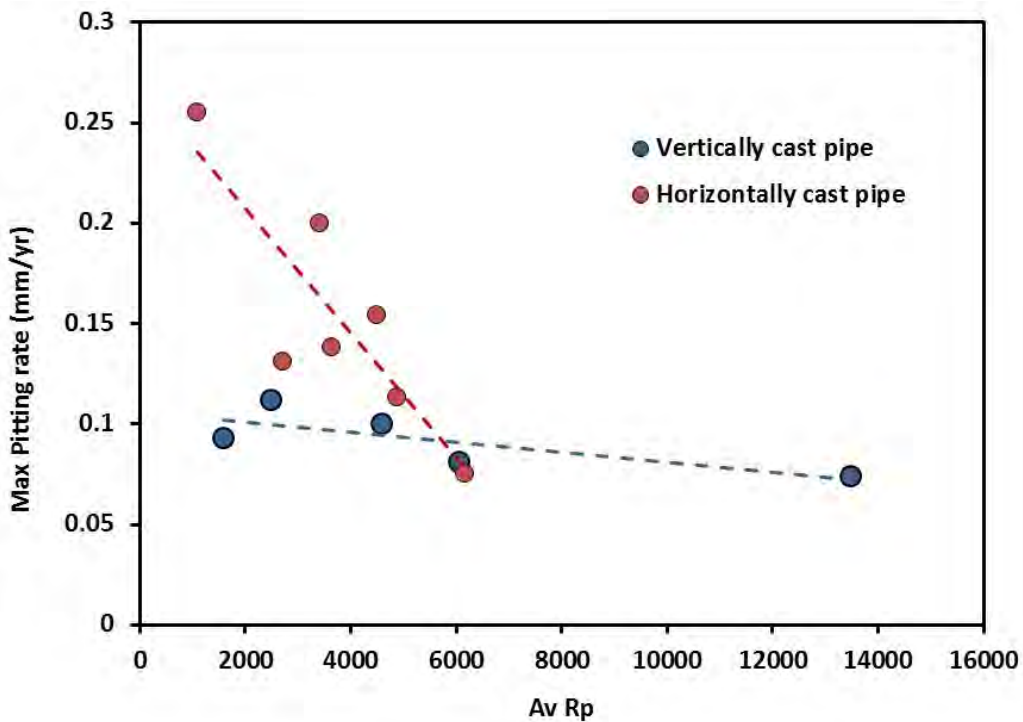


Figure 14. Comparing the correlations between horizontal and vertically cast pipe. Dashed lines are lines of best fit as shown in the previous two figures.

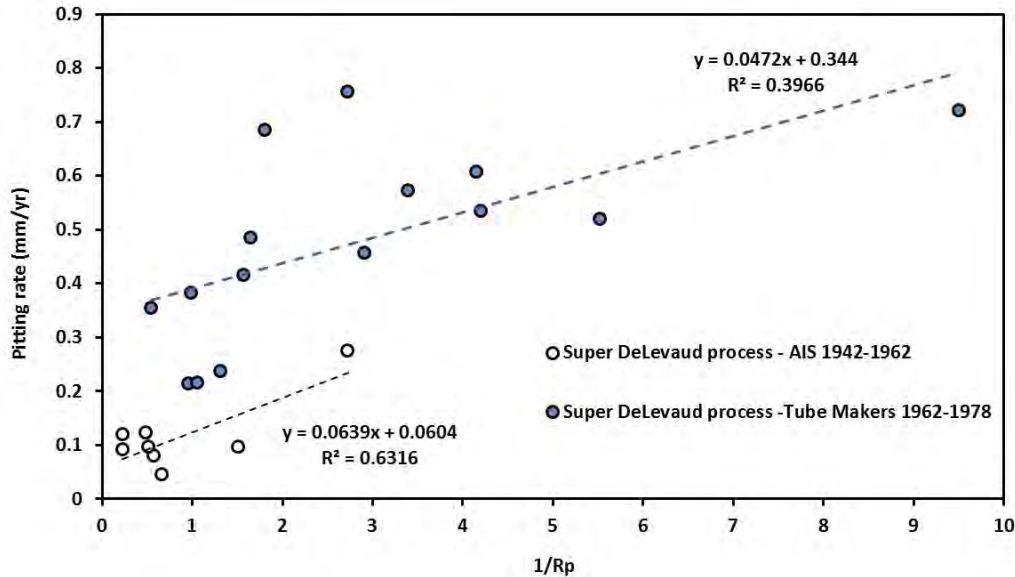


Figure 15. Correlations of 1/Rp against observed pitting rates for pipes manufactured during the period. (Data from Hay, 1984). Note that mode of casting is estimated from installation date.

Concluding Note on Issues Relating to Time Dependent Corrosion Trends

The non-linear nature of the corrosion process, the focus of LPR on electron transfer processes and the possible role of changing pipe manufacturing techniques all indicate that the addition of a pipe age factor into the LPR predictive model may improve model prediction of corrosion rates particularly for older pipes. The extent of this correction will depend on the non-linearity of the corrosion behaviour over time and will most likely have to be estimated from a more extensive analysis of the data of Romanoff or any other time series data that becomes available. Whether it will be possible to include a separate modification for pipe manufacturing method or simply roll that into the age correction factor will have to be further investigated and most likely will ultimately depend on the availability of sufficient data to make possible the distinction between the impact of the age of pipe and manufacturing method on the predicted rate of corrosion.

Issues Relating to Moisture Content of the Soil

Soil is a heterogeneous material consisting of a range of differently sized solid particles interspersed with a network of pores of varying diameters. Soil moisture levels can range from oven dried (essentially all pores are air filled) up to saturated (all pores are water filled – see Figure 16, left). In natural settings soils generally only become saturated after prolonged rain events and then only temporarily so. Without further rain the moisture in saturated soils will drain under gravity until the soil reaches what is known as “field capacity” at which point water has drained from the larger macro-pores but a sizeable amount is still retained in the smaller macro-pores and finer pore structures (Figure 16, middle). If there is no further rain input the combined effects of evaporation and water uptake from vegetation will act to further lower the moisture content of the soil until a point is reached where the only remaining moisture is physically/chemically bonded to the soil particles so well that it cannot be removed by plant suction. This point is known as the wilt

point (WP) (Figure 16 right) – so called because plants wilt at this level of soil moisture. If there is no further moisture input soil levels can fall below the wilt point however this process is slow as the available moisture in the soil is tightly bound to the soil particles. Thus, generally speaking, the wilt point represents the lower bound of the soil moisture content of the soil.

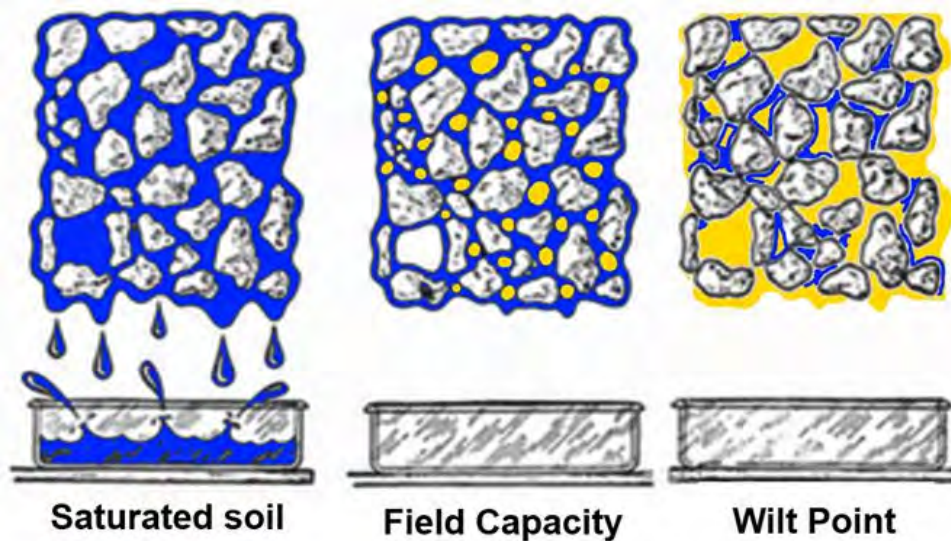


Figure 16. Schematic representation of the three different soil moisture states of soils

The presence of moisture in the soil is necessary for corrosion of cast iron pipe to take place as water is the essential electrolyte required to support the electrochemical corrosion process (Roberge, 2008). Uhlig in Revie (2011) notes that the moisture content of the soil is the only variable in underground corrosion proven to have a measurable effect and consequently the use of soil moisture in models predicting buried pipe corrosion rates is almost universal (for example see Gemmel, 1952; Penhale, 1958; Noyce and Ritchie, 1979).

The relationship between soil moisture levels and the rate of corrosion however is complex. Previous studies (Romanoff, 1957; Gupta and Gupta, 1979; Glazov et al., 2006) for example have observed that the corrosivity of soils towards mild steel is low at small soil moisture levels and increases as the soil becomes wetter before again decreasing as the soil moisture tends towards saturated. Gupta and Gupta (1979) suggested that the maximum is reached when the soil moisture is at approximately 65% of the soil’s water holding capacity. Dafter (2014c) observed that corrosion of buried cast iron pipes was most rapid when the soil moisture content was about halfway between the wilt point and the soil’s field capacity. At this point the conductivity of the soil is sufficient to minimise the ohmic resistance to the electrochemical reaction without being so moist as to stifle the reaction by slowing the transport of oxygen through the (partially water filled) soil pore structure. As the corrosion process is related to the ease at which ions can be transported through the soil structure it stands to reason that it is not the absolute soil moisture content that is important as much as the degree of saturation of the existing pore structure (i.e., what proportion of the pore structure is air filled and what proportion is water filled). As pore volume and pore structure is dependent on soil texture it is important that the effects of soil moisture is considered separately for different soil types (e.g., sandy or clay soils).

In Activity 3 Rob Petersen (see also Petersen and Melchers, 2013) has also identified the long-term soil moisture saturation level as one of the prime variables in the modelling of cast iron

pipe corrosion. The long-term corrosion data shown for example in Figure 17 clearly shows differing corrosion trends over time for soils of differing moisture content.

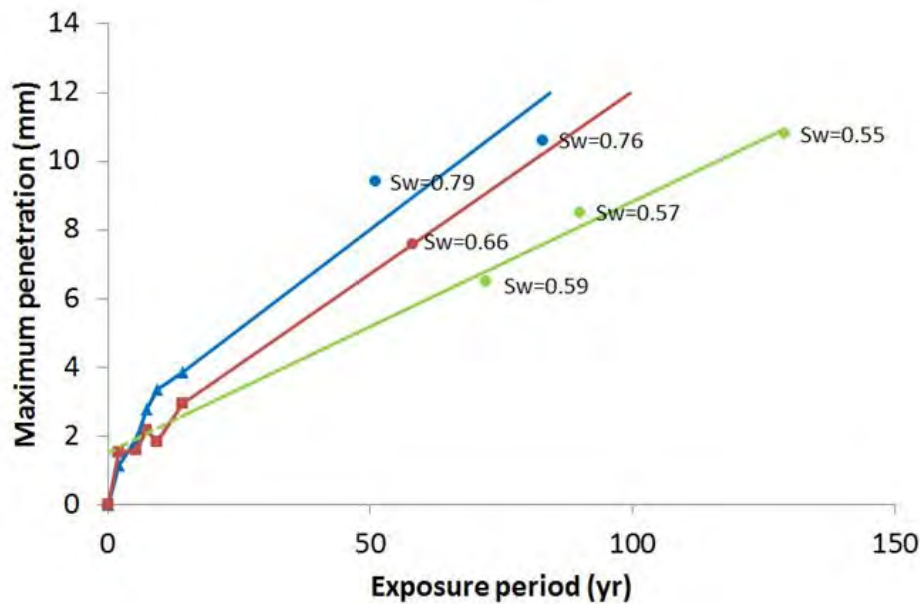


Figure 17. Impact of soil moisture on cast iron rates of corrosion (image taken from Rob Petersen's Activity 3 results)

As previously discussed, LPR measurements conducted by PCA Echologics are currently conducted on soil samples after their soil moisture has been adjusted to the wilt point irrespective of the original soil moisture content of the sample when collected or the long-term soil moisture level of the soil at the site in question (Ferguson and Nicholas, 1992). This practice would appear to be at odds with the findings quoted above which indicate that rates of corrosion are dependent on the soil moisture content.

The questions that naturally arise are: (1) why is the test conducted at the soil wilt point and secondly and (2) does the use of the wilt point increase the level of uncertainty in the corrosion rate prediction. In answer to the first query it would appear that use of a wilt point soil moisture level was originally advocated by Hay (1984) who suggested that the wilt point moisture level is an extremely common condition in Australian soils (Heathcote and Nicholas, 1998). It should be noted however that the Hay's study was conducted during an exceptionally dry period (this is stated as a possible reason why he found only a very poor relationship between soil moisture levels and corrosion activity). If his observations in regard to wilt point were based on the samples he took during this study then they may have conveyed a false impression as to the general level of moisture present in soils.

To investigate the assumption that the wilt point is a good indicator of long-term soil moisture levels a survey of long-term soil moisture data reported at the soil monitoring network located in the upper Hunter Valley (Rüdiger et al., 2007) was compared to the calculated wilt point. The comparison (Figures 18 to 20) shows that the average soil moisture is generally considerably higher than the wilt point. Data presented by Dafer (2014c, Figure 21) in which he compares the one-off soil moisture values determined for the grab samples used in his study against experimentally determined wilt point and field capacity levels also indicates that the "normal" soil moisture levels generally lie somewhere between the wilt point and the field capacity.

From a physical point of view this would make sense. As has been discussed previously the wilt point generally represents the lower limit of the soil moisture content and the field capacity the upper limit. Soils cannot hold moisture levels greater than the field capacity except over very short periods after considerable rainfall. Without rainfall, evaporation and plant uptake will force moisture levels lower however once the moisture level has decreased to the wilt point it is generally difficult to further remove water from the soil structure via the normally available processes (evaporation, plant uptake, drainage) as water molecules are chemically and physically absorbed onto the surface of soil particles. In practice soil moisture levels will generally fluctuate between the wilt point/field capacity extremes hence it is likely that the average moisture level lies somewhere between these two levels.

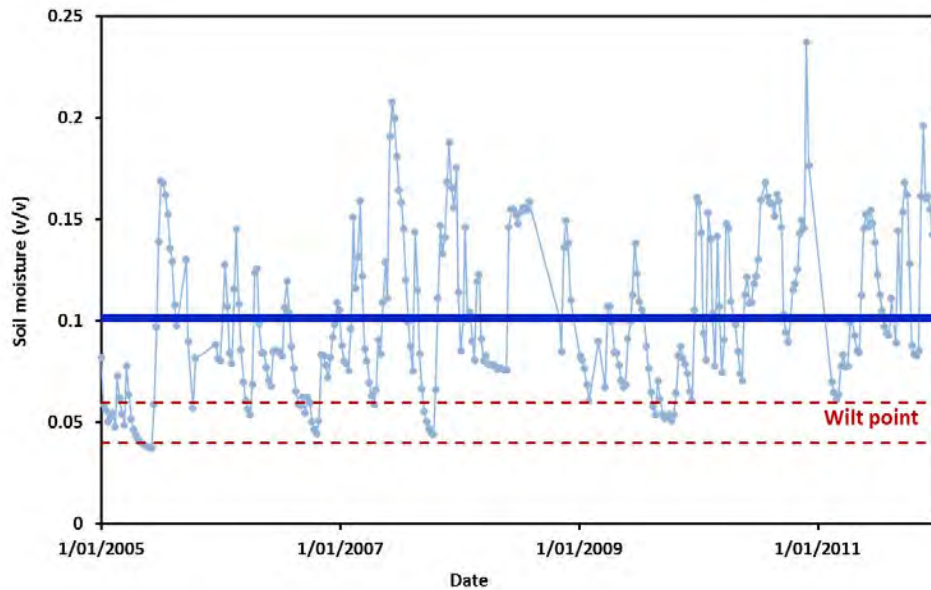


Figure 18. Comparison of long-term soil moisture trends and wilt point for sandy soils (150 mm depth). Blue data points are observed soil moisture levels; dark blue line is long-term average; red dashed lines represent the likely wilt point range.

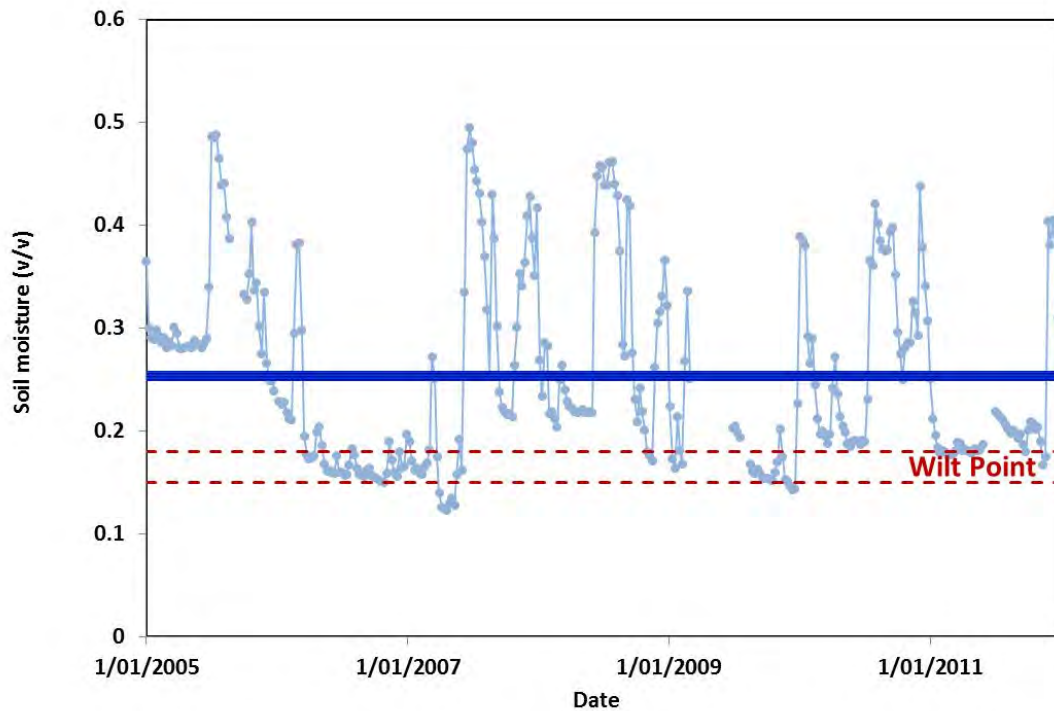


Figure 19. Comparison of long-term soil moisture trends and wilt point for a clay soil (150 mm depth). Blue data points are observed soil moisture levels; dark blue line is long-term average; red dashed lines represent the likely wilt point range.

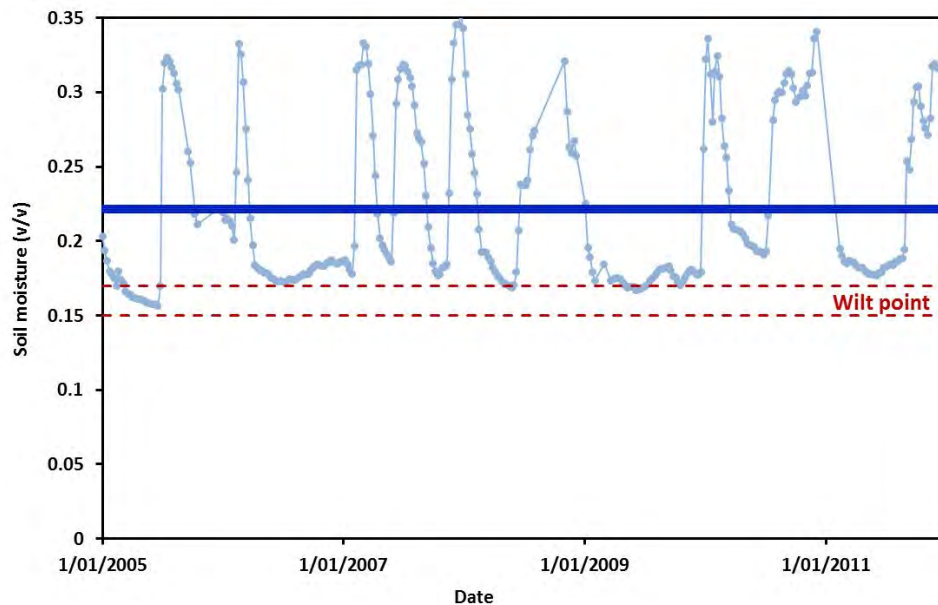
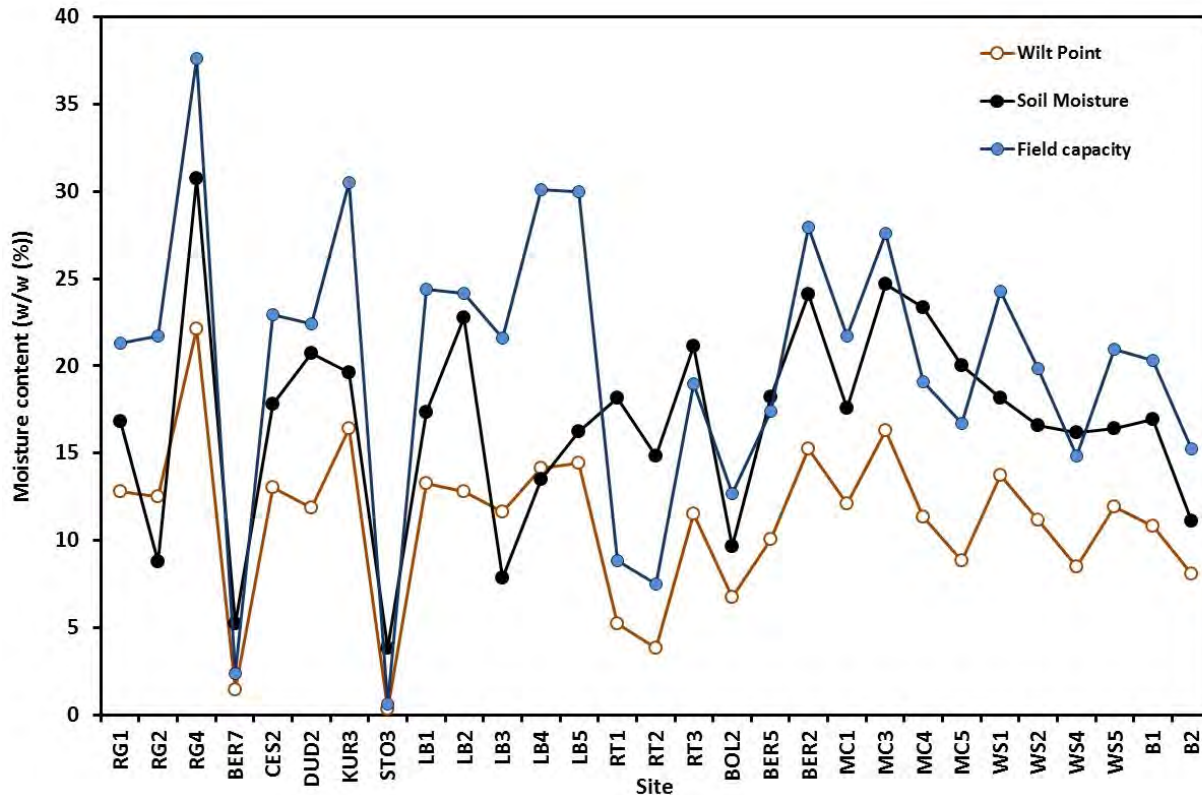


Figure 20. Comparison of long-term soil moisture trends and wilt point for a sandy soil (750mm depth). Blue data points are observed soil moisture levels; dark blue line is long-term average; red dashed lines represent the likely wilt point range.



Source: Adapted from Dafter 2014c.

Figure 21. A comparison wilt point, field capacity and measured (one off) soil moisture levels recorded during a corrosion survey of Hunter Water cast iron pipes

In correspondence with PCA personnel (pers. comm. Phil Ferguson) it has been suggested that despite the seeming inconsistencies in conducting the LPR test at the wilt point (WP), corrosion predictions made from LPR tests conducted at the WP moisture level still manage to reflect the aggressive nature of soils which are known to be quite sodden. Just how this is accomplished however is not clear. One possibility is that the wilt point for a given soil is dependent on the structure and chemistry of the soil. For example, an analysis of a wide range of soils (Saxton and Rawls, 2006) suggests that the wilt point is positively correlated against clay and organic matter content and negatively correlated against sand content. Thus, while the LPR test is conducted at the wilt point for an individual soil it is important to realise that this level of soil moisture will vary from soil to soil and that carrying out the test at the varying wilt point levels for the different soils may in some fashion allow the LPR tests to reflect factors (such as soil structure) which affect ion transport through the soil which ultimately have a bearing on the corrosion rate.

On a more practical level carrying out the LPR test with a soil sample dried to its wilt point does impart an important advantage in running the test in that it allows for more consistent packing of the LPR test cell. Soils with high moisture content are less workable than dry soils and consequently the risk of air gaps is higher in LPR tests conducted with wetter soils. Both PCA Echologics (pers. comm. Phil Ferguson) and Dafter (2014b) note the importance to the final test result of the manner in which the LPR cell is packed. (For example, PCA Echologics places a great deal of importance on how the cell is packed and has established a rigorous methodology for doing

so). The work undertaken by Dafter (2014b) has also highlighted the significant impact that soil compaction has on the outcome of the LPR test:

- (1) Poor compaction of the soil results in air gaps at the soil/metal interface thereby reducing the working area of the electrode actually undergoing polarisation – effectively this is equivalent to working with a smaller electrode and ultimately the rate of corrosion will be overestimated.
- (2) The presence of air gaps increases the potential for crevice corrosion of the electrodes significantly reducing the life of the electrodes.
- (3) Air gaps cause a substantial degree of variation in the measured values of R_p .

Thus, while it may appear from a corrosion standpoint that it might be more appropriate to run the LPR test at the normal soil moisture content on a practical level the best approach appears to be to continue carrying out the tests at the wilt point but include a soil moisture correction factor in the $R_p \rightarrow$ Corrosion rate algorithm which corrects for the long-term average soil saturation level of the soil in question.

Backfill Type and Quality

It has been noted by Dafter (2014b) that the use of the LPR test to predict corrosion rates works best when the water pipe in question is buried in uniform native soils. LPR soil samples are obtained (when possible) approximately 300mm away from the pipe at its midline depth. When the pipe is buried in the native soil it is therefore likely that the soil sampled in this fashion for the LPR test is indicative of the soil in contact with the pipe and hence from a corrosion point of view is relevant to determining the rate of corrosion.

There are however a number of scenarios where the soil in contact with, and surrounding the pipe, is not native and/or not uniform and in such cases the soil that is sampled and LPR tested is not indicative of the soil in contact with the pipe. These fall into 4 main categories:

- (1) Where the pipe is surrounded by a heterogeneous native soils (e.g., containing rocks, lumps of clay etc. or comprising a number of different soil horizons – see Figure 22 A)
- (2) Where the pipe is surrounded by a well formed, uniform imported sandy fill material
- (3) Where the pipe is surrounded by a poorly formed imported material through which is mixed some of the original native soil
- (4) Pipes are bedded on hard native soils and the remainder of the excavation is filled with loose and variable backfill material

As noted by PCA Echologics (pers. comm. Phil Ferguson), the use of imported fill and hence scenarios (2) to (4) are only relevant to pipes laid after ~1960. Also, it is their experience that the heterogeneity of the backfill is more likely to be the result of either horizontal or vertical stratification of the filling material and native soils (Figure 22 (B and C)). Phil also notes that heterogeneity of backfill is not a common cause of pipe failure.

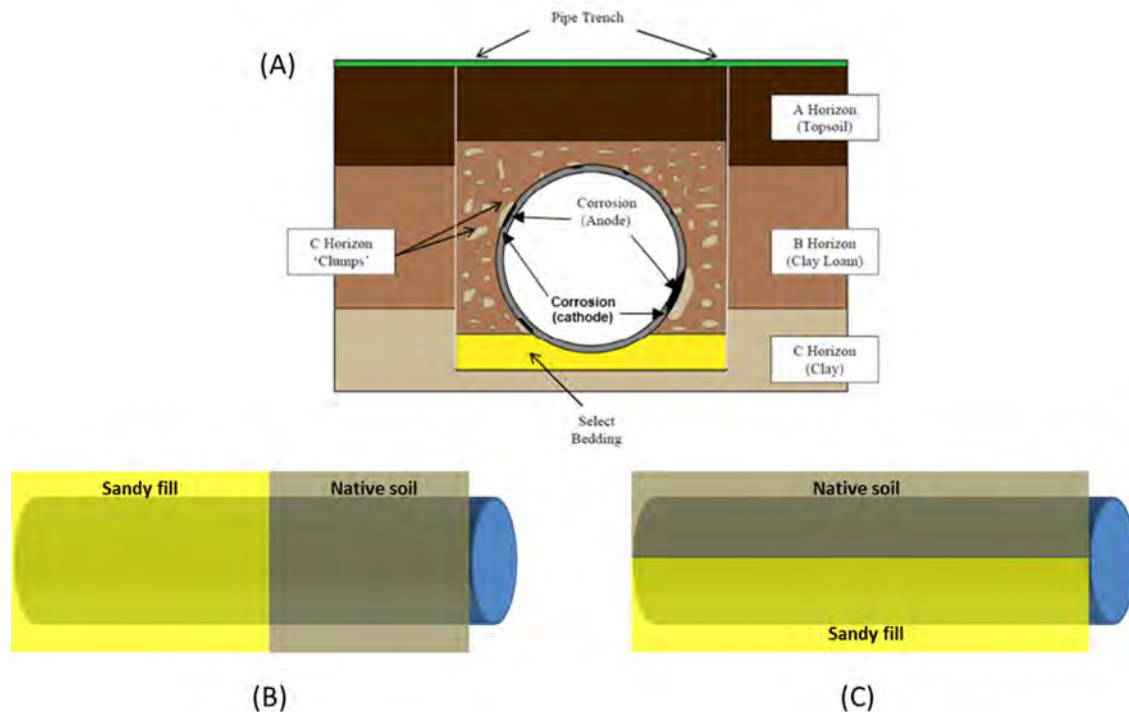
This backfill issue is important as it has been observed that localised corrosion rates of pipes in contact with heterogeneous backfill material (be it native soil, imported fill or a mixture of the two) is significantly higher than in uniform “natural” soils (e.g., see Norin and Vinka 2003). Dafter (2014c) also notes for example that corrosion observed on sand surrounded pipes is often

the result of native soil infiltrating the imported bedding. Contact of the pipe with one or more soil structures can occur over relatively small distances (of the order of cm) or over much larger distances which may induce higher levels of corrosion driven by, for example, differential aeration cells (Ferguson and Nicholas, 1992, Petersen and Melchers, 2012) or differences in the ease at which critical chemical species (oxygen, ferrous ions...) can move through the soil surrounding the pipe. The resultant differential nature of the local environment is then thought to drive areas of localised corrosion of cast iron pipe.

It should be stressed that the basic problem here is one of representative soil sampling and is not specific to LPR testing but will apply to any “spot measurement” technique, or even continuous techniques without sufficient resolution. In the case of LPR testing the impact of a non-representative soil sampling on the predicted (as opposed to the real corrosion behaviour) depends on which of the above scenarios is applicable. In scenario (2) for example where the pipe is surrounded by a well formed ~100 mm thick, uniform imported sandy fill material observed corrosion rates are generally very low (<0.05mm/yr). In these cases, LPR predictions made from sampling of native soils (which lies outside the sandy fill) in the same location are likely to over-predict the rate of corrosion. Conversely, where native soils have intruded into the sandy imported fill (or lumps of clay or rocky material are present in native fill) the LPR test may considerably under-estimate the rate of corrosion.

Because of the likely random nature of this problem it will be the most difficult to address in a quantitative sense. One possible strategy to address this issue is to employ a more intense sampling regime (i.e., more frequent than every 50-100m) however given that the scale of such phenomena can be in the order of centimetres it is likely that any practical level of soil sampling may not capture the heterogeneity of the soil environment. A second approach which is more in line with the focus of Activity 4b, (i.e., improvement of the $R_p \rightarrow$ Corrosion algorithm), would be the inclusion of an additional risk factor for areas in which a heterogeneous soil environment is known to be present. A further alternative, as suggested by Dafter (2014b), would be to limit the application of the LPR technique to cast iron pipes buried wholly in native soil.

The sampling strategy approach will be investigated as a part of Activity 4c while the risk factor approach is recommended for Activity 4b.3 which is focused on the improvement of the $R_p \rightarrow$ Corrosion model.



Source: Adapted from Dafter 2014c (top).

Figure 22. Corrosion of pipe buried in mixed soil horizons with distributed soil strata. (A) when lumps of foreign material are distributed through soil. Note the anode of the corrosion cells lie under the clump while the cathode is likely to reside at the edge of the clump. (B) and (C) when native soil and foreign fill material adjoin.

SUMMARY AND SUGGESTED FOCUS FOR ACTIVITY 4B.3 WORK

The purpose of this report, in conjunction with the more theoretical analysis conducted previously, is to examine the application of the linear polarisation resistance (LPR) technique to the prediction of corrosion rates of buried cast iron pipes and in doing so suggest areas in which improvements can be made to the prediction of corrosion rates using LPR tests.

Four possible factors have been identified whose inclusion in the $R_p \rightarrow$ Corrosion rate algorithm may improve prediction accuracy:

1. The method of pipe manufacture: An analysis carried out by Dafter (2014a, 2014c) indicates that the relationship between LPR R_p value and the max pit depth may be different for pipes manufactured by different techniques (for example vertically or horizontally cast). Dafter (2014c) speculated that this may be (at least in part) due to differences in the original bitumen coating applied to the pipes however there is no direct evidence to support this. By considering a separate calibration equation for each pipe class or adjusting coefficients to account for pipe type it may be possible to improve the accuracy of the corrosion prediction.
2. The age of the pipe.: The available data indicates that cast iron pitting rates decrease over time. This decrease may be due to the changing nature of the corrosion process itself – moving from corrosion limited by the kinetics of the corrosion reaction to a

- system where mass transport limitations are the rate limiting factor. The LPR test is fundamentally an examination of corrosion processes that are dominant at the beginning of the corrosion process and consequently there is a possibility that LPR predictions of corrosion rates might benefit from an adjustment to account for the slow-down in pitting rates over time. It is important to note however that there may not be a clear distinction between the effects of pipe age, pipe manufacturing method and other factors that impact on the corrosion process which have changed over time (for example the methods used to bury the pipe). To improve the model predictions the strategy should ideally be to account for both the age of pipe and the means of manufacture in the formulation of an improved predictive model. However, the limitations in the data currently available may mean that a single correction factor to account for the combined effect of pipe age and manufacturing method will be the used in the improved predictive model.
3. Soil moisture (saturation) level: Soil moisture content is an important factor in determining rates of cast iron pipe corrosion but LPR tests are always conducted at the wilt point soil moisture level regardless of the soil moisture conditions at the pipe site. Analysis of soil moisture data suggests that many cases the wilt point is not representative of the average long-term soil moisture content of the soil and hence running the test at the wilt point may increase uncertainties in the model prediction. Application of a correction factor to account for the impact of long-term soil moisture levels may be beneficial and should be investigated.
 4. Backfill type and quality: Both Matt Dafter and PCA Echologics acknowledge that the LPR technique works best when native soils are used as backfill. A non-uniform soil environment (due to for example the presence of lumps of clay/rocky material or native soil intrusion into imported sandy fill) has the potential to produce extremely localised corrosion phenomena. Because of the likely random nature of this problem it will be difficult to address in a quantitative sense. Possible strategies include more intense sampling and subsequent statistical analysis leading to the inclusion of an additional risk factor for areas in which this type of backfill is known to be in place. The sampling strategy/statistical approach will be investigated as a part of Activity 4c while the risk factor approach is recommended for Activity 4b.3 which is focused on the improvement of the $R_p \rightarrow$ Corrosion model. A further alternative, as suggested by Dafter (2014b), would be to limit the application of the LPR technique to cast iron pipes buried wholly in native soil. (Currently PCA Echologics manages analysis involving sandy backfill statistically as the imported soil is, with very few exceptions, much less corrosive)

It is recommended that Activity 4b.3, in which an improved $R_p \rightarrow$ Corrosion rate prediction model is to be developed, should investigate if the inclusion of the above factors into the prediction algorithm.

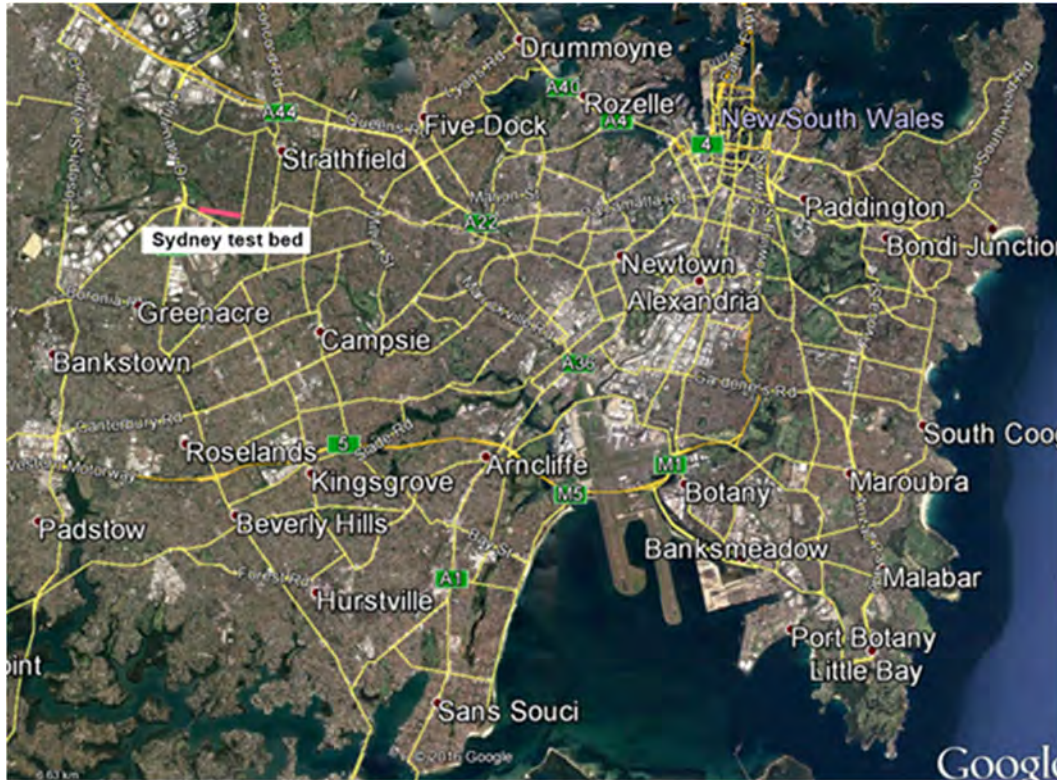
REFERENCES

- Dafter, M. (2014a). "Using LPR to predict underground corrosion of cast iron watermain. Paper 051." ACA 2014 conference. November 2014, Darwin.

- Dafter, M. R. (2014c). "Electrochemical testing of soils for long-term prediction of corrosion of ferrous pipes." Faculty of Engineering and Built Environment, The University of Newcastle. p.H.D.
- Farrag, K. (2010). "Evaluation of External Corrosion-Rate Using Polarization Resistance and Soil Properties. Final report."
- Ferguson, P. H. and D. M. F. Nicholas (1992). "External corrosion of buried iron and steel water mains." *Corrosion Australasia* 17(4): 7-10.
- Gemmel, G. D. (1952). "An investigation of the corrosive effects of soils on steel plates." *New Zealand Journal of Science and Technology* 33: 287.
- Glazov, N., S. Ukhlovsev, I. Reformatskaya, A. Podobaev and I. Ashcheulova (2006). "Corrosion of carbon steel in soils of varying moisture content." *Protection of Metals* 42(6): 601-608.
- Gupta, S. K. and B. K. Gupta (1979). "The critical soil moisture content in the underground corrosion of mild steel." *Corrosion Science* 19(3): 171-178.
- Hay, L. (1984). "The Influence of soil properties on the performance of underground pipelines." Department of soil science, The Faculty of Agriculture, The University of Sydney.
- Heathcote, M. and D. Nicholas (1998). "Life assessment of large cast iron watermains. UWRAA report no. 146."
- Makar, J. M. and B. B. Rajani (2000). "Grey cast iron water pipe metallurgy. National Research Council report NRCC-44241."
- Melchers, R. E. (2014). "Microbiological and abiotic processes in modelling longer-term marine corrosion of steel." *Bioelectrochemistry* 97(0): 89-96.
- Nicholas, D. and G. Moore (2009). "Corrosion of ferrous watermains: past performance and future prediction - a review." *Corrosion and Materials* 34(2): 33-40.
- Norin, M. and T. G. Vinka (2003). "Corrosion of carbon steel in filling material in an urban environment." *Materials and Corrosion* 54(9): 641-651.
- Noyce, R. W. and J. M. Ritchie (1979). "Michigan galvanised metal culvert corrosion study, Transportation Research Board.
- Penhale, H. R. (1958). "Corrosion of mild steel in some New Zealand soils." *New Zealand Journal of Science* 1: 52.
- Petersen, R. B. and R. E. Melchers (2012). "Long-term corrosion of cast iron cement lined pipes." *Corrosion and Prevention* 2012, 11-14 Nov 2012, Melbourne, Australia
- Petersen, R. B. and R. E. Melchers (2013). "Modelling the long-term corrosion of cast iron pipes." *Corrosion and Prevention* 2013, 10-13 Nov 2013, Brisbane, Australia
- Revie, R. W. (2011). "Uhlig's Corrosion Handbook", Wiley.
- Ricker, R. E. (2010). "Analysis of Pipeline Steel Corrosion Data From NBS (NIST) Studies Conducted Between 1922-1940 and Relevance to Pipeline Management." *Journal of Research of the National Institute of Standards and Technology* 115(5): 373-392.
- Roberge, P. (2008). "Corrosion Engineering : Principles and Practice: Principles and Practice", McGraw-Hill (publishers). New York.
- Romanoff, M. (1957). "Underground Corrosion. National Bureau of Standards Circular 579."
- Rossum, J. R. (1969). "Prediction of pitting rates in ferrous metals from soil parameters." *Journal (American Water Works Association)* 61(6): 305-310.
- Rüdiger, C., G. Hancock, H. M. Hemakumara, B. Jacobs, J. D. Kalma, C. Martinez, M. Thyer, J. P. Walker, T. Wells and G. R. Willgoose (2007). "Goulburn River experimental catchment data set." *Water Resour. Res.* 43(10): W10403.

- Saxton, K. E. and W. J. Rawls (2006). "Soil Water Characteristic Estimates by Texture and Organic Matter for Hydrologic Solutions." *Soil Science Society of America Journal* 70(5): 1569-1578.
- Wells, T. (2014). "Report on Current Knowledge of Theoretical basis of Linear Polarisation Resistance. Activity 4b.1 (available on the Critical Water Pipes project site <http://www.criticalpipes.com/>)."

11.5.5 Activity 4c: Soils Data for Verona St Test Bed Site



Source: Map data © 2016 Google.

Figure 11.70. Location of the Verona St test bed

The Verona St test consists of one and a half kilometres of pipeline that Sydney Water decommissioned in 2010 due to its poor condition. Figure 11.70 shows the map of the area in Strathfield, Sydney where the test bed lies. Cement lined cast iron pipes of approximately 665 mm OD were laid along the bed in 1922. The soil along the test bed is generally heavy clay – particularly at pipe depth (general 1.5 to 2 m below the ground surface). The general layout of the test bed and sampling locations are shown in Figure 11.71.

Soil samples were taken at various locations along the test bed. Initial samples were taken to coincide with pipe exhumation to enable soil properties to be directly compared with corrosion behaviour. Later samples were taken when soil moisture sensors were installed along the bed. Samples were generally taken at the mid depth of the pipe immediately adjacent to the pipe. However, samples were also taken above and below the pipe to enable the level of local variability to be assessed (Figure 11.72).

Spacing between samples generally ranged from 5 to 50 m however three high density sampling locations were also sampled (Figure 11.73) to help determine the level of local variability in soil characteristics. At these points samples were taken ~0.5 m apart.

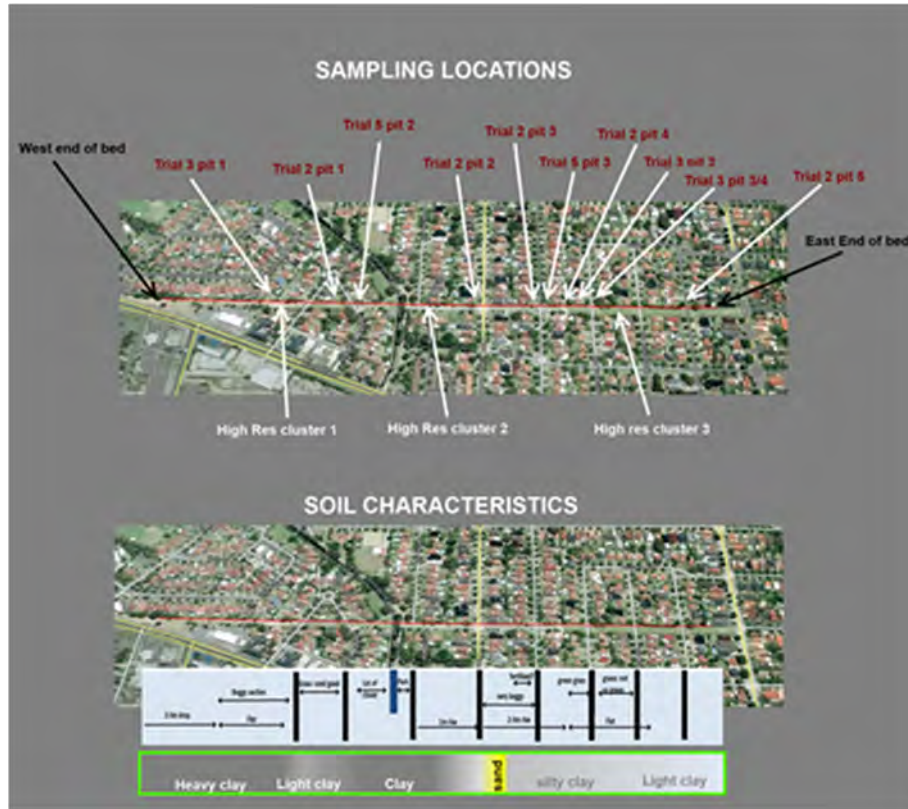


Figure 11.71. General layout of Verona St test bed

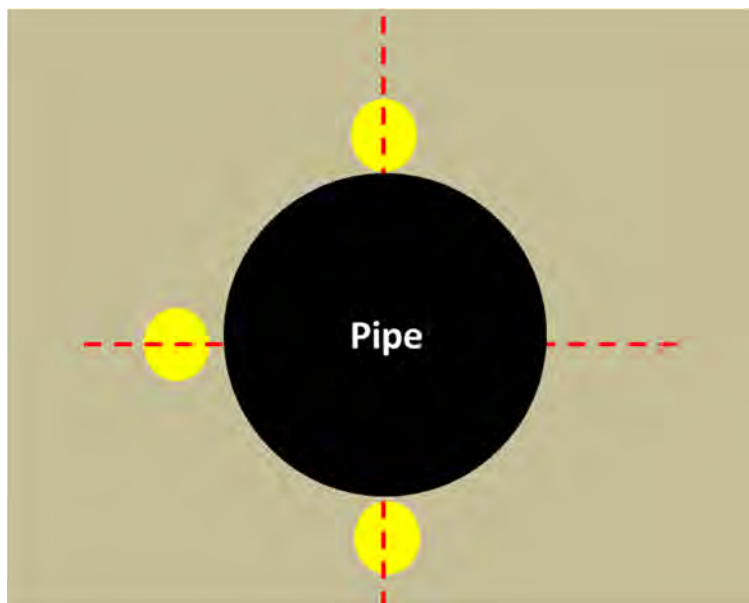


Figure 11.72. Sampling above and below the water pipe

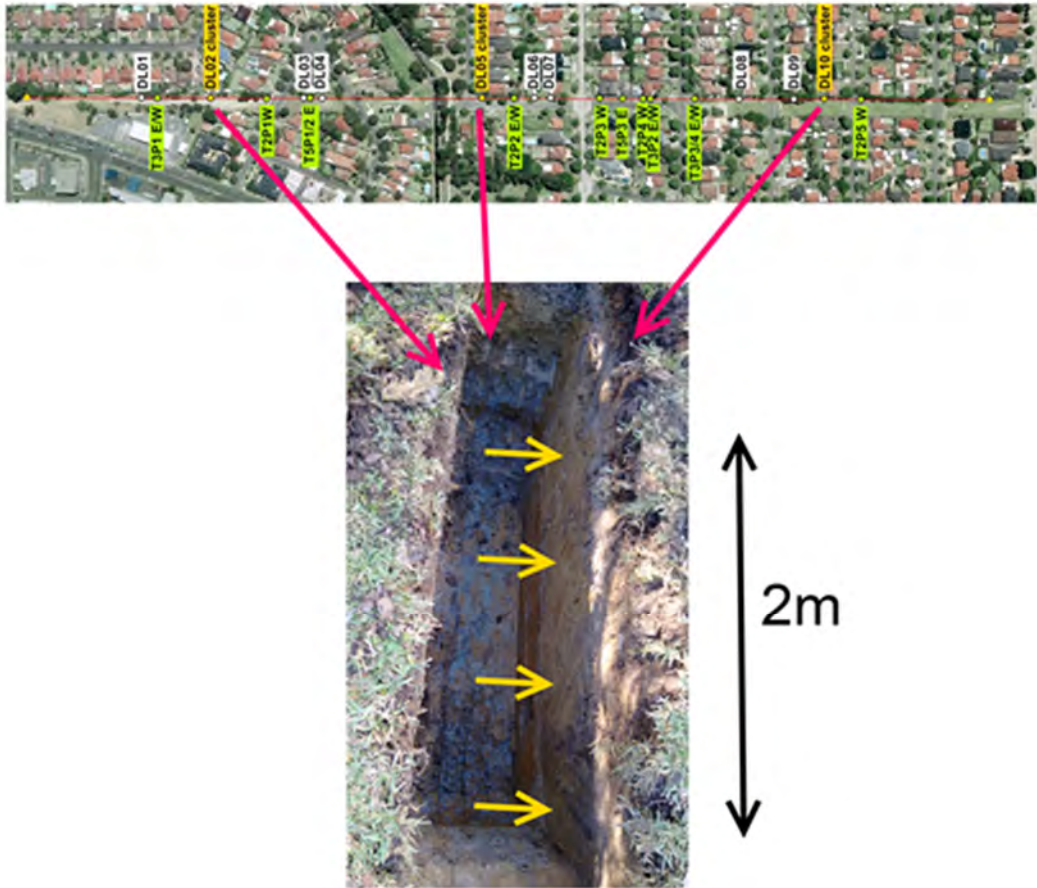


Figure 11.73. Location of high sample density clusters and remaining soil sampling sites

Soil samples were analysed for a variety of properties (Table 11.6). All testing was conducted at a National Association of Testing Authorities (NATA) registered commercial laboratory. Undisturbed soil samples were also taken for bulk density determination. Samples were also collected for Linear Polarisation resistance analysis (see Activity 4b).

Soil properties are listed in Table 11.7 to Table 11.15. Data was used to determine the presence and extent of spatial patterns in soil properties. The variation in properties along the test bed is shown in Figures Figure 11.74 to Figure 11.77. Clustered sample properties are shown as yellow points in the graphs. Variation in soil properties for samples taken above, beside and below the pipe is shown in Figure 11.78. As reported in the project summary the spatial variability of the data for all variables was considerable even at very small spacing between samples and consequently no discernible spatial trends were evident. A semi-variogram analysis was conducted (see Figure 11.78 to Figure 11.81) to determine the range over which neighbouring samples were correlated. The random fluctuations in variance around a flat trend observed in these figures indicates that there is no spatial correlation between soil properties.

Table 11.6
Soil testing undertaken

Soil property	Test method reference(s)
Texture class	AS4419-2003
Moisture content	AS4454-2012 or AS1289.2.1.4-2005
pH	Rayment and Lyons (2010) 4A1 and 4B1 and B2
Resistivity	AS1289.4.4.1-1997
Chloride	Rayment and Lyons (2010) 5A1; APHA Cl B
Sulphate	AS4419-2003
Nitrate	APHA NO3 E
Phosphate	Rayment and Lyons (2010) 9C1
Total organic carbon	Rayment and Lyons (2010) 6B3
Conductivity	Rayment and Lyons (2010) 3A1
Field capacity	Abbot TS (Ed) (1987) Soil testing service – Methods and Interpretation, Dept of Agriculture NSW (Publisher)
Permanent wilt point	
	McIntyre (1974)

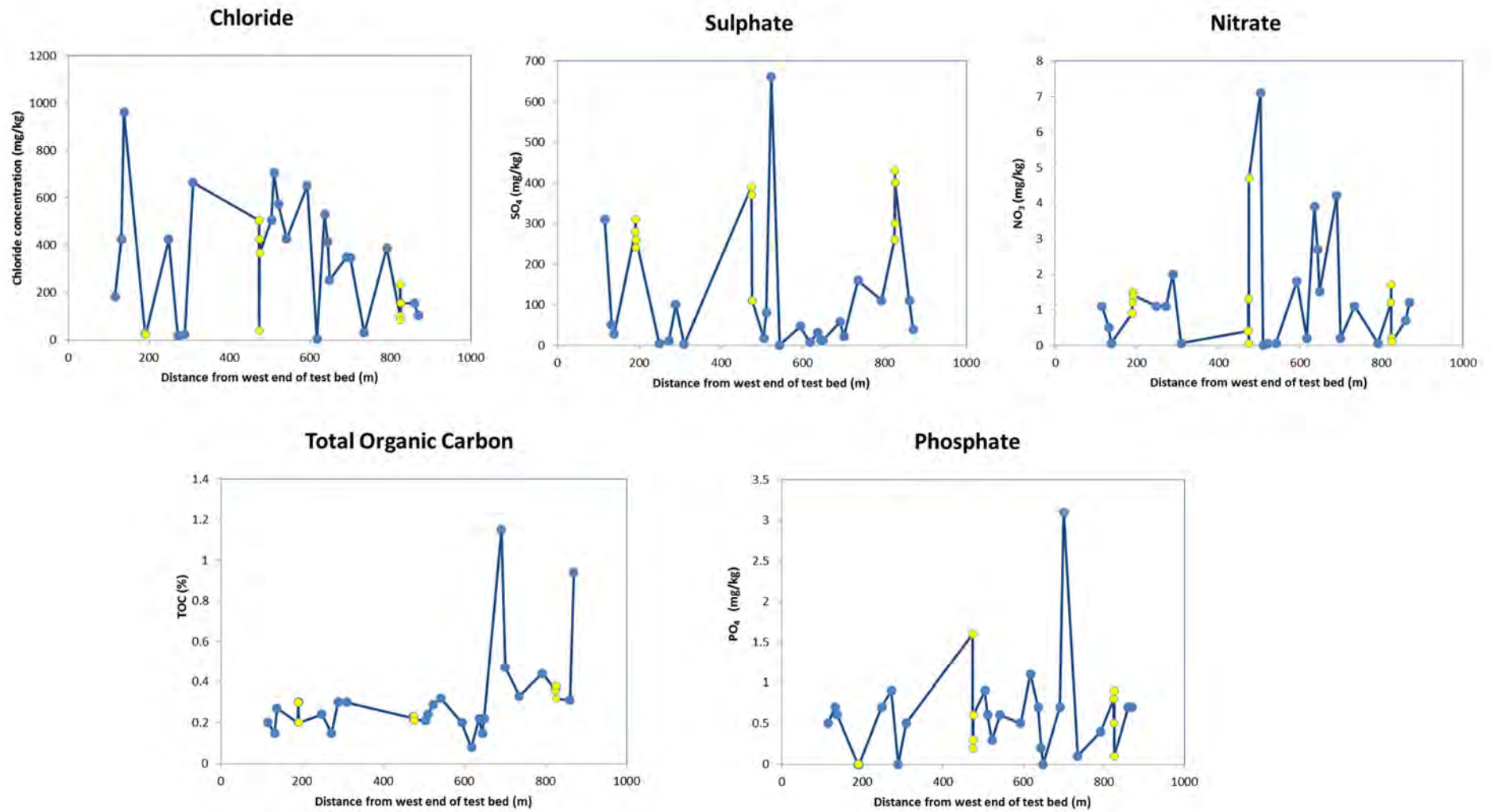


Figure 11.74 Variation in soil chemistry along the length of the Verona St test bed

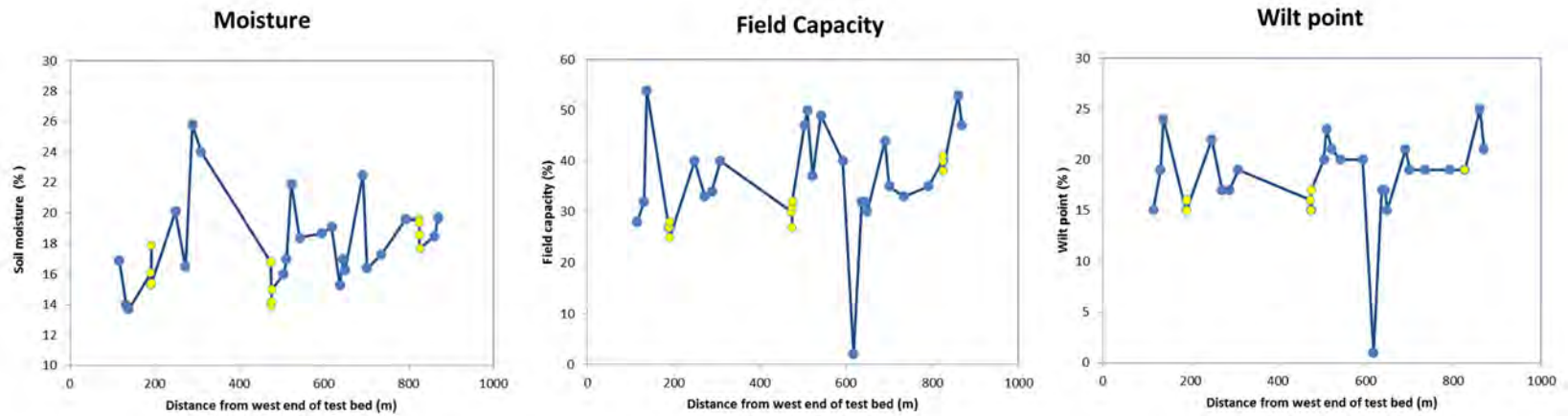


Figure 11.75. Variation in soil moisture properties along the length of the Verona St test bed

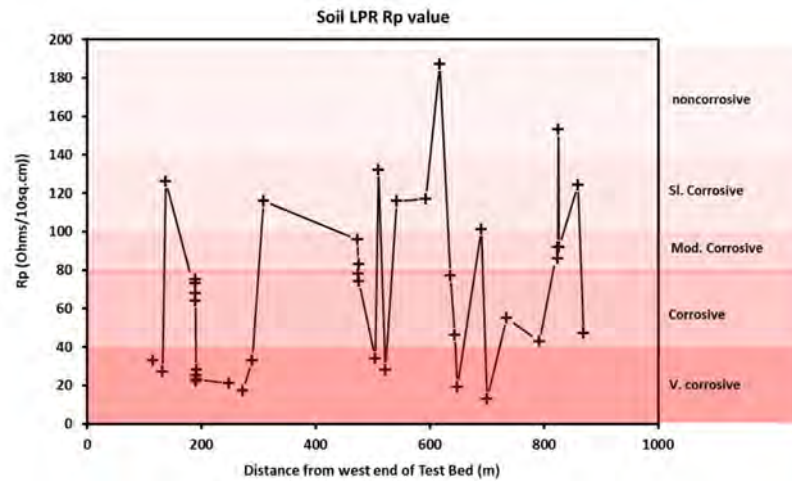


Figure 11.76. Variation in Linear Polarised Resistance Rp values at mid-pipe depth along the length of the test bed. Shaded regions show the predicted corrosivity ranges.

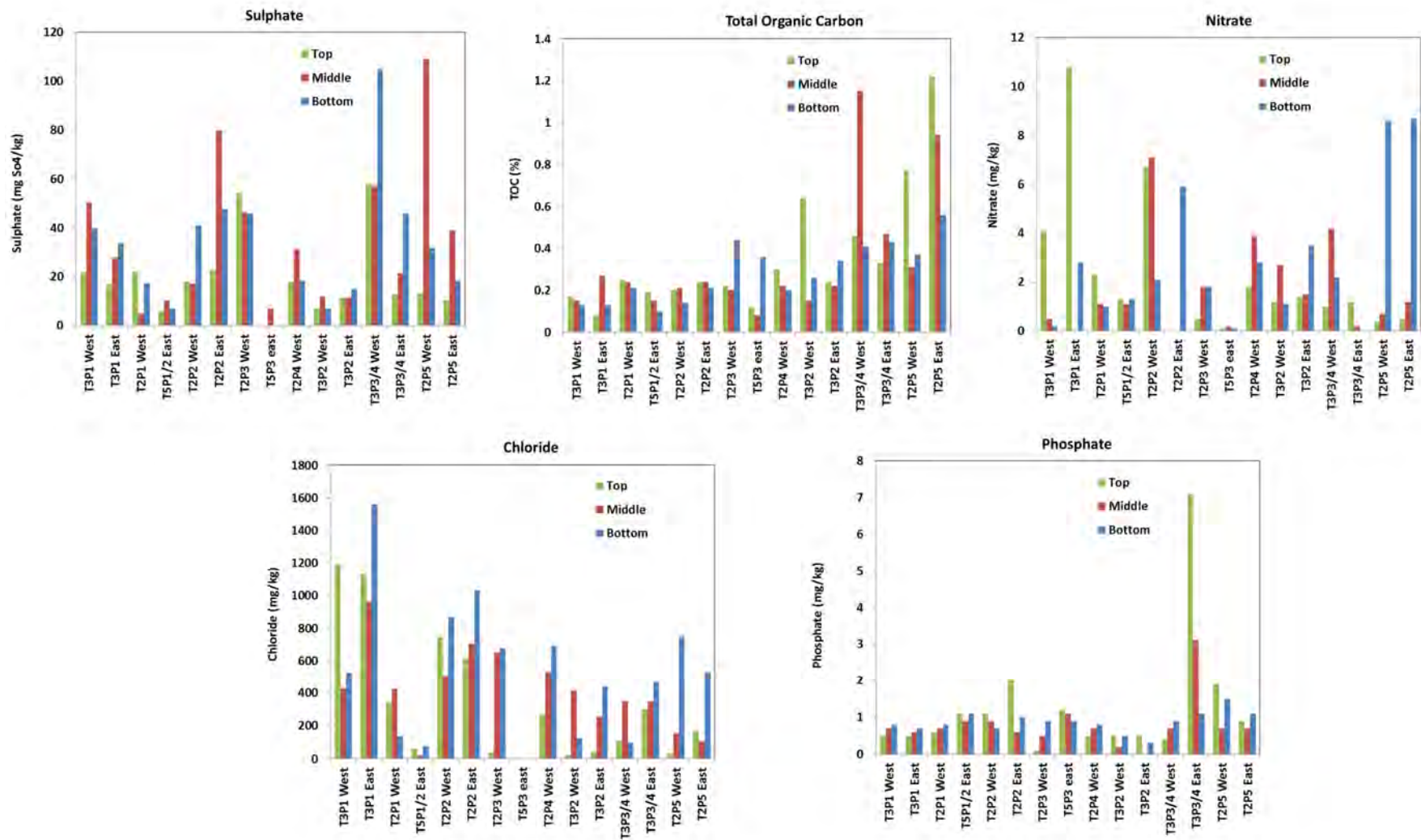


Figure 11.77. Soil chemical properties observed at the top of the pipe, adjacent to the mid depth point of the pipe and immediately underneath the pipe at various sampling pits

Table 11.7
Location and soil texture for samples taken at pipe depth along the Verona St test bed

Sample ID	Easting	Northing	Distance from West end	Texture
DL01	321908.6	6248702.4	115.3	Silty Clay
T3P1 West M	321924.1	6248698.6	131.8	Medium Clay
T3P1 East M	321930.1	6248698.6	137.8	Silty Clay
DL02+500mm to west	321981.4	6248692.6	189.4	Silty Clay
DL02	321981.9	6248692.5	189.9	Silty Clay
DL02+1m to east	321982.8	6248692.4	190.9	Silty Clay
DL02+1.6m to east	321983.5	6248692.3	191.5	Silty Clay
T2P1 West M	322039.6	6248683.4	248.5	Medium Clay
T5P1/2 East M	322081.0	6248680.6	272	MEDIUM CLAY
DL03	322079.7	6248678.7	288.6	Silty Clay
DL04	322099.9	6248675.9	309	LIGHT CLAY
DL05 +500mm to West	322263.3	6248654.7	473.9	LIGHT CLAY
DL05	322263.9	6248654.7	474.5	MEDIUM CLAY
DL05 + 1m to east	322264.9	6248654.5	475.5	LIGHT CLAY
DL05 + 1.5m to east	322265.4	6248654.4	476	LIGHT CLAY
T2P2 West M	322293.0	6248648.8	504.1	LIGHT CLAY
T2P2 east M	322299.5	6248648.8	510.5	MEDIUM CLAY
DL06	322310.8	6248648.2	522	LIGHT CLAY
DL07	322330.5	6248645.8	542.1	MEDIUM CLAY
T2P3 West M	322381.3	6248637.4	593.1	LIGHT CLAY
T5P3 East M	322405.3	6248634.8	617.2	SAND
T2P4 West M	322424.2	6248632.1	636.4	SILTY CLAY
T3P2 West M	322431.7	6248630.9	644	LIGHT CLAY
T3P2 East M	322436.2	6248630.9	648.6	LIGHT CLAY
T3P3/4 West M	322477.4	6248624.7	690.6	SILTY CLAY
T3P3/4 East M	322487.6	6248621.3	700.1	Light clay
DL08	322521.5	6248619.0	734.6	MEDIUM CLAY
DL09	322578.0	6248611.4	791.6	MEDIUM CLAY
DL10 +500mm West	322610.0	6248606.8	823.9	MEDIUM CLAY
DL10	322610.5	6248606.7	824.4	MEDIUM CLAY
DL10+800mm East	322611.3	6248606.7	825.2	MEDIUM CLAY
DL10+1.3m East	322611.7	6248606.5	825.7	MEDIUM CLAY
T2P5 West M	322645.4	6248600.7	859.9	Light clay
T2P5 East M	322655.0	6248599.1	869.1	Sandy clay

Table 11.8
Chemistries of soil properties taken at pipe depth along the Verona St test bed

Sample ID	Cl- mg/kg	SO4 mg SO4 / kg	Nitrate mg/kg	Phosphate mg/kg	TOC %
DL01	184	310	1.1	0.5	0.2
T3P1 West M	426.2	50.6	0.5	0.7	0.15
T3P1 East M	962.4	27.9	0.05	0.6	0.27
DL02+500mm to west	28.1	280	0.9	0	0.2
DL02	30.7	310	1.2	0	0.3
DL02+1m to east	27.2	240	1.5	0	0.3
DL02+1.6m to east	23.1	260	1.4	0	0.2
T2P1 West M	425.3	5	1.1	0.7	0.24
T5P1/2 East M	18.8	10.3	1.1	0.9	0.15
DL03	23.9	100	2	0	0.3
DL04	665.6	2.5	0.05	0.5	0.3
DL05 +500mm to West	505.7	390	0.4	1.6	0.22
DL05	39.2	370	1.3	0.2	0.23
DL05 + 1m to east	425.7	110	0.05	0.3	0.23
DL05 + 1.5m to east	367.1	110	4.7	0.6	0.21
T2P2 West M	507	17.1	7.1	0.9	0.21
T2P2 east M	705.9	80	0	0.6	0.24
DL06	573.2	660	0.05	0.3	0.29
DL07	427.8	<5	0.05	0.6	0.32
T2P3 West M	651.7	46.3	1.8	0.5	0.2
T5P3 East M	3.5	6.9	0.2	1.1	0.08
T2P4 West M	530	31.3	3.9	0.7	0.22
T3P2 West M	415.3	12	2.7	0.2	0.15
T3P2 East M	253.2	11.6	1.5	0	0.22
T3P3/4 West M	350	57.3	4.2	0.7	1.15
T3P3/4 East M	348.5	21.5	0.2	3.1	0.47
DL08	31.2	160	1.1	0.1	0.33
DL09	388.7	110	0.05	0.4	0.44
DL10 +500mm West	101.3	260	1.2	0.8	0.36
DL10	235.5	430	1.7	0.5	0.37
DL10+800mm East	85.5	300	0.2	0.9	0.38
DL10+1.3m East	155.9	400	0.1	0.1	0.32
T2P5 West M	154.8	109	0.7	0.7	0.31
T2P5 East M	103.8	39	1.2	0.7	0.94

Table 11.9
Moisture, texture and density properties of soil samples taken at pipe depth along the Verona St test bed

Sample ID	Moisture % (w/v)	FC %	WP %	Bulk density (g/cc)	Sand	Silt	Clay
DL01	16.9	28	15	1.93	35	25	40
T3P1 West M	14	32	19				
T3P1 East M	13.7	54	24				
DL02+500mm to west	16.1	27	15		29	27	44
DL02	15.3	27	16	1.92	29	26	45
DL02+1m to east	17.9	28	16		34	24	42
DL02+1.6m to east	15.4	25	15		34	22	44
T2P1 West M	20.1	40	22				
T5P1/2 East M	16.5	33	17				
DL03	25.8	34	17	1.86	27	31	42
DL04	24	40	19	1.93	29	28	43
DL05 +500mm to West	16.8	30	16		48	15	37
DL05	13.9	27	15	2.16	46	17	37
DL05 + 1m to east	14.2	31	15		46	15	39
DL05 + 1.5m to east	15	32	17		49	16	35
T2P2 West M	16	47	20				
T2P2 east M	17	50	23				
DL06	21.9	37	21	1.9	20	32	48
DL07	18.4	49	20	1.98	17	25	58
T2P3 West M	18.7	40	20				
T5P3 East M	19.1	2	1				
T2P4 West M	15.3	32	17				
T3P2 West M	17	32	17				
T3P2 East M	16.3	30	15				
T3P3/4 West M	22.5	44	21				
T3P3/4 East M	16.4	35	19				
DL08	17.3	33	19	1.98	29	26	45
DL09	19.6	35	19	1.91	41	15	44
DL10 +500mm West	19.6	40	19		29	21	50
DL10	19.4	41	19	2.08	29	26	45
DL10+800mm East	18.6	40	19		28	25	47
DL10+1.3m East	17.7	38	19		26	26	48
T2P5 West M	18.5	53	25				
T2P5 East M	19.7	47	21				

Table 11.10**Soil textures of samples taken above, beside and below the pipe along the Verona St test bed**

Site ID	Texture		
	Bottom	Middle	Top
T3P1 West	Silty Clay	Medium Clay	Light Clay
T3P1 East	Medium Clay	Silty Clay	Light Clay
T2P1 West	Medium Clay	Medium Clay	Medium Clay
T5P1/2 East	LIGHT CLAY	MEDIUM CLAY	SILTY CLAY
T2P2 West	FINE SANDY CLAY LOAM	LIGHT CLAY	LIGHT CLAY
T2P2 East	MEDIUM CLAY	MEDIUM CLAY	SILTY CLAY
T2P3 West	LIGHT CLAY	LIGHT CLAY	LIGHT CLAY
T5P3 east	SAND	SAND	SAND
T2P4 West	SILTY CLAY	SILTY CLAY	SILTY CLAY
T3P2 West	LIGHT CLAY	LIGHT CLAY	MEDIUM CLAY
T3P2 East	SILTY CLAY	LIGHT CLAY	LIGHT CLAY
T3P3/4 West	SILTY CLAY	SILTY CLAY	SILTY CLAY
T3P3/4 East	Light clay	Light clay	Sandy clay
T2P5 West	Light clay	Light clay	Light clay
T2P5 East	SILTY CLAY	Sandy clay	SILTY CLAY

Table 11.11
Soil moisture properties for samples taken above, beside and below pipe along the Verona St test bed

Site ID	Field Capacity (%)			Permanent Wilt Point (%)		
	Bottom	Middle	Top	Bottom	Middle	Top
T3P1 West	37	32	42	19	19	21
T3P1 East	47	54	57	21	24	22
T2P1 West	33	40	50	18	22	22
T5P1/2 East	28	33	27	13	17	11
T2P2 West	33	47	37	12	20	17
T2P2 East	46	50	44	23	23	23
T2P3 West	41	40	43	20	20	21
T5P3 east	2	2	2	1	1	1
T2P4 West	31	32	30	16	17	17
T3P2 West	34	32	29	18	17	15
T3P2 East	30	30	28	14	15	15
T3P3/4 West	44	44	43	21	21	22
T3P3/4 East	33	35	35	18	19	17
T2P5 West	59	53	35	24	25	17
T2P5 East	34	47	33	17	21	16

Table 11.12
Soil chemistries for samples taken above, beside and below pipe along the Verona St test bed

	Chloride (mg/kg)			Sulphate (1:5) mg So4/kg			Nitrate Nitrogen NO3-N (mg/kg)			Phosphate (mg/kg)		
	Bottom	Middle	Top	Bottom	Middle	Top	Bottom	Middle	Top	Bottom	Middle	Top
T3P1 West	526.2	426.2	1193.3	39.9	50.6	22	0.2	0.5	4.1	0.8	0.7	0.5
T3P1 East	1561.1	962.4	1133.1	33.8	27.9	17	2.8	0	10.8	0.7	0.6	0.5
T2P1 West	132.5	425.3	343.9	17.4	5	22.1	1	1.1	2.3	0.8	0.7	0.6
T5P1/2 East	79.6	18.8	61.2	6.9	10.3	6.1	1.3	1.1	1.3	1.1	0.9	1.1
T2P2 West	869.6	507	744.3	41	17.1	18	2.1	7.1	6.7	0.7	0.9	1.1
T2P2 East	1031.9	705.9	612.7	47.7	80	22.9	5.9	0	0	1	0.6	2
T2P3 West	676.7	651.7	40.6	46	46.3	54.3	1.8	1.8	0.5	0.9	0.5	0.1
T5P3 east	<7	<7	<7	<5	6.9	<5	0.1	0.2	0.1	0.9	1.1	1.2
T2P4 West	692.5	530	271.8	18.4	31.3	17.8	2.8	3.9	1.8	0.8	0.7	0.5
T3P2 West	123.5	415.3	22.8	6.9	12	6.9	1.1	2.7	1.2	0.5	0.2	0.5
T3P2 East	438.6	253.2	43.6	15.1	11.6	11.6	3.5	1.5	1.4	0.3	0	0.5
T3P3/4 West	93.9	350	107.2	105	57.3	58	2.2	4.2	1	0.9	0.7	0.4
T3P3/4 East	466.3	348.5	303	45.9	21.5	12.9	0	0.2	1.2	1.1	3.1	7.1
T2P5 West	750.5	154.8	33.9	31.8	109	13.2	8.6	0.7	0.4	1.5	0.7	1.9
T2P5 East	526.7	103.8	171.4	18.2	39	10.5	8.7	1.2	0.5	1.1	0.7	0.9

Table 11.13
Soil moisture and densities for samples taken above, beside and below pipe along the Verona St test bed

	Moisture (% w/v)			Bulk Density (g/ml)		
	Bottom	Middle	Top	Bottom	Middle	Top
T3P1 West	16.1	14	16	1.13	1.16	1.13
T3P1 East	18.1	13.7	16.8	1.22	1.09	1.15
T2P1 West	17.4	20.1	19.5	0.99	1.12	1.22
T5P1/2 East	17.9	16.5	10.1	1.22	1.04	1.14
T2P2 West	16.1	16	17.6	1.18	1.19	1.13
T2P2 East	15.8	17	17	1.06	1.17	1.17
T2P3 West	20.2	18.7	21.6	1.06	1.1	1.08
T5P3 east	19.3	19.1	20.4	1.48	1.49	1.49
T2P4 West	15.3	15.3	16.3	1.1	1.14	1.13
T3P2 West	17	17	16.4	1.14	1.16	1.17
T3P2 East	22.5	16.3	15.4	1.16	1.16	1.16
T3P3/4 West	21	22.5	19.4	1.01	0.98	1.12
T3P3/4 East	18.6	16.4	15.8	1.04	0.99	1.12
T2P5 West	21.2	18.5	19.1	0.99	1.12	1.01
T2P5 East	16.3	19.7	17.6	1.1	1.23	1.25

Table 11.14
Soil properties for clustered samples - Verona St test bed

Sample ID	Distance from neighbours (m)	Texture	Cl mg/kg	SO4 ²⁻ mg SO4 / kg	NO ₃ -N mg/kg	PO ₄ mg/kg
DL02+500mm to west	0	Silty Clay	28.1	280	0.9	0
DL02	0.5	Silty Clay	30.7	310	1.2	0
DL02+1m to east	1.5	Silty Clay	27.2	240	1.5	0
DL02+1.6m to east	2.1	Silty Clay	23.1	260	1.4	0
DL05 +500mm to West	0	LIGHT CLAY	505.7	390	0.4	1.6
DL05	0.6	MEDIUM CLAY	39.2	370	1.3	0.2
DL05 + 1m to east	1.6	LIGHT CLAY	425.7	110	0.05	0.3
DL05 + 1.5m to east	2.1	LIGHT CLAY	367.1	110	4.7	0.6
DL10 +500mm West	0	MEDIUM CLAY	101.3	260	1.2	0.8
DL10	0.5	MEDIUM CLAY	235.5	430	1.7	0.5
DL10+800mm East	1.3	MEDIUM CLAY	85.5	300	0.2	0.9
DL10+1.3m East	1.8	MEDIUM CLAY	155.9	400	0.1	0.1

Table 11.15
Soil moisture and textural properties for clustered samples - Verona St test bed

Sample ID	Moisture (%w/v)	Field Capacity %	Wilt Point capacity %	Clay	Silt	Sand
DL02+500mm to west	16.1	27	15	44	27	29
DL02	15.3	27	16	45	26	29
DL02+1m to east	17.9	28	16	42	24	34
DL02+1.6m to east	15.4	25	15	44	22	34
DL05 +500mm to West	16.8	30	16	37	15	48
DL05	13.9	27	15	37	17	46
DL05 + 1m to east	14.2	31	15	39	15	46
DL05 + 1.5m to east	15	32	17	35	16	49
DL10 +500mm West	19.6	40	19	50	21	29
DL10	19.4	41	19	45	26	29
DL10+800mm East	18.6	40	19	47	25	28
DL10+1.3m East	17.7	38	19	48	26	26

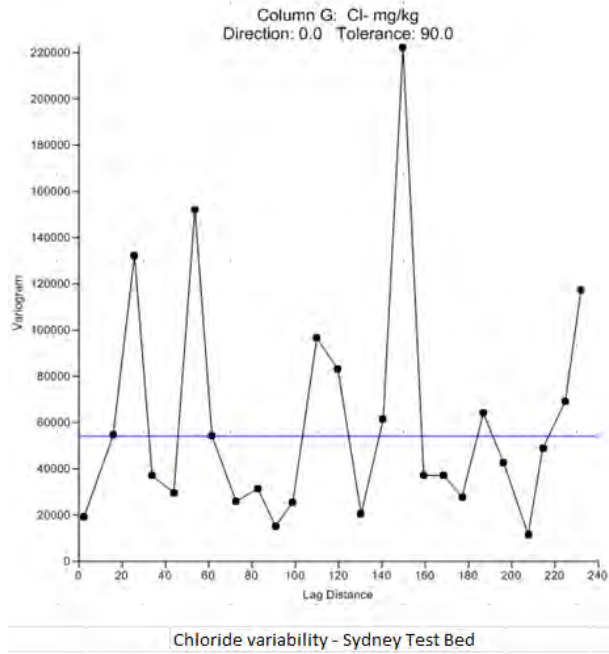


Figure 11.78. Semi variogram of soil chloride variability. The random fluctuations around a flat trend indicates that there was no spatial correlation between soil properties.

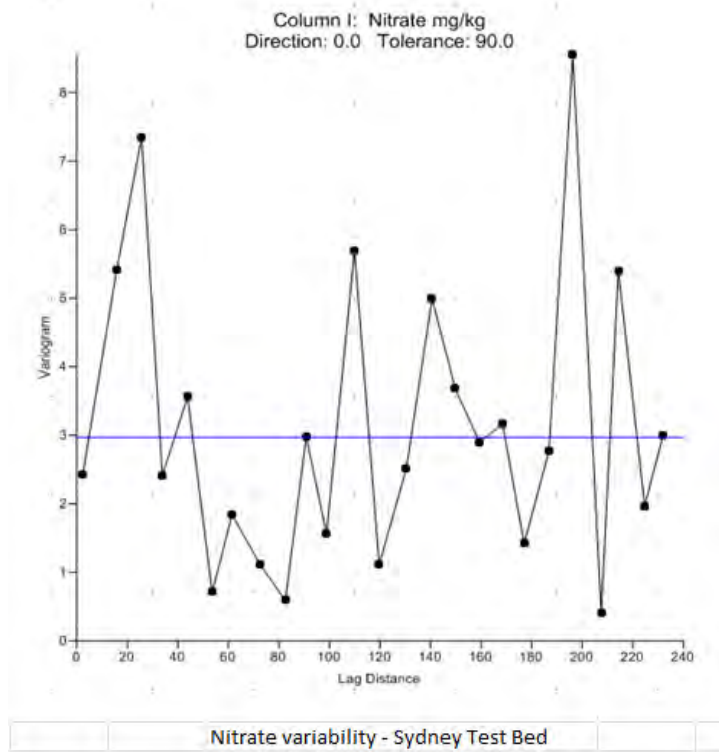
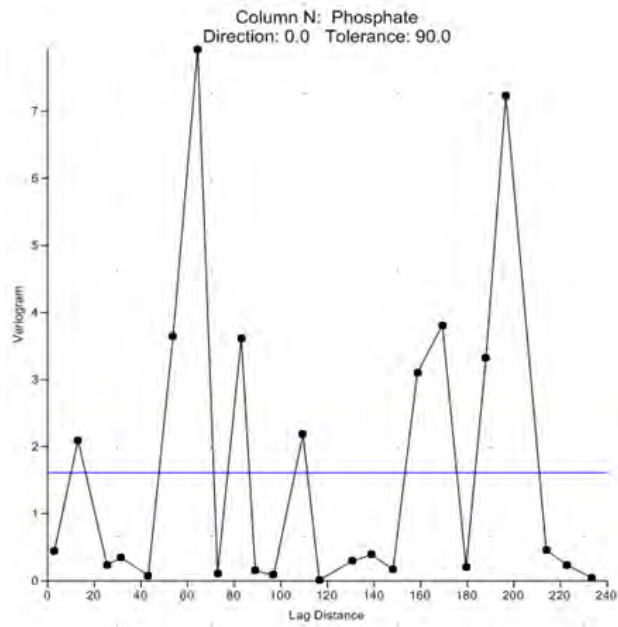
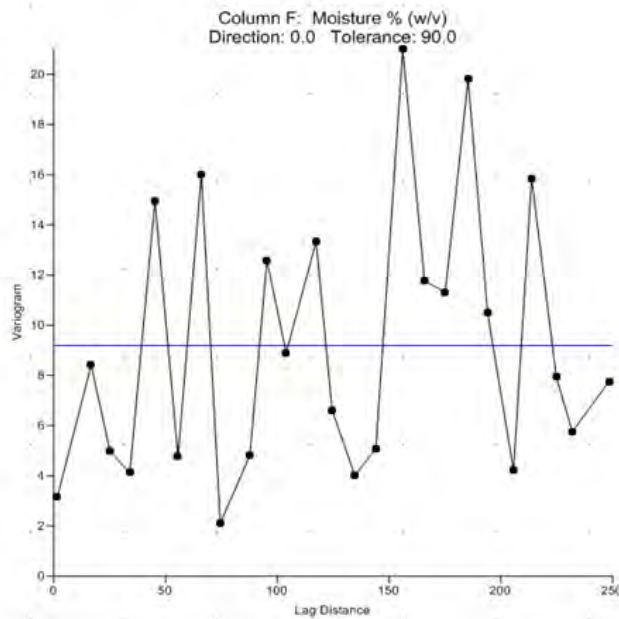


Figure 11.79. Semi variogram of soil nitrate variability. The random fluctuations around a flat trend indicates that there was no spatial correlation between soil properties.



Phosphate variability - Sydney Test Bed

Figure 11.80. Semi variogram of soil phosphate variability. The random fluctuations around a flat trend indicates that there was no spatial correlation between soil properties.



Soil moisture variability - Sydney Test Bed

Figure 11.81. Semi variogram of soil moisture variability. The random fluctuations around a flat trend indicates that there was no spatial correlation between soil properties.

11.5.6 Activity 4c: Soils Data for Perth Subiaco and Fremantle Sites

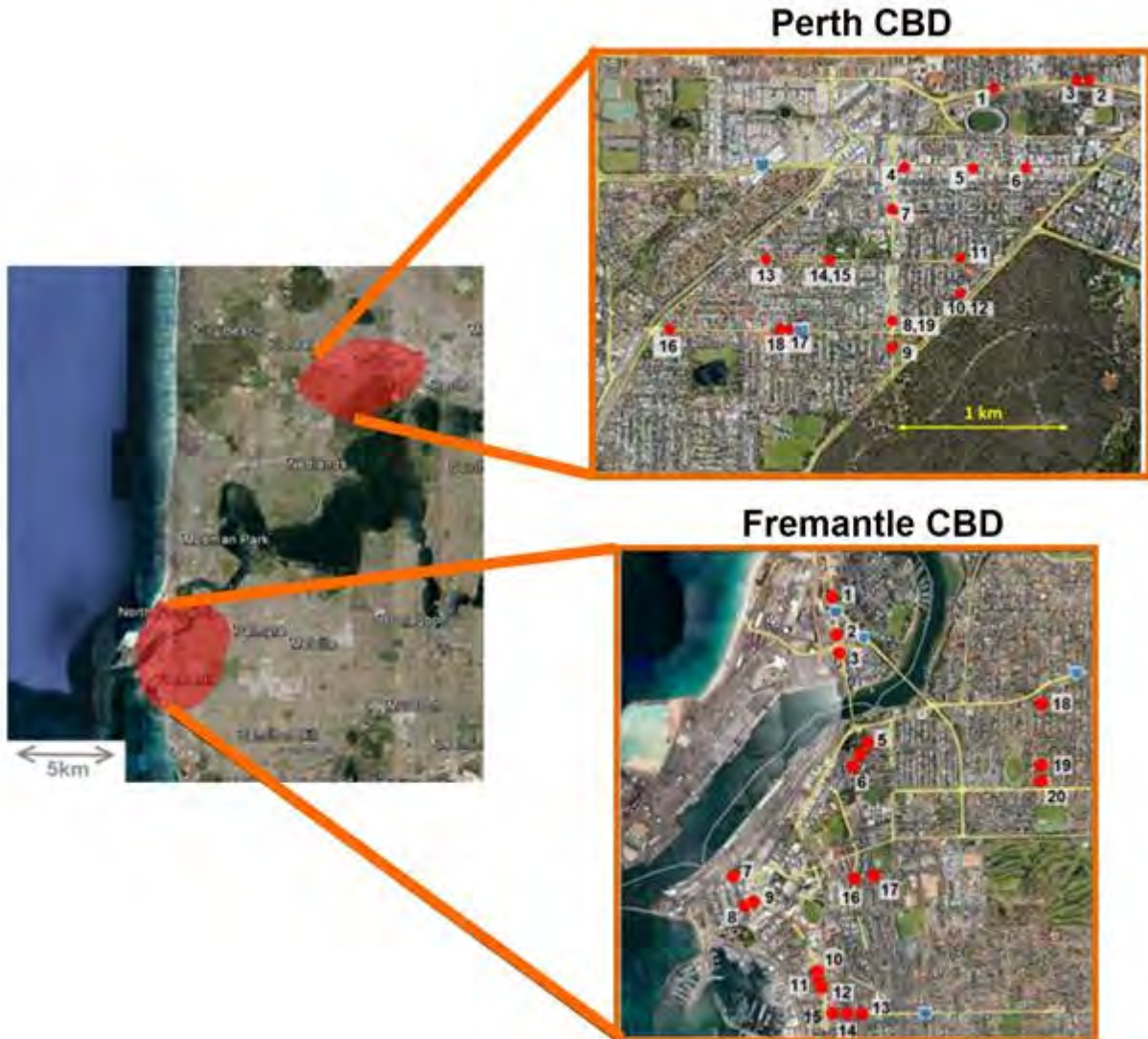


Figure 11.82. Location of the Perth and Fremantle soil sampling locations

Soil sampling campaigns were also conducted in the Perth and Fremantle CBD areas in Western Australia. In these locations the soils are predominantly sandy and so offer a contrast to the clay rich soils of the Sydney sampling sites. All samples were taken at pipe depth with the distance between adjacent samples ranging from 2 m to 3 km at the Perth site and 30 m to 3 km apart at the Fremantle location. Sample collection and analysis followed the same procedures as detailed earlier for the Sydney test site. Soil properties for the Fremantle sites are listed in Table 11.16 and Table 11.17. Soil property variogram analyses for Fremantle samples are shown in Figure 11.83 to Figure 11.86. Perth data are shown in Table 11.18 to Table 11.20 and semi variogram figures shown in Figure 11.87 to Figure 11.89.

Table 11.16

Location of Fremantle soil samples and dates in which pipes laid at those locations. Also, moisture content and resistivity values for those locations are listed.

Loc #	Easting (m)	Northing (m)	When pipe installed	Moisture Content (%)	Resistivity
1	382246.2	6455206.8	1969.0	12.6	6990
2	382293.6	6454911.1	1969.0	2.9	11100
3	382325.2	6454765.8	1969.0	5.9	9900
4	382554.1	6454017.6	1934.0	3.8	9170
5	382553.3	6454011.4	1934.0	14.3	10800
6	382453.7	6453856.3	1934.0	9	5260
7	381492.1	6452934.7	1958.0	6	6900
8	381632.9	6452731.2	1961.0	6.3	5350
9	381578.5	6452709.6	1961.0	7	9710
10	382170.8	6452164.0	1980.0	8	5240
11	382197.3	6452102.6	1980.0	9.7	6800
12	382206.4	6452071.5	1980.0	7.7	4220
13	382542.4	6451845.4	1932.0	14	3920
14	382427.3	6451839.8	1932.0	11.5	7410
15	382329.3	6451838.6	1932.0	10.3	5590
16	382470.7	6452949.7	1927.0	12.8	2700
17	382613.4	6452963.1	1927.0	6.4	2500
21	382634.7	6452962.6	1905.0	3	5880
18	383969.5	6454367.7	1933.0	6	2600
19	383975.9	6453877.2	1933.0	6.7	8400
20	383975.7	6453751.6	1933.0	5.5	3010

Table 11.17
Soil chemistries of Fremantle soil samples

Sample ID	Total Alkalinity as CaCO ₃	Bicarbonate Alkalinity as CaCO ₃	Carbonate Alkalinity as CaCO ₃	Sulfate as SO ₄ ²⁻	Chloride	Nitrite as N (Sol.)	Nitrate as N (Sol.)	Nitrite + Nitrate as N (Sol.)	Reactive Phosphorus as P	Total Organic Carbon
1	1970	1920	51	20	10	<0.1	0.4	0.4	0.2	0.32
2	653	593	60	<10	<10	<0.1	<0.1	<0.1	<0.1	0.05
3	2180	2120	66	<10	<10	<0.1	0.3	0.3	<0.1	0.22
4	668	640	28	<10	20	<0.1	0.2	0.2	0.2	0.45
5	1380	1320	63	<10	20	<0.1	<0.1	<0.1	<0.1	0.21
6	776	749	27	<10	20	<0.1	0.4	0.4	<0.1	0.34
7	781	744	37	<10	<10	<0.1	0.3	0.3	0.2	0.09
8	1080	1030	47	20	10	<0.1	0.3	0.3	0.3	0.12
9	386	361	25	<10	<10	<0.1	0.2	0.2	0.3	0.06
10	833	789	44	10	40	<0.1	0.4	0.4	0.3	0.1
11	478	447	31	10	30	<0.1	0.1	0.1	0.2	0.12
12	414	380	34	<10	<10	<0.1	7.6	7.6	0.3	0.09
13	2350	2320	34	30	20	0.5	11.9	12.4	<0.1	0.36
14	1740	1700	48	10	20	<0.1	3	3	<0.1	0.19
15	2170	2110	60	50	3	<0.1	0.6	0.6	0.3	0.58
16	1630	1570	58	60	90	<0.1	2.6	2.6	<0.1	0.59
17	2080	1930	150	20	80	0.2	0.1	0.3	0.7	0.23
21	268	232	36	20	30	0.1	1.5	1.6	0.4	0.11
18	103	92	12	10	60	<0.1	1.4	0.4	0.7	0.36
19	47	41	6	<10	10	0.1	1.7	1.8	0.3	0.56
20	27	27	<1	10	30	0.2	0.3	0.5	0.7	0.29

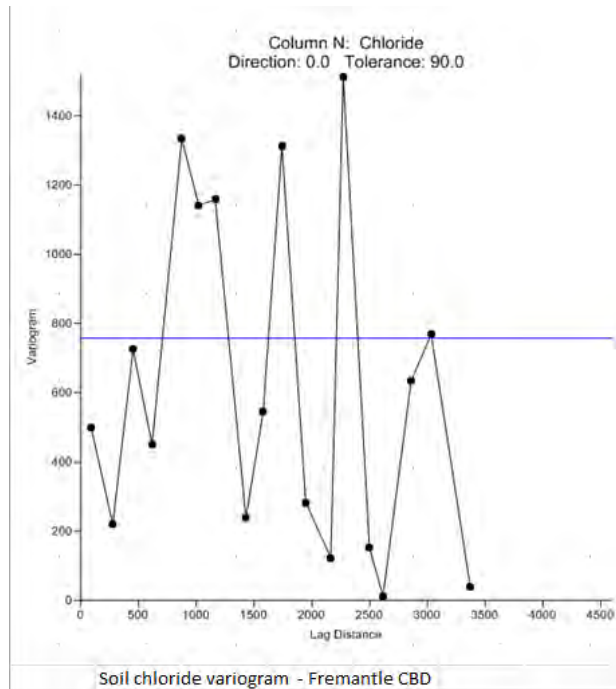


Figure 11.83. Semi variogram of soil chloride variability (Fremantle sites). The random fluctuations around a flat trend indicates that there was no spatial correlation between soil properties.

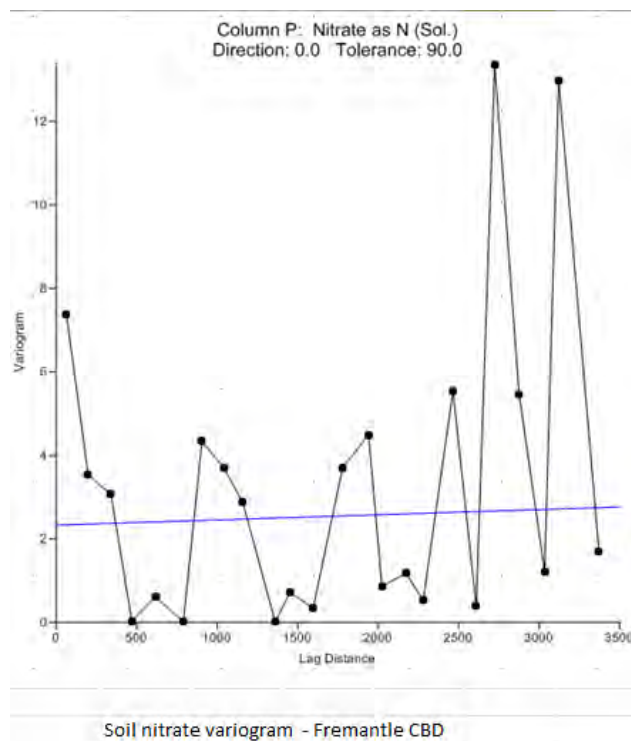


Figure 11.84. Semi variogram of soil nitrate variability (Fremantle sites). The random fluctuations around a flat trend indicates that there was no spatial correlation between soil properties.

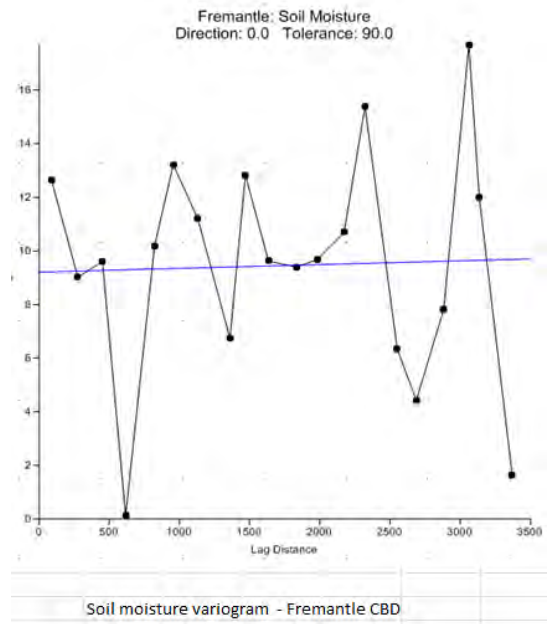


Figure 11.85. Semi variogram of soil moisture variability (Fremantle sites). The random fluctuations around a flat trend indicates that there was no spatial correlation between soil properties.

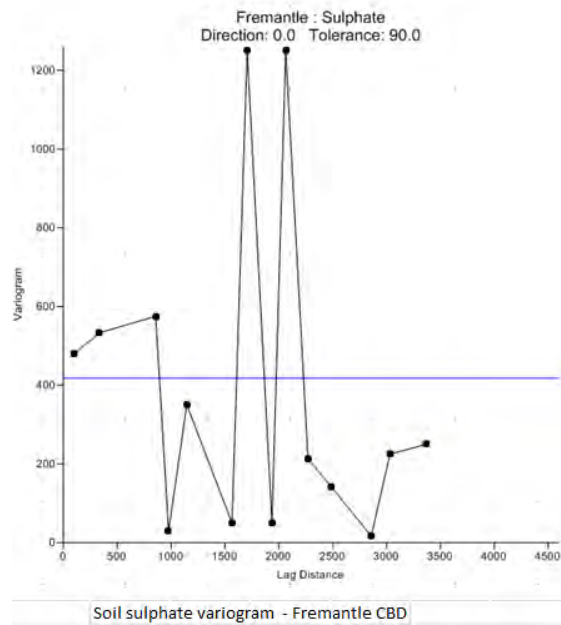


Figure 11.86. Semi variogram of soil sulphate variability (Fremantle sites). The random fluctuations around a flat trend indicates that there was no spatial correlation between soil properties.

Table 11.18
Locations, soil texture/colour, conductivity and moisture levels for Perth CBD samples

Sample ID	Eastings (m)	Northings (m)	Colour	Texture	Conductivity	Moisture
1	389470.373	6465326.82	Yellowish Brown	Sand	13	1.4
2	390070.609	6465375.746	Dark Yellowish	Sand	10	1.4
3	390011.979	6465377.555	Dark Yellowish	Sand	22	3
4	388916.453	6464825.922	Brown	Sand	38	5.5
5	389348.697	6464820.738	Dark Yellowish	Sand	68	4.8
6	389676.753	6464825.833	Dark Yellowish	Sand	66	<1
7	388846.247	6464562.188	Dark Yellowish	Sand	91	1.8
8	388851.443	6463866.422	Dark Yellowish	Sand	62	1.7
9	388849.225	6463696.475	Dark Yellowish	Sand	49	1.8
10	389269.96	6464043.28	Dark Yellowish	Sand	27	5
11	389270.035	6464263.013	Dark Brown	Sand	25	1.8
12	389269.707	6464048.852	Dark Yellowish	Sand	27	5
13	388056.184	6464242.819	Dark Yellowish	Sand	24	2
14	388453.204	6464241.279	Dark Brown	Sand	12	4.2
15	388452.055	6464242.597	Yellowish Brown	Sand	15	1.1
16	387447.014	6463800.987	Brown	Sand	56	2.2
17	388159.899	6463799.937	Dark Yellowish	Sand	30	1.3
18	388197.161	6463798.016	Dark Greyish Brown	Sand	5	1.7
19	388849.476	6463864.771	Dark Yellowish	Sand	88	1.3

Table 11.19
Soil chemistries and densities for Perth CBD samples

Sample ID	Resistivity	Total Alkalinity as CaCO₃	Bicarbonate Alkalinity as CaCO₃	Carbonate Alkalinity as CaCO₃	Bulk Density
1	76900	13	13	<1	1.555
2	5260	4	4	<1	
3	45400	10	10	<1	1.594
4	12000	28	28	<1	
5	14700	53	48	5	1.771
6	15200	85	78	7	1.644
7	5290	89	77	12	
8	16100	56	50	7	1.584
9	20400	52	44	8	1.706
10	37000	23	22	1	
11	11800	4	4	<1	1.52
12	37000	23	22	1	
13	41700	7	7	<1	1.633
14	83300	11	11	<1	1.66
15	17500	6	6	<1	
16	3910	8	8	<1	1.658
17	7690	1	1	<1	
18	9800	5	5	<1	1.717
19	5400	39	37	2	

Table 11.20
Soil chemistries for Perth CBD samples continued

Sample ID	Total Alkalinity as CaCO₃	Carbonate Alkalinity as CaCO₃	Sulfate as SO₄ 2-	Chloride	Nitrite as N (Sol.)	Nitrate as N (Sol.)	Nitrite + Nitrate as N (Sol.)	Reactive Phosphorus as P
1	13	<1	<10	30	0.4	0.8	1.2	1.4
2	4	<1	<10	20	<0.1	0.6	0.6	0.3
3	10	<1	<10	40	0.2	0.3	0.5	1
4	28	<1	<10	20	0.1	0.3	0.4	0.6
5	53	5	<10	20	0.2	0.3	0.5	0.6
6	85	7	10	20	0.2	1	1.2	0.7
7	89	12	40	40	<0.1	0.6	0.6	0.2
8	56	7	<10	40	0.2	1	1.2	1
9	52	8	<10	10	0.2	0.6	0.8	0.8
10	23	1	<10	20	0.2	0.4	0.6	0.7
11	4	<1	20	30	0.1	0.4	0.5	0.9
12	23	1	<10	20	0.2	0.4	0.6	0.7
13	7	<1	20	40	0.4	0.5	0.9	1.4
14	11	<1	<10	20	0.3	1.2	1.5	1.1
15	6	<1	<10	20	0.1	0.6	0.7	0.6
16	8	<1	10	100	0.3	0.5	0.8	1
17	1	<1	<10	60	0.1	0.2	0.3	0.4
18	5	<1	<10	<10	<1	0.3	0.3	0.2
19	39	2	20	60	<0.1	0.5	0.5	0.3

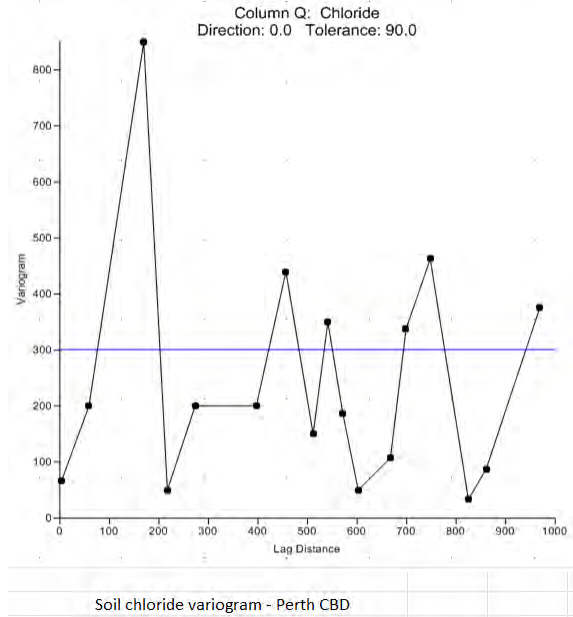


Figure 11.87. Semi variogram of soil chloride variability (Perth sites). The random fluctuations around a flat trend indicates that there was no spatial correlation between soil Rp values.

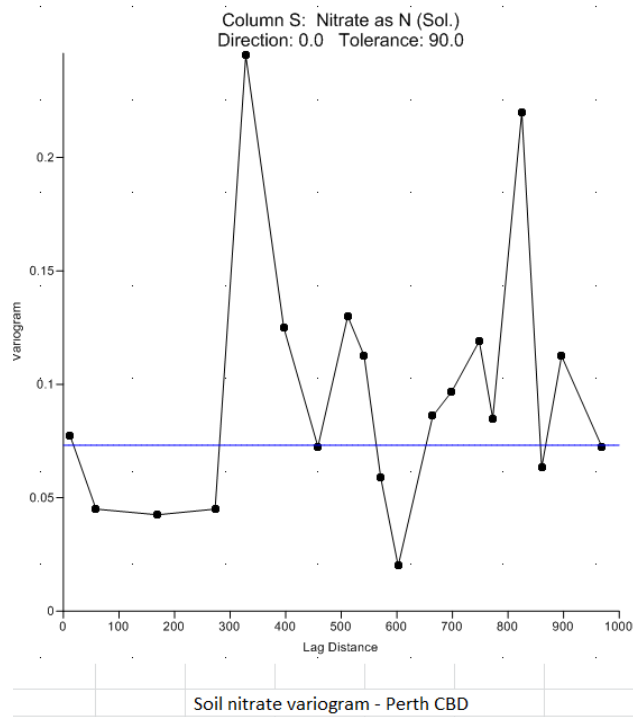


Figure 11.88. Semi variogram of soil nitrate variability (Perth sites). The random fluctuations around a flat trend indicates that there was no spatial correlation between soil Rp values.

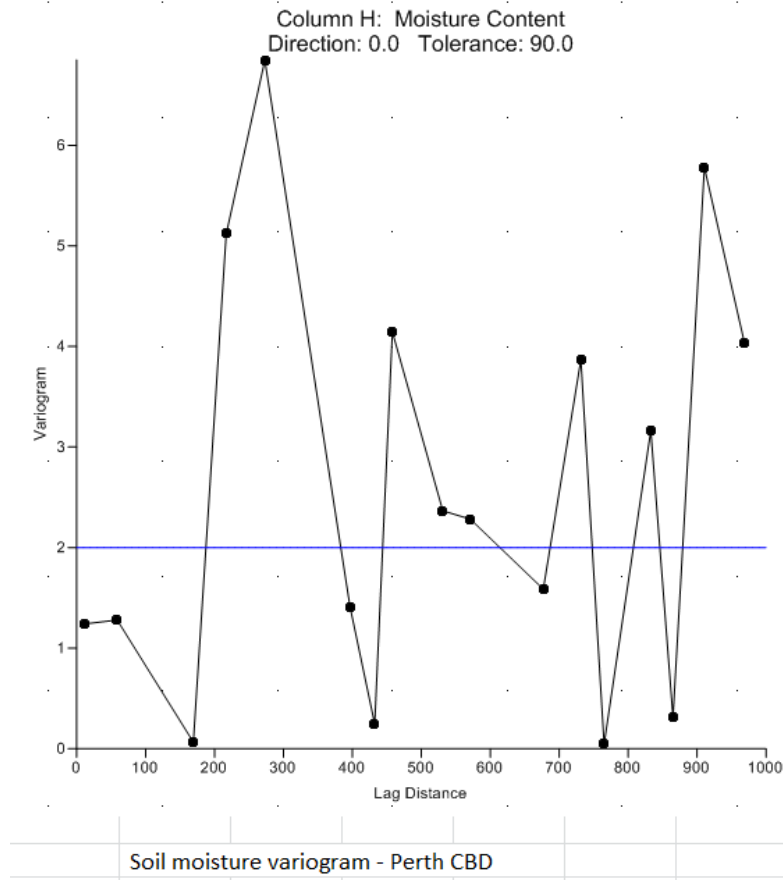


Figure 11.89. Semi variogram of soil moisture variability (Perth sites). The random fluctuations around a flat trend indicates that there was no spatial correlation between soil Rp values.

As reported in the project summary the spatial variability of the data for all variables mirrored that observed earlier for the Sydney samples, that is, there was no discernible correlation between neighbouring sample soil properties irrespective of how closely the samples were taken.

The consequence of the lack of correlation is that there is no meaningful method of interpolating soil properties from a finite, practical sampling survey. Instead a survey of soil samples can only be used to determine the likely average value (and likely variation around that average) of soil properties that will be observed throughout the sampled region.

11.5.7 Activity 4c: Long-Term Soil Moisture Data for Verona St Test Bed (Sydney)

Long-term soil moisture was carried out at the Verona Street test bed in order to determine the following:

- (1) The variation in soil moisture at pipe depth over time
- (2) The variation in long-term soil moisture trends over distance

To monitor the soil moisture content 10 soil moisture sensors were installed along the length of the Sydney Water Verona St test bed. The sensors (MadgeTech SMR101A loggers coupled with Echo EC-3 moisture sensors (Figure 11.90)) were installed in July 2015.



Figure 11.90. Logger/sensor unit deployed for long-term soil moisture studies

The monitors were programmed to record soil moisture data every 10 minutes. All the sensors were installed in close proximity to the centreline of the pipe in the original backfill (Figure 11.91). Care was taken to choose locations that haven't been disturbed for other experiments (see locations in Table 11.21). To install the moisture sensors trenches were dug at each location of sufficient depth to install the sensor at the mid height of the pipe.

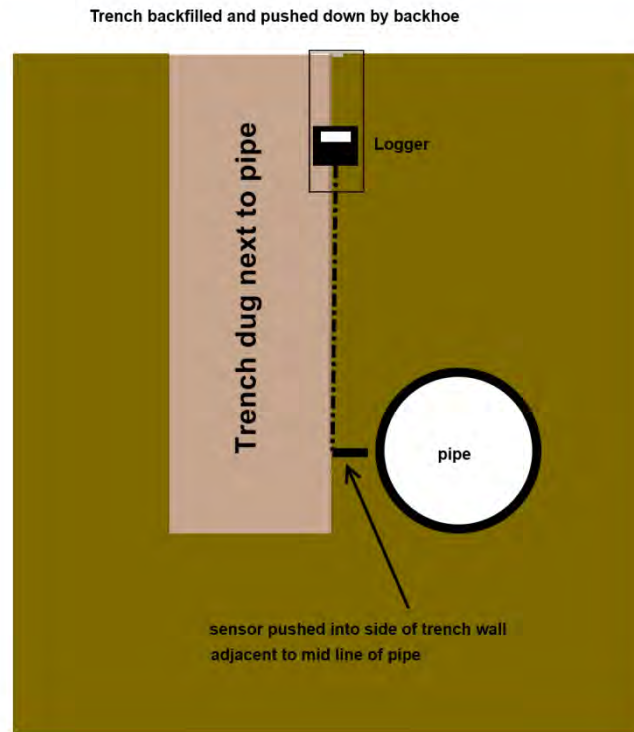


Figure 11.91. Placement of SM sensors next to pipe



Figure 11.92. Soil moisture sensor location next along the test bed

Table 11.21
Locations of long-term soil moisture sensors

Sensor ID	Latitude (°)	Longitude (°)
Sensor 1	-33.887018°	151.074193°
Sensor 2	-33.887120°	151.074980°
Sensor 3	-33.887263°	151.076036°
Sensor 4	-33.887294°	151.076252°
Sensor 5	-33.887511°	151.078020°
Sensor 6	-33.887573°	151.078527°
Sensor 7	-33.887603°	151.078743°
Sensor 8	-33.887869°	151.080802°
Sensor 9	-33.887951°	151.081416°
Sensor 10	-33.888002°	151.081761°

11.5.7.1 Results

During the course of the trial there were a number of failures. Sensor 3 failed almost immediately upon installation. Sensors 2, 7 and 9 began reporting highly variable readings after 5, 9 and 5 months respectively, most likely due to moisture infiltration into the logger. All remaining sensors were still functioning at the time of writing this report.

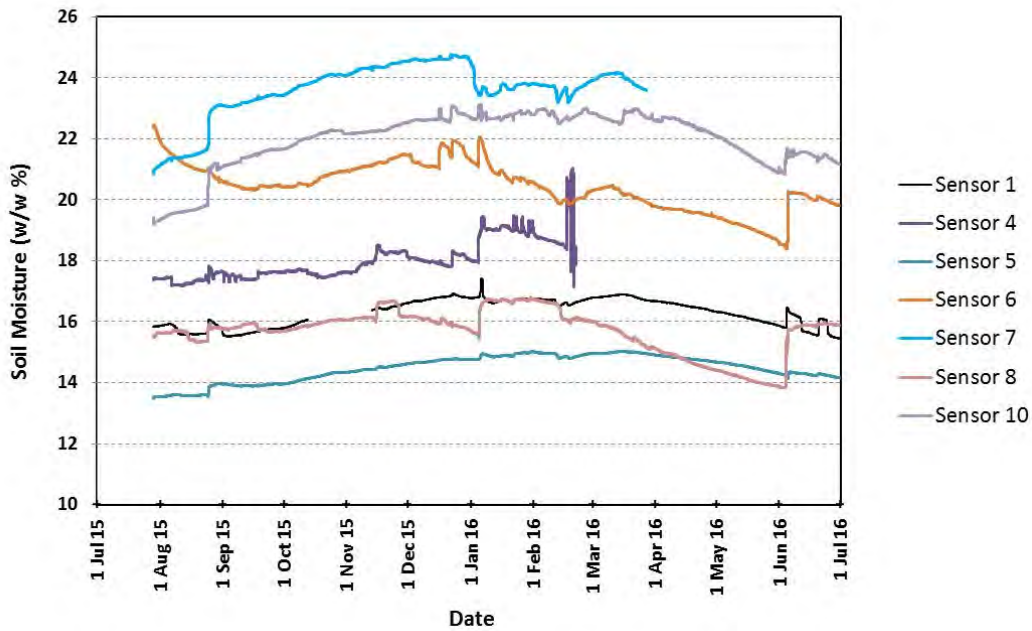


Figure 11.93. Long-term trends in soil moisture along the Verona St test bed at mid pipe depth

The data from functioning sensors is shown in Figure 11.93. The general trend over time was consistent at all locations. Namely that after a settling period of several months the trend in soil moisture over time was fairly constant at any given location. At the depth of the sensors (1.5 to 2m) there was only a muted response to rainfall events (Figure 11.94). This was due to 3 reasons: (1) the depth of the sensors; (2) the nature of the soil surrounding the pipe (clay) which dampened transport of moisture throughout the soil column and (3) the fact that the soil moisture was likely already at or close to the field capacity at all sites (again see Figure 11.94).

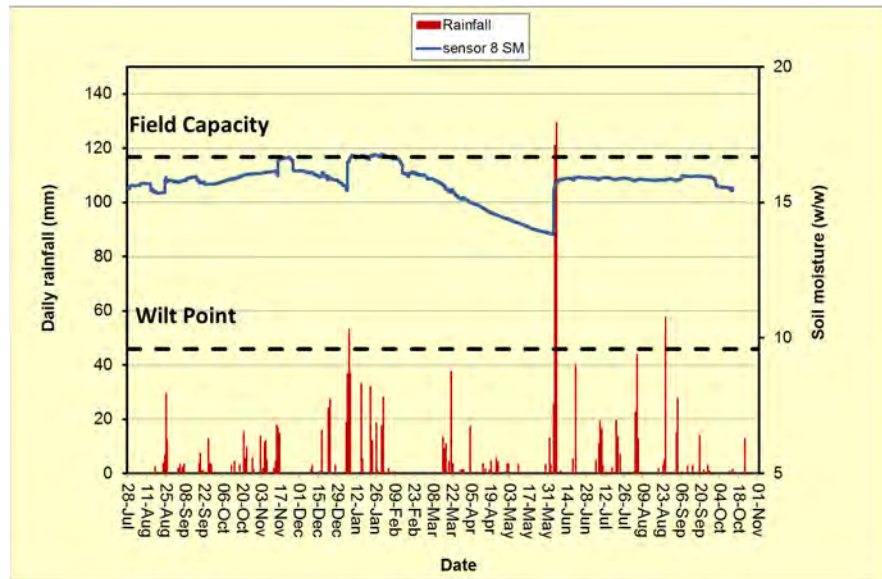


Figure 11.94. Response of sensor 8 soil moisture level to local rainfall

Inspection of Figure 11.93 however reveals that while soil moisture was relatively constant over time at all locations there was a considerable degree of variation in soil moisture between sites even across the length of the test bed. This degree of spatial variation is in accordance with the level of variation observed in one off soil moisture measurements taken from grab samples throughout the course of the study. Figure 11.95 shows the average of the long-term soil moisture data plotted with one off soil moisture data obtained throughout the study – in both cases there was a considerable degree of variability even on small spatial scales.

11.5.7.2 Summary

A number of long-term soil moisture monitors have been installed along the length of the Sydney Water Verona St test bed at pipe depth to determine the nature of long-term trends in soil moisture that impact on corrosion rates for cast iron pipes.

Results obtained after almost a year of operations show that soil moisture is relatively steady over time at each location and is not overly sensitive to rainfall events. A considerable site to site variation in moisture levels however was observed which is in accordance with findings obtained from the analysis of grab samples.

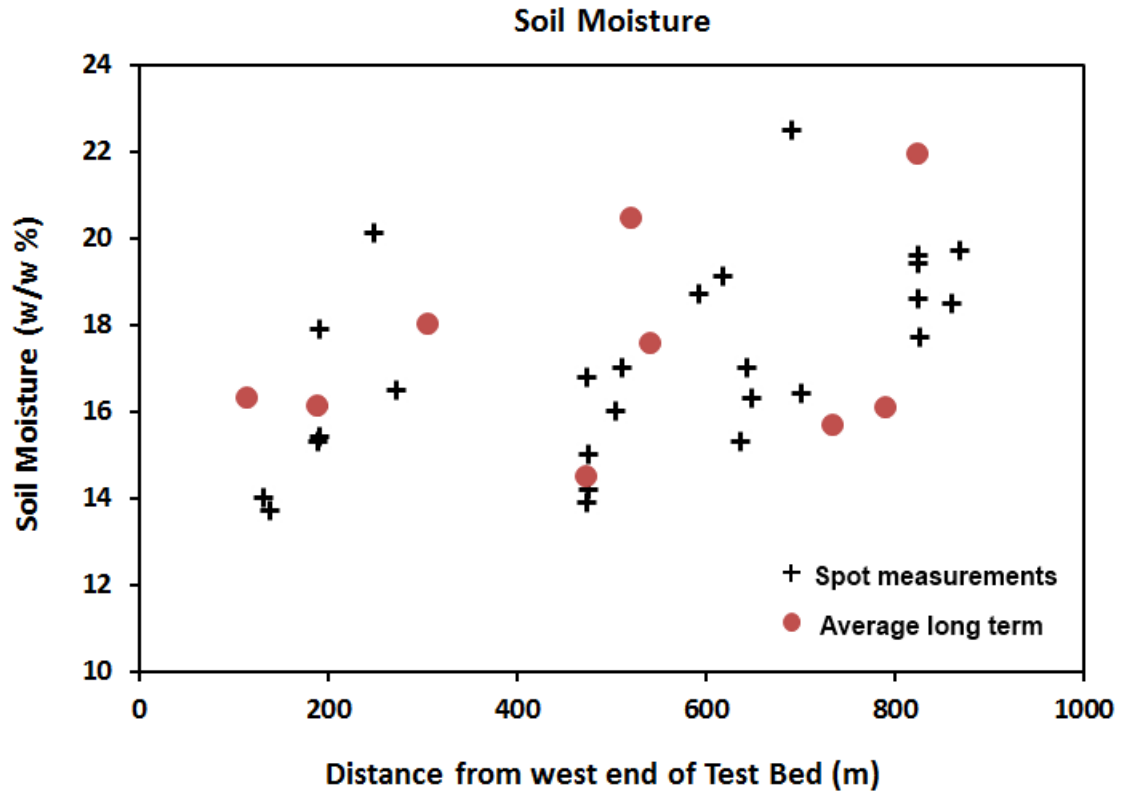


Figure 11.95. Variation in soil moisture levels along the length of the Verona St test bed

REFERENCES

- Adamchuk, V.I., Hummel, J.W., Morgan, M.T., and Upadhyaya, S.K. 2004. "On-the-go soil sensors for precision agriculture." *Computers and Electronics in Agriculture*, 44(1), 71-91.
- Anderson, T.L. 2005. *Fracture mechanics: fundamentals and applications*. Boca Raton, FL: CRC Press.
- ASME. 2012. *Manual for determining the remaining strength of corroded pipelines: A supplement to ASME B31 code for pressure piping. ASME B31*. New York: American Society of Mechanical Engineers, American National Standards Institute.
- ASTM International. 2004. *E 8M – 04. Standard test methods for tension testing of metallic materials*. West Conshohocken, PA: ASTM International.
- ASTM International. 2008a. *E 399-08. Standard test method for linear-elastic plane-strain fracture toughness K_{Ic} of metallic materials*. West Conshohocken, PA: ASTM International
- ASTM International. 2008b. *E 1820-08. standard test method for measurement of fracture toughness*. West Conshohocken, PA: ASTM International.
- ASTM International. 2009. *E 9-09. Standard test methods of metallic materials at room temperature*. West Conshohocken, PA: ASTM International.
- ASTM International. 2010. *A247 – 10. Standard test method for evaluating the microstructure of graphite iron castings*. West Conshohocken, PA: ASTM International.
- ASTM International. 2013a. *E466. Standard practice for conduction force controlled constant amplitude axial fatigue tests of metallic materials*. West Conshohocken, PA: ASTM International.
- ASTM International. 2013b. *E 647 - 13. Standard test method for measurement of fatigue crack growth rates*. West Conshohocken, PA: ASTM International.
- Australian Iron and Steel. 1941. *Cast iron pipes*. Sydney, Australia: AIS.
- Bah, A., Balasundram, S.K., and Husni, H.A. 2012. "Sensor technologies for precision soil nutrient management and monitoring." *American Journal of Agricultural and Biological Sciences*, 7(1), 43-49.
- Bárdossy, A., and Lehmann, W. 1998. "Spatial distribution of soil moisture in a small catchment. Part 1: geostatistical analysis." *Journal of Hydrology*, 206(1–2), 1-15.
- Belmonte, H.M.S., Mulheron, M., Smith, P.A., Ham, A., Wescombe, K., and Whiter, J. 2008. "Weibull-based methodology for condition assessment of cast iron water mains and its application." *Fatigue & Fracture of Engineering Materials & Structures*, 31, 370-385.
- Brevis, W., Susmel, L. and Boxall, J. 2014. Investigating in-service failures of water pipes from a multiaxial notch fatigue point of view: A conceptual study. In *Proceedings of the Institution of Mechanical Engineers, Part C: Journal of Mechanical Engineering Science*.
- British Standards. 1938. *Cast iron pipes. BS 78*. London: British Standards Institute.
- Brocca, L., Melone, F., Moramarco, T., and Morbidelli, R., 2010. "Spatial-temporal variability of soil moisture and its estimation across scales." *Water Resources Research*, 46(2).
- Brocca, L., Morbidelli, R., Melone, F., and Moramarco, T., 2007. "Soil moisture spatial variability in experimental areas of central Italy." *Journal of Hydrology*, 333(2–4), 356-373.

- Cambardella, C.A., Moorman, T.B., Parkin, T.B., Karlen, D.L., Novak, J.M., Turco, R.F., and Konopka, A.E. 1994. "Field-scale variability of soil properties in central Iowa soils." *Soil Science Society of America Journal*, 58(5).
- Cassa, A., Van Zyl, J., and Laubscher, R. 2010. "A numerical investigation into the effect of pressure on holes and cracks in water supply pipes." *Urban Water Journal*, 7, 109-120.
- Chan, D.C.C. 2014. Study of pipe-soil-climate interaction of buried water and gas pipes. PhD thesis. Civil Engineering, Monash University: Melbourne.
<http://arrow.monash.edu.au/vital/access/manager/Repository/monash:130371>.
- Chan, D., Kodikara, J.K., Rajeev, P., and Robert, D. Forthcoming. Field study of large diameter cast iron water pipe buried under a roadway. Not yet submitted.
- Chan, D., Shannon, B., and Kodikara, J. 2016. Relative importance of external factors on pipe performance. In *Proceedings of OzWater 2016*, 10–12 May, Melbourne, Australia.
- Conlin, R.M., and Baker, T.J. 1991. *Application of fracture mechanics to the failure behaviour of buried cast iron mains*. Wokingham, UK: Transport Research Laboratory.
- Cole, I.S., and Marney, D. 2012. "The science of pipe corrosion: A review of the literature on the corrosion of ferrous metals in soils." *Corrosion Science*, 56, 5-16.
- Dafter, M. 2013. Long term corrosion of buried watermains compared with short term electrochemical testing. Corrosion and Prevention, 10-13 Nov 2013, Brisbane, Australia.
- Dafter, M. 2014a. Using LPR to predict underground corrosion of cast iron watermains. Paper 051. ACA 2014 conference. November 2014, Darwin.
- Dafter, M.R. 2014b. Electrochemical testing of soils for long-term prediction of corrosion of ferrous pipes. PhD dissertation, The University of Newcastle.
- De Lannoy, G.J.M., Verhoest, N.E.C., Houser, P.R., Gish, T.J., and Van Meirvenne, M. 2006. "Spatial and temporal characteristics of soil moisture in an intensively monitored agricultural field (OPE3)." *Journal of Hydrology*, 331(3–4), 719-730.
- Ehsani, M.R., Upadhyaya, S.K., Slaughter, D., Shafii, S., and Pelletier, M. 1999. "A NIR technique for rapid determination of soil mineral nitrogen." *Precision Agriculture*, 1(2), 219-236.
- Famiglietti, J.S., Rudnicki, J.W., and Rodell, M. 1998. "Variability in surface moisture content along a hillslope transect: Rattlesnake Hill, Texas." *Journal of Hydrology*, 210(1–4), 259-281.
- Fahimi, A., Evans, T.S., Farrow, J., Jesson, D.A., Mulheron, M.J., and Smith, P.A. 2016. "On the residual strength of aging cast iron trunk mains: Physically-based models for asset failure." *Materials Science and Engineering: A*, 663, 204–212.
- Falque, R., Vidal-Calleja, T., Valls Miro, J., Lingnau, D., and Russell, D. 2014, Background segmentation to enhance remote field eddy current signals. Australasian Conference on Robotics & Automation (ACRA), Melbourne, Australia.
- Falque, R., Vidal-Calleja, T., Dissanayake, G., and Valls Miro, J. 2016, From the skin-depth equation to the inverse RFEC sensor model. IEEE International Conference on Control, Automation, Robotics and Vision (ICARCV), Phuket, Thailand.
- Falque, R., Vidal-Calleja, T., and Valls Miro, J. 2015. Kidnapped laser-scanner for evaluation of RFEC tool. IEEE/RSJ International Conference on Intelligent Robots and Systems (IROS), Hamburg, Germany.
- Farrag, K. 2010. *Evaluation of External Corrosion-Rate Using Polarization Resistance and Soil Properties*. Washington, DC: U. S. Department of Transportation.

- Ferguson, P.H. 2010a. Condition assessment of pressure water mains - is it worth doing? ASCE Pipelines Conference 2010, Keystone, Colorado. August 28-September 1, 2010.
- Ferguson, P.H. 2010b. Smoke and mirrors. Which condition assessment techniques work. North American Society for Trenchless technology (NASTT) No-dig Show, Chicago, Illinois. May 2-7, 2010.
- Ferguson, P.H., and Nicholas, D.M.F. 1992. "External corrosion of buried iron and steel water mains." *Corrosion Australasia*, 17, 7-10.
- Fontana, M.G. 2005. *Corrosion Engineering*. New York: Tata McGraw-Hill.
- Gould, S. 2011. A study of the failure of buried reticulation pipes in reactive soils. Doctor of Philosophy, Monash University.
- Hope, D., Zhu, W., Gries, C., Oleson, J., Kaye, J., Grimm, N.B., and Baker, L.A. 2005. "Spatial variation in soil inorganic nitrogen across an arid urban ecosystem." *Urban Ecosystems*, 8(3-4): 251-273.
- Hadfield, P. 2014. "Failure prediction of critical pipes and pipe leak management." *Utility Magazine*, 3, 42-45.
- Heathcote, M., and Nicholas, D. 1998. *Life assessment of large cast iron water mains*. Melbourne: Urban Water Research Association of Australia.
- Huang, X., Skidmore, E.L., and Tibbz, G. 1999. Spatial variability of soil properties along a transect of CRP and continuously cropped land. 10th International soil conservation organisation meeting. Purdue University.
- Ji, J., Zhang, C., Kodikara, J., and Yang, S.-Q. 2015a. "Prediction of stress concentration factor of corrosion pits on buried pipes by least squares support vector machine." *Engineering Failure Analysis*, 55: 131-138.
- Ji, J., Zhang, C., and Kodikara, J. 2015b. Lifetime Reliability Assessment of Buried Pipelines Subjected to Corrosion. Symposium on Reliability of Engineering System, SRES 2015, Oct. 15-17, 2015, Hangzhou, China.
- Ji, J., Robert, D.J., Zhang, C., Zhang, D., and Kodikara, J. 2016. "Probabilistic physical modelling of corroded cast iron pipes for lifetime prediction." *Structural Safety*, DOI: 10.1016/j.strusafe.2016.09.004.
- Jiang, R., Robert, D., Hutchinson, C., Zhao, X.L., and Kodikara, J. 2016. Leak-before-break in cast iron mains a failure analysis of a catastrophic pipe burst on Harris Street Sydney. In *Proceedings of the IWA World Water Congress and Exhibition 2016*, 9-14 Oct., Brisbane, Australia.
- Kerry, R., Oliver, M.A., and Frogbrook, Z.L. 2010. "Sampling in precision agriculture." In *Geostatistical Applications for Precision Agriculture*, M.A. Oliver (Ed.). Dordrecht, Netherlands: Springer.
- Kear, G., Flatley, I., and Jones, S. 2006. Application of polarisation resistance measurements for the estimation of corrosion rates of galvanised steel structures in Soils. Corrosion and Protection 06 Conference, Grand Chancellor Hotel, Hobart Australia, 19-22 November 2006. Paper No. 127.
- Kleiner, Y., Rajani, B., and Krysz, D. 2013. "Performance of ductile iron pipes. I: Characterization of external corrosion patterns." *Journal of Infrastructure Systems*, 19, 108-119.
- Kodikara, J., Valls Miro, J., and Melchers, R. 2016. "Failure prediction of critical cast iron pipes." *Advances in Water Research*, 26(3), 6-11.

- Korres, W., Reichenau, T.G., Fiener, P., Koyama, C.N., Bogen, H.R., Cornelissen, T., Baatz, R., Herbst, M., Diekkrüger, B., Vereecken, H., and Schneider, K. 2015. "Spatio-temporal soil moisture patterns – A meta-analysis using plot to catchment scale data." *Journal of Hydrology*, 520, 326-341.
- Lauzon, J.D., O'Halloran, I.P., Fallow, D.J., von Bertoldi, A.P., and Aspinall, D. 2005. "Spatial variability of soil test phosphorus, potassium, and pH of Ontario soils." *Agronomy Journal*, 97(2), 524-532.
- Lim, K., Wong, L., Wong, K.C., and Kodikara, J.K. 2016. "Distributed fiber optic sensors for monitoring pressure and stiffness changes in out-of-round pipes." *Structural Control and Health Monitoring*, 23(2): 303–314.
- Liu, D. K., Dissanayake, G., Valls Miro, J., and Waldron, K. 2014. Infrastructure robotics: Research challenges and opportunities. International Symposium on Automation and Robotics in Construction and Mining, Sydney, Australia, pp. 43-49.
- McBratney, A.B., Webster, R., and Burgess, T.M. 1981. "The design of optimal sampling schemes for local estimation and mapping of regionalized variables—I: Theory and method." *Computers & Geosciences*, 7(4), 331-334.
- McIntyre, D.S. 1974. "Water retention and the moisture characteristic." In *Methods of Analysis for Irrigated Soils*. (Ed. J. Loveday) Tech. Comm. No. 54. Common Agric. Bur. (Publisher) England.
- Makar, J.M., and McDonald, S.E. 2007. "Mechanical behavior of spun-cast gray iron pipe." *Journal of Materials in Civil Engineering*, 19, 826–833.
- Melchers, R.E., and Petersen, R.B. 2016. Romanoff's soil corrosion data deconstructed. In *Proc. Conf. Corrosion and Prevention*, Auckland, New Zealand, Nov 13-16, Aust. Corrn. Assn., Melbourne.
- Mumovic, D., and Santamouris, M. 2013. *A Handbook of sustainable building design and engineering: An integrated approach to energy, health and operational performance.* London: Routledge.
- Nicholas, D., and Moore, G. 2009. "Corrosion of ferrous water mains: past performance and future prediction—a review." *Corrosion and Materials*, 34, 33–40.
- Nicholas, D., Ferguson, P., and Dafter, M. 2011. Electrochemical determination of corrosion rates of water mains in soils: a review. 18th International Corrosion Congress. Perth, Australia. 20-24th November 2011.
- Norin, M., and Vinka, T.G. 2003. "Corrosion of carbon steel in filling material in an urban environment." *Materials and Corrosion*, 54, 641-651.
- OAG. 2014. *Water corporation management of water pipes*. Perth, Australia: Office of the Auditor General.
- Pandey, V., and Pandey, P.K. 2010. "Spatial and temporal variability of soil moisture." *International Journal of Geosciences*, 1(2), 87-98.
- Petersen, R.B., and Melchers, R.E. 2012. Long-term corrosion of cast iron cement lined pipes. In *Proc. ACA conference, Corrosion & Prevention*, 2012, 11-14 Nov., Melbourne.
- Petersen, R.B., Dafter, M., and Melchers, R.E. 2013a. Modelling the long-term corrosion of cast iron pipes. In *Proc. ACA Conference*, Nov 10-13, Brisbane, Aust. Corrn. Assn.
- Petersen, R.B., Dafter, M., and Melchers, R.E. 2013b Long-term corrosion of buried cast iron water mains: field data collection and model calibration, In *Proc. LESAM - Strategic Asset Management of Water and Wastewater Infrastructure Conf*, Sydney, Australia. 10-13 September 10-12.

- Petersen, R.B., and Melchers, R.E. 2014. Long term corrosion of buried cast iron pipes in native soils. *Corrosion & Prevention 2013*. Darwin, Australia: Aust. Corrn. Assn.
- Petersen, R.B., and Melchers, R.E. 2015. The bi-modal corrosion behaviour of ferrous metals buried in soil. In *Proc. Conf. Corrosion & Prevention*, Adelaide, 15–18 Nov., Aust. Corrn. Assn.
- Petersen, R.B., and Melchers, R.E. 2016a. Predicting the corrosion of cast iron pipes. In *Proc. Conf. OzWater 16*, Melbourne, May 10-12, Aust. Water Assoc.
- Petersen, R.B., and Melchers, R.E. 2016b. Model for the long-term corrosion of cast iron pipes buried in soil. In *Proc. Conf. IALCCE*, Delft, The Netherlands, Oct 16-19.
- Petersen, R.B., and Melchers, R.E. 2016c. Factors involved in the long-term corrosion of buried cast iron. In *Proc. Conf. Corrosion and Prevention*, Auckland, New Zealand, Nov 13-16, Aust. Corrn. Assn.
- Petersen, R.B., Melchers, R.E., and Wells, T. 2016. *The long-term corrosion of cast iron in soil environments*. Newcastle, Australia: Centre for Infrastructure Performance and Reliability, The University of Newcastle.
- Rajani, B., and Kleiner, Y. 2010. Fatigue failure of large-diameter cast iron mains. *Water Distribution Systems Analysis 2010*, Tucson, USA.
- Rajani, B., and Kleiner, Y. 2013. *Fracture failure of large diameter cast iron water mains*. Project #4035. Denver, CO: Water Research Foundation.
- Rajani, B., Kleiner, Y., Krys, D., and Scientific, C. 2011. *Long-term performance of ductile iron pipes*. Project #3036. Denver, CO: Water Research Foundation.
- Rajani, B., Lewandowski, J., and Margevicius, A. 2012. “Failure analysis of cast iron trunk main in Cleveland, Ohio.” *Journal of Failure Analysis and Prevention*, 12, 217-236.
- Rajani, B., Makar, J., Mcdonald, S., Zhan, C., Kuraoka, S., Jen, C.-K., and Viens, M. 2000. *Investigation of grey cast iron water mains to develop a methodology for estimating service life*. Project #280. Denver, CO: AwwaRF and AWWA.
- Rajeev, P., Kodikara, J., Chiu, W.K., and Kuen, T. 2013a. “Distributed optical fibre sensors and their applications in pipeline monitoring.” *Key Engineering Materials*, 558: 424–434.
- Rajeev P., Kodikara J., Robert, D., Zeman, P., and Rajani, B. 2013b. Factors contributing to large diameter water pipe failure as evident from failure inspection, LESAM 2013 – IWA Leading edge strategic asset management, 10–12 Sep., Sydney, Australia.
- Rajeev, P., Kodikara, J., Robert, D., Zeman, P., and Rajani, B. 2014. “Factors contributing to large diameter water pipe failure.” *Water Asset Management Journal*, 10(3): 9–14.
- Rathnayaka, S.U.P. 2016. A study of water pressure influence on failure of large diameter water pipelines. PhD thesis. Civil Engineering, Monash University: Melbourne, 2016. <http://arrow.monash.edu.au/vital/access/manager/Repository/monash:172826>.
- Rathnayaka, S., Robert, D.J., Rajeev, P., and Kodikara, J. 2013. A review of the pressure transient effects on water distribution main failures, International Conference on Structural Engineering & Construction Management-ICSECM 2013, 13–15 Dec., Kandy, Sri Lanka.
- Rathnayaka, S., Keller, R., Kodikara, J., and Chik, L. 2016a. “Numerical simulation of pressure transients in water supply networks as applicable to critical water pipe asset management.” *Journal of Water Resources Planning and Management*, 142(6): 04016006.

- Rathnayaka, S., Shannon, B., Rajeev, P., and Kodikara, J. 2016b. "Monitoring of pressure transients in water supply networks." *Journal of Water Resources Management*, 30(2): 471–485.
- Rathnayaka, S., Shannon, B., Zhang, C., and Kodikara, J. 2016c. "Introduction of leak-before-break (LBB) concept for cast iron water pipes on the basis of laboratory experiments." *Urban Water Journal*, DOI: 10.1080/1573062X.2016.1274768.
- Rathnayaka, S., Shannon, B., Robert, D., and Kodikara, J. 2016d. "Experimental evaluation of bursting capacity of corroded grey cast iron water pipeline." *Structure and Infrastructure Engineering*, 21 March 2017.
- Rathnayaka, S., Shannon, B., Vahid, S., Guo, M., Sinclair, D., and Kodikara, J. 2016e. Reducing severity of pressure transients in water supply networks-a case study. In *Proceedings of OzWater 2016*, 10–12 May, Melbourne, Australia.
- Rayment, G.E., and Lyons, D.J. 2010. *Soil chemical methods – Australasia*. Clayton, Vic, Australia: CSIRO Publishing.
- Rezaei, H., Ryan, B., and Stoianov, I. 2015. "Pipe failure analysis and impact of dynamic hydraulic conditions in water supply networks." *Procedia Engineering*, 119, 253–262.
- Robert, D., Rajeev, P., Kodikara, J., and Rajani, B. 2016b. "Equation to predict maximum pipe stress incorporating internal and external loadings on buried pipes." *Canadian Geotechnical Journal*, 53(8): 1315–1331.
- Robert, D. J., Jiang, R., Rajeev, P., and Kodikara, J. 2016a. "Contribution of cement mortar lining to structural capacity of cast iron water mains." *Materials Journal*, 113(03): 295–306.
- Romanoff, M. 1957. *Underground corrosion, National Bureau of Standards Circular 579*. Washington, DC: US Government Printing Office.
- Schijve, J. 2001. *Fatigue of structures and materials*. Netherlands: Springer.
- Scott, R.J. 1990. *Reticulation water mains 1857 to 1990*. Melbourne: Melbourne Water.
- Scully, J.R. 2000. "Polarization resistance method for determination of instantaneous corrosion rates." *Corrosion*, 56, 199-218.
- Seica, M., and Packer, J. 2004. "Mechanical properties and strength of aged cast iron water pipes." *Journal of Materials in Civil Engineering*, 16, 69-77.
- Shannon, B., Rathnayaka, S., Zhang, C., and Kodikara, J. 2016b. Lessons learnt on pipe failure mechanisms from observation of exhumed cast iron pipes. In *Proceedings of OzWater 2016*, 10–12 May, Melbourne, Australia.
- Shannon, B., Rathnayaka, S., Zhang, C., and Kodikara, J. 2016c. Lessons learnt from laboratory pipe burst tests. In *Proceedings of the IWA World Water Congress & Exhibition 2016*, 9–14 Oct., Brisbane, Australia.
- Shannon, B., Jiang, R., Ji, J., Chan, D., and Kodikara, J. 2016a. Investigation of cohort properties for Australian cast iron water mains. In *Proceedings of the IWA World Water Congress & Exhibition 2016*, 9–14 Oct., Brisbane, Australia.
- Shi, L., Sun, L., Vidal-Calleja, T., and Valls Miro, J. 2015. Kernel-specific gaussian process for prediction in pipe wall thickness mapping, Australasian Conference on Robotics & Automation (ACRA), Canberra, Australia.
- Shi, L., and Valls Miro, J. 2016. Towards optimized and reconstructable sampling inspection of pipe integrity for improved efficiency of NDT. IWA World Water Congress, Brisbane, Australia.

- Shi, L., Valls Miro, J., Rajalingam, J., Wood, R., and Vitanage, D. 2016a. High precision GPS aided in-pipe distance calibration for satellite image-based pipeline mapping. Ozwater'16: Australia's International Water Conference and Exhibition (OzWater), Melbourne, Australia.
- Shi, L., Valls Miro, J., Zhang, T., Vidal-Calleja, T., Sun, L., and Dissanayake, G. 2016b. Constrained sampling of 2.5D probabilistic maps for augmented inference. IEEE/RSJ International Conference on Intelligent Robots and Systems (IROS), Daejeon, Korea.
- Shi, L., Valls Miro, J., Vidal-Calleja, T., Vitanage, D., and Rajalingam, J. 2017. Innovative data driven "along-the-pipe" condition assessment for critical water mains. Ozwater'17: Australia's International Water Conference and Exhibition (OzWater), Melbourne, Australia.
- Skinner, B., Vidal-Calleja, T., Valls Miro, J., De Bruijn, F., and Falque, R. 2014. 3D point cloud upsampling for accurate reconstruction of dense 2.5D thickness maps. Australasian Conference on Robotics & Automation (ACRA), Melbourne, Australia.
- Su, D., Valls Miro, J., and Vidal-Calleja, T. 2015. Modelling in-pipe acoustic signal propagation for condition assessment of multi-layer water pipelines. IEEE Conference on Industrial Electronics and Applications (ICIEA), Auckland, New Zealand.
- Sun, L., Vidal-Calleja, T., and Valls Miro, J. 2015. Bayesian fusion using conditionally independent submaps for high resolution 2.5D mapping. IEEE International Conference on Robotics and Automation (ICRA), Seattle, USA.
- Sun, L., Vidal-Calleja, T., and Valls Miro, J. 2016. Gaussian markov random fields for fusion in information form, IEEE International Conference on Robotics and Automation (ICRA), Stockholm, Sweden.
- Sun, L., Vidal-Calleja, T., and Valls Miro, J. 2017. Coupling conditionally independent submaps for large-scale 2.5D mapping with gaussian markov random fields. IEEE International Conference on Robotics and Automation (ICRA), Singapore.
- Ulapane, N., Alempijevic, A., Vidal-Calleja, T., Valls Miro, J., Rudd, J., and Roubal, M. 2014. Gaussian process for interpreting pulsed eddy current signals for ferromagnetic pipe profiling. IEEE Conference on Industrial Electronics and Applications (ICIEA), Hangzhou, China.
- Valls Miro, J., and Shi, L. 2016. "Aiming for the holy grail: pipe condition assessment along critical mains from limited inspections." *Utility Magazine*, 10, 90-92.
- Valls Miro, J., Rajalingam, J., Vidal-Calleja, T., De Bruijn, F., Wood, R., Vitanage, D., Ulapane, N., Wijerathna, B., and Su, D. 2013. A live test bed for the advancement of condition assessment and failure prediction research on critical pipes. IWA Leading-Edge conference on Strategic Asset Management of Water and Wastewater Infrastructures (LESAM), Sydney, Australia.
- Valls Miro, J., Vidal-Calleja, T., De Bruijn, F., Ulapane, N., Wijerathna, B., Su, D., Rajalingam, J., Wood, R., and Vitanage, D. 2014. "A live test bed for the advancement of condition assessment and failure prediction research on critical pipes." *Water Asset Management International*, 10(2), 3-8.
- Vidal-Calleja, T., Su, D., De Bruijn, F., and Valls Miro, J. 2014a. Learning spatial correlations for Bayesian fusion in pipe thickness mapping. IEEE International Conference on Robotics and Automation (ICRA), Hong Kong, China.

- Vidal-Calleja, T., Valls Miro, J., Martin, F., Lingnau, D., and Russell, D. 2014b. Automatic detection and verification of pipeline construction elements with multi-modal data. IEEE/RSJ International Conference on Intelligent Robots and Systems (IROS), Chicago, USA.
- Vitanage, D.C., Kodikara, J., and Allen, G. 2013. Collaborative research on condition assessment and pipe failure prediction of critical water mains, LESAM 2013 – IWA Leading edge strategic asset management, 10–12 Sep., Sydney, Australia.
- Vitanage, D., Kodikara, J., and Allen, G. 2014. “Collaborative research on condition assessment and pipe failure prediction for critical water mains.” *Water Asset Management Journal*, 10(3), 15–18.
- Vitanage, D., and Zhang, D. 2014. *Using data analytics to prioritise high risk critical pipe failure*. Sydney, Australia: Sydney Water.
- Western, A.W., Blöschl, G., and Grayson, R.B. 1998. “Geostatistical characterisation of soil moisture patterns in the Tarrawarra catchment.” *Journal of Hydrology*, 205(1–2), 20-37.
- Wijerathna, B., Vidal-Calleja, T., Kodagoda, S., Zhang, Q., and Valls Miro, J. 2013. Multiple defect interpretation based on gaussian processes for MFL technology. In *Proc. SPIE 8694, Nondestructive Characterization for Composite Materials, Aerospace Engineering, Civil Infrastructure, and Homeland Security 2013*, San Diego, California, USA.
- Wijerathna, B., Kodagoda, S., Valls Miro, J., and Dissanayake, G. 2015. Iterative coarse to fine approach for interpretation of defect profiles using MFL measurements. IEEE Conference on Industrial Electronics and Applications (ICIEA), Auckland, New Zealand.
- Wikipedia. 2008. Wikipedia’s “Structured-light 3D scanner” entry. Image 3-proj2cam.svg by Vanessa Ezekowitz. https://en.wikipedia.org/wiki/Structured-light_3D_scanner.
- Wong, L., Chiu, W.K., Lim, K., and Kodikara, J. 2014. Distributed strain sensing for structural health monitoring. In *Proceedings of Singapore Aerospace Technology & Engineering Conference*, 10 Feb., SunTec City, Singapore.
- Wong, L., Rathnayaka, S., Chiu, W.K., and Kodikara, J. 2016c. Fatigue damage monitoring of a cast iron pipeline using distributed optical fibre sensors. In the 6th Asia Pacific Workshop on Structural Health Monitoring, 7–9 Dec., Hobart, Australia.
- Wong, L., Chowdhury, N., Wang, J., Chiu, W., and Kodikara, J. 2016a. “Fatigue damage monitoring of a composite step lap joint using distributed optical fibre sensors.” *Materials*, 9(5), 374.
- Wong, L., Lim, K., Chiu, W.K., Kodikara, J., and Chowdhury, N. 2016b. “Using water hammer effects for the detection of localised anomaly along a LDPE pipeline with distributed optical fibre sensors.” *Structural Control and Health Monitoring*, DOI:10.1002/stc.1975.
- Wong, L., Chiu, W.K., and Kodikara, J. 2017a. “Using distributed optical fibre sensor to enhance structural health monitoring of a pipeline subjected to hydraulic transient excitation.” *Structural Health Monitoring, International*. pp 1-15 DOI: 10.1177/1475921717691036.
- Wong, L., Chiu, W.K., and Kodikara, J. 2017b. “Using transient excitation for the structural health monitoring of a long small diameter pipeline with a distributed optical fibre sensor.” *Structural Health Monitoring*. DOI: 10.1177/1475921717691036.
- WSAA (Water Services Association of Australia). 2009. *National Performance Report 2007/2008*. Melbourne, Australia: WSAA.
- Yang, L., Wei, W., Chen, L., Jia, F., and Mo, B. 2012. "Spatial variations of shallow and deep soil moisture in the semi-arid Loess Plateau, China." *Hydrol. Earth Syst. Sci.*, 16(9): 3199-3217.

- Yao, X., Fu, B., Lü, Y., Sun, F., Wang, S., and Liu, M. 2013. "Comparison of four spatial interpolation methods for estimating soil moisture in a complex terrain catchment." *PLoS ONE*, 8(1): e54660.
- Zhang, C., Ji, J., Kodikara, J., and Rajani, B. 2017a. "Hyperbolic constitutive model to study cast iron pipes in 3-D nonlinear finite element analyses." *Engineering Failure Analysis*, <http://dx.doi.org/10.1016/j.engfailanal.2017.01.003>.
- Zhang, C., Rathnayaka, S., Shannon, B., Ji, J., and Kodikara, J. 2017b. "Numerical interpretation of pressurized corroded cast iron pipe tests." *International Journal of Mechanical Sciences*, 128-129, 116-124.



City West Water™



Melbourne Water



MONASH University



QUEENSLAND Urban Utilities



SA Water



Sydney WATER



THE UNIVERSITY OF NEWCASTLE AUSTRALIA



UNIVERSITY OF TECHNOLOGY SYDNEY



WATER CORPORATION



Yarra Valley Water



THE Water Research FOUNDATION



1199 North Fairfax Street, Suite 900
Alexandria, VA 22314-1445
www.werf.org | werf@werf.org

6666 West Quincy Avenue
Denver, CO 80235-3098
www.waterrf.org | info@waterrf.org